DESIGN CONCEPT
FOR THE
ADVANCED RADAR TEST BED (ARTB)
(VOLUME II: APPENDICES)

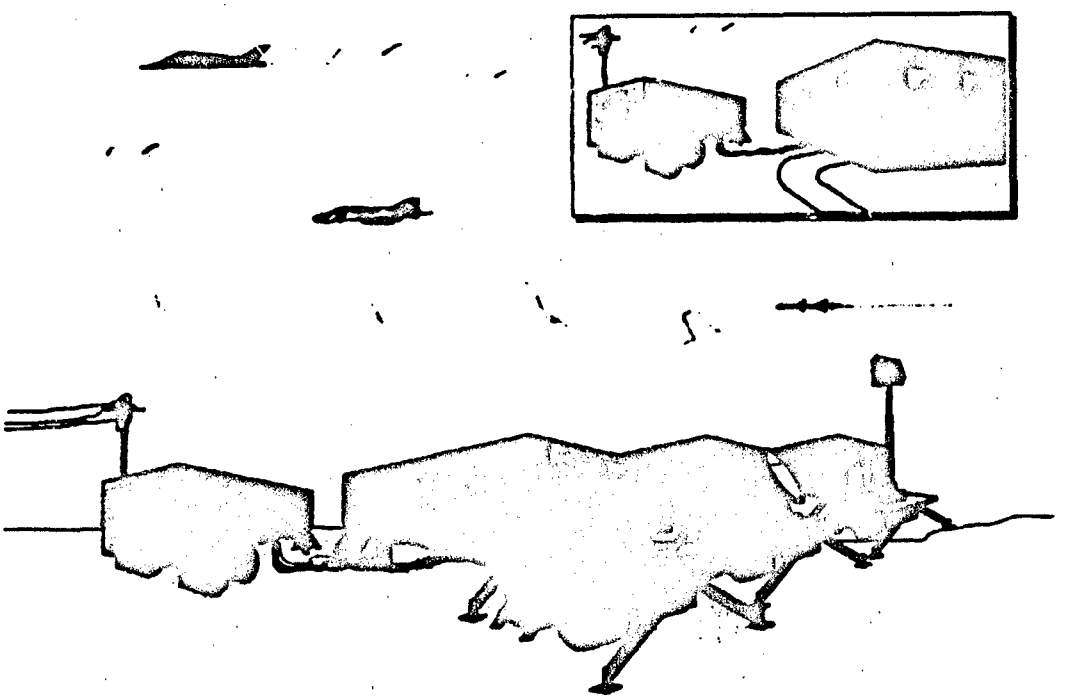

Prepared for:

U.S. Army Space and Strategic Defense Command
(Attn: CSSD-CR-P)
Huntsville, Alabama

Prepared by:

SCIENTIFIC RESEARCH CORPORATION
2300 Windy Ridge Parkway Suite 400 South
Atlanta, Georgia 30067

31 December 1994

AD NUMBER

AD-B205 248

NEW LIMITATION CHANGE

TO

DISTRIBUTION STATEMENT A -
Approved for public release; Distribution unlimited.

Limitation Code: 1

FROM

DISTRIBUTION STATEMENT -

Limitation Code:

AUTHORITY

Janet E. Mosher, Phillips Lab., Kirtland AFB, N.M.

DESIGN CONCEPT

FOR THE

ADVANCED RADAR TEST BED (ARTB)

Prepared for:

U.S. Army Space and Strategic Defense Command
(Attn: CSSD-CR-P)
Huntsville, Alabama 35807-3801

CONTRACT NO. DASG60-91-C-0118
Contract Start Date: 30 August 1991
Contract End Date: 31 December 1994

Prepared by:

SCIENTIFIC RESEARCH CORPORATION
2300 Windy Ridge Parkway Suite 400 South
Atlanta, Georgia 30067

Principal Investigator - Dr. James Beard, (404) 859-9161
Project Engineer - Mr. Jeff Smart, (404) 859-9161

Authenticated by _____
Program Manager

Date 26 May 1995

Approved by _____
Vice President, Sensors

Date 26 MAY 95

SECTION 1
TECHNICAL PROPOSAL

1.0 INTRODUCTION

This proposal responds to the Broad Area Announcement of FY91 Research Opportunities of the SDIO Innovative Science and Technology Directorate, Reference Number SDIO 90-18, listed as topical area number (4) Self Adaptive Processing and Simulation. A collaborative industrial and university team (Scientific Research Corporation, Metric Systems Corporation and Clemson University), proposes to perform research consisting of the two primary tasks and associated sub-tasks described in subsequent sections of this proposal.

The proposed industrial-university team has decades of experience in providing advanced technology-oriented research and development as well as manufacturing support for the United States government and industry. With combined partnership resources of more than 3000 personnel located throughout the United States and overseas, consisting primarily of scientists, engineers, analytical and product personnel, the proposed team represents a wide spectrum of research, development, engineering, manufacturing, test and evaluation, and operational activities. Facilities and laboratories are available to support effectively a variety of experimental and scientific investigations.

Recent research and development activities have included providing focus for emerging technologies and directing research programs that required the skills of highly specialized scientists and engineers. For example, advanced sensor and communication technologies for phased arrays and high power systems have been investigated to determine their potential for meeting specialized rapid prototyping requirements. In addition to laboratory experiments and basic research ranging from components to large space, terrestrial, and platform systems, associated studies included computer-aided analysis of highly accurate transportable measurement systems that could be used at a variety of geographically disbursed test sites.

1.1 TECHNICAL AREAS PROPOSED

Two primary tasks are proposed that consists of research and development directly related to the advancement of Simulation Technologies. Particular tasks and associated sub-tasks proposed are as follows: (Task I) Experimental Modular System and Critical Component Research (System Control and Processing Modules, IF Waveform Generation, High Power Transmitters, RF modules, and Antenna Elements); and (Task II) Analytical and Experimental Studies (system vulnerabilities utilizing all-source data, and emerging technologies such as signal processing and multi-target detection). The relationship of these various tasks and sub-tasks, shown in Figure 1, is discussed in subsequent paragraphs.

The research proposed will be performed by industrial and university engineering and computer science professionals, who will focus on developing solutions to defense problems. Industry will be providing emerging technologies for evaluation and will also support proposed research activities.

Our research team has the technical experience and special facilities required to effectively support experimental and associated critical components research program. Additionally, this team could also perform optional applied research and prototyping tasks. The costs, risks, and transportability limitations associated with the development of high fidelity simulations have frequently precluded their effective utilization as test assets. It is therefore proposed that component developments (low cost emitters with full effective radiated power and high-fidelity signals) be integrated with emerging phased array and processing technologies to build multiple-use, experimental modular test assets. Research activities will include evaluation and subsequent development of a real-time programmable signal processor that will operate in a multi-target environment. A real-time multicomputer laboratory will be utilized for studying transputer-based architectures for radar signal processing. This facility can also support research work in the use of sophisticated signal processing techniques needed for real-time detection and tracking in a multi-target environment.

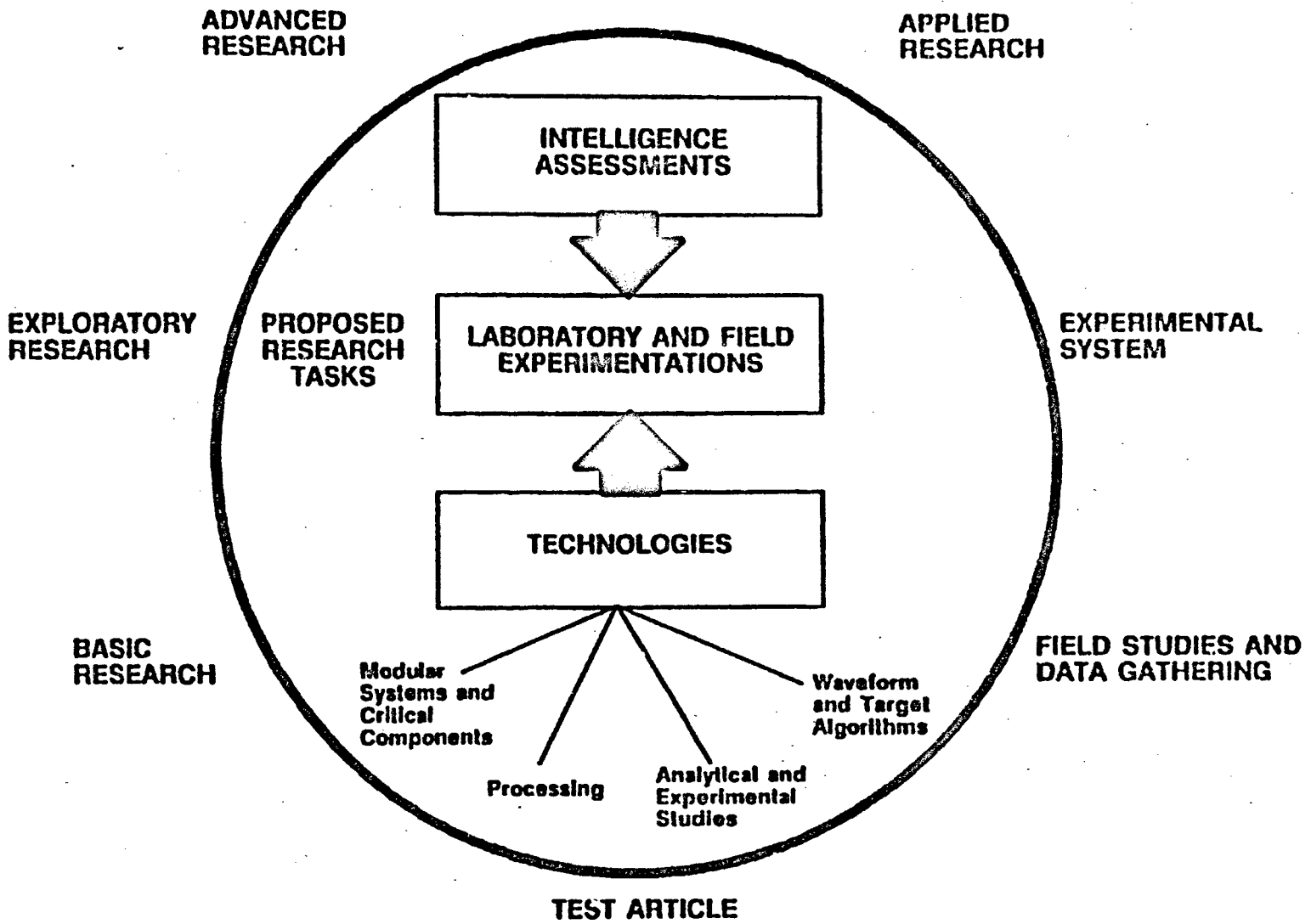

FIGURE 1. CONNECTIVITY OF RESEARCH TASKS

Such experimental modules could be designed to simulate ground based sensors and airborne missile parameters for strategic as well as tactical systems that must operate in high clutter and multipath environments as part of an integrated air defense system. Both early warning and terminal tracking elements could be connected with adaptive networks and efficient data systems to perform a variety of functions. Critical component technologies may include: (1) complex phased arrays and sub-arrays; (2) variable waveform generators; (3) high average power transmitter components; (4) knowledge-based modules and associated machine intelligence; (5) ultra-stable sources; and (6) support networks.

1.1.1 TASK I: EXPERIMENTAL MODULAR SYSTEM AND CRITICAL COMPONENT RESEARCH

Historically, simulation/simulator test asset developments have been program specific with limited flexibility or transportability. In addition to meeting flexibility and versatility requirements, simulation system developments need to be cost effective. In a down scaled defense environment, it is clear that the U.S. can neither construct realistic war fighting assets nor simulate advanced systems in the absence of cost saving technologies. In this proposal, a number of technological advancements are identified which are expected to provide an order of magnitude reduction in system development costs. The proposed modular system research activities will provide the foundation for sub-element assessments and subsequent individual component developments. Alternatives specified will utilize both near-term and advanced technologies.

Technical Approach

Effective target acquisition, tracking and interceptor research and their supporting technologies require timely development of modules that can be integrated, adaptive, multi-spectral, and technically sophisticated. A natural evolution, therefore, is the creation of a multiple emulation system with flexible, transportable, and low-cost design features. Such a system will replicate characteristics of power and signal sources that would be encountered in a variety of operational environments. Realistic testing scenarios will

consider the fact that signal densities include a complex mix of missile and air defense systems. The test article to be developed must therefore employ highly integrated electronics and RF modules with reconfigurable elements that replicate a variety of sensors and missile control systems. Operational requirements may also include adaptive processes and coherent sidelobe-canceller techniques to extract information on targets that are embedded in a background of high clutter.

Transportability for field experimentations will be enhanced with a miniaturized modular approach. The system could be broken down at convenient interface points for transport and re-deployment at a new location and re-connected at defined interface points. The enhanced versatility, transportability, and reliability of such a modular design make it a most attractive option.

One example of a modular design element is a knowledge-based subsystem that allows the user operational flexibility in configuring the system to perform a variety of processing functions. Developmental options include flexible selection of a set of IF hardware for generating the appropriate timing pulses and waveforms to produce the desired radiated signals. The received signals will be processed at IF and fed to a data acquisition system for recording or, with appropriate software, processing could provide dynamic feedback to the system to provide a real-time response capability for more sophisticated simulation requirements. Expandable frequency coverage will be provided by a collection of frequency translation modules. Interchangeable antenna subsystems at the RF port of such a translation module will allow the user to customize the radiated signal pattern to satisfy various requirements. This approach permits timely development of a baseline system with enhancement capabilities and provides for the addition of new modules for major performance upgrades. A modular programmable system with faithfully replicated performance bands will be developed. The system will be suitable for a variety of experimental and developmental support missions. It will provide flexibility in a domain where little specific information is currently available, and it will allow rapid reconfiguration of sub-elements as additional data become available.

The basic elements of a design concept that will capitalize on enabling technologies to achieve these objectives are shown in Figure 2. The centralized control and operator interface functions shown in this diagram could be implemented in a simplistic general purpose front-end processor. Alternatively, a more complex parallel processor could be used to construct complex waveforms and perform signal processing functions. The intermediate frequency (IF) waveform generation, time synchronization, and IF reception functions may be implemented with readily available hardware and software. The high power transmit sections needed for amplification and generation of the appropriate RF waveform must be developed. They would also be used to produce the perspective radiating apertures that perform beam steering and RF collimation.

Commonalities of digital and low power RF components will be exploited to reduce development costs. An extension of this concept may include development of a single front-end processor and IF waveform generator to control and produce low power waveforms for multiple users. New requirements could therefore be satisfied in the low power section of the system by modifying existing software. A standard interface will be implemented between the IF sections and high power RF components; however, multiple RF heads and radiating apertures may be required due to present technology limitations in high power generation systems. Future enhancements could be achieved with the addition of a new antenna or RF module with minimal impact on the other system components.

System Control and Processing Modules

System control and processing functions are typically performed by a general purpose processing system. Functions of the processor include providing an intuitive user interface and control for the system. For example, simulation waveform parameters are typically established by the processor for down-loading to the waveform generator.

FIGURE 2. MODULAR SYSTEM COMPONENTS

A viable implementation of a realistic user interface entails high level operator interaction to specify alternative test scenarios. For example, such a system may automatically retrieve a prioritized list of candidate emitters utilizing knowledge-based systems that characterize specific targets, missile characteristics and performance envelopes. Operators could have embedded software that would modify the candidate emitters list subject to new intelligence data. Alternative concepts could use artificial intelligence techniques to assist in candidate emitter selection. For instance, geographic mapping and emulation probabilities could be factored into the emitter selection process, thereby reducing operator interaction. Other functions provided by the processor may include measurement of actual emanations.

Processor functions may also encompass dynamic adjustment of transmit waveforms based on threat environment characteristics. In a typical encounter, systems are likely to cycle through a predictable change in transmit waveform as targets are detected and engaged. For example, radar waveforms may transition from search/acquisition modes of operation to target track, and from target track to target engagement. Waveform transitions serve to alert enemy forces of weapon status and provide additional confirmation of system identity. While transitions are not critical to counter surveillance, they may play a substantial role in "end game" deception. The processor will therefore be responsible for processing return energy, scoring detections, establishing target tracks, controlling the direction of antenna radiation, calculating transmit waveform parameters, selecting the appropriate RF module, and monitoring system status.

IF Waveform Generation

Control signals generated by the processor are sent to the waveform generator which consists of low frequency and wide bandwidth components that are capable of producing a variety of signal characteristics. This development approach exploits the commonality of digital and low power RF components to generate waveforms for arbitrary RF requirements utilizing IF baseband modules. Multi-system simulation can therefore be achieved since all waveforms, regardless of final frequency, can be originated at

baseband or IF thereby providing increased flexibility and expandability. Further, the baseband and IF waveforms can be generated by hardware that is small, light, and inexpensive.

In the modular system proposed, RF waveforms required to simulate threat emissions can be derived utilizing IF baseband components. These low power, low frequency waveforms can be constructed in digital format using available computer hardware and software. This permits the design, construction, and modification of waveforms for current as well as future requirements. Digital representation of a particular waveform can therefore be used to drive an Arbitrary Waveform Synthesizer which in turn provides an analog baseband input to the IF generator. The IF generator provides an analog signal which is converted to the appropriate frequency, amplified, and then propagated through the antenna. This direct digital synthesis technique will be utilized to build the baseband waveform in software and the resultant digital representation will provide an input to a synthesizer or digital-to-analog converter.

This technique provides several advantages over traditional analog baseband waveform generation techniques such as:

- very fine frequency and phase resolution,
- flat and predictable response over a wide bandwidth,
- low phase noise,
- minimal adjustment/drift,
- low analog component count,
- easy implementation of alternative modulations, and
- low power consumption.

Some of the advantages realized with analog waveform generation systems include:

- possibility of generating higher frequencies,
- [illegible] spurious noise performance,
- smoother frequency chirps,

- easy implementation of analog modulators, and
- lower cost for simplistic (static) requirements.

By extending this system concept, it is possible for waveform generation to be accomplished by mimicking actual signals and providing them as an input to the basic system for signal regeneration. This process has the potential to provide the mechanism for integrating new requirements into simulator assets with minimal software development; however, fundamental research is required to determine feasibility, flexibility, and effectiveness of the system.

High Power Transmitters

Low power waveforms generated by the IF hardware require further processing to convert the signal to the appropriate RF and establish the proper output power. In the modular design approach, these functions are implemented in a high power RF module.

While the problems encountered in the low power sections of the modular design are well understood, high power components are typically the largest, heaviest, and most costly portions of the system. For example, the high power transmitter draws large amounts of current at high voltage levels thus dictating power plant requirements. Stable operation of the transmitter often requires liquid cooling, which produces additional repercussions on system design. Consequently, simulator developments tend to revolve around design constraints associated with the transmitter.

Transmitter designs are typically dictated by RF tube selection. The situation is complicated by the fact that RF tubes are highly specialized to specific systems; therefore, design of a new system often involves construction of a new tube. While hundreds of tubes with differing characteristics have been manufactured, there are at least two dozen parameters required to specify their operation. Consequently, a slight deviation in system requirements often results in a new tube development program.

The transmitter design approach proposed utilizes a master oscillator power amplifier architecture. The master oscillator will be used to convert the signal generated by the IF hardware, or it can be eliminated if low power RF signals are supported directly by the waveform generator. High power amplifiers will provide the appropriate gain. Although vacuum tubes are commonly used as the amplifier in applications requiring high output power, alternative approaches involving the coherent summation of outputs from low-power components will be investigated. Among the candidate tubes, CFAs and cavity-coupled TWTs probably hold the most promise for near term applications.

Figure 3 illustrates the percentage bandwidth versus peak power output of various tubes in the S- to X- band range of operation. In the power region of interest, Klystron bandwidth is less than ten percent of the center frequency, whereas the bandwidth of coupled cavity TWTs and CFAs is approximately thirty percent. While it is notable that helically wound TWTs possess even greater bandwidths, these tubes can be unreliable at high power levels. Bandwidth constraints are critical to simulator developments due to the requirement for multi-system simulation. It is clear that multiple tubes will be required to span the complete frequency range of interest. However, wider tube bandwidths will reduce cost and complexity.

Operating efficiency affords another measure for tube comparison. Figure 4 illustrates a plot of efficiency versus bandwidth for several high power tubes. Low efficiency devices generally require large amounts of prime power to deliver substantial output power. Consequently, low transmit efficiency can translate into a large power supply. In addition, energy not coupled to the RF field is usually converted into heat which translates into increased cooling requirements. At ten percent bandwidth, CFA efficiency is approximately 60 percent in comparison to the 25-35 percent efficiency of TWTs and Klystrons. In addition to the relatively high efficiency of CFAs, these devices are smaller in comparison to TWTs and Klystrons. However, the gain and dynamic range of CFAs

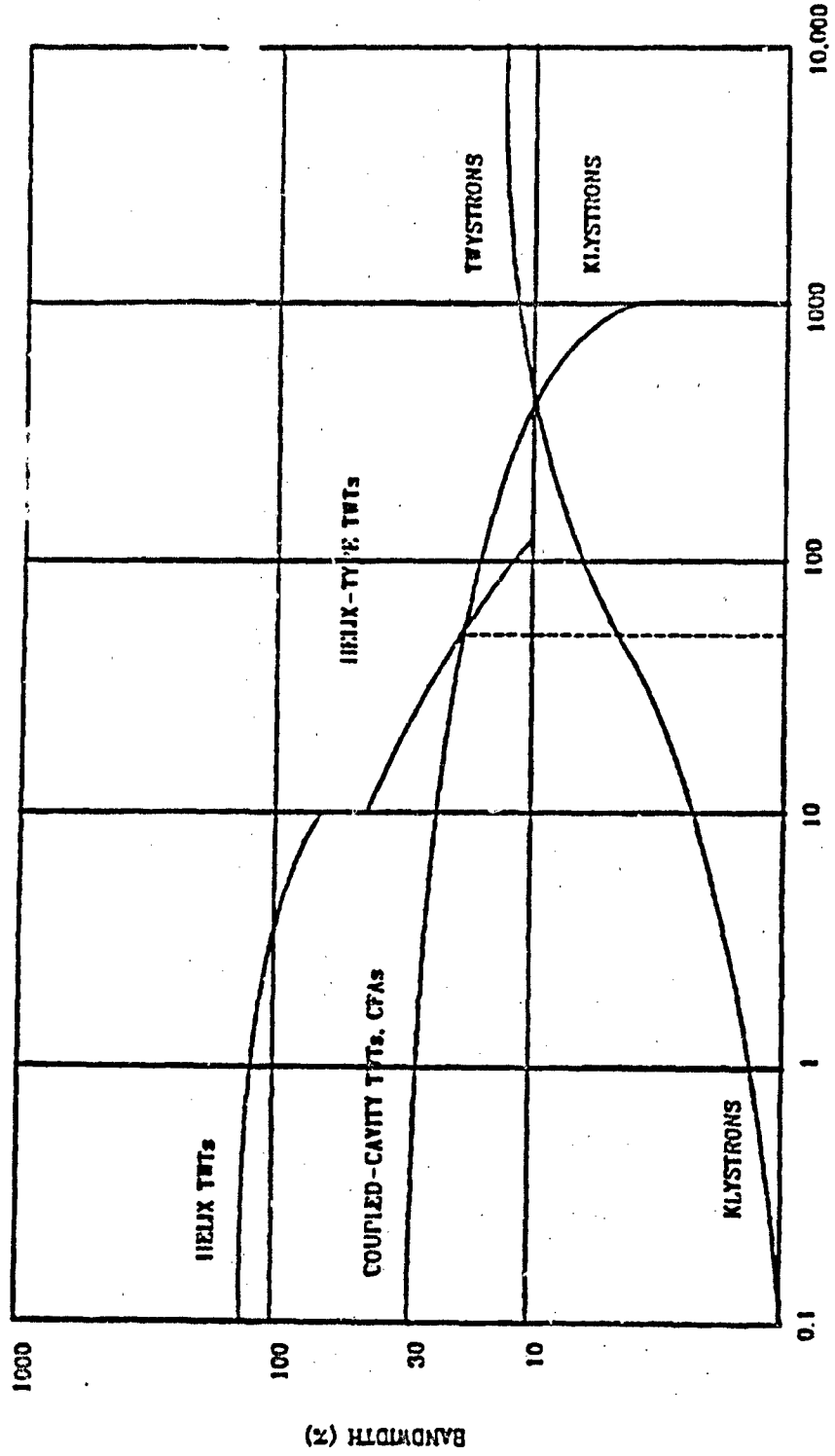

FIGURE 3. PEAK POWER VS. BANDWIDTH

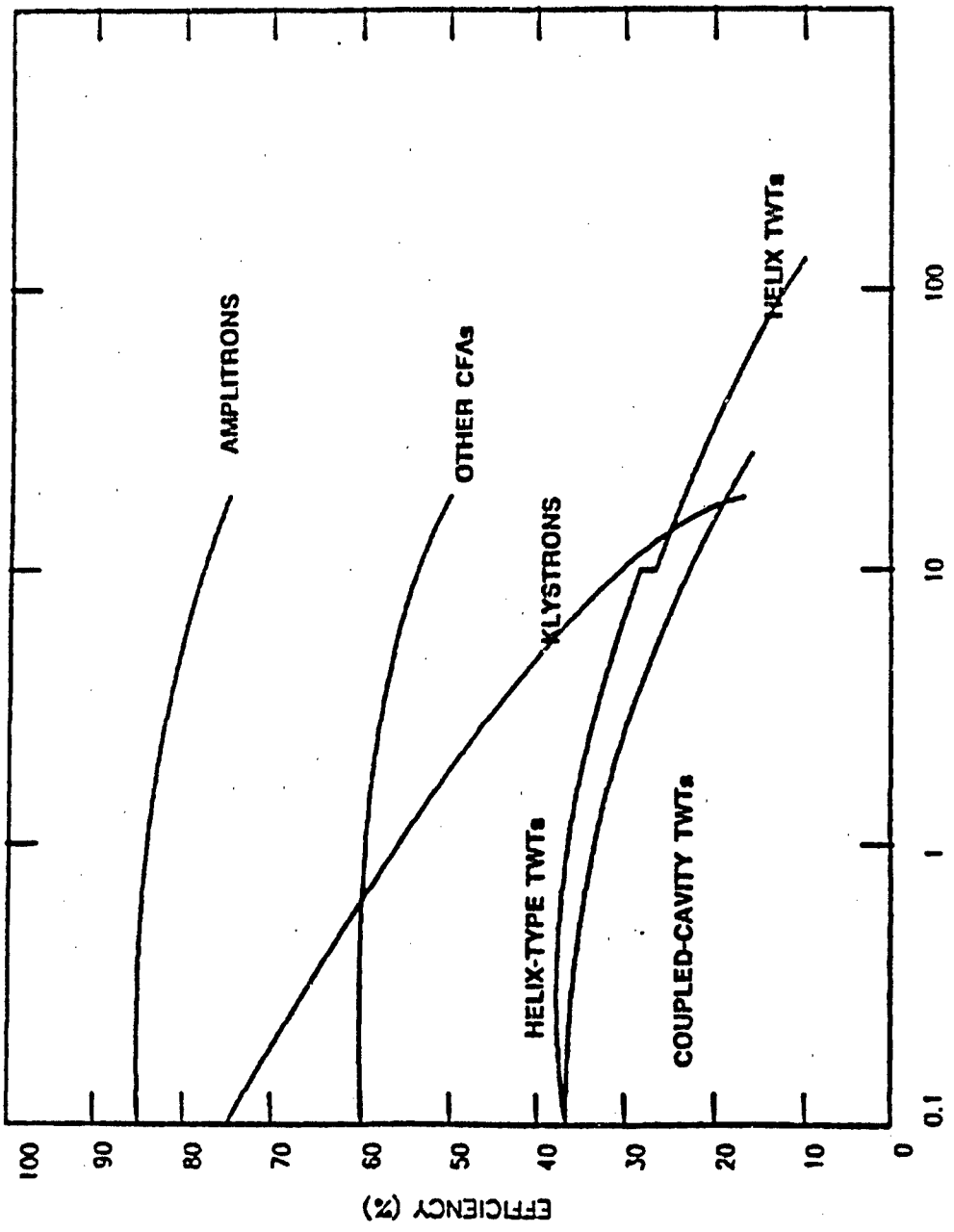

FIGURE 4. EFFICIENCY VS. BANDWIDTH FOR VARIOUS TUBES

are small in comparison to other tube types. A typical high power CFA possesses a 6-30 dB gain with a dynamic range of 3-20 dB. In comparison, high power TWTs and Klystrons possess typical gains of 30-70 dB with dynamic ranges of 40-80 dB.

While detail design trade-offs are best conducted after a thorough investigation of waveform characteristics, some general conclusions are possible at this juncture. In applications where size and weight are of primary concern, a two-stage transmitter design may afford the most flexibility. The output from the IF hardware could be connected to a solid state amplifier, or a relatively small TWT. The first stage output would feed a high power CFA. This configuration affords the benefits of the gain-bandwidth product displayed by TWTs and solid state devices, and would also exploit the efficiency of high power CFAs. Power supply voltage would be minimized since TWTs operate at low power and CFAs are more efficient. For example, a typical one megawatt TWT might require a power supply capable of producing 90 KV while a comparable CFA requires only 40 KV. Some of the disadvantages of the two-stage approach include pulse compression, increased noise, and relatively more complex circuitry. In operational scenarios not constrained by space limitations, Klystrons provide a viable mechanism for achieving high power output with minimal waveform distortion. Recent research in Klystron development has produced devices that manifest extremely high peak power with low phase noise.

Aperture Trade-offs

The RF energy generated by the transmitter requires further amplification and coupling into a free-space environment. Amplification is achieved by translating omni-directional emanations into highly directive field patterns and establishing a proper impedance match. Recent technological advancements have made it possible for radiating apertures to couple RF energy into free space with increased efficiency while providing multi-functional capability. Consequently, the U.S. has progressed from a defense posture based on the proliferation of a multitude of single-mode, single- function systems to one composed of highly advanced assets possessing multi-function capabilities. For example, from a radar

perspective, the roles of air surveillance, target acquisition, target tracking, and missile guidance have traditionally been performed by different systems. However, modern systems are capable of accomplishing these functions in a single integrated package. To accomplish the multi-function mission, the system must rapidly distribute transmit energy over large areas. Search, track and guidance dwells must be interleaved on a millisecond basis while maintaining precise control over the direction and composition of the transmit waveform. These requirements generally dictate the utilization of phased-array technology. By employing a phased-array, the proposed system will be able to track multiple targets simultaneously while controlling missiles and performing search functions.

Advanced phased-arrays are usually composed of thousands of independently controlled radiating elements. Traditionally, corporate feed structures utilizing individual phase shifters for each element have been employed. Due to the complexity of the feed structure, beam steering logic, and associated electronics, it is no surprise that the antenna is one of the major cost drivers in phased array systems.

Phased Array Alternatives

Most new systems include increased reliance on multi-function elements that utilize phase array technologies in their implementation. Since the cost of simulating such systems is highly dependent on the antenna structure, our investigation will focus on alternative means of imitating the scan pattern displayed by a phased-array.

The major trade-offs in performance encountered with alternative arrays include higher RMS sidelobe levels, reduced field of view, and reduced antenna gain. The resultant antenna is still capable of scanning the volume covered by the organic asset in the same amount of time with the same spot size but with reduced main beam power, decreased capability for multiple target tracking, and increased sidelobe levels. The net result is that stringent requirements may be placed on the transmitter and phase shifter elements

because of increased power requirements arising from a reduced element count. Statistically thinning the elements from the array requires a more complex feed system.

A small aperture array will also require high transmitter and phase shifter element power due to a reduced element count. However, the feed network can be simplified, as compared to that of the thinned array, due to element symmetry and the absence of terminated elements. Element symmetry also reduces sidelobe levels as compared to a thinned array. Increased beamwidth due to the physically smaller antenna aperture is the major sacrifice in antenna performance.

The high-gain element array maintains the gain of the full aperture with fewer elements. Therefore, full array ERP can be supported with the same transmitter and phase shifters while maintaining a narrow beamwidth. RMS sidelobes are low but grating lobes become prominent due to the relative element spacing. This approach provides the greatest cost savings of the four alternatives but has the disadvantage of a limited field-of-view.

A combination of high-gain elements in a statistically thinned array is another technique which could be used to simulate phased-array antennas at a reduced cost. This approach also demonstrates an increase in grating lobe levels due to increased element spacings as well as increased sidelobe levels resulting from the thinned array. The antenna would require increased transmitter and phase shifter power handling capability. Cost is increased due to the difficulty in implementing a space feed.

Micro-strip Patched Arrays

Mechanical designs reduce phased-array simulator costs by substituting electronically complex apertures with rudimentary mechanical components. Element reduction techniques attempt an equivalent goal by decreasing the number of active radiators. A third possible approach involves the utilization of low cost, highly reliable, electronic components. Phased-array price reduction through low cost component development is an area that is receiving increasing levels of attention due to the extensive utilization of

large conformal and planar arrays in both the government and private sectors. The primary technology for investigation in these endeavors is silicon based integrated circuit techniques. The advantage of constructing the elements in this manner is that the manufacturing process is reliable, repeatable, precise and cost effective for relatively large quantities.

Figure 5 illustrates a single element of a micro-strip patched array. A PTFE (Teflon), non-woven, glass laminate material is constructed with the appropriate relative permitivity. Alternatives involving a silicon substrate with phosphorus or boron implantation are possible. Aluminum metalization on one side of the wafer forms the ground plane while the elements are typically constructed from DUROID 5870 material with a dielectric constant of 2.2. The resonant frequency of an element constructed in this manner is given by

$$(f_r)_{mn} = \frac{1}{(2\Pi\sqrt{\mu_o \epsilon})\left(\left(\frac{m\Pi}{l}\right)^2 + \left(\frac{n\Pi}{w}\right)^2\right)^{1/2}}$$

where "l" and "w" are the patch dimensions and "m" and "n" are the mode numbers. The lowest resonant frequency occurs at m=1 and n=0 when l>w. For example, one inch elements display a peak radiation response of approximately 2.9 GHz. Single elements bandwidths are generally limited by substrate thickness to less than 10 percent of the resonant frequency. Therefore, high-Q (narrow bandwidth) limitations have traditionally restricted the utilization of micro-strip patched arrays to narrow band transmissions.

Recent endeavors by the Strategic Defense Initiative Office (SDIO) have revived interest in micro-strip patched array applications for radar and communications systems developments. The primary stumbling block has been bandwidth limitations. While it is possible to support the instantaneous bandwidth of most radar and communications systems (other than chirp) with micro-strip patched arrays, it is not possible to support

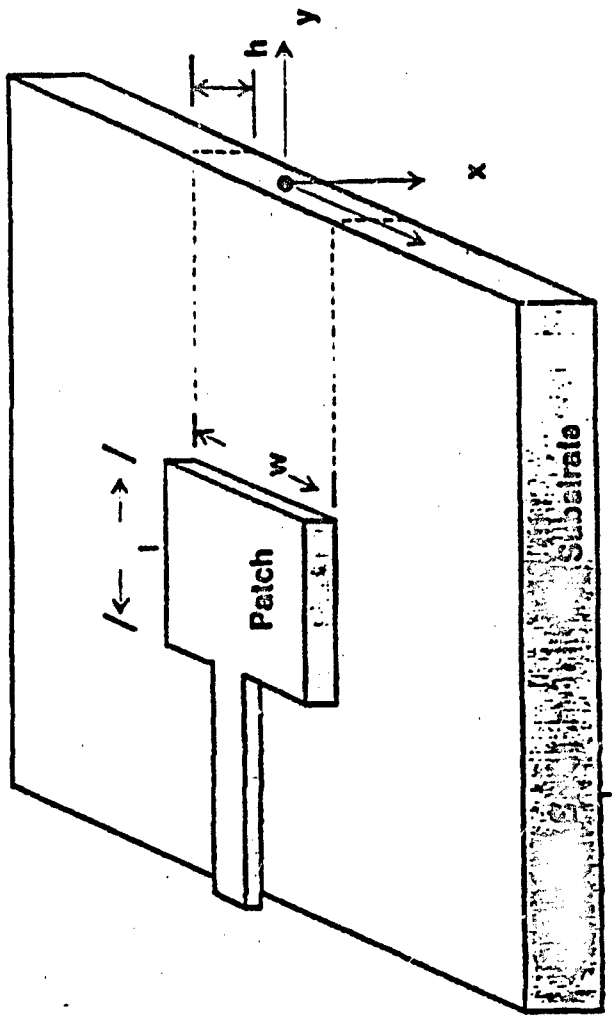

FIGURE 6. SINGLE-LAYER MICROSTRIP PATCH ELEMENT

typical dynamic (tunable) bandwidths without appreciable losses using single-layer designs.

Preliminary developments based on multi-layer concepts are reported to satisfy the wide bandwidth requirement. The underpendings of this approach are based on concepts borrowed from RF radio developments. In particular, it is possible to construct a wide bandwidth receiver by employing multiple high-Q amplifying stages. The receiver bandwidth can be narrowed by adjusting the amplifiers to the same resonance, or it can be widened by slightly detuning the individual stages. A graphical representation of the wide bandwidth concept is illustrated in Figure 6 for a two-stage amplifier design. The concept is implemented in micro-strip antennas by employing multiple layers. Each layer is analogous to a single amplifying stage. Detuning between stages is accomplished by designing layers with different resonance. Therefore, by increasing the size of the lower conductive layer relative to the upper layer, wide bandwidth operation is achieved. Single element, multi-layer prototypes have been developed which have displayed bandwidths on the order of 23% at 3:1 VSWRs.

Applications of wide bandwidth micro-strip patched arrays in the proposed modular design are numerous. The bandwidth of the antenna lends feasibility to the concept of multi-simulation applications. Reduced antenna weight decreases the payload requirements for the host platform, and the possibility of constructing conformal configurations enables the development of low profile structures.

Scope of Task I Research

Assessments and experimental sub-tasks will be completed for a hierarchy of flexible modules capable of satisfying a multiplicity of developmental and testing requirements. These include:

1. Assessment of critical functions to assist in defining and solving parameter optimization problems.

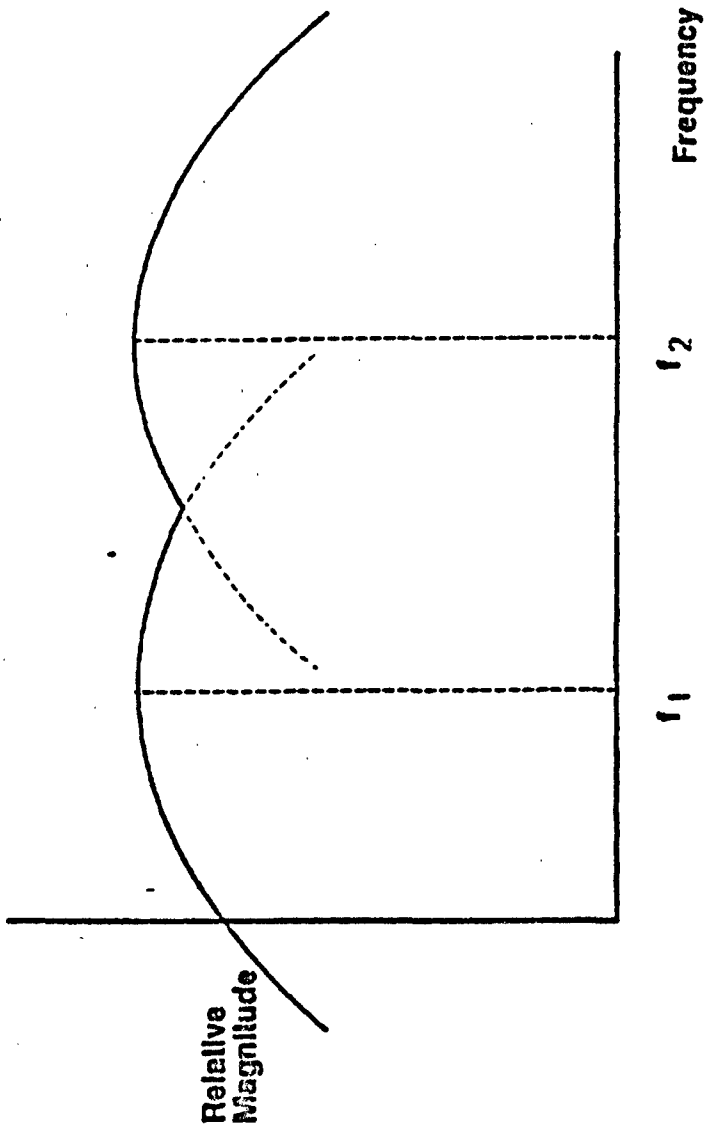

FIGURE 6. WIDE BANDWIDTH RESPONSE

2. Definition of architectures, objectives, and sub-elements, including operational interactions.
3. Scientific investigation and development of emerging technology modules for utilization in the development of an experimental system based on a combination of intelligence and signal sources.
4. Analysis and trade-off in support of programmatic decisions.
5. Definition of plans and functional specifications for a prototype system.

As test assets continue to evolve to meet future requirements, the design principles proposed will become more attractive. Implementation of the proposed modular design concept is therefore a very effective way to prepare for the future. The ability to capture a waveform, store it, modify it according to new requirements, and feed it into a waveform generator could provide the most cost effective means of implementing new requirements. This process will provide a mechanism for the expedient upgrade of test assets to parallel strategic and tactical weapon system developments. The flow chart depicting these activities is shown in Figure 7.

1.1.2 TASK II: ANALYTICAL AND EXPERIMENTAL STUDIES

Proposed technologies to be integrated into effective test assets must be adaptive, multi-spectral, flexible and accurate to support laboratory as well as free-space testing of weapon systems. Testing scenarios require replication of environments consisting of a combination of complex signal sources and information flows between various sensors, weapon control systems and missile systems. This task therefore will support the concepts and experimentations defined in Tasks I and II. Subsystem and component technology studies will include vulnerability assessments, emerging technology studies for miniaturized low-cost systems, and signal processing investigations.

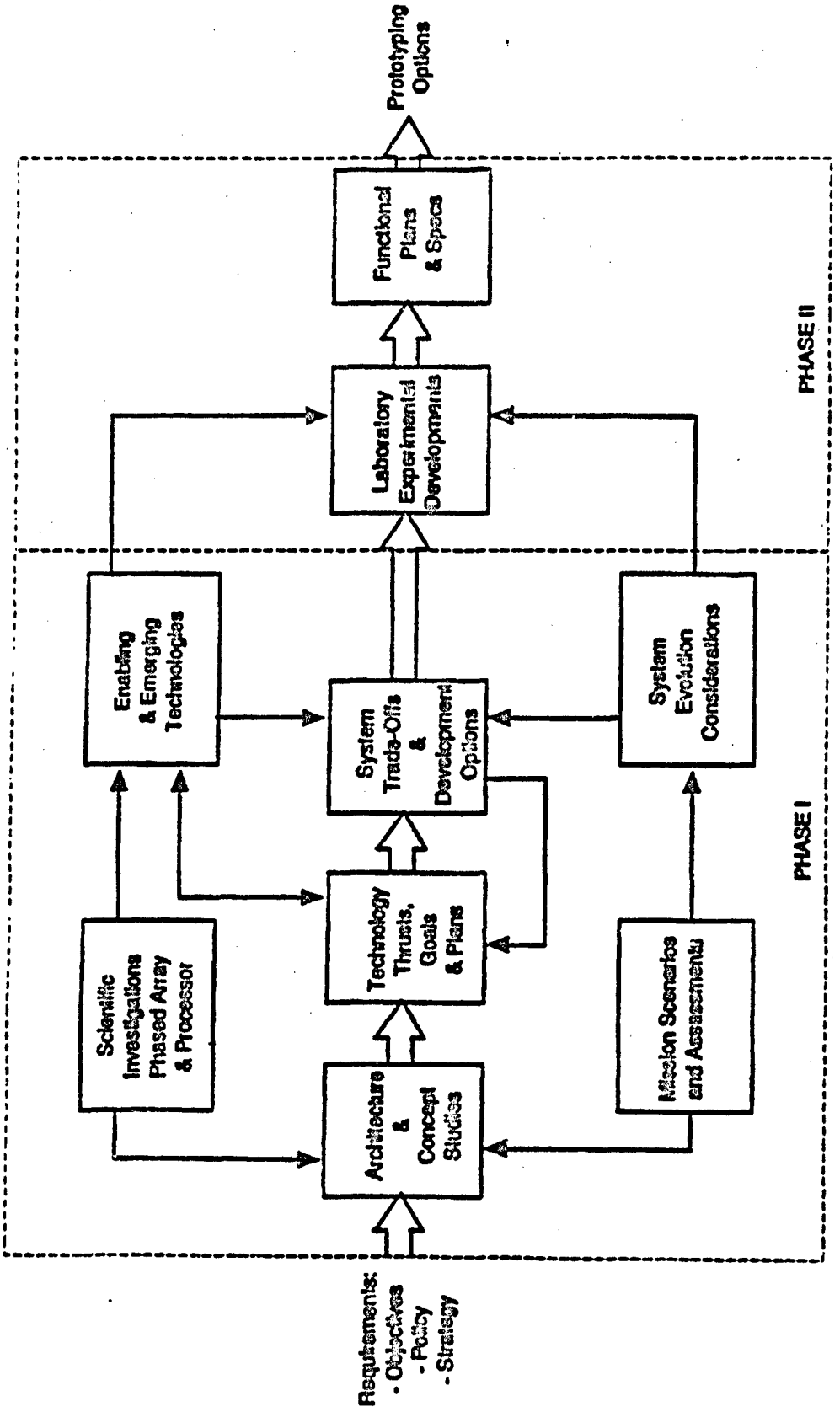

FIGURE 7. SYSTEM DEVELOPMENT FLOW DIAGRAM

Vulnerability Assessments

This sub-task consists of the development of characteristics and parameters of a dynamically evolving threat environment, including platform, weapon and missile systems. Multiple intelligence sources will be utilized to provide comprehensive support for subsequent development of a high-fidelity, flexible, transportable experimental test asset system. Specific activities will include the following:

1. Definition of the requirements and missions for a representative deployment environment.
2. Selection and specification of conflict scenarios in sufficient detail to allow identification of systems involved in engagements, including terminal homing.
3. Establishment of a data structure that permits parameters and characteristics of threat systems to be identified in sufficient detail for trade-off analysis and subsequent identification of critical component developments, as well as the integration of adaptive hardware and software with simulation developments.

Adaptive Clutter Rejection Filtering Investigations

Low altitude ground clutter, particularly in urban or semi-urban environments, can be quite specular in character. Fixed bandwidth clutter rejection filters (e.g. MTI) may be inadequate, where it is difficult to discriminate between target returns and clutter returns on the basis of spectral properties. An adaptive least squares algorithm may be configured to operate on complex-valued data sequences to determine an inverse, autoregressive, model-based impulse response filter for clutter rejection. This algorithm is stable and can be implemented with fixed point arithmetic. Additional work is needed to determine an appropriate vectorization to provide for efficient real-time implementations.

In situations where the signal-to-clutter ratios are small or where the clutter spectrum may be broadened by radar system phase instabilities, clutter rejection may not be desirable. Previous work concerning pulse doppler radar used to detect weak distributed targets has

shown that clutter rejection filtering may reduce the signal sensitivity to the point where detection is unreliable. Modelling techniques which preserve the second order properties of the radar return signal are being investigated as a means of target detection and tracking in the presence of strong ground clutter. A modified PRONY algorithm based upon an autoregressive model of the radar return spectrum is being used to identify distributed targets without the benefits of clutter rejection filtering.

Signal Processing in Non-Homogeneous Clutter Environments

In this sub-task we propose to investigate the application of intelligent systems to constant false alarm rate (CFAR) detection in the presence of non-homogeneous clutter. The presence of non-homogeneous clutter and the presence of interfering targets associated with a multiple target environment can seriously degrade the performance of conventional CFAR radar detection including GO-CFAR and SO-CFAR processors. Non-homogeneous clutter can be an appropriate characterization of an ECM environment. Earlier work has indicated that what is needed even in a single target environment is a multi-algorithm processor with associated integration of the processor outputs so that performance robustness is achieved over a wide class of potential clutter environments. Our proposed approach is to use intelligent system technology as a means of integrating various processors. Algorithm outputs can be combined based upon rules defined through analysis of non-homogeneous clutter environments.

1.2 SUMMARY OF PROPOSED RESEARCH CONTRIBUTION TO EXPERIMENTAL AND TESTING PROGRAMS

The research activities proposed can assist in providing an order of magnitude cost savings in processing and simulation/simulator developments. Timely insertion of advanced technologies will be stimulated by new and innovative ideas and collaborative partnerships. In addition to having successfully completed projects on several related research programs, the university and industry research team proposed can effectively transition from conceptual research activities to major industrial prototyping utilizing existing facilities and product experience. Personnel in each phase can therefore provide

a wide range of scientific and highly specialized disciplines with access to facilities and clearances that will permit performance at the highest special activity levels. These characteristics have historically permitted investigative studies and developmental options on programs similar to those proposed in an accurate and timely manner. Elements of the proposed research may necessitate integration of diverse all-source information as well as complex technologies. Effective integration of these activities will be accomplished in an even-handed manner with the academic and industrial capabilities described in previous sections of this proposal.

Specifications and components will be developed for a modular programmable test asset system to assist the SDIO Innovative Science and Technology Directorate and the U.S. Army Strategic Defense Command and their customers as they deal with a dynamically evolving threat environment. The spin-off of advanced processing and associated technologies will accurately assist in the replication of various threat signatures as well as provide for experimentations and modeling of blue systems. Each element of our proposed research will be complementary in solving a multiplicity of direct and related innovative science and technology program objectives. For example, there are numerous defense-related computational problems that can not be met by traditional algorithmic computing techniques. Emerging technologies offers the possibility of real-time performance for a large class of computing problems facing the Strategic Defense mission. By forming partnerships on the leading edge of computing, simulation developments and instrumentation technologies, we provide a team for rapidly assessing the potential for research as well as developing innovative solutions for a dynamically evolving threat environment.

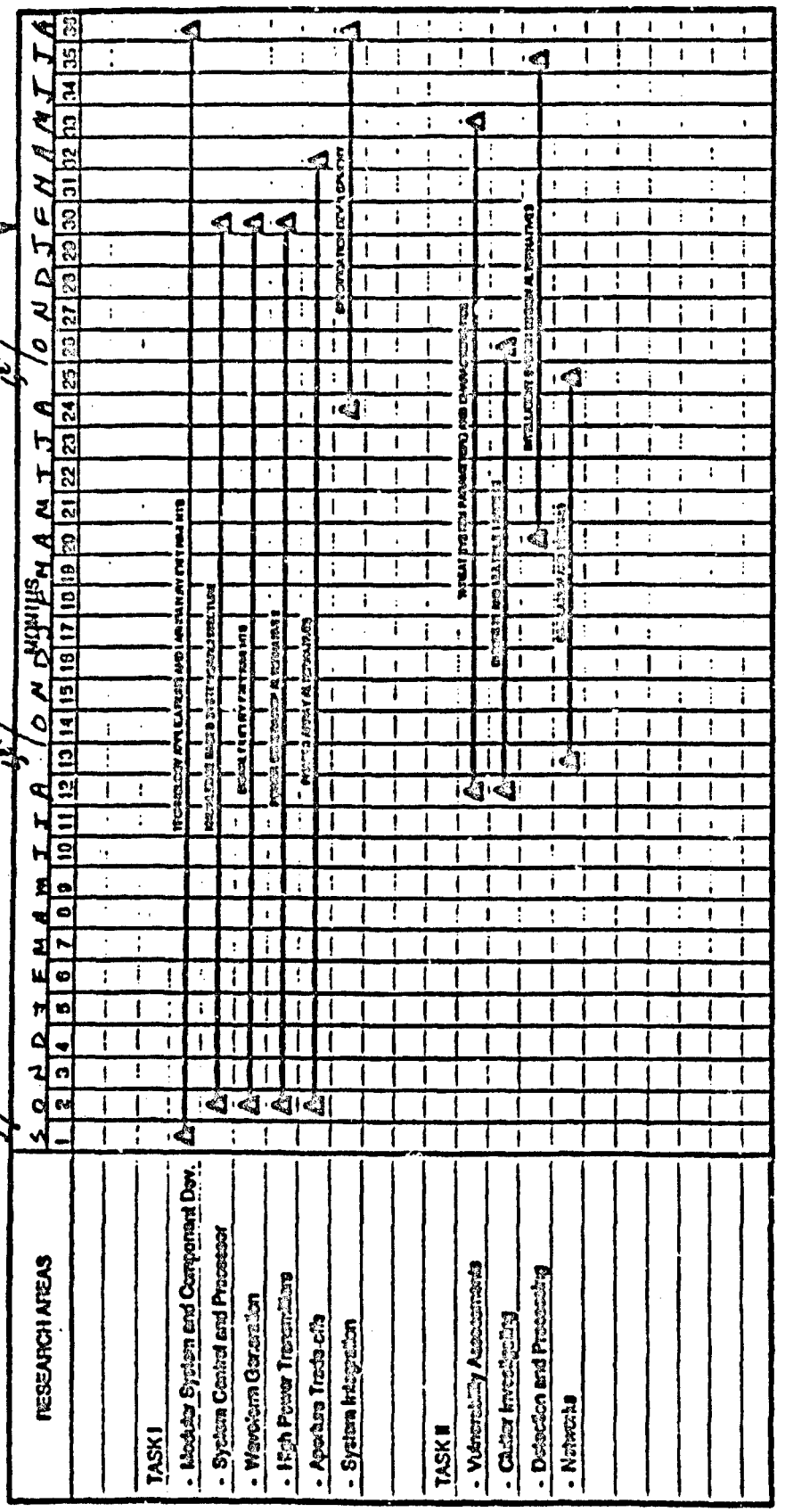

FIGURE 8. SCHEDULE OF EVENTS

B-1: HF Phase Reference Exciter Design

A schematic diagram of an HF phase reference source exciter is shown in **Figure B-1.** The schematic does not show all parameter values such as gain, attenuation, etc. Instead, its intent is to show the minimal required components to provide the subsystem function. Exact parameter values are based on the element characteristics, interrelationships and requirements. The design concept should be clear enough however to enable the identification of those parameters and subsystem element requirements.

This exciter schematic incorporates the van / trailer division to accommodate reconfigurability. It also provides for a spare phase lock signal at the trailer and a stable clock source for the timing and control (T&C) subsystem. There is no requirement for the transmitted signal phase reference and the T&C reference clock to be phase locked however. It should be noted that the stable master oscillator (Stamo) provides the phase lock signal to the COHO, STALO-2 and STALO-1 phase locked oscillator sources. The waveform generation signal is an input to the exciter. That signal is used to modulate the COHO signal for both regular and chirped transmissions. The mixers are protected either by necessary attenuators or isolators to prevent reflections back into the device and subsequent non-desired mixing products.

The saw expansion system inputs include a system select and pulse gate. The system select is used in the event multiple time-bandwidth products are required for a single system or multiple systems. The pulse gate gates the output of the SAW expansion system to the desired output pulse width. The pulse gate may or may not be supplied by the SAW expansion system. If the pulse gate is supplied by the expansion system, the expansion system will require the waveform generator input for timing purposes. In either case, the pulse gate or waveform generator will be a timing and control (T&C) supplied signal. The SAW expansion system is shown with a coaxial path around the device via coaxial switches for operation in or out of the chirped mode.

In the event that the radar characteristics are changed, only the circuitry associated with STALO-1 in the trailer and the output to the transmitter will require possible hardware replacement. It is possible to use a microwave frequency synthesizer for STALO-1 and a tunable

YIG filter on the exciter output. Circulators and amplifiers can be selected to cover over an octave of bandwidth. The phase noise of the exciter output may not be optimal however. In tactical low PRF emulations, this may not be a problem.

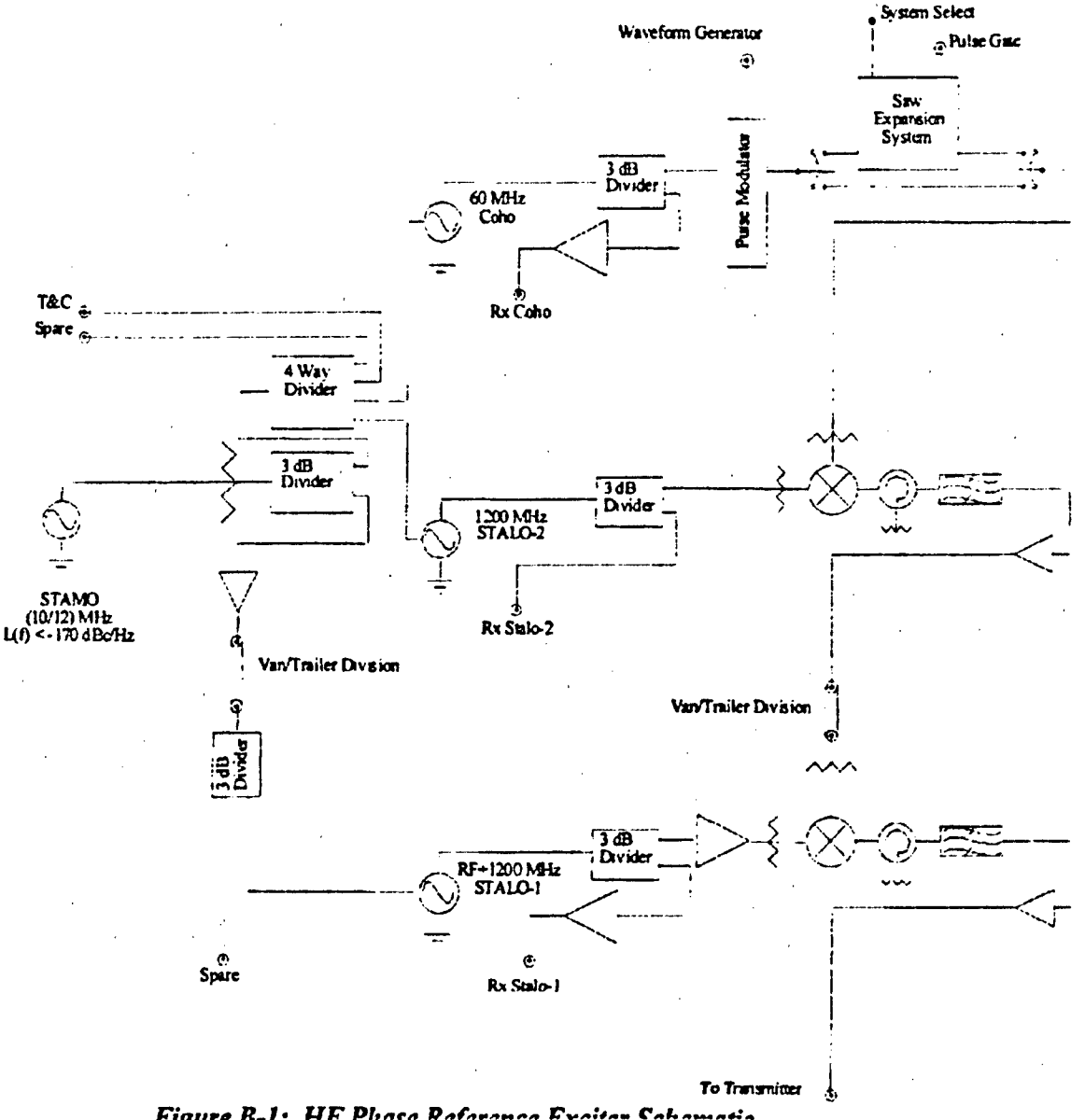

Figure B-1: HF Phase Reference Exciter Schematic

B-2 UHF/L-Band Phase Reference Exciter Design

The schematic diagram of the UHF/L-Band Phase reference exciter is shown in **Figure B-2.** This schematic includes the required power dividers, anticipated mixer protection techniques and the proposed van/trailer division. Many of the same schematic features apply here as they did in the HF phase lock source implementation. In this implementation, only one path between the van and trailer is required.

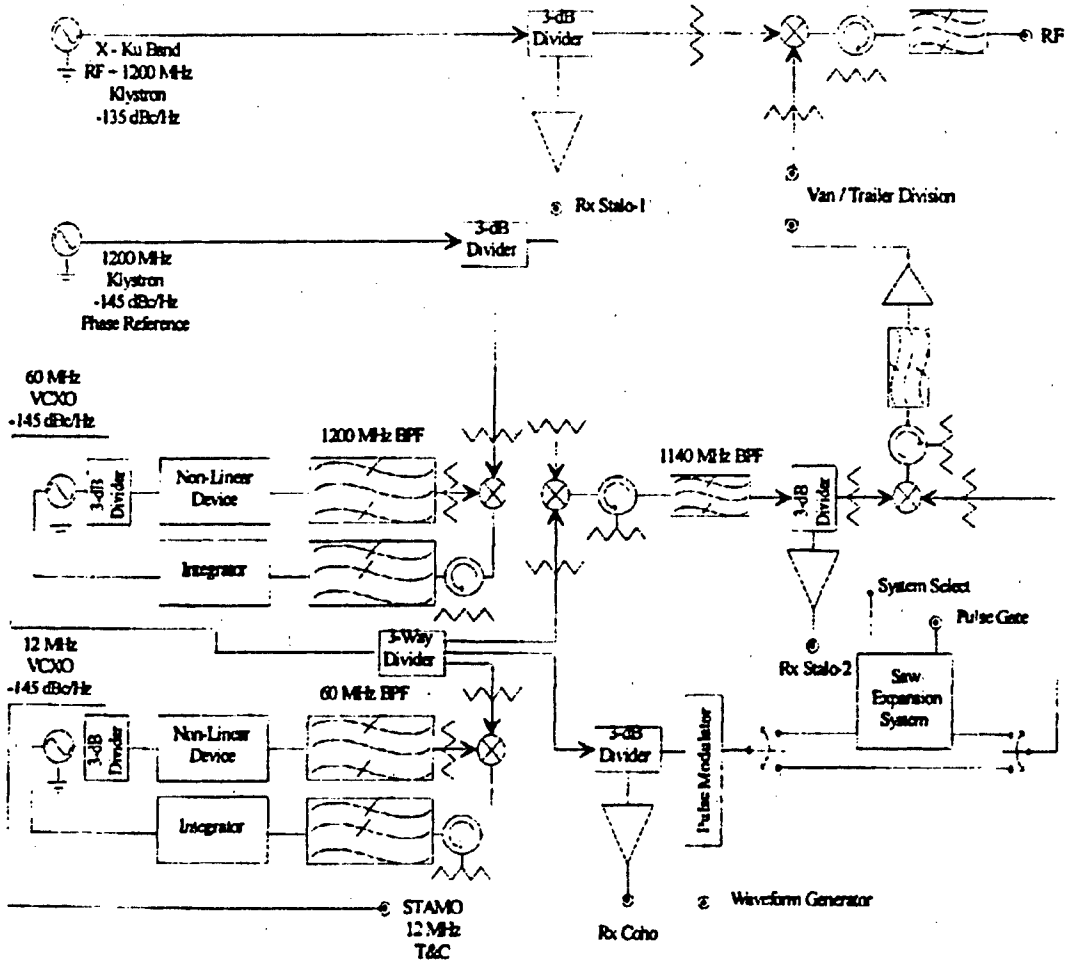

Figure B-2: UHF/L-Band Phase Reference Exciter Schematic

The discussion of the phase locked loops may begin with the VCOs. The VCO phase noise requirement is such that their noise is no higher than the 1.2 GHz klystron's. The non-linear device provides harmonics of the VCO signal. The appropriate harmonic is selected with the bandpass filter. Appropriate implies the VCO harmonic is equivalent in frequency with its phase lock source. The phases of the VCO harmonic and phase lock source will be driven into the normal phase quadrature condition required by the PLLs. The PLL mixer ports are protected by isolation devices. System sensitivity is preserved by the preclusion of added intermodulation products as a result of reflections The PLL mixer output is low pass filtered. There is no reason that the filter 3 dB bandwidth should be higher than 10 Hz. The circuits will be in sinusoidal steady state after initial power-up and will remain there during operation. Any phase noise degradation by the non-linear device will be substantially reduced by the low pass filter and the following integrator. The integrator phase noise improvement will of course be proportional to the radian frequency of the phase noise. The resultant control signal provided to the VCO should be a spectrally pure DC signal of theoretically zero amplitude. The VCO quiescent frequency will be that of the desired frequency output.

RADAR CALCULATIONS
TABLE OF CONTENTS

Representative Low PRF Case

Receiver and Signal Processor Subsystem Performance Analysis

Specified Radar Parameters

$c = 3 \cdot 10^8$ m./sec. (velocity of light)

$f = 14 \cdot 10^9$ Hz (transmitted frequency)

$\lambda := \frac{c}{f}$ m. (transmitted center frequency wavelength) $\lambda = 0.0214$ m.

$PRF = 4000$ Hz (transmitted pulse repition frequency)

$R_{max} = \frac{c}{PRF \cdot 2}$ m. (maximum unambiguous range) $R_{max} = 3.75 \cdot 10^4$ m.

$\sigma_{min} = .1$ sq. m. (minimum specified target cross-section area)

$P_t = 50000$ W. (transmitter output power)

$\tau_{pulse} = 9 \cdot 10^{-6}$ sec. (Expanded transmitted pulsewidth in seconds)

$B_{chirp} = 2.5 \cdot 10^6$ Hz (Pulse Compression Chirp Bandwidth)

$N = 32$ (Number of FFT Integrations = Number of frequency bins in a PRF)

$DopBinBW = \frac{PRF}{N}$ (Resultant Doppler Bin Bandwidth) $DopBinBW = 125$ Hz

$MinSIR = 0$ dB (Required SIR for Pd and Pfa for Swerling I target)

$SubClutVis = 75$ dB (Specified subclutter visiblity)

$ClutFiltRej = 0$ dB (Specified clutter filter rejection)

$k = 1.38 \cdot 10^{-23}$ watts/(deg.K * Hz) (Boltzman's constant)

$F = 2.512$ (Receiver Noise Figure = 4 dB)

$MaxSNR_{AD} = 75$ dB (Measured A/D signal-to-noise ratio)

Derivation of Compressed Pulsewidth

The envelope of the received compressed pulse and the envelope of the transmitted expanded pulse are related by a fourier transform. Assuming that the expanded transmit pulse is rectangular in shape and having a duration of nine microseconds, the envelope and thus the pulsewidth of the compressed pulse can be determined. The time sidelobes will be reduced to 35 dB below that of the main lobe by Taylor (Tschebycheff error) weighting of the FFT samples. The losses associated with the main lobe broadening will also be calculated.

Assumptions:

SLL := 35 dB (Forced time sidelobe level maximum value.)

nbar := 5 (Number of sidelobes to be held at the maximum sidelobe level.)

Calculations:

nhits := 99 (Arbitrary odd number of time samples incident upon the expanded pulse envelope.)

Nsamp := 4096 (Total number of fft time samples.)

$fsamp := \frac{nhits}{\tau_{pulse}}$ $fsamp = 1.1 \cdot 10^7$ Hz (Sampling frequency)

i := 0.. nhits - 1 kk := nhits.. Nsamp - 1 (Time indicies, i - time index on expanded pulse envelope, kk - time index after expanded pulse envelope.)

$j := 0.. \frac{Nsamp}{2} - 1$ (FFT frequency index)

$t_i := \frac{\tau_{pulse}}{nhits} \cdot i$ sec. $t_{kk} := \frac{\tau_{pulse}}{nhits} \cdot kk$ sec.

$b_i := 1$ $b_{kk} := 0$ (FFT sample values.)

$B := fft(b)$ $B_j := |B_j| + 10^{-10}$ (Calculate the magnitude of the fft of the expanded pulse envelope and prevent a zero quantity.)

$Max := B_0$ $B_j := \frac{B_j}{Max}$ $B_j := 20 \cdot \log(B_j)$ (Normalize and calculate the logrithmic magnitude.)

$f_j := \frac{fsamp}{Nsamp} \cdot j$ Hz (Calculate the center frequency of each of the FFT frequency bins.)

$t_j := \frac{\tau_{pulse}}{B_{chirp}} \cdot f_j$ sec. (Calculate the equivalent time for each fft bin center frequency.)

Compute the Taylor Window for the Pulse Compression

$R := 10^{\frac{SLL}{20}}$ $A := \frac{acosh(R)}{\pi}$ (Calculate constant related to desired sidelobe level.)

$\sigma := \frac{nbar}{\sqrt{A^2 + \left(nbar - \frac{1}{2}\right)^2}}$ (Scaling factor)

$m := 1 .. nbar - 1$ $n := 0 .. nbar - 1$ $n1 := 1 .. nbar - 1$ (Indices for calculation of Taylor coefficients)

$$FF_n := \frac{((nbar-1)!)^2 \cdot \prod_m \left[1 - \frac{n^2}{\sigma^2 \cdot \left[A^2 + \left(m - \frac{1}{2}\right)^2\right]}\right]}{(nbar-1+n)! \cdot (nbar-1-n)!}$$

$x := 0 .. \frac{nhits - 1}{2}$ (Taylor coefficient index)

$L := nhits - 1$ (Total length of the number of time samples)

$$Taylor_x := \frac{1}{2 \cdot \pi} \cdot \left[FF_0 + 2 \cdot \sum_{n1} FF_{n1} \cdot \cos\left[\frac{n1 \cdot \pi \cdot x}{\left(\frac{L}{2}\right)}\right]\right]$$ (Calculate the Taylor coefficients)

$\eta := \frac{1}{FF_0 + 2 \cdot \sum_{n1} (FF_{n1})^2}$ $\eta = 0.81$ $20 \cdot \log(\eta) = -1.85$ dB (Efficiency of the Taylor weighting)

$L_{taylor} := \left(\frac{1}{\eta}\right)^2$ (Loss coefficient for range equation) $L_{taylor} = 1.532$

$W_x := Taylor_{\left(\frac{nhits-1}{2}\right) - x}$ $W_{\left(\frac{nhits-1}{2}\right) + x} := Taylor_x$ (Assign the appropriate Taylor coefficient to each time sample.)

$wb_i := W_i \cdot b_i$ $wb_{kk} = 0$ (Weight the expanded pulse samples with the Taylor coefficients.)

$WB = fft(wb)$ $WB_j := |WB_j| + 10^{-10}$ (Calculate the magnitude of the fft of the weighted expanded pulse and prevent a zero quantity.)

$Max := WB_0$ $WB_j := \frac{WB_j}{Max} \cdot \eta$ $WB_j := 20 \log(WB_j)$ (Normalize, apply the efficiency calculated and calculate the logrithmic magnitude.)

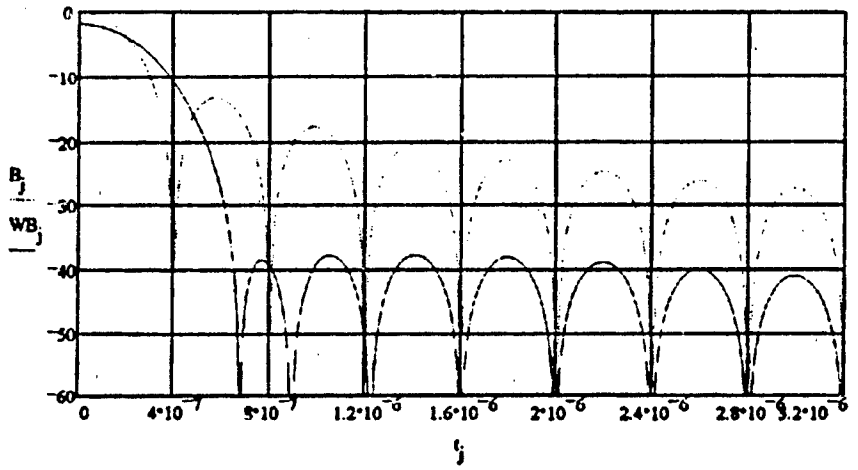

The above plot shows the effects of the pulse compression both with and without the Taylor weighting. The weighted compressed pulse is plotted with the efficiency applied. The classic definition of the compressed unweighted pulsewidth is 1/chirp bandwidth. In this case it would be 0.4 microseconds. As shown above, the actual main lobe null to null pulsewidth is twice that or 0.8 microseconds. The 0.4 microsecond pulsewidth actually yields the -4dB pulsewidth which is similiar to the classic definition of the bandwidth of a rectangular pulse. Therefore, the pulsewidth of the weighted pulse will be measured from the -4dB points.

$$WB_j = \frac{10^{\frac{WB_j}{20}}}{\eta} \qquad WB_j := 20 \cdot \log(WB_j)$$ (Convert the weighted fft back to linear, remove the efficiency and convert back to logrithmic.)

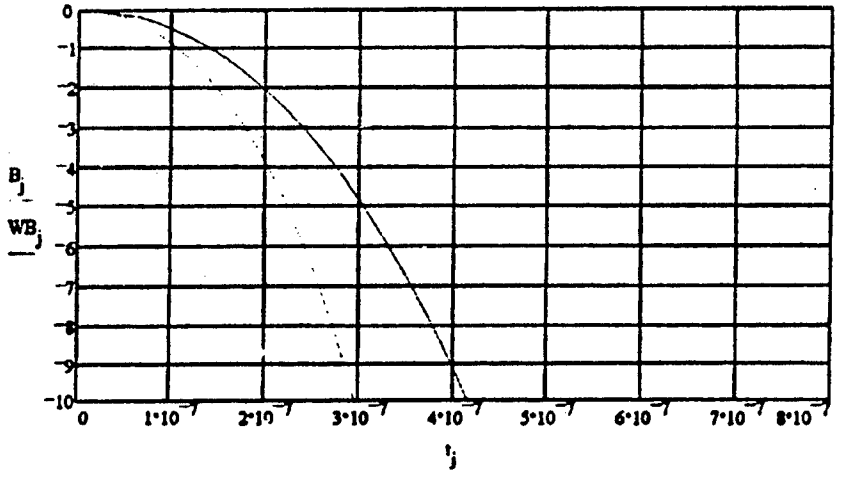

Inspecting the above plot of the normalized unweighted and weighted main lobes shows that the weighted main lobe -4dB pulsewidth is approximately 0.55 microseconds.

$\tau_{comp} = 0.55 \cdot 10^{-6}$ sec. (Compressed and weighted pulsewidth)

$B_{comp} = \frac{1}{\tau_{comp}}$ $B_{comp} = 1.82 \cdot 10^{6}$ Hz (Compressed and weighted pulse bandwidth)

Derivation of Receiver Gain

The receiver should be designed to amplify the signal as much as possible without increasing the noise floor of the system. This accomplished increasing the gain of the receiver until the noise in the receiver is equal to the noise floor introduced by the A/D converter. Therefore, to calculate the receiver gain, the noise power introduced into the system by the A/D converter must first be calculated.

Assumptions:

$V_{pp} := 2.0$ v. (Maximum peak-to-peak voltage level for converter)

$R_{load} := 50$ ohms (A/D Converter Input Impedance)

$T := 290$ deg. Kelvin (ambient temperature)

$T_A := 100$ deg. Kelvin (antenna noise temperature)

$L_A := 1.413$ (losses between the antenna and receiver = 1.5 dB)

$L_{mm} := 1.413$ (Mismatched receiver S/N ratio loss = 1.5 dB)

Calculations:

$$V_{rms} := \frac{V_{pp}}{2 \cdot \sqrt{2}} \quad V_{rms} = 0.71 \quad \text{v. (Maximum A/D RMS voltage)}$$

$$Pmax_{AD} := \frac{V_{rms}^2}{R_{load}} \quad Pmax_{AD} = 0.01 \quad \text{W. (Maximum A/D average power = 10 dBm)}$$

$$Pfloor_{AD} := 10 \cdot \log\left(\frac{Pmax_{AD}}{10^{-3}}\right) - MaxSNR_{AD} \quad Pfloor_{AD} = -65 \quad \text{dBm (A/D noise floor)}$$

$$Pfloor_{AD} := 10^{-3} \cdot 10^{\frac{Pfloor_{AD}}{10}} \quad \text{W (Convert from dBm units to Watts)}$$

It is assumed that the noise power in the receiver measured within the bandwidth of the compressed pulse is attenuated by a factor of the compression ratio through the SAW line filter sub-system. Therefore, the noise power incident on the A/D converter is given by:

$$G_o := \frac{Pfloor_{AD} \cdot L_A \cdot (\tau_{pulse} \cdot B_{comp})}{k \cdot \left[T \cdot (L_A \cdot F - 1) + T_A\right] \cdot B_{comp} \cdot (L_{taylor} \cdot L_{mm})}$$

(Receiver Gain to match Receiver Noise Floor to A/D Noise Floor given antenna noise temp., loss between receiver and antenna, SAW filter losses and the receiver noise figure.)

$10 \cdot \log(G_o) = 52.05$ dB

Derivation of Receiver Pre-AGC Dynamic Range

Having calculated the receiver gain, the maximum input to the receiver can now be calculated by removing the calculated gain of the receiver from the maximum input power to the A/D converter.

Assumptions:

None

Calculations:

$$Pmax_{AD} = 10\log\left(\frac{Pmax_{AD}}{.001}\right) \quad dBm$$

$$Pmax_{RX} = Pmax_{AD} - 10\log(G_o) \qquad Pmax_{RX} = -42.05 \quad dBm$$

The minimum signal input to the receiver such that the signal at the A/D converter input is equal to the noise floor may be calculated by removing the maximum SNR of the A/D from the maximum input power to the receiver.

$$Pfloor_{RX} = Pmax_{RX} - MaxSNR_{AD} \qquad Pfloor_{RX} = -117.05 \quad dBm$$

Derivation of the Clutterless Receiver Automatic Gain Control Requirements

The receiver automatic gain control (AGC) will serve to prevent the receiver from being saturated by excessive clutter returns or close range targets. The AGC will also provide for constant angle tracking sensitivity (volts per degree error) over large signal dynamic range variations and target range.

The AGC will be applied to the middle stages of the amplifier chain to preserve the receiver noise figure and the maximum undistorted output of the final stage. The AGC control signal will be derived from the filtered pulse compression matched filter output. The AGC will control the acquisition and track sum channel as well as the difference azimuth and elevation track channel gains.

To determine the requirements of the AGC, some estimate of the level of incoming signals must be made. Therefore, a discussion of target signal dynamic range is included. Assuming full receiver gain, a comparison of the receiver input that will saturate the A/D converter to the expected target signal dynamics will provide the minimum requirements of the AGC.

Assumptions:

$\tau_{recovery} := 10^{-6}$ sec. (Duplexer recovery time)

$\sigma_{max} := 100$ m^2 (Maximum expected target RCS)

$G_A := 20000$ (Calculated Antenna Gain = 43 dBi)

$L_{xmtr} := 1.318$ (Loss between the transmitter and the antenna = 1.2 dB)

$L_{2way} := 1.413$ (Round trip loss between antenna and target = 1.5 dB)

Calculations:

Target Dynamic Range

The minimum target detection range is determined by the duplexer recovery time and the transmitted pulsewidth.

$$R_{min} := c \cdot \frac{\tau_{pulse} - \tau_{recovery}}{2} \qquad R_{min} = 1.5 \cdot 10^{3} \text{ m. (Minimum detection range of the radar)}$$

The cross section of a target at the minimum through the maximum ranges can now be calculated which corresponds to the maximum and minimum unattenuated signal voltage the A/D can handle.

$tr := 1,2..\frac{R_{max}}{100}$ (target range index)

$R_{tr} := 100 \cdot tr$ m. (target range)

$Pmax\_RX_{tr} := Pmax_{RX}$ (maximum unattenuated receiver input for A/D saturation)

$Pfloor\_RX_{tr} := Pfloor_{RX}$ (minimum unattenuated receiver input to match A/D noise floor)

$$Pmin\sigma_{RX_{tr}} := \frac{P_t \cdot G_A^2 \cdot \sigma_{min} \cdot \lambda^2}{(4\cdot\pi)^3 \cdot (R_{tr})^4 \cdot L_{xmtr} \cdot L_{2way} \cdot L_A} \text{ W.}$$

(Power received from smallest specified target (.1 sq. m.) versus required tracking range.)

$$Pmin\sigma_{RX_{tr}} := if\left(R_{tr} > R_{min}, 10\log\left(\frac{Pmin\sigma_{RX_{tr}}}{.001}\right), -200\right) \text{ dBm}$$

(Convert to dBm units)

$$Pmax\sigma_{RX_{tr}} := \frac{P_t \cdot G_A^2 \cdot \sigma_{max\_} \cdot \lambda^2}{(4\cdot\pi)^3 \cdot (R_{tr})^4 \cdot L_{xmtr} \cdot L_{2way} \cdot L_A} \text{ W.}$$

(Power received from largest expected target (100 sq. m.) versus required tracking range.)

$$Pmax\sigma_{RX_{tr}} := if\left(R_{tr} > R_{min}, 10\log\left(\frac{Pmax\sigma_{RX_{tr}}}{.001}\right), 200\right) \text{ dBm}$$

(Convert to dBm units)

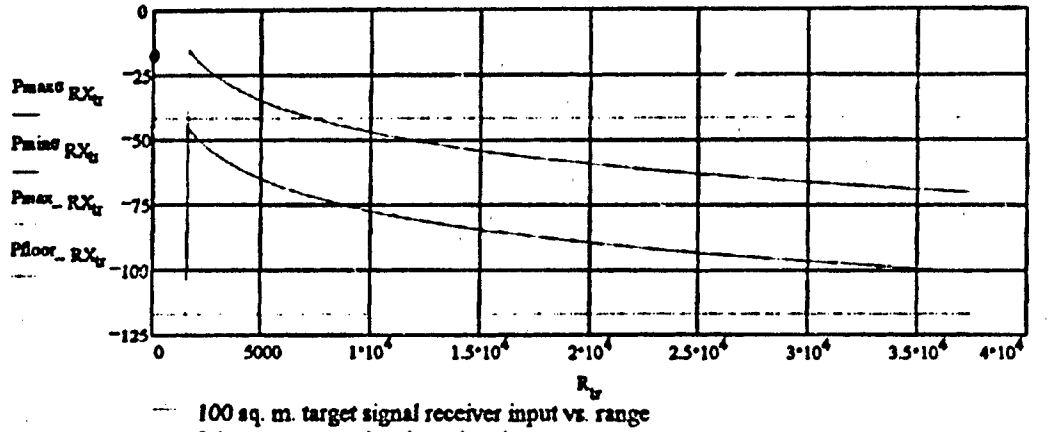

— 100 sq. m. target signal receiver input vs. range
— 0.1 sq. m. target signal receiver input vs. range
--- maximum receiver input to match A/D saturation level
--- minimum receiver input to match noise floor

Clutterless AGC Minimum Requirements

$$Pbig = \frac{P_t \cdot G_A^2 \cdot \sigma_{max\_} \cdot \lambda^2}{(4\cdot\pi)^3 \cdot (R_{min})^4 \cdot L_{xmtr} \cdot L_{2way} \cdot L_A} \text{ W.}$$ (Power received from largest expected target (100 sq. m.) at minimum range.)

$Pbig = 10 \cdot \log\left(\frac{Pbig}{.001}\right)$ dBm (Convert to dBm units) $Pbig = -14.59$ dBm

$AGC = (Pbig - Pmax_{RX}) + 20$ $AGC = 47.46$ dB (Minimum required dynamic range of AGC with a 20 dB safety margin.)

The above calculation assumes that the gain of the receiver is set to the value that matches the noise floor of the receiver to that of the A/D converter, that the threshold for AGC operation is 10 dB less than the A/D saturation receiver input level and that the maximum receiver input for AGC operation is 10 dB greater than that of the largest target at the shortest range.

Derivation of the Minimum Detectable Signal

Previously, the receiver gain was calculated to equalize the noise power in the receiver measured within the 4 dB bandwidth of the compressed pulsewidth to the noise power in the A/D converter also measured in a pulsewidth of bandwidth. The effect of range gating implemented in the form of decimating the digitized range lines will be to alias the thermal noise in the pulsewidth of receiver bandwidth into the PRF bandwidth of the FFT. The FFT will divide this noise power evenly into N bins of bandwidth, where N is the number of pulses in the FFT. The target Doppler which is contained in only one bin for I/Q processing will compete against only one bin of noise. Therefore, the effective system thermal noise floor must be modified.

Assumptions:

None

Calculations:

$$thermal_{noise} = \frac{Pfloor_{AD}}{N}$$ (Noise Power in a FFT bin of bandwidth)

$$10 \cdot \log\left(\frac{thermal_{noise}}{10^{-3}}\right) = -80.05 \quad dBm$$

Therefore, given the effective processing gain, N, for the number of pulses used in the FFT, the minimum detectable signal power which will be detected by the radar can be calculated. The range of signal powers is given by the dynamic range of the A/D converter plus the coherent processing gain.

$DR_{system} = MaxSNR_{AD} + 10 \cdot \log(N) - MinSIRdB$ (Detectable target cross section dynamic range)

$DR_{system} = 90.05$ dB

$Pmds_{AD} = Pmax_{AD} - DR_{system}$ dBm (Minimum detectable signal power at the input to the A/D converter.)

$Pmds_{AD} = -80.05$ dBm

$Pmds_{RX} = Pmds_{AD} - 10 \cdot \log(G_o)$ (Minimum detectable signal power at the input to the receiver.)

$Pmds_{RX} = -132.1$ dBm

$Pmds\_RX_{tr} = Pmds_{RX}$

Derivation of Sidelobe and Mainbeam Clutter Power

The return signals for a pulsed radar system include scatter from not only the desired targets but from undesired objects as well. These undesired objects are collectively called clutter and can include things such as the ground, structures on the ground, birds, insects, chaff, weather precipitation and many others. It is a well documented fact that modelling clutter for radar analysis is difficult at best and usually takes the form of a collection of simplifying assumptions with documented ground reflectivities. This analysis will also make several assumptions that will result in a calculatable effective clutter radar cross section.

The simplifying assumptions made here include:

1. There will be no terrestrial structures either natural or man made present within the radar's field of view. Any natural vegetation or ground surface irregularities will be accounted for with the assumed ground reflectivity.
2. There will be no airborne clutter such as birds, precipitation, etc.
3. The antenna lobe structure will be assumed to be perfectly symmetric in a volume of revolution around boresight in the non-scanned mode. In the scanned mode, the resultant grating lobes will necessarily be accounted for.
4. The antenna lobes of interest will illuminate the ground uniformly within their half-power beamwidths.

The cross section of ground seen by the radar is a function of the transmit pulsewidth and the antenna beamwidth. For distances close to the radar, the antenna beamwidth limits the illuminated ground area. For distances far from the radar, the pulsewidth of the transmitted signal limits the illuminated area. For airborne radar, the determination of which case to use is made by using the calculation method that produces the maximum ground return. The scenarios are different for ground based radar and airborne radar . For airborne radar, if the main lobe is pointing down, the main lobe is typically the most significant ground illuminator. The ground based radar is typically concerned with airborne targets. As such, the main lobe is usually above horizon and the only contributors to the ground clutter are the sidelobes. Any sidelobes that will produce ground returns will be those that are physically directed below horizontal. The radar antenna will only be a few meters off the ground. Any contributing ground patches will be the same distance from the antenna as the target is from the antenna. This is due to range gating. Range gating limits the received clutter energy. Only the patches of ground illuminated by the sidelobes that are within the same "range bin" as the target will contribute to the clutter power competing with the target. Since the target range will be significantly larger than the height of the antenna, the patch size will be both pulsewidth and beamwidth limited. It will be radially pulsewidth limited and azimuthally beamwidth limited.

Assumptions:

$HA := 10$ m. (antenna height above ground)

$\theta_T := 0$ deg. (target angle above horizon)

$N_{SL} := 6$ (highest order antenna sidelobe effectively contributing to clutter)

$n_{SL} := 0..N_{SL}$ (nth sidelobe contributing to clutter, 0th = mainbeam)

$Gsl_0 := 10^{\frac{10\log(G_A)-0}{10}}$ (Main Beam Gain) $10\log(Gsl_0) = 43.01$ dB

$\theta bw_0 = .85$ deg. (Main Beam HPBW)

$\phi pa_0 := 0$ deg. (Main Beam Pointing Angle)

$Gsl_1 = 10^{\frac{10\log(G_A)-21.1}{10}}$ (1st Sidelobe Gain)

$\theta bw_1 := .429$ deg. (1st SL HPBW)

$\phi pa_1 = 1.32$ deg. (1st SL Pointing Angle)

$Gsl_2 := 10^{\frac{10\log(G_A)-22}{10}}$ (2nd Sidelobe Gain)

$\theta bw_2 = .536$ deg. (2nd SL HPBW)

$\phi pa_2 := 2.0$ deg. (2nd SL Pointing Angle)

$Gsl_3 = 10^{\frac{10\log(G_A)-22.5}{10}}$ (3rd Sidelobe Gain)

$\theta bw_3 := .536$ deg. (3rd SL HPBW)

$\phi pa_3 = 2.95$ deg. (3rd SL Pointing Angle)

$Gsl_4 := 10^{\frac{10\log(G_A)-22.3}{10}}$ (4th Sidelobe Gain)

$\theta bw_4 = .643$ deg. (4th SL HPBW)

$\phi pa_4 := 3.428$ deg. (4th SL Pointing Angle)

$Gsl_5 := 10^{\frac{10\log(G_A)-21.5}{10}}$ (5th Sidelobe Gain)

$\theta bw_5 = .643$ deg. (5th SL HPBW)

$\phi pa_5 := 4.285$ deg. (5th SL Pointing Angle)

$Gsl_6 = 10^{\frac{10\log(G_A)-26}{10}}$ (6th Sidelobe Gain)

$\theta bw_6 := .643$ deg. (6th SL HPBW)

$\phi pa_6 := 5.143$ deg. (6th SL Pointing Angle)

$\sigma_0 := 0.01$ (Ground reflection coefficient = -20 dB)

Calculations:

A low PRF radar exhibits unambiguous range. As such, the clutter power received competing with the target is only the power received from the range bin of interest. Therefore, there is no need to sum clutter power from ambiguous ranges nor is there a need to provide for special clutter range indices.

$$HT_{tr} := HA + \left[R_{tr} \cdot \sin\left(\theta_T \cdot \left(\frac{2 \cdot \pi}{360} \right) \right) \right] \quad \text{m. (target altitude above ground)}$$

SEP = the physical seperation between the target and clutter point

The antenna, target and clutter point form a plane. The radius from the antenna to the target and clutter point = R. The physical separation between the target and clutter point can be calculated by:

$$\sin\left[\frac{\phi pa_{n\,SL}}{2} \cdot \left(\frac{2 \cdot \pi}{360} \right) \right] = \frac{\left(\frac{SEP_{n\,SL,tr}}{2} \right)}{R_{tr}}$$

or

$$SEP_{n\,SL,tr} := 2 \cdot R_{tr} \cdot \sin\left[\frac{\phi pa_{n\,SL}}{2} \cdot \left(\frac{2 \cdot \pi}{360} \right) \right] \quad \text{m. (separation between target and clutter patch)}$$

When viewed from above, the apparent angle between the clutter patch and the target with the antenna at the vertex is a function of :

$$\theta tilt_{n\,SL,tr} := if\left(n_{SL} > 0, asin\left(\frac{HT_{tr}}{SEP_{n\,SL,tr}} \right), 0 \right) \quad \text{rad.}$$

(Since the separation is fixed by range and sidelobe angle, an argument greater than one would indicate the invalidity of the sidelobe causing clutter return for a target of the indicated range and height.)

$$\theta app_{n\,SL,tr} := if\left(n_{SL} > 0, if\left(\frac{HT_{tr}}{SEP_{n\,SL,tr}} < 1, \phi pa_{n\,SL} \cdot \cos\left(\theta tilt_{n\,SL,tr} \right), 0 \right), 0 \right) \quad \text{deg.}$$

The tilt angle is the angle subtended by the ground and the line between the clutter patch and target.

The apparent distance from the antenna to the clutter point when viewed from above is a function of:

$$\theta G_{tr} := asin\left(\frac{HA}{R_{tr}} \right) \quad \text{rad.}$$

$$Rcp_{tr} := R_{tr} \cdot \cos\left(\theta G_{tr} \right) \quad \text{m.} \quad \text{(apparent distance from antenna to the clutter patch when viewed from above.)}$$

For the pulsewidth limited case, the main beam ground clutter return may be calculated as follows. The intersection of the ground and main beam forms a hyperbola.

$a = HA \cdot \cot\left(\frac{2 \cdot \pi}{360} \cdot \frac{\theta bw_0}{2}\right)$ (Half length of the major axis which is the separation between origin which is the antenna location and the hyperbola vertex which is the closest ground point which is illuminated by the main beam.)

$b = HA$ (Half length of the minor axis.)

In rectangular coordinates, assuming the center is the origin, the equation for a hyperbola is given as:

$$\frac{x^2}{a^2} - \frac{y^2}{b^2} = 1,$$

$y_{T_{tr}} = b \cdot \sqrt{\frac{(Rcp_{tr})^2}{a^2} - 1}$ m. (Y axis extent of hyperbola assuming target along x axis.)

$\gamma_{tr} = 2 \cdot \operatorname{atan}\left(\frac{y_{T_{tr}}}{Rcp_{tr}}\right)$ rad. (Azimuth angular coverage of ground clutter patch of main beam.)

$$mbAcp_{tr} = if\left(\frac{HA}{Rcp_{tr}} < 1, if\left(Rcp_{tr} > a, \frac{c \cdot \tau_{comp}}{2 \cdot \cos(\theta G_{tr})} \cdot \frac{\gamma_{tr}}{2 \cdot \pi} \cdot Rcp_{tr}, 0\right), 0\right)$$

For the pulsewidth limited case, a single illuminated patch size is given by:

$$Acp_{n_{SL},tr} = if\left[\left(\frac{HT_{tr}}{SEP_{n_{SL},tr}}\right) < 1, \left[\left(\frac{c \cdot \tau_{comp}}{2}\right) \cdot \frac{R_{tr} \cdot \theta bw_{n_{SL}} \cdot \left(\frac{2 \cdot \pi}{360}\right)}{\cos(\theta G_{tr})}\right], 0\right] \quad m^2$$

There will be two identical patches based on antenna sidelobe symmetry. Therefore, the total clutter patch area for a sidelobe pair can be described by:

$$Acp_{n_{SL},tr} = if\left[n_{SL} > 0, if\left[\left(\frac{HT_{tr}}{SEP_{n_{SL},tr}}\right) < 1, \frac{c \cdot \tau_{comp}}{\cos(\theta G_{tr})} \cdot R_{tr} \cdot \theta bw_{n_{SL}} \cdot \left(\frac{2 \cdot \pi}{360}\right), 0, mbAcp_{tr}\right]\right] m^2$$

The ground reflectivity varies as a function of terrain, structures, ground conductivity, ground dielectric constant, frequency, grazing angle and vegetation. There have been numerous studies documented to determine the average ground clutter reflection coefficient. For Ku band, a reasonable reflection coefficient is 0.01 or -20 dB.

$\sigma_0 = 0.01$

Therefore, for the sidelobes considered, the total effective ground clutter RCS may be described by:

$$\sigma c_{tr} = \sigma_o \cdot \sum_{n_{SL}} Acp_{n_{SL},tr} \quad \text{sq. m.}$$

The total power returned to the receiver from the clutter patches may be computed using the radar range equation. Since each sidelobe pair corresponds to different gain levels, the total effective ground clutter calculated above must be modified in the range equation.

$$Pc_{RX_{tr}} = \frac{P_t \cdot \lambda^2 \cdot \sigma_o}{(4 \cdot \pi)^3 \cdot (R_{tr})^4 \cdot L_{xmtr} \cdot L_{2way} \cdot L_A} \cdot \sum_{n_{SL}} \left(Gsl_{n_{SL}}\right)^2 \cdot Acp_{n_{SL},tr} \quad \text{W.}$$

$$Pc_{RX_{tr}} := if\left(R_{tr} > R_{min}, if\left(Pc_{RX_{tr}} > 0, 10 \cdot \log\left(\frac{Pc_{RX_{tr}}}{.001}\right), -200\right), -200\right) \quad \text{dBm}$$

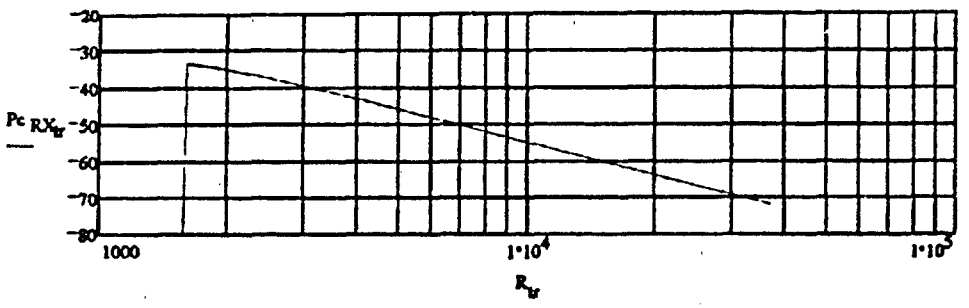

Derivation of Spurious False Target Power Levels

Spurious signals in a radar of sufficient magnitude will appear as false targets. The spurious signals may be caused by a variety of sources such as transmitter harmonics, transmitter spurious signals, transmitter amplitude and phase variations over the pulse bandwidth, I/Q detector phase and amplitude imbalances, linear frequency modulation (LFM) non-linearities, etc. Once the effects of I/Q imbalances and windowing are known, the transmitter spurious signals can be specified to be below the maximum acceptable level. Transmitter harmonics are filtered. The pulse bandwidth will only be a small percentage of the transmitter bandwidth. Variations over the pulse bandwidth will be negligible. The spurs resulting from LFM non-linearities may be accounted for by the SAW device manufacturer.

This example considers a clutter signal and a target signal at 562.5 Hz doppler frequency which is 75 dB below the clutter signal. 562.5 Hz is the lowest doppler frequency detectable following clutter blanking. Thus, this is the worst case clutter and target return acceptable to the radar. The composite signal is broken into in-phase and quadrature components. The "unwindowed" spectrum is calculated, and then the 75 dB Dolph-Tschebycheff window is applied to the received pulses to reduce leakage of target doppler into adjacent bins.

Assumptions:

$\phi := 5$ deg. (Maximum phase mismatch between I and Q channels)

$A := -0.5$ dB (Maximum amplitude mismatch between I and Q channels)

$A := 10^{\frac{A}{20}}$ $A = 0.94$ (Convert to linear)

Calculations:

Frequency of the clutter (Hz): $f0 := \frac{PRF}{N} \cdot 0$ Hz $f0 = 0$ Hz

Frequency of the target (Hz): $f1 := \frac{PRF}{N} \cdot 4.5$ Hz $f1 = 562.5$

Signal to Clutter Ratio: $SCR := ClutFiltRej - SubClutVis$ $SCR = -75$

Relative linear magnitude: $m1 := 10^{\frac{SCR}{20}}$ $m1 = 1.78 \cdot 10^{-4}$

$i := 0..N-1$ $t_i := \frac{i}{PRF}$

$f_i := \cos(2 \cdot \pi \cdot f0 \cdot t_i) + m1 \cdot \cos(2 \cdot \pi \cdot f1 \cdot t_i)$ $g_i := \left(\cos\left(2 \cdot \pi \cdot f0 \cdot t_i + \frac{\pi}{2} + \frac{\pi \cdot \phi}{180}\right) - m1 \cdot \cos\left(2 \cdot \pi \cdot f1 \cdot t_i + \frac{\pi}{2} + \frac{\pi \cdot \phi}{180}\right)\right) \cdot A$

$h_i := f_i + (0 + i) \cdot g_i$

$H := cfft(h)$ (Compute the FFT of the unwindowed I&Q data)

$$M := \text{if}\left[\left(\frac{f0}{\frac{PRF}{N}}\right) - \text{floor}\left[\frac{f0}{\left(\frac{PRF}{N}\right)}\right] > .5, \text{ceil}\left(\frac{f0}{\frac{PRF}{N}}\right), \text{floor}\left(\frac{f0}{\frac{PRF}{N}}\right)\right] \qquad max := |H_M|$$

$$H_i := \text{if}\left(\frac{|H_i|}{max} < 10^{-10}, -210, 20\cdot\log\left(\frac{|H_i|}{max}\right)\right)$$

(Computes the magnitude of this FFT and normalize the magnitude spectrum by the maximum value which is H_M in this case)

Now apply a 75dB Dolph-Chebychev window to the I&Q data

$SLL := -SCR + MinSIR \qquad SLL = 75$

$$RR := 10^{\frac{SLL}{20}} \qquad A := \cosh\left[\left(\frac{1}{N-1}\right)\cdot\text{acosh}(RR)\right]$$

(Calculate constant related to desired sidelobe level.)

$n := 1..\frac{N}{2}$ (Indices for calculation of Dolph coefficients)

$$Dolph_n := \sum_{q=n}^{\frac{N}{2}} \frac{(-1)^{\frac{N}{2}-q}\cdot A^{(2\cdot q)-1}\cdot\left(q+\frac{N}{2}-2\right)!\cdot\left[\left(2\cdot\frac{N}{2}\right)-1\right]}{(q-n)!\cdot(q-n-1)!\cdot\left(\frac{N}{2}-q\right)!}$$

(n must be even)

$x := 0..\frac{N}{2}-1$ (Total length of the number of time samples)

$w_x := Dolph_{\frac{N}{2}-x} \qquad w_{\frac{N}{2}+x} := Dolph_{x+1}$ (Assign the appropriate Taylor coefficient to each time sample.)

$hw_i := f_i\cdot w_i + (0-i)\cdot g_i\cdot w_i$

$HW := cfft(hw)$ (Compute the FFT of the windowed I&Q data

$max := |HW_M|$

$HW_i := \text{if}\left(\frac{|HW_i|}{max} < 10^{-10}, -210, 20\cdot\log\left(\frac{|HW_i|}{max}\right)\right)$ (Compute the normalized magnitude in dB of this FFT)

$HW_7 = -77.02$	dB	$HW_{25} = -77.09$	dB	$H_7 = -93.12$	dB	$H_{25} = -104.71$	dB
$HW_6 = -76.33$	dB	$HW_{26} = -75.57$	dB	$H_6 = -88.73$	dB	$H_{26} = -104.22$	dB
$HW_5 = -71.15$	dB	$HW_{27} = -74.9$	dB	$H_5 = -79.21$	dB	$H_{27} = -102.12$	dB

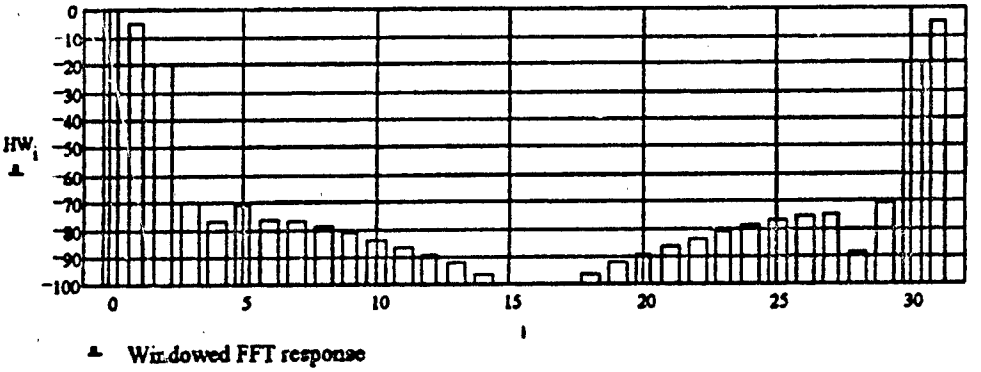

▲ Windowed FFT response

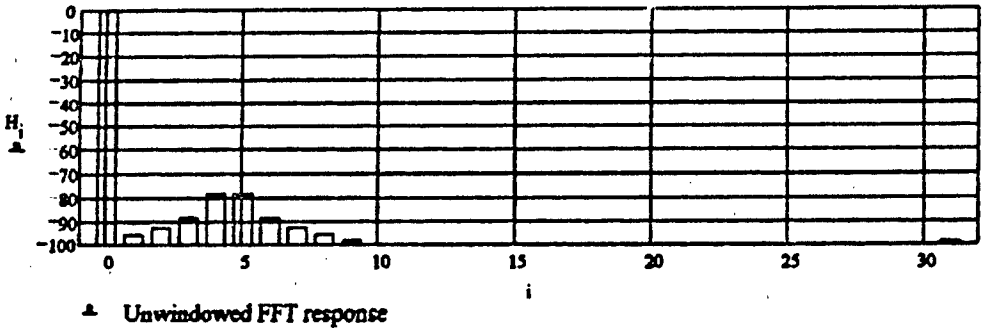

▲ Unwindowed FFT response

The above windowed FFT response indicates the ability to see the -75 dB target in the clutter and I/Q imbalances after clutter blanking. Based on HW_5 and HW_{27}, the fifth doppler FFT bin and the closest doppler FFT in magnitude after clutter blanking, there is sufficient margin for the minimum signal to interference ratio. This is a worst case margin. The target is minimal and at the lowest useable doppler frequency after clutter blanking. If the target signal increases, the doppler frequency increases or if the I/Q imbalances improve, the target signal margin above increases.

Derivation of System Phase and Clutter Spectral Leakage Noise Floor

To optimize detection, the clutter phase noise floor of the system should be specified such that it is a minimum number of dB below the required minimum subclutter visibility. 13 dB is typical for 50% probability of detection and 10^{-6} probability of false alarm. The clutter noise floor will be the result of the phase noise of the oscillators used in upconversion / downconversion chain of the radar as well as transmitter thermal and phase noise.

The analysis is started by modeling the phase noise envelope of the worst phase noise contributor. A Bode plot of the noise skirt can be drawn using poles to mark the knee points in the curve. The Bode plot approach is used to derive a plot of L(f), the phase noise spectral density, which is defined as the ratio of the single sideband phase noise power per Hertz relative to the carrier power. The plot will be used to also set the maximum allowable total noise contributions from the other components in the exciter / transmitter chain.

Assumptions:

$n_1 = 1$ (Phase Noise pole order. 1 => 20 dB/decade, 0.5 => 10 dB/decade, ...)

$f_{c1} = 10$ Hz (Phase Noise carrier offset frequency)

$dBL1 = -75$ dBc/Hz (Maximum allowable phase noise magnitude @ fc1)

$n_2 = 0.0625$ (Phase noise pole order. 1 => 20 dB/decade, 0.5 => 10 dB/decade, ...)

$f_{c2} = 10000$ Hz (Phase Noise carrier offset frequency)

$dBL2 = -135$ dBc/Hz (Maximum allowable phase noise magnitude @ fc2)

$f_{break} = 10000$ (L(f) break frequency)

Calculations:

$f = 10, 1000 .. \frac{B_{comp}}{2}$ Hz (Phase noise skirt frequency range of interest)

$$f_{3dB1} = \frac{f_{c1}}{\sqrt{\frac{1}{\left(10^{\frac{dBL1}{10}}\right)^{\frac{1}{n_1}}} - 1}}$$

(Flicker phase noise 3dB frequency)

$f_{3dB1} = 0$ (Hz)

$$L_1(f) := \left[\frac{1}{1-\left(\frac{f}{f_{3dB1}}\right)^2}\right]^{n1}$$ (Flicker noise average power per Hertz relative to carrier)

$$f_{3dB2} = \frac{f_{c2}}{\sqrt{\left(\frac{1}{10^{\frac{dB1.2}{10}}}\right)^{\frac{1}{n2}} - 1}}$$ (White phase noise 3dB frequency)

$f_{3dB2} = 0$ (Hz)

$$L_2(f) := \left[\frac{1}{1+\left(\frac{f}{f_{3dB2}}\right)^2}\right]^{n2}$$ (White noise average power per Hertz relative to carrier)

$L(f) := if(f<10000, L_1(f), L_2(f))$ (Oscillator phase noise average power per Hertz relative to the carrier power, dBc/Hz)

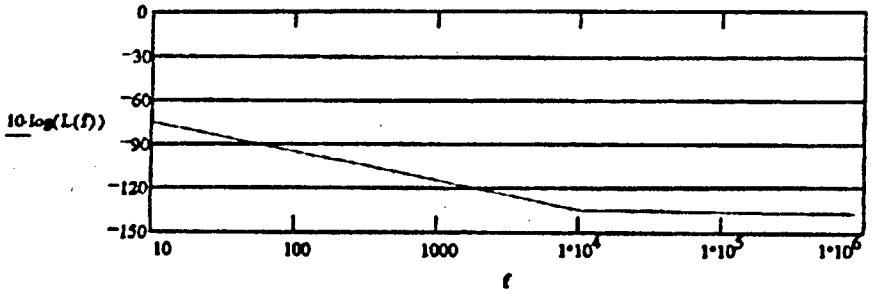

When a signal returns from a target and is downconverted by the same oscillator, some of the phase noise of the oscillator will be canceled due to correlation. This is known as range correlation effect. The improvement in the phase noise skirt of the output waveform can be calculated for a given range delay. In this example, the transmitter is the largest contributor to the transmitted noise floor level and thus the reange correlation effect does not apply.

$M = \frac{B_{comp}}{PRF}$ (number of spectral lines contained with pulsewidth's spectral mainlobe)

$\Delta f := \frac{PRF}{N}$ (bandwidth of an FFT bin in Hertz)

$m = 1 .. \frac{M - 1}{2}$ (clutter spectral line index)

$kk = 1 .. \frac{N - 2}{2}$ (FFT bin index)

First, the average noise power is computed relative to the carrier in an FFT bin's bandwidth which results from the clutter spectral line at the fundamental carrier frequency.

$Pcarrier_{kk} = \Delta f \cdot L(kk \cdot \Delta f)$ dBc (Average upper sideband phase noise power resulting from the carrier)

$Pcarrier_{N-kk} = Pcarrier_{kk}$ dBc (Average lower sideband phase noise power resulting from the carrier)

Next, the average power relative to the carrier in a bin's bandwidth which results from the replicas of the clutter spectral lines to the left (or negative frequencies) of the fundamental carrier frequency is added.

$$Pneg_{kk} = \sum_{m} \Delta f \cdot L(kk \cdot \Delta f - m \cdot PRF) \cdot \left[\frac{\sin\left[\pi \cdot \left[\frac{m \cdot PRF}{\left(\frac{B_{comp}}{2}\right)}\right]\right]}{\pi \cdot \left[\frac{m \cdot PRF}{\left(\frac{B_{comp}}{2}\right)}\right]} \right]^{-2}$$

$$Pneg_{N-kk} = \sum_{m} \Delta f \cdot L((N - kk) \cdot \Delta f + (m - 1) \cdot PRF) \cdot \left[\frac{\sin\left[\pi \cdot \left[\frac{m \cdot PRF}{\left(\frac{B_{comp}}{2}\right)}\right]\right]}{\pi \cdot \left[\frac{m \cdot PRF}{\left(\frac{B_{comp}}{2}\right)}\right]} \right]^{2}$$

Finally, the average noise power relative to the carrier contribution from the replicas of the clutter spectral lines to the right (or positive frequencies) of the fundamental carrier is added. Again, the noise power is calculated in a bandwidth of an FFT bin.

$$Ppos_{kk} := \sum_{m} \Delta f \cdot L((N - kk)\cdot\Delta f + (m - 1)\cdot PRF)\cdot \left[\frac{\sin\left[\pi\cdot\left[\frac{m\cdot PRF}{\left(\frac{B_{comp}}{2}\right)}\right]\right]}{\pi\cdot\left[\frac{m\cdot PRF}{\left(\frac{B_{comp}}{2}\right)}\right]} \right]^2$$

$$Ppos_{N-kk} := \sum_{m} \Delta f \cdot L(kk\cdot\Delta f + m\cdot PRF)\cdot \left[\frac{\sin\left[\pi\cdot\left[\frac{m\cdot PRF}{\left(\frac{B_{comp}}{2}\right)}\right]\right]}{\pi\cdot\left[\frac{m\cdot PRF}{\left(\frac{B_{comp}}{2}\right)}\right]} \right]^2$$

$$Pnoise_{kk} := Pcarrier_{kk} + Pneg_{kk} + Ppos_{kk}$$

$$Pnoise_{N-kk} := Pcarrier_{N-kk} + Pneg_{N-kk} + Ppos_{N-kk}$$

$$kk := 0..N - 1$$

$$Pnoise_{kk} := if\left(Pnoise_{kk} < 10^{-15}, 10^{-15}, Pnoise_{kk}\right)$$

Decimation of the sampled waveform into range bins coherently aliases the phase noise in the kk^{th} doppler bin with the kk^{th} doppler bin of each PRF line within the compressed pulse bandwidth. Decimation also coherently aliases the signal in the kk^{th} doppler bin with the kk^{th} doppler bin of each PRF line. Therefore, the signal to clutter phase noise ratio in each doppler bin remain unchanged through the decimation process.

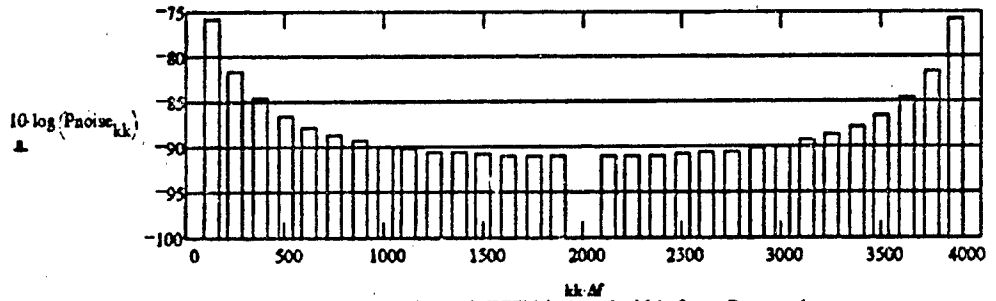

Phase noise power in each FFT bin bandwidth from Rmax clutter

The subclutter visibility is also dependant upon the window applied to the range samples. A 75 dB Dolph-Chebycheff window can be applied to a sample clutter return to calculate the "windowed" spectrum. Based on the above clutter phase noise calculation and the following "windowed" clutter calculation, a total subclutter visibility may be specified.

Frequency of the clutter (Hz): $f0 = 0$ Hz

$i = 0..N-1 \qquad t_i := \frac{i}{PRF}$

$f_i := \cos(2\cdot\pi\cdot f0\cdot t_i)$ (In phase clutter signal.) $\qquad g_i := \cos\left(2\cdot\pi\cdot f0\cdot t_i + \frac{\pi}{2}\right)$ (Quadrature clutter signal)

$h_i := f_i + (0-i)\cdot g_i$

$H := cfft(h)$ (Compute the FFT of the unwindowed I&Q data)

$$M := if\left[\left|\left(\frac{f0}{\frac{PRF}{N}}\right) - floor\left[\left(\frac{f0}{\frac{PRF}{N}}\right)\right]\right| > .5, ceil\left(\frac{f0}{\frac{PRF}{N}}\right), floor\left(\frac{f0}{\frac{PRF}{N}}\right)\right] \qquad max := |H_M|$$

$$H_i := if\left(\frac{|H_i|}{max} < 10^{-10}, -210, 20\cdot\log\left(\frac{|H_i|}{max}\right) - ClutFiltRej\right)$$

(Compute the magnitude of this FFT and normalize the magnitude spectrum by the maximum value which is H_M in this case)

Now apply a 75 Dolph-Chebychev window to the I&Q data.

$hw_i := f_i\cdot w_i + (0+i)\cdot g_i\cdot w_i$

$HW := cfft(hw)$ (Compute the FFT of the windowed I&Q data)

$max := |HW_M|$

$$HW_i := \text{if}\left(\frac{|HW_i|}{\max} < 10^{-10}, -210, 20\cdot\log\left(\frac{|HW_i|}{\max}\right) - \text{ClutFiltRej}\right)$$ (Compute the normalized magnitude in dB of this FFT)

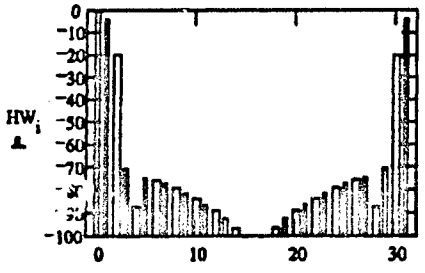

▲ Windowed Normalized Clutter

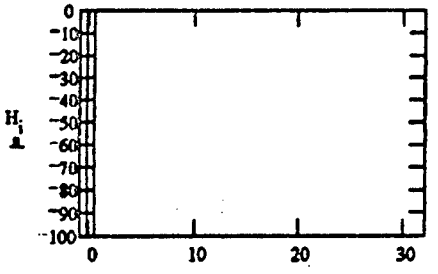

▲ Unwindowed Normalized Clutter

Comparing the previously calculated normalized clutter phase noise and the windowed normalized clutter, the subclutter visibility after clutter blanking may be safely specified as 75 dB. Therefore, any in band spurious signals from the transmitter and SAW devices must be less than the previously calculated maximum allowable average phase noise relative to the carrier power.

$SubCVis_{-i} := -SubClutVis$ dB

$SubCVis_{RX_{tr}} := Pc_{RX_{tr}} - SubClutVis$ (Visibility relative to the calculated received clutter power.)

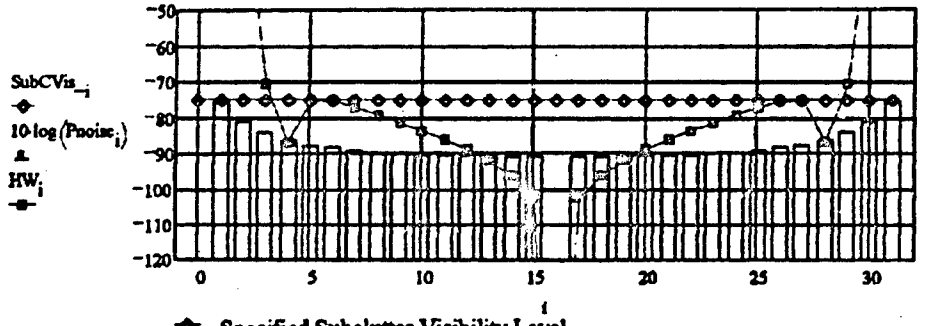

◆ Specified Subclutter Visibility Level
▲ Calculated Rmax Clutter Phase Noise
◆ Calculated Windowed Clutter Spectral Leakage

The above graph compares the specified subclutter visibility level, the calculated phase noise and the window spectral leakage effects on the clutter. The maximum allowable phase noise from the other components in the exciter / transmitter chain may be specified to be 10 dB below the worst case phase noise contributor versus frequency. Therefore, the total exciter noise including the noise contributions of phase, thermal, jitter and acoustic sources must be no greater than -65 dBc/Hz at 10 Hz away from the carrier and no greater than -145 dBc/Hz at 10 kHz away from the carrier.

Derivation of Overall System Detection Performance

The graph below exploits the results of all the previous calculations except AGC. The plots shows the expected receiver input levels for the 100 square meter target, the 0.1 square meter target and the calculated clutter return with its respective phase noise. They are compared to the receiver input level that would saturate the A/D converter and the minimum detectable signal.

$AGC_{low_{tr}} = Pmax_{RX} - 10$ dBm (Threshold of AGC operation)

$AGC_{hi_{tr}} := Pbig - 10$ dBm (Upper minimum limit of AGC operation)

$AGC = (Pbig - Pmax_{RX}) + 20$ $AGC = 47.46$ dB (Minimum required dynamic range of AGC with a 20 dB safety margin.)

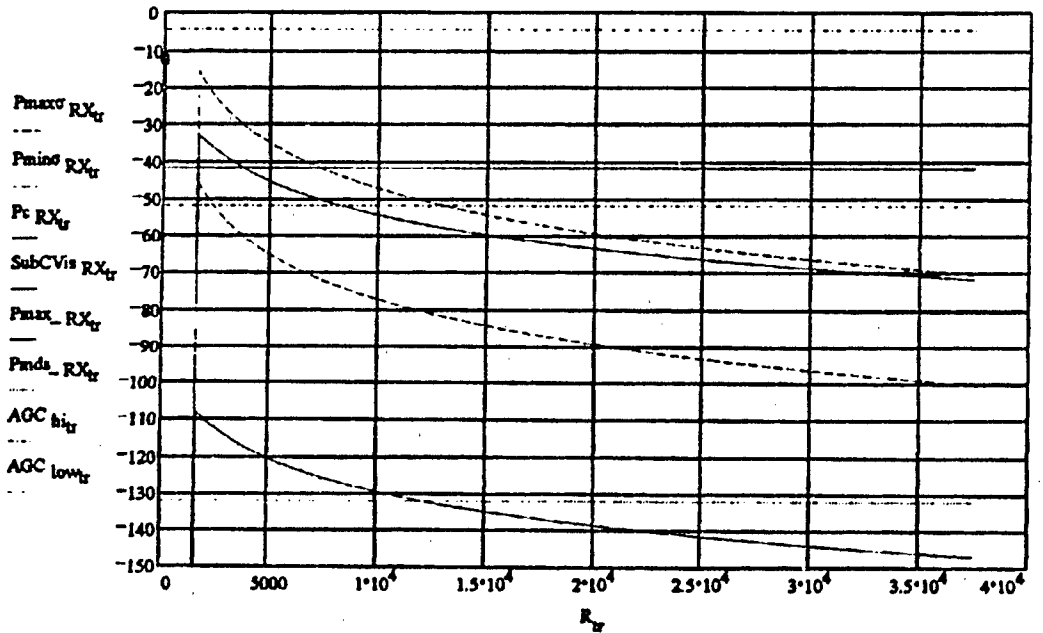

- 100 sq. m. target signal receiver input vs. range
- 0.1 sq. m. target signal receiver input vs. range
- Calculated received clutter power
- Visibility relative to clutter power received
- Maximum receiver input to match A/D saturation level
- Minimum detectable signal receiver input level
- Upper minimum limit of receiver AGC operation
- Lower threshold of receiver AGC operation

Representative Medium PRF Case

Receiver and Signal Processor Subsystem Performance Analysis

Specified Radar Parameters

$c = 3 \cdot 10^{8}$ m./sec. (velocity of light)

$f = 10 \cdot 10^{9}$ Hz (transmitted center frequency)

$\lambda := \frac{c}{f}$ m. (transmitted center frequency wavelength) $\lambda = 0.03$ m.

$R_{max} = 150000$ m. (maximum specified range)

$\sigma_{min} = 1$ sq. m. (minimum specified target cross-section area)

$P_t = 80000$ W. (transmitter output power)

$\tau_{pulse} = 5.25 \cdot 10^{-6}$ sec. (Expanded transmitted pulsewidth in seconds)

$B_{chirp} := 0 \cdot 10^{6}$ Hz (Pulse Compression Chirp Bandwidth)

PRF := 15000 Hz (transmitted pulse repition frequency)

DopBinBW := 900 Hz (Specified Doppler bin bandwidth)

$N := \text{floor}\left(\frac{PRF}{DopBinBW}\right)$ (Number of FFT Integrations = Number of frequency bins in a PRF)

N = 16

MinSIR = 0 dB (Required SIR for Pd and Pfa for Swerling I target)

$\tau_{comp} = \tau_{pulse}$ sec. (Compressed and weighted pulsewidth)

$B_{comp} := \frac{1}{\tau_{comp}}$ $B_{comp} = 1.9 \cdot 10^{5}$ Hz (Compressed and weighted pulse bandwidth)

SubClutVis := 90 dB (Specified subclutter visibility)

ClutFiltRej := 30 dB (Specified clutter filter rejection)

$k = 1.38 \cdot 10^{-23}$ watts/(deg.K * Hz) (Boltzman's constant)

F = 2.512 (Receiver Noise Figure = 4 dB)

$MaxSNR_{AD} = 75$ dB (Measured A/D signal-to-noise ratio)

Derivation of Receiver Gain

The receiver should be designed to amplify the signal as much as possible without increasing the noise floor of the system. This accomplished increasing the gain of the receiver until the noise in the receiver is equal to the noise floor introduced by the A/D converter. Therefore, to calculate the receiver gain, the noise power introduced into the system by the A/D converter must first be calculated.

Assumptions:

$V_{pp} = 2.0$ v. (Maximum peak-to-peak voltage level for converter)

$R_{load} = 50$ ohms (A/D Converter Input Impedance)

$T = 290$ deg. Kelvin (ambient temperature)

$T_A = 100$ deg. Kelvin (antenna noise temperature)

$L_A = 1.5849$ (losses between the antenna and receiver = 2.0 dB)

$L_{mm} = 1.4125$ (Mismatched receiver S/N ratio loss = 1.5 dB)

Calculations:

$$V_{rms} = \frac{V_{pp}}{2\cdot\sqrt{2}} \quad V_{rms} = 0.71 \quad \text{v. (Maximum A/D RMS voltage)}$$

$$Pmax_{AD} = \frac{V_{rms}^2}{R_{load}} \quad Pmax_{AD} = 0.01 \quad \text{W. (Maximum A/D average power = 10 dBm)}$$

$$Pfloor_{AD} = 10\cdot\log\left(\left(\frac{Pmax_{AD}}{10^{-3}}\right)\right) - MaxSNR_{AD} \quad Pfloor_{AD} = -65 \quad \text{dBm (A/D noise floor)}$$

$$Pfloor_{AD} = 10^{-3}\cdot 10^{\frac{Pfloor_{AD}}{10}} \quad \text{W (Convert from dBm units to Watts)}$$

It is assumed that the noise power in the receiver measured within the bandwidth of the pulse. Therefore, the noise power incident on the A/D converter is given by:

$$G_o = \frac{Pfloor_{AD}\cdot L_A\cdot(\tau_{pulse}\cdot B_{comp})}{k\cdot\left[T\cdot(L_A\cdot F - 1) + T_A\right]\cdot B_{comp}\cdot L_{mm}}$$

(Receiver Gain to match Receiver Noise Floor to A/D Noise Floor given antenna noise temp., loss between receiver and antenna, SAW filter losses and the receiver noise figure.)

$10\cdot\log(G_o) = 51.46$ dB

Derivation of Receiver Pre-AGC Dynamic Range

Having calculated the receiver gain, the maximum input to the receiver can now be calculated by removing the calculated gain of the receiver from the maximum input power to the A/D converter.

Assumptions:

None

Calculations:

$$Pmax_{AD} = 10\log\left(\frac{Pmax_{AD}}{.001}\right) \quad dBm$$

$$Pmax_{RX} = Pmax_{AD} - 10\log(G_o) \qquad Pmax_{RX} = -41.46 \quad dBm$$

The minimum signal input to the receiver such that the signal at the A/D converter input is equal to the noise floor may be calculated by removing the maximum SNR of the A/D from the maximum input power to the receiver.

$$Pfloor_{RX} = Pmax_{RX} - MaxSNR_{AD} \qquad Pfloor_{RX} = -116.46 \quad dBm$$

Derivation of the Clutterless Receiver Automatic Gain Control Requirements

The receiver automatic gain control (AGC) will serve to prevent the receiver from being saturated by excessive clutter returns or close range targets. The AGC will also provide for constant angle tracking sensitivity (volts per degree error) over large signal dynamic range variations and target range.

The AGC will be applied to the middle stages of the amplifier chain to preserve the receiver noise figure and the maximum undistorted output of the final stage. The AGC control signal will be derived from the matched filter output. The AGC will control the acquisition and track sum channel as well as the difference azimuth and elevation track channel gains.

To determine the requirements of the AGC, some estimate of the level of incoming signals must be made. Therefore, a discussion of target signal dynamic range is included. Assuming full receiver gain, a comparison of the receiver input that will saturate the A/D converter to the expected target signal dynamics will provide the minimum requirements of the AGC.

Assumptions:

$\tau_{recovery} = 10^{-6}$ sec. (Duplexer recovery time)

$\sigma_{max\_} = 100$ m^2 (Maximum expected target RCS)

$G_A = 20000$ (Antenna Gain = 43 dBi)

$L_{xmtr} = 1.5849$ (Loss between the transmitter and the antenna = 2.0 dB)

$L_{2wsy} = 1.2589$ (Round trip loss between antenna and target = 1.0 dB)

Calculations:

Target Dynamic Range

The minimum target detection range is determined by the duplexer recovery time and the transmitted pulsewidth.

$$R_{min} = c \cdot \frac{\tau_{pulse} + \tau_{recovery}}{2} \qquad R_{min} = 937.5 \quad \text{m. (Minimum detection range of the radar)}$$

The radar returns of the target at the minimum through the maximum ranges can now be calculated and compared to the maximum and minimum signals the A/D can handle.

$tr := 1 .. \frac{R_{max}}{250}$ (target range index)

$R_{tr} := 250 \cdot tr$ m. (target range)

$Pmax\_RX_{tr} := Pmax_{RX}$ (maximum unattenuated receiver input for A/D saturation)

$Pfloor\_RX_{tr} := Pfloor_{RX}$ (minimum unattenuated receiver input to match A/D noise floor)

$$Pmin\sigma_{RX_{tr}} := \frac{P_t \cdot G_A^2 \cdot \sigma_{min} \cdot \lambda^2}{(4\cdot\pi)^3 \cdot (R_{tr})^4 \cdot L_{xmtr} \cdot L_{2way} \cdot L_A} \text{ W.}$$ (Power received from smallest specified target (.1 sq. m.) versus required tracking range.)

$$Pmin\sigma_{RX_{tr}} := 10 \cdot \log\left(\frac{Pmin\sigma_{RX_{tr}}}{.001}\right) \text{ dBm}$$ (Convert to dBm units)

$$Pmax\sigma_{RX_{tr}} := \frac{P_t \cdot G_A^2 \cdot \sigma_{max\_} \cdot \lambda^2}{(4\cdot\pi)^3 \cdot (R_{tr})^4 \cdot L_{xmtr} \cdot L_{2way} \cdot L_A} \text{ W.}$$ (Power received from largest expected target (100 sq. m.) versus required tracking range.)

$$Pmax\sigma_{RX_{tr}} := 10 \cdot \log\left(\frac{Pmax\sigma_{RX_{tr}}}{.001}\right) \text{ dBm}$$ (Convert to dBm units)

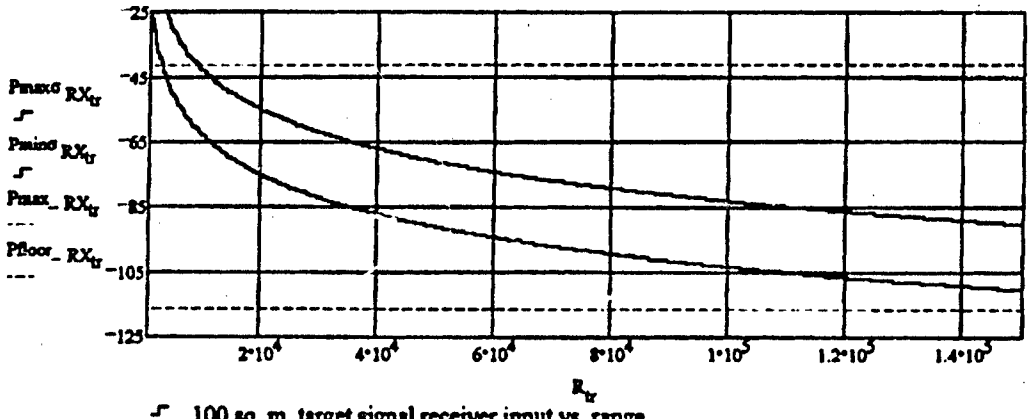

100 sq. m. target signal receiver input vs. range
1 sq. m. target signal receiver input vs. range
maximum receiver input to match A/D saturation level
minimum receiver input to match noise floor

AGC Minimum Requirements

$$Pbig = \frac{P_t \cdot G_A^2 \cdot \sigma_{max} \cdot \lambda^2}{(4\cdot\pi)^3 \cdot (R_{min})^4 \cdot L_{xmtr} \cdot L_{2way} \cdot L_A}$$ W. (Power received from largest expected target (100 sq. m.) at minimum range.)

$Pbig = 10 \cdot \log\left(\frac{Pbig}{.001}\right)$ dBm (Convert to dBm units) $Pbig = -2.26$ dBm

$AGC = (Pbig - Pmax_{RX}) + 20$ $AGC = 59.2$ dB (Minimum required dynamic range of AGC with a 20 dB safety margin.)

The above calculation assumes that the gain of the receiver is set to the value that matches the noise floor of the receiver to that of the A/D converter, that the threshold for AGC operation is 10 dB less than the A/D saturation receiver input level and that the maximum receiver input for AGC operation is 10 dB greater than that of the largest target at the shortest range.

Derivation of the Minimum Detectable Signal

Previously, the receiver gain was calculated to equalize the noise power in the receiver measured within the 4 dB bandwidth of the compressed pulsewidth to the noise power in the A/D converter also measured in a pulsewidth of bandwidth. The effect of range gating implemented in the form of decimating the digitized range lines will be to alias the thermal noise in the pulsewidth of receiver bandwidth into the PRF bandwidth of the FFT. The FFT will divide this noise power evenly into N bins of bandwidth, where N is the number of pulses in the FFT. The target Doppler which is contained in only one bin for I/Q processing will compete against only one bin of noise. Therefore, the effective system thermal noise floor must be modified.

Assumptions:

None

Calculations:

$$thermal_{noise} := \frac{Pfloor_{AD}}{N}$$ (Noise Power in a FFT bin of bandwidth)

$$10 \cdot \log\left(\frac{thermal_{noise}}{10^{-3}}\right) = -77.04 \quad dBm$$

Therefore, given the effective processing gain, N, for the number of pulses used in the FFT, the minimum detectable signal power which will be detected by the radar can be calculated. The range of signal powers is given by the dynamic range of the A/D converter plus the coherent processing gain.

$DR_{system} = MaxSNR_{AD} + 10 \cdot \log(N) - MinSIR$ dB (Detectable target cross section dynamic range)

$DR_{system} = 87.04$ dB

$Pmds_{AD} = Pmax_{AD} - DR_{system}$ dBm (Minimum detectable signal power at the input to the A/D converter.)

$Pmds_{AD} = -77.04$ dBm

$Pmds_{RX} = Pmds_{AD} - 10 \cdot \log(G_o)$ (Minimum detectable signal power at the input to the receiver.)

$Pmds_{RX} = -128.5$ dBm

$Pmds\_RX_u = Pmds_{RX}$

Derivation of Sidelobe and Mainbeam Clutter Power

The return signals for a pulsed radar system include scatter from not only the desired targets but from undesired objects as well. These undesired objects are collectively called clutter and can include things such as the ground, structures on the ground, birds, insects, chaff, weather precipitation and many others. It is a well documented fact that modelling clutter for radar analysis is difficult at best and usually takes the form of a collection of simplifying assumptions with documented ground reflectivities. This analysis will also make several assumptions that will result in a calculatable effective clutter radar cross section.

The simplifying assumptions made here include:

1. There will be no terrestrial structures either natural or man made present within the radar's field of view. Any natural vegetation or ground surface irregularities will be accounted for with the assumed ground reflectivity.
2. There will be no airborne clutter such as birds, precipitation, etc.
3. The antenna lobe structure will be assumed to be perfectly symmetric in a volume of revolution around boresight in the non-scanned mode. In the scanned mode, the resultant grating lobes will necessarily be accounted for.
4. The antenna lobes of interest will illuminate the ground uniformly within their half-power beamwidths.

The cross section of ground seen by the radar is a function of the transmit pulsewidth and the antenna beamwidth. For distances close to the radar, the antenna beamwidth limits the illuminated ground area. For distances far from the radar, the pulsewidth of the transmitted signal limits the illuminated area. For airborne radar, the determination of which case to use is made by using the calculation method that produces the maximum ground return. The scenarios are different for ground based radar and airborne radar . For airborne radar, if the main lobe is pointing down, the main lobe is typically the most significant ground illuminator. The ground based radar is typically concerned with airborne targets. As such, the main lobe is usually above horizon and the only contributors to the ground clutter are the sidelobes. Any sidelobes that will produce ground returns will be those that are physically directed below horizontal. The radar antenna will only be a few meters off the ground. Any contributing ground patches will be the same distance from the antenna as the target is from the antenna. This is due to range gating. Range gating limits the received clutter energy. Only the patches of ground illuminated by the sidelobes that are within the same "range bin" as the target will contribute to the clutter power competing with the target. Since the target range will be significantly larger than the height of the antenna, the patch size will be both pulsewidth and beamwidth limited. It will be radially pulsewidth limited and azimuthally beamwidth limited.

Assumptions:

$HA = 3$ m.	(antenna height above ground)
$\theta_T = 0.5$ deg.	(target angle above horizon)
$N_{SL} = 6$	(highest order antenna sidelobe effectively contributing to clutter)
$n_{SL} := 1..N_{SL}$	(nth sidelobe contributing to clutter)

$Gsl_0 = 10^{\frac{10\log(G_A)-0}{10}}$ (Main Beam Gain) $10\log(Gsl_0) = 43.01$

$\theta bw_0 = .85$ deg. (Main Beam HPBW)

$\phi pa_0 = 0$ deg. (Main Beam Pointing Angle)

$Gsl_1 = 10^{\frac{10\log(G_A)-24}{10}}$ (1st Sidelobe Gain)

$\theta bw_1 := .429$ deg. (1st SL HPBW)

$\phi pa_1 = 1.25$ deg. (1st SL Pointing Angle)

$Gsl_2 = 10^{\frac{10\log(G_A)-32}{10}}$ (2nd Sidelobe Gain)

$\theta bw_2 = .536$ deg. (2nd SL HPBW)

$\phi pa_2 = 2.2$ deg. (2nd SL Pointing Angle)

$Gsl_3 = 10^{\frac{10\log(G_A)-32}{10}}$ (3rd Sidelobe Gain)

$\theta bw_3 = 1.$ deg. (3rd SL HPBW)

$\phi pa_3 = 24.5$ deg. (3rd SL Pointing Angle)

$Gsl_4 = 10^{\frac{10\log(G_A)-32.5}{10}}$ (4th Sidelobe Gain)

$\theta bw_4 = .643$ deg. (4th SL HPBW)

$\phi pa_4 = 3.125$ deg. (4th SL Pointing Angle)

$Gsl_5 = 10^{\frac{10\log(G_A)-32.5}{10}}$ (5th Sidelobe Gain)

$\theta bw_5 = 18.5$ deg. (5th SL HPBW)

$\phi pa_5 = 4.285$ deg. (5th SL Pointing Angle)

$Gsl_6 = 10^{\frac{10\log(G_A)-34}{10}}$ (6th Sidelobe Gain)

$\theta bw_6 = 1.$ deg. (6th SL HPBW)

$\phi pa_6 = 26.5$ deg. (6th SL Pointing Angle)

$\sigma_0 := 0.01$ (Ground reflection coefficient = -20 dB)

Calculations:

A medium PRF radar exhibits ambiguous range. As such the clutter power received competing with the target is the power received from all the ambiguous ranges. Therefore, targets at a far range will compete with close range, mid-range and far range clutter. Mathematically, the range can be broken into sections of length equal to the unambigous range.

$R_{un} = \frac{c}{2 \cdot PRF}$ m. (Unambiguous range.) $R_{un} = 1 \cdot 10^4$ m.

nseg = 20 (Number of segments the unambiguous range is divided into.)

$segL = \frac{R_{un}}{nseg}$ m. (Segment length) segL = 500 m.

$m_r := 1 .. floor\left(\frac{R_{max}}{R_{un}}\right)$ (Unambiguous range length index.) $floor\left(\frac{R_{max}}{R_{un}}\right) = 15$

$n_r := 1 .. nseg$ (Range index within each unambiguous range length segment.)

$cR_{m_r,n_r} = \left[\left(m_r - 1\right) \cdot R_{un}\right] + \left(n_r \cdot segL\right)$ m. (Range for clutter calculations which will be equated with the target range.)

$HT_{m_r,n_r} = HA + \left[cR_{m_r,n_r} \cdot \sin\left[\theta_T \cdot \left(\frac{2 \cdot \pi}{360}\right)\right]\right]$ m. (Target altitude above ground. *Clutter range is equal to range of target from antenna.*)

SEP = the physical seperation between the target and clutter point

The antenna, target and clutter point form a plane. The radius from the antenna to the target and clutter point = cR. The physical separation between the target and clutter point can be calculated by:

$$\sin\left[\frac{\phi pa_{n_{SL}}}{2} \cdot \left(\frac{2 \cdot \pi}{360}\right)\right] = \frac{\left(\frac{SEP\left(n_{SL}, m_r, n_r\right)}{2}\right)}{cR_{m_r,n_r}}$$

or

$SEP\left(n_{SL}, m_r, n_r\right) = 2 \cdot cR_{m_r,n_r} \cdot \sin\left[\frac{\phi pa_{n_{SL}}}{2} \cdot \left(\frac{2 \cdot \pi}{360}\right)\right]$ m. (separation between target and clutter patch)

When viewed from above, the apparent angle between the clutter patch and the target with the antenna at the vertex is a function of :

$$\theta tilt(n_{SL}, m_r, n_r) := if\left(n_{SL} > 0, asin\left(\frac{HT_{m_r,n_r}}{SEP(n_{SL}, m_r, n_r)}\right), 0\right) \text{ rad.}$$

(Since the separation is fixed by range and sidelobe angle, an argument greater than one would indicate the invalidity of the sidelobe causing clutter return for a target of the indicated range and height.)

$$\theta app(n_{SL}, m_r, n_r) := if\left(n_{SL} > 0, if\left(\frac{HT_{m_r,n_r}}{SEP(n_{SL}, m_r, n_r)} < 1, tpa_{n_{SL}} \cdot \cos(\theta tilt(n_{SL}, m_r, n_r)), 0\right), 0\right) \text{ deg.}$$

The tilt angle is the angle subtended by the ground and the line between the clutter patch and target.

The apparent distance from the antenna to the clutter point when viewed from above is a function of:

$$\theta G_{m_r,n_r} := if\left(\frac{HA}{cR_{m_r,n_r}} < 1, asin\left(\frac{HA}{cR_{m_r,n_r}}\right), \frac{\pi}{2}\right) \text{ rad.}$$

$$Rcp_{m_r,n_r} := cR_{m_r,n_r} \cdot \cos(\theta G_{m_r,n_r}) \text{ m.}$$ (apparent distance from antenna to the clutter patch when viewed from above.)

For the pulsewidth limited case, the main beam ground clutter return may be calculated as follows. The intersection of the ground and main beam forms a hyperbola.

$a := HA \cdot \cot\left(\frac{2 \cdot \pi}{360} \cdot \frac{\theta bw_0}{2}\right)$ (Half length of the major axis which is the separation between origin which is the antenna location and the hyperbola vertex which is the closest ground point which is illuminated by the main beam.)

$b := HA$ (Half length of the minor axis.)

In rectangular coordinates, assuming the center is the origin, the equation for a hyperbola is given as:

$$\frac{x^2}{a^2} - \frac{y^2}{b^2} := 1$$

$$y_{T_{m_r,n_r}} := b \cdot \sqrt{\frac{(Rcp_{m_r,n_r})^2}{a^2} - 1} \text{ m.}$$ (Y axis extent of hyperbola assuming target along x axis.)

$$\gamma_{m_r,n_r} := 2 \cdot atan\left(\frac{y_{T_{m_r,n_r}}}{Rcp_{m_r,n_r}}\right) \text{ rad.}$$ (Azimuth angular coverage of ground clutter patch of main beam.)

$$mbAcp_{m_r,n_r} := if\left(\frac{HA}{cR_{m_r,n_r}} < 1, if\left(Rcp_{m_r,n_r} > a, \frac{c \cdot \tau comp}{2 \cdot \cos(\theta G_{m_r,n_r})} \cdot \frac{\gamma_{m_r,n_r}}{2 \cdot \pi} \cdot Rcp_{m_r,n_r}, 0\right), 0\right)$$

For the pulsewidth limited case, a single illuminated patch size is given by:

$$Acp(n_{SL}, m_r, n_r) := if\left[\left(\frac{HT_{m_r,n_r}}{SEP(n_{SL}, m_r, n_r)}\right) < 1, \left[\frac{\left(\frac{c \cdot \tau_{comp}}{2}\right)}{\cos(\theta G_{m_r,n_r})} \cdot cR_{m_r,n_r} \cdot \theta bw_{n_{SL}} \cdot \left(\frac{2 \cdot \pi}{360}\right)\right], 0\right] \quad m^2$$

There will be two identical patches based on antenna sidelobe symmetry. Therefore, the total clutter patch area for a sidelobe pair can be described by:

$$Acp(n_{SL}, m_r, n_r) := if\left[n_{SL} > 0, if\left[\left(\frac{HT_{m_r,n_r}}{SEP(n_{SL}, m_r, n_r)}\right) < 1, \frac{c \cdot \tau_{comp} \cdot cR_{m_r,n_r} \cdot \theta bw_{n_{SL}}}{\cos(\theta G_{m_r,n_r})} \cdot \left(\frac{2 \cdot \pi}{360}\right), 0\right], mbAcp_{m_r,n_r}\right]$$

The ground reflectivity varies as a function of terrain, structures, ground conductivity, ground dielectric constant, frequency, grazing angle and vegetation. There have been numerous studies documented to determine the average ground clutter reflection coefficient. For Ku band, a generous reflection coefficient is 0.01 or -20 dB.

$\sigma_o := .01$

Therefore, for the sidelobes considered, the total effective ground clutter RCS may be described by:

$$\sigma c_{m_r,n_r} := \sigma_o \cdot \sum_{n_{SL}} Acp(n_{SL}, m_r, n_r) \quad m^2$$

The total power returned to the receiver from the clutter patches may be computed using the radar range equation. Since each sidelobe pair corresponds to different gain levels, the total effective ground clutter calculated above must be modified in the range equation.

The clutter returns from all the ambiguous ranges must be folded into the clutter power received for the first unambiguous range segment. Beyond that segment, the clutter power competing with the target energy will be equivalent for each following unambiguous range length segment.

$$mnPc_{RX_{n_r}} := \frac{P_t \cdot \lambda^2 \cdot \sigma_o}{(4 \cdot \pi)^3} \cdot \sum_{n_{SL}} (Gsl_{n_{SL}})^2 \cdot \sum_{m_r} if\left[cR_{m_r,n_r} > R_{min}, \frac{Acp(n_{SL}, m_r, n_r)}{(cR_{m_r,n_r})^4}, 0\right] \quad W.$$

$$Pc_{RX_{tr}} := mnPc_{RX_{floor}\left[\left(\frac{R_{tr}}{R_{un}} - floor\left(\frac{R_{tr}}{R_{un}}\right)\right) \cdot neg - 1\right]}$$

$$Pc_{RX_{tr}} := if\left(Pc_{RX_{tr}} > 0, 10\cdot\log\left(\frac{Pc_{RX_{tr}}}{.001}\right), -200\right) \quad dBm$$

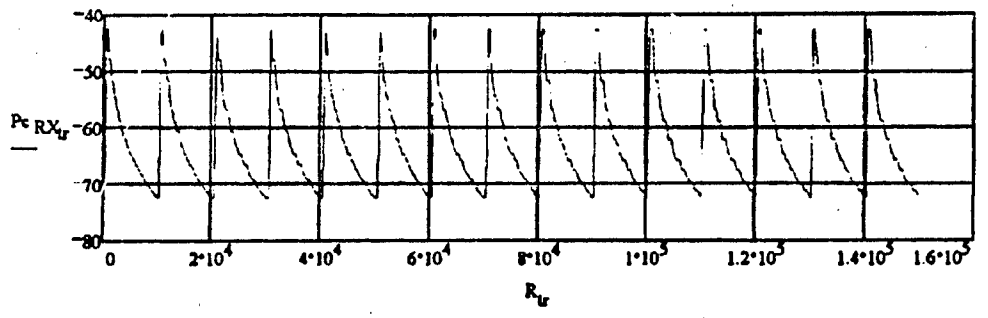

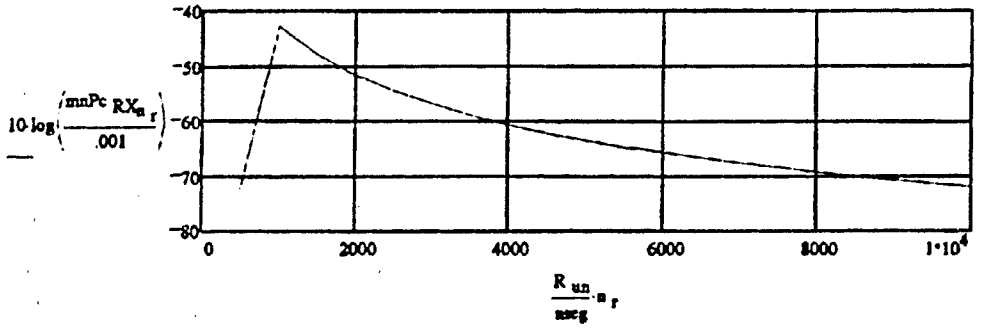

Derivation of Spurious False Target Power Levels

Spurious signals in a radar of sufficient magnitude will appear as false targets. The spurious signals may be caused by a variety of sources such as transmitter harmonics, transmitter spurious signals, transmitter amplitude and phase variations over the pulse bandwidth, I/Q detector phase and amplitude imbalances, linear frequency modulation (LFM) non-linearities, etc. Once the effects of I/Q imbalances and windowing are known, the transmitter spurious signals can be specified to be below the maximum acceptable level. Transmitter harmonics are filtered. The pulse bandwidth will only be a small percentage of the transmitter bandwidth. Variations over the pulse bandwidth will be negligible. The spurs resulting from LFM non-linearities may be accounted for by the SAW device manufacturer.

This example considers a clutter signal and a target signal at the minimum doppler frequency which is SCR dB below the clutter signal. The minimum doppler frequency is the lowest doppler frequency detectable following clutter blanking. Thus, this is the worst case clutter and target return acceptable to the radar. The composite signal is broken into in-phase and quadrature components. The "unwindowed" spectrum is calculated, and then a window is applied to the received pulses to reduce leakage of target doppler into adjacnt bins.

Assumptions:

$\phi := 5$ deg. (Maximum phase mismatch between I and Q channels)

$A := .5$ dB (Maximum amplitude mismatch between I and Q channels)

$A := 10^{\frac{A}{20}}$ $A = 0.9441$ (Convert to linear)

Calculations:

Frequency of the clutter (Hz): $f0 := \frac{PRF}{N} \cdot 0$ Hz $f0 = 0$ Hz

Frequency of the target (Hz): $f1 := \frac{PRF}{N} \cdot 2.5$ Hz $f1 = 2.34 \cdot 10^{3}$ Hz

Signal to Clutter Ratio: $SCR := ClutFiltRej - SubClutVis$ $SCR = -60$ dB

Relative linear mag: $m1 := 10^{\frac{SCR}{20}}$ $m1 = 0.001$

$i := 0..N-1$ $t_i := \frac{i}{PRF}$

$f_i := \cos\left(2 \cdot \pi \cdot f0 \cdot t_i\right) + m1 \cdot \cos\left(2 \cdot \pi \cdot f1 \cdot t_i\right)$ $g_i := \left(\cos\left(2 \cdot \pi \cdot f0 \cdot t_i + \frac{\pi}{2} + \frac{\pi \cdot \phi}{180}\right) + m1 \cdot \cos\left(2 \cdot \pi \cdot f1 \cdot t_i - \frac{\pi}{2} + \frac{\pi \cdot \phi}{180}\right)\right) \cdot A$

$h_i := f_i + (0 + i) \cdot g_i$

$H := cfft(h)$ (Compute the FFT of the unwindowed I&Q data)

$M := \text{floor}\left(\frac{f0}{\frac{PRF}{N}}\right)$ $\quad max := |H_M|$ (Compute the magnitude of this FFT and normalize the magnitude spectrum by the maximum value which is H_M in this case)

$H_i := \text{if}\left(\frac{|H_i|}{max} < 10^{-10}, -210, 20 \cdot \log\left(\frac{|H_i|}{max}\right) - ClutFiltRej\right)$

Now apply a Dolph window to the I&Q data to set the appropriate sidelobe level (SLL)

$SLL := -SCR + MinSIR$ $\quad SLL = 60$

$RR := 10^{\frac{SLL}{20}}$ $\quad A := \cosh\left[\left(\frac{1}{N-1}\right) \cdot \text{acosh}(RR)\right]$ (Calculate constant related to desired sidelobe level.)

$n := 1 .. \frac{N}{2}$ (Indices for calculation of Dolph coefficients)

$$Dolph_n := \sum_{q=n}^{\frac{N}{2}} \frac{(-1)^{\frac{N}{2}-q} \cdot A^{(2 \cdot q)-1} \cdot \left(q + \frac{N}{2} - 2\right)! \cdot \left[\left(2 \cdot \frac{N}{2}\right) - 1\right]}{(q-n)! \cdot (q+n-1)! \cdot \left(\frac{N}{2} - q\right)!}$$ (n must be even)

$x := 0 .. \frac{N}{2} - 1$

$W_x := Dolph_{\frac{N}{2}-x}$ $\quad W_{\frac{N}{2}+x} := Dolph_{x+1}$ (Assign the appropriate Taylor coefficient to each time sample.)

$hw_i := f_i \cdot W_i - (0 + i) \cdot g_i \cdot W_i$ (Weight the target samples with the Taylor coefficients.)

$HW := cfft(hw)$ (Compute the FFT of the windowed I&Q data

$max := |HW_M|$

$HW_i := \text{if}\left(\frac{|HW_i|}{max} < 10^{-10}, -210, 20 \cdot \log\left(\frac{|HW_i|}{max}\right) - ClutFiltRej\right)$ (Compute the normalized magnitude in dB of this FFT)

$HW_3 = -88.87$ dB	$HW_{13} = -95.85$ dB	$H_3 = -94.21$ dB	$H_{13} = -113.58$ dB
$HW_4 = -91.04$ dB	$HW_{12} = -90.33$ dB	$H_4 = -103.67$ dB	$H_{12} = -114.33$ dB
$HW_5 = -93.16$ dB	$HW_{11} = -93.17$ dB	$H_5 = -107.9$ dB	$H_{11} = -114.57$ dB

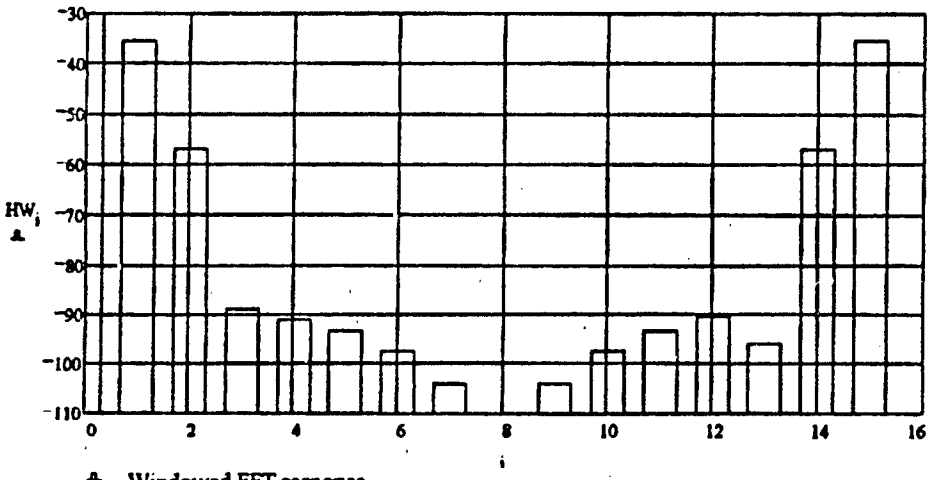

Windowed FFT response

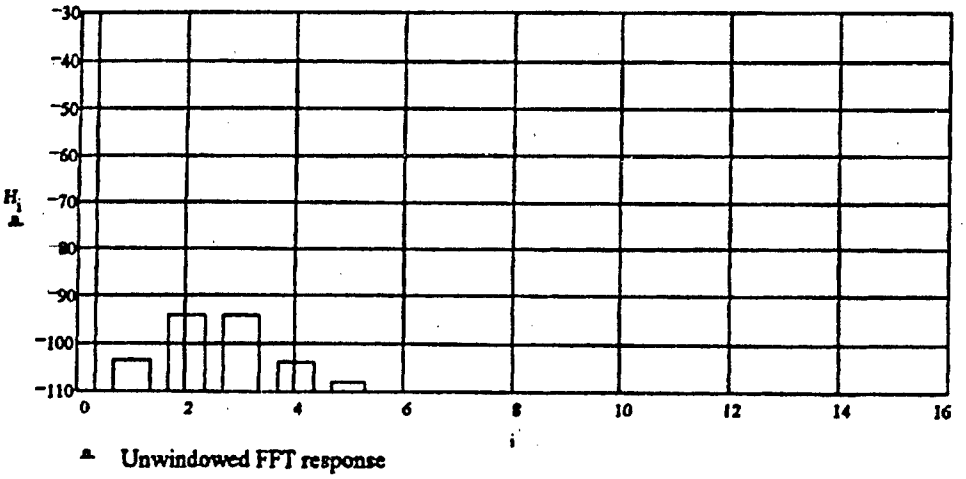

Unwindowed FFT response

The above windowed FFT response indicates the ability to see the target in the clutter and I/Q imbalances after clutter blanking. The target is minimal and at the lowest useable doppler frequency after clutter filtering and blanking.

Derivation of System Phase and Clutter Spectral Leakage Noise Floor

To optimize the receiver design, the clutter noise floor of the system should be specified such that it is a minimum number of dB below the achieveable thermal noise floor. 10 to 15 dB is typical. The clutter noise floor will be the result of the phase noise of the oscillators used in upconversion / downconversion chain of the radar as well as supply voltage ripple in the transmitter. The objective is to design the system so that the phase noise of the worst case oscillator is the limiting factor on the system's clutter phase noise. Usually it is the highest frequency oscillator. In some cases, a multiple stage upconversion scheme is used so that low frequency oscillators with superior phase noise performance can be used to arrive at the transmit frequency.

The analysis is started by modeling the phase noise envelope of the worst phase noise oscillator. A Bode plot of the oscillator skirt can be drawn using poles to mark the knee points in the curve. The Bode plot approach is used to derive a plot of L(f), the phase noise spectral density, which is defined as the ratio of the single sideband phase noise power per Hertz relative to the carrier power. The plot will be used to also set the maximum allowable total noise contributions from the other components in the exciter / transmitter chain.

Assumptions:

$n_1 := 1$ (Phase Noise pole order. 1 => 20 dB/decade, 0.5 => 10 dB/decade, ...)

$f_{c1} := 10$ Hz (Phase Noise carrier offset frequency)

$dBL1 := -75$ dBc/Hz (Maximum allowable phase noise magnitude @ fc1)

$n_2 := 0.0625$ (Phase noise pole order. 1 => 20 dB/decade, 0.5 => 10 dB/decade, ...)

$f_{c2} := 10000$ Hz (Phase Noise carrier offset frequency)

$dBL2 := -135$ dBc/Hz (Maximum allowable phase noise magnitude @ fc2)

$f_{break} := 10000$ (L(f) break frequency)

Calculations:

$f := 10, 1000 .. \frac{B_{comp}}{2}$ Hz (Phase noise skirt frequency range of interest)

$$f_{3dB1} := \frac{f_{c1}}{\sqrt{\frac{1}{\left(10^{\frac{dBL1}{10}}\right)^{\frac{1}{n_1}}} - 1}}$$ (Flicker phase noise 3dB frequency)

$f_{3dB1} = 0$ (Hz)

$$L_1(f) := \left[\frac{1}{1+\left(\frac{f}{f_{3dB1}}\right)^2}\right]^{-a1}$$ (Flicker noise average power per Hertz relative to carrier)

$$f_{3dB2} := \frac{f_{c2}}{\sqrt{\left(\frac{1}{10^{\frac{dBL2}{10}}}\right)^{\frac{1}{a2}} - 1}}$$ (White phase noise 3dB frequency)

$f_{3dB2} = 0$ (Hz)

$$L_2(f) := \left[\frac{1}{1+\left(\frac{f}{f_{3dB2}}\right)^2}\right]^{a2}$$ (White noise average power per Hertz relative to carrier)

$L(f) := if(f<10000, L_1(f), L_2(f))$ (Oscillator phase noise average power per Hertz relative to the carrier power, dBc/Hz)

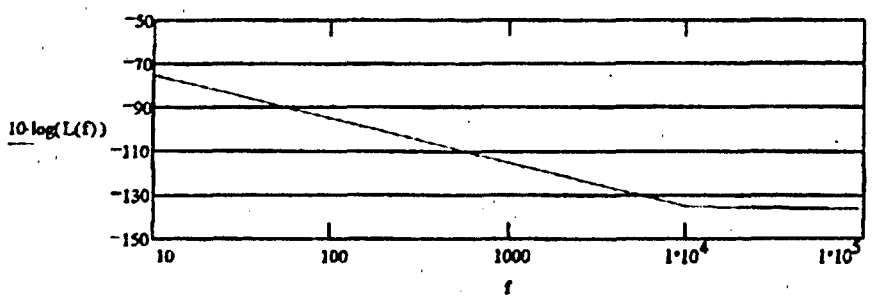

When a signal returns from a target and is downconverted by the same oscillator, some of the phase noise of the oscillator will be canceled due to correlation. This effect is known as the range correlation effect. The improvement in the phase noise skirt of the output waveform can be modeled for a given rang delay. In this example, the transmitter is the largest contributor to the transmitted noise floor level and thus the reange correlation effect does not apply.

$M := \frac{B_{comp}}{PRF}$ (number of spectral lines contained with pulsewidth's spectral mainlobe)

$\Delta f := \frac{PRF}{N}$ (bandwidth of an FFT bin in Hertz)

$m := 1 .. \frac{M - 1}{2}$ (clutter spectral line index)

$kk := 1 .. \frac{N - 2}{2}$ (FFT bin index)

First, the average noise power is computed relative to the carrier in an FFT bin's bandwidth which results from the clutter spectral line at the fundamental carrier frequency.

$Pcarrier_{kk} := \Delta f \cdot L(kk \cdot \Delta f)$ dBc (Average upper sideband phase noise power resulting from the carrier)

$Pcarrier_{N-kk} := Pcarrier_{kk}$ dBc (Average lower sideband phase noise power resulting from the carrier)

Next, the average power relative to the carrier in a bin's bandwidth which results from the replicas of the clutter spectral lines to the left (or negative frequencies) of the fundamental carrier frequency is added.

$$Pneg_{kk} := \sum_{m} \Delta f \cdot L(kk \cdot \Delta f + m \cdot PRF) \cdot \left| \frac{\sin\left[\pi \cdot \left[\frac{m \cdot PRF}{\left(\frac{B_{comp}}{2}\right)}\right]\right]}{\pi \cdot \left[\frac{m \cdot PRF}{\left(\frac{B_{comp}}{2}\right)}\right]} \right|^2$$

$$Pneg_{N-kk} := \sum_{m} \Delta f \cdot L((N - kk) \cdot \Delta f + (m - 1) \cdot PRF) \cdot \left| \frac{\sin\left[\pi \cdot \left[\frac{m \cdot PRF}{\left(\frac{B_{comp}}{2}\right)}\right]\right]}{\pi \cdot \left[\frac{m \cdot PRF}{\left(\frac{B_{comp}}{2}\right)}\right]} \right|^2$$

Finally, the average noise power relative to the carrier contribution from the replicas of the clutter spectral lines to the right (or positive frequencies) of the fundamental carrier is added. Again, the noise power is calculated in a bandwidth of an FFT bin.

$$Ppos_{kk} := \sum_{m} \Delta f \cdot L((N - kk)\cdot\Delta f + (m - 1)\cdot PRF)\cdot \left[\frac{\sin\left[\pi\cdot\left[\frac{m\cdot PRF}{\left(\frac{B_{comp}}{2}\right)}\right]\right]}{\pi\cdot\left[\frac{m\cdot PRF}{\left(\frac{B_{comp}}{2}\right)}\right]}\right]^2$$

$$Ppos_{N-kk} := \sum_{m} \Delta f \cdot L(kk\cdot\Delta f - m\cdot PRF)\cdot \left[\frac{\sin\left[\pi\cdot\left[\frac{m\cdot PRF}{\left(\frac{B_{comp}}{2}\right)}\right]\right]}{\pi\cdot\left[\frac{m\cdot PRF}{\left(\frac{B_{comp}}{2}\right)}\right]}\right]^2$$

$$Pnoise_{kk} := Pcarrier_{kk} + Pneg_{kk} - Ppos_{kk}$$

$$Pnoise_{N-kk} := Pcarrier_{N-kk} + Pneg_{N-kk} + Ppos_{N-kk}$$

$$kk := 0..N - 1$$

$$Pnoise_{kk} := if\left(Pnoise_{kk} < 10^{-15}, 10^{-15}, Pnoise_{kk}\right)$$

Decimation of the sampled waveform into range bins coherently aliases the phase noise in the kk^{th} doppler bin with the kk^{th} doppler bin of each PRF line within the pulse bandwidth. Decimation also coherently aliases the signal in the kk^{th} doppler bin with the kk^{th} doppler bin of each PRF line. Therefore, the signal to clutter phase noise ratio in each doppler bin remain unchanged through the decimation process.

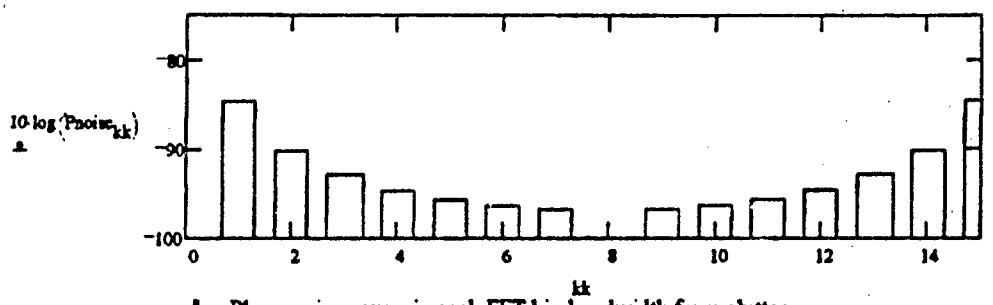

▲ Phase noise power in each FFT bin bandwidth from clutter

The subclutter visibility is also dependant upon the window applied to the range samples. A 60 dB Dolph window can be applied to clutter return samples that have been previously clutter notch attenuated by 30 dB to calculate the "windowed" spectrum. Based on the above clutter phase noise calculation and the following "windowed" clutter calculation, a total subclutter visibility may be specified.

Frequency of the clutter (Hz): $f0 := \frac{PRF}{N} \cdot 0 \quad Hz \quad f0 = 0$

$i := 0 .. N - 1 \qquad t_i := \frac{i}{PRF}$

$f_i := \cos(2 \cdot \pi \cdot f0 \cdot t_i)$ (In phase clutter signal.) $\quad g_i := \cos\left(2 \cdot \pi \cdot f0 \cdot t_i + \frac{\pi}{2}\right)$ (Quadrature clutter signal)

$h_i := f_i + (0 - i) \cdot g_i$

$H := cfft(h)$ (Compute the FFT of the unwindowed I&Q data)

$M := floor\left(\frac{f0}{\frac{PRF}{N}}\right) \qquad max := |H_M|$

(Compute the magnitude of this FFT and normalize the magnitude spectrum by the maximum value which is H_M in this case)

$H_i := if\left(\frac{|H_i|}{max} < 10^{-10}, -210, 20 \cdot \log\left(\frac{|H_i|}{max}\right) - ClutFiltRej\right)$

Now apply the Dolph window to the I&Q data.

$hw_i := f_i \cdot W_i - (0 + i) \cdot g_i \cdot W_i$

$HW := cfft(hw)$ (Compute the FFT of the windowed I&Q data)

$max := |HW_M|$

$$HW_i := if\left(\frac{|HW_i|}{max} < 10^{-10}, -210, 20\cdot\log\left(\frac{|HW_i|}{max}\right) - ClutFiltRej\right)$$ (Compute the normalized magnitude in dB of this FFT)

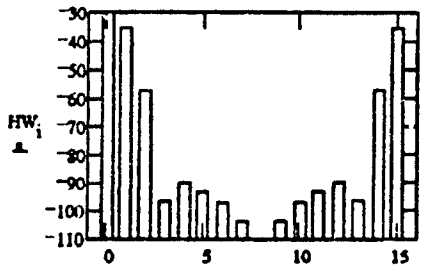

▲ Windowed Normalized Clutter

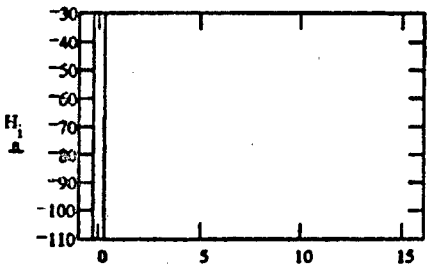

▲ Unwindowed Normalized Clutter

Comparing the previously calculated normalized clutter phase noise and the windowed normalized clutter, the subclutter visibility after clutter blanking may be safely specified as 90 dB. Therefore, any in band spurious signals from the transmitter and SAW devices must be less than the carrier in decibels by the sum of the required subclutter visibility and the minimum signal to interference ratio.

$SubCVis_{-i} := -SubClutVis$

$SubCVis_{RX_{tr}} = Pc_{RX_{tr}} - SubClutVis$ (Visibility relative to the calculated received clutter power.)

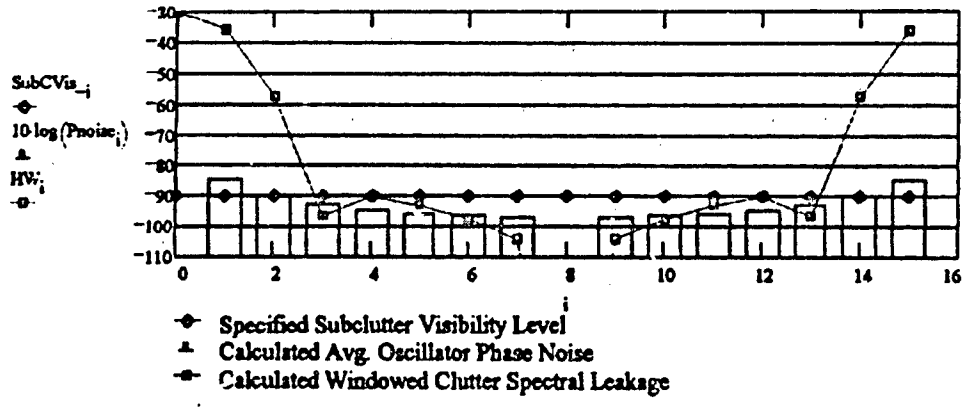

◆ Specified Subclutter Visibility Level
▲ Calculated Avg. Oscillator Phase Noise
Calculated Windowed Clutter Spectral Leakage

The above graph compares the specified subclutter visibility level, the calculated average oscillator phase noise and the window effects on the clutter. The maximum allowable phase noise from the components in the exciter chain may be specified to be 10 dB below the transmitter phase noise versus frequency. Therefore, the total transmitter noise including the noise contributions of phase, thermal, jitter and acoustic sources must be no greater than -85 dBc/Hz at 10 Hz away from the carrier and no greater than -145 dBc/Hz at 10 kHz away from the carrier.

Derivation of Overall System Detection Performance

The graph below exploits the results of all the previous calculations except AGC. The plots shows the expected receiver input levels for the 100 square meter target, the 1 square meter target and the calculate clutter return with its respective phase noise. They are compared to the receiver input level that would saturate the A/D converter and the minimum detectable signal.

$AGC_{low_{tr}} := Pmax_{RX} - 10$ dBm (Threshold of AGC operation)

$AGC_{hi_{tr}} = Pbig + 10$ dBm (Upper minimum limit of AGC operation)

$AGC := (Pbig - Pmax_{RX}) - 20$ $AGC = 59.2$ dB (Minimum required dynamic range of AGC with a 20 dB safety margin.)

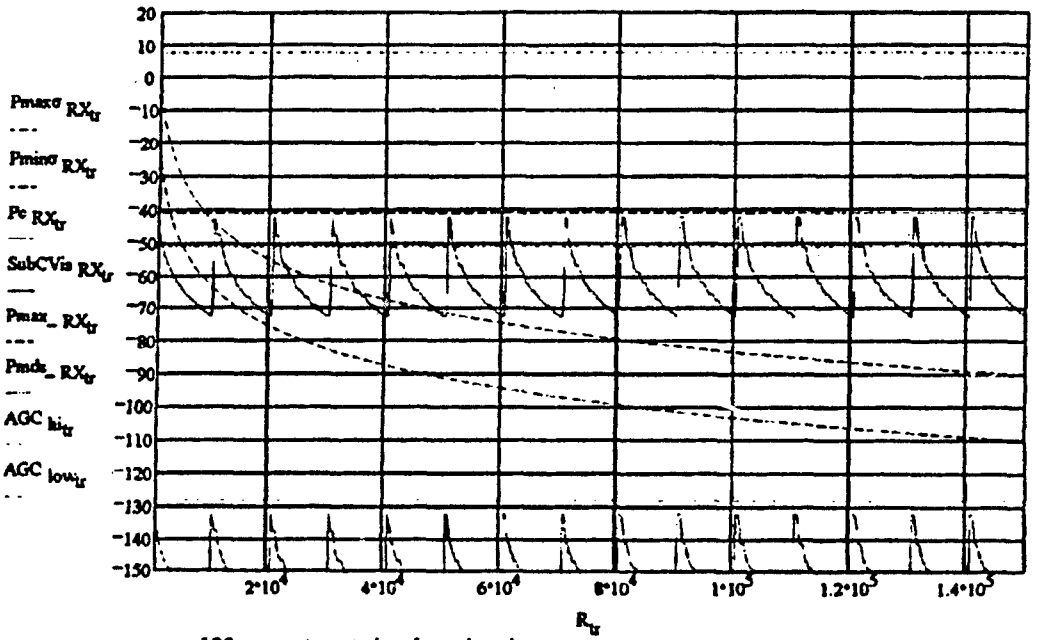

--- 100 sq. m. target signal receiver input vs. range
--- 1 sq. m. target signal receiver input vs. range
— Calculated received clutter power
— Specified visibility relative to clutter power received
--- Maximum receiver input to match A/D saturation level
··· Minimum detectable signal receiver input level
··· Upper minimum limit of receiver AGC operation
··· Lower threshold of receiver AGC operation

Representative High PRF Case

Receiver and Signal Processor Subsystem Performance Analysis

Specified Radar Parameters

$c = 3 \cdot 10^8$ m./sec. (velocity of light)

$f = 10 \cdot 10^9$ Hz (transmitted center frequency)

$\lambda := \frac{c}{f}$ m. (transmitted center frequency wavelength) $\lambda = 0.03$ m.

$R_{max} = 150000$ m. (maximum specified range)

$\sigma_{min} = 1$ sq. m. (minimum specified target cross-section area)

$P_t = 80000$ W. (transmitter output power)

$\tau_{pulse} = .75 \cdot 10^{-6}$ sec. (Expanded transmitted pulsewidth in seconds)

$B_{chirp} := 0 \cdot 10^6$ Hz (Pulse Compression Chirp Bandwidth)

PRF = 105000 Hz (transmitted pulse repition frequency)

DopBinBW = 900 Hz (Specified Doppler bin bandwidth)

$N := \text{floor}\left(\frac{PRF}{DopBinBW}\right)$ (Number of FFT Integrations = Number of frequency bins in a PRF)

N = 116

MinSIR = 0 dB (Required SIR for Pd and Pfa for Swerling I target)

$\tau_{comp} = \tau_{pulse}$ sec. (Compressed and weighted pulsewidth)

$B_{comp} = \frac{1}{\tau_{comp}}$ $B_{comp} = 1.33 \cdot 10^6$ Hz (Compressed and weighted pulse bandwidth)

SubClutVis := 95 dB (Specified subclutter visibility)

ClutFiltRej = 30 dB (Specified clutter filter rejection)

$k = 1.38 \cdot 10^{-23}$ watts/(deg.K * Hz) (Boltzman's constant)

F = 2.512 (Receiver Noise Figure = 4 dB)

$MaxSNR_{AD} := 75$ dB (Measured A/D signal-to-noise ratio)

Derivation of Receiver Gain

The receiver should be designed to amplify the signal as much as possible without increasing the noise flo of the system. This accomplished increasing the gain of the receiver until the noise in the receiver is equal to the noise floor introduced by the A/D converter. Therefore, to calculate the receiver gain, the noise pow introduced into the system by the A/D converter must first be calculated.

Assumptions:

$V_{pp} := 2.0$ v. (Maximum peak-to-peak voltage level for converter)

$R_{load} := 50$ ohms (A/D Converter Input Impedance)

$T := 290$ deg. Kelvin (ambient temperature)

$T_A := 100$ deg. Kelvin (antenna noise temperature)

$L_A := 1.5849$ (losses between the antenna and receiver = 2.0 dB)

$L_{mm} := 1.4125$ (Mismatched receiver S/N ratio loss = 1.5 dB)

Calculations:

$V_{rms} := \frac{V_{pp}}{2 \cdot \sqrt{2}}$ $V_{rms} = 0.71$ v. (Maximum A/D RMS voltage)

$Pmax_{AD} := \frac{V_{rms}^2}{R_{load}}$ $Pmax_{AD} = 0.01$ W. (Maximum A/D average power = 10 dBm)

$Pfloor_{AD} := 10 \cdot \log\left(\left|\frac{Pmax_{AD}}{10^{-3}}\right|\right) - MaxSNR_{AD}$ $Pfloor_{AD} = -65$ dBm (A/D noise floor)

$Pfloor_{AD} := 10^{-3} \cdot 10^{\frac{Pfloor_{AD}}{10}}$ W (Convert from dBm units to Watts)

It is assumed that the noise power in the receiver measured within the bandwidth of the pulse. Therefore, t noise power incident on the A/D converter is given by:

$$G_0 := \frac{Pfloor_{AD} \cdot L_A \cdot (\tau_{pulse} \cdot B_{comp})}{k \cdot [T \cdot (L_A \cdot F - 1) + T_A] \cdot B_{comp} \cdot L_{mm}}$$

(Receiver Gain to match Receiver Noise Floor to A/D Noise Floor given antenna noise temp., loss between receiver and antenna, SAW filter losses and the receiver noise figure.)

$10 \cdot \log(G_0) = 43.01$ dB

Derivation of Receiver Pre-AGC Dynamic Range

Having calculated the receiver gain, the maximum input to the receiver can now be calculated by removing the calculated gain of the receiver from the maximum input power to the A/D converter.

Assumptions:

None

Calculations:

$$Pmax_{AD} = 10\log\left(\frac{Pmax_{AD}}{.001}\right) \quad dBm$$

$$Pmax_{RX} = Pmax_{AD} - 10\log(G_o) \qquad Pmax_{RX} = -33.01 \quad dBm$$

The minimum signal input to the receiver such that the signal at the A/D converter input is equal to the noise floor may be calculated by removing the maximum SNR of the A/D from the maximum input power to the receiver.

$$Pfloor_{RX} = Pmax_{RX} - MaxSNR_{AD} \qquad Pfloor_{RX} = -108.01 \quad dBm$$

Derivation of the Clutterless Receiver Automatic Gain Control Requirements

The receiver automatic gain control (AGC) will serve to prevent the receiver from being saturated by excessive clutter returns or close range targets. The AGC will also provide for constant angle tracking sensitivity (volts per degree error) over large signal dynamic range variations and target range.

The AGC will be applied to the middle stages of the amplifier chain to preserve the receiver noise figure and the maximum undistorted output of the final stage. The AGC control signal will be derived from the matched filter output. The AGC will control the acquisition and track sum channel as well as the difference azimuth and elevation track channel gains.

To determine the requirements of the AGC, some estimate of the level of incoming signals must be made. Therefore, a discussion of target signal dynamic range is included. Assuming full receiver gain, a comparison of the receiver input that will saturate the A/D converter to the expected target signal dynamics will provide the minimum requirements of the AGC.

Assumptions:

$\tau_{recovery} = 10^{-6}$ sec. (Duplexer recovery time)

$\sigma_{max\_} = 100$ m^2 (Maximum expected target RCS)

$G_A = 20000$ (Antenna Gain = 43 dBi)

$L_{xmtr} = 1.5849$ (Loss between the transmitter and the antenna = 2.0 dB)

$L_{2way} = 1.2589$ (Round trip loss between antenna and target = 1.0 dB)

Calculations:

Target Dynamic Range

The minimum target detection range is determined by the duplexer recovery time and the transmitted pulsewidth.

$$R_{min} = c\cdot\frac{\tau_{pulse} - \tau_{recovery}}{2} \qquad R_{min} = 262.5 \text{ m. (Minimum detection range of the radar)}$$

The radar returns of the target at the minimum through the maximum ranges can now be calculated and compared to the maximum and minimum signals the A/D can handle.

$tr := 1 .. \frac{R_{max}}{1000}$ (target range index)

$R_{tr} := 1000 \cdot tr \ m.$ (target range)

$Pmax\_RX_{tr} := Pmax_{RX}$ (maximum unattenuated receiver input for A/D saturation)

$Pfloor\_RX_{tr} := Pfloor_{RX}$ (minimum unattenuated receiver input to match A/D noise floor)

$$Pmin\sigma_{RX_{tr}} := \frac{P_t \cdot G_A^2 \cdot \sigma_{min} \cdot \lambda^2}{(4 \cdot \pi)^3 \cdot (R_{tr})^4 \cdot L_{xmtr} \cdot L_{2way} \cdot L_A} W.$$ (Power received from smallest specified target (.1 sq. m.) versus required tracking range.)

$$Pmin\sigma_{RX_{tr}} := 10 \cdot \log\left(\frac{Pmin\sigma_{RX_{tr}}}{.001}\right) dBm$$ (Convert to dBm units)

$$Pmax\sigma_{RX_{tr}} := \frac{P_t \cdot G_A^2 \cdot \sigma_{max\_} \cdot \lambda^2}{(4 \cdot \pi)^3 \cdot (R_{tr})^4 \cdot L_{xmtr} \cdot L_{2way} \cdot L_A} W.$$ (Power received from largest expected target (100 sq. m.) versus required tracking range.)

$$Pmax\sigma_{RX_{tr}} := 10 \cdot \log\left(\frac{Pmax\sigma_{RX_{tr}}}{.001}\right) dBm$$ (Convert to dBm units)

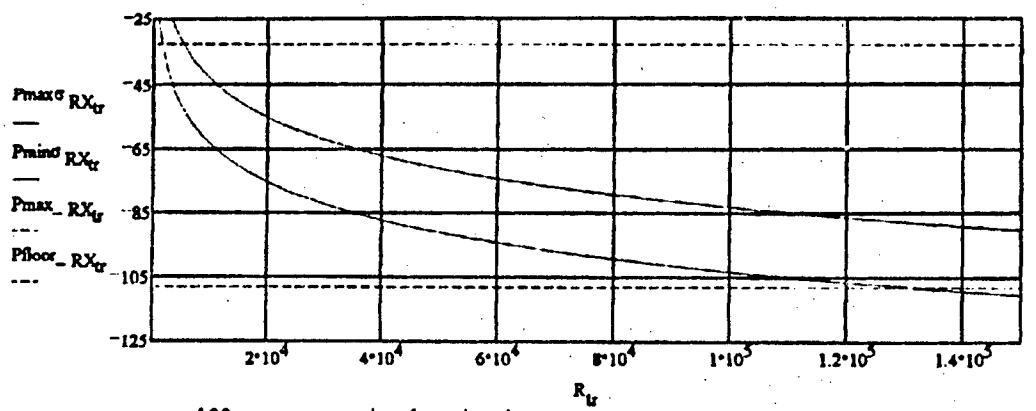

— 100 sq. m. target signal receiver input vs. range
— 1 sq. m. target signal receiver input vs. range
--- maximum receiver input to match A/D saturation level
--- minimum receiver input to match noise floor

AGC Minimum Requirements

$$Pbig := \frac{P_t \cdot G_A^2 \cdot \sigma_{max\_} \cdot \lambda^2}{(4\cdot\pi)^3 \cdot (R_1)^4 \cdot L_{xmtr} \cdot L_{2way} \cdot L_A}$$ W. (Power received from largest expected target (100 sq. m.) at minimum range.)

$Pbig := 10 \cdot \log\left(\frac{Pbig}{.001}\right)$ dBm (Convert to dBm units) Pbig = -3.38 dBm

$AGC := (Pbig - Pmax_{RX}) + 20$ AGC = 49.63 dB (Minimum required dynamic range of AGC with a 20 dB safety margin.)

The above calculation assumes that the gain of the receiver is set to the value that matches the noise floor of the receiver to that of the A/D converter, that the threshold for AGC operation is 10 dB less than the A/D saturation receiver input level and that the maximum receiver input for AGC operation is 10 dB greater than that of the largest target at the shortest range.

Derivation of the Minimum Detectable Signal

Previously, the receiver gain was calculated to equalize the noise power in the receiver measured within the 4 dB bandwidth of the compressed pulsewidth to the noise power in the A/D converter also measured in a pulsewidth of bandwidth. The effect of range gating implemented in the form of decimating the digitized range lines will be to alias the thermal noise in the pulsewidth of receiver bandwidth into the PRF bandwidth of the FFT. The FFT will divide this noise power evenly into N bins of bandwidth, where N is the number of pulses in the FFT. The target Doppler which is contained in only one bin for I/Q processing will compete against only one bin of noise. Therefore, the effective system thermal noise floor must be modified.

Assumptions:

None

Calculations:

$$\text{thermal}_{\text{noise}} = \frac{\text{Pfloor}_{\text{AD}}}{N} \qquad \text{(Noise Power in a FFT bin of bandwidth)}$$

$$10 \cdot \log\left(\frac{\text{thermal}_{\text{noise}}}{10^{-3}}\right) = -85.64 \qquad \text{dBm}$$

Therefore, given the effective processing gain, N, for the number of pulses used in the FFT, the minimum detectable signal power which will be detected by the radar can be calculated. The range of signal powers is given by the dynamic range of the A/D converter plus the coherent processing gain.

$$DR_{\text{system}} = \text{MaxSNR}_{\text{AD}} + 10 \cdot \log(N) - \text{MinSIR} \quad \text{dB}$$

(Detectable target cross section dynamic range)

$$DR_{\text{system}} = 95.64 \quad \text{dB}$$

$$\text{Pmds}_{\text{AD}} = \text{Pmax}_{\text{AD}} - DR_{\text{system}} \quad \text{dBm}$$

(Minimum detectable signal power at the input to the A/D converter.)

$$\text{Pmds}_{\text{AD}} = -85.64 \quad \text{dBm}$$

$$\text{Pmds}_{\text{RX}} = \text{Pmds}_{\text{AD}} - 10 \cdot \log(G_0)$$

(Minimum detectable signal power at the input to the receiver.)

$$\text{Pmds}_{\text{RX}} = -128.65 \quad \text{dBm}$$

$$\text{Pmds\_RX}_{tr} = \text{Pmds}_{\text{RX}}$$

Derivation of Sidelobe and Mainbeam Clutter Power

The return signals for a pulsed radar system include scatter from not only the desired targets but from undesired objects as well. These undesired objects are collectively called clutter and can include things such as the ground, structures on the ground, birds, insects, chaff, weather precipitation and many others. It is a well documented fact that modelling clutter for radar analysis is difficult at best and usually takes the form of a collection of simplifying assumptions with documented ground reflectivities. This analysis will also make several assumptions that will result in a calculatable effective clutter radar cross section.

The simplifying assumptions made here include:

1. There will be no terrestrial structures either natural or man made present within the radar's field of view. Any natural vegetation or ground surface irregularities will be accounted for with the assumed ground reflectivity.
2. There will be no airborne clutter such as birds, precipitation, etc.
3. The antenna lobe structure will be assumed to be perfectly symmetric in a volume of revolution around boresight in the non-scanned mode. In the scanned mode, the resultant grating lobes will necessarily be accounted for.
4. The antenna lobes of interest will illuminate the ground uniformly within their half-power beamwidths.

The cross section of ground seen by the radar is a function of the transmit pulsewidth and the antenna beamwidth. For distances close to the radar, the antenna beamwidth limits the illuminated ground area. For distances far from the radar, the pulsewidth of the transmitted signal limits the illuminated area. For airborne radar, the determination of which case to use is made by using the calculation method that produces the maximum ground return. The scenarios are different for ground based radar and airborne radar . For airborne radar, if the main lobe is pointing down, the main lobe is typically the most significant ground illuminator. The ground based radar is typically concerned with airborne targets. As such, the main lobe is usually above horizon and the only contributors to the ground clutter are the sidelobes. Any sidelobes that will produce ground returns will be those that are physically directed below horizontal. The radar antenna will only be a few meters off the ground. Any contributing ground patches will be the same distance from the antenna as the target is from the antenna. This is due to range gating. Range gating limits the received clutter energy. Only the patches of ground illuminated by the sidelobes that are within the same "range bin" as the target will contribute to the clutter power competing with the target. Since the target range will be significantly larger than the height of the antenna, the patch size will be both pulsewidth and beamwidth limited. It will be radially pulsewidth limited and azimuthally beamwidth limited.

Assumptions:

$HA := 23$ m. (antenna height above ground)

$\theta_T := 0.5$ deg. (target angle above horizon)

$N_{SL} := 6$ (highest order antenna sidelobe effectively contributing to clutter)

$n_{SL} := 1..N_{SL}$ (nth sidelobe contributing to clutter)

$Gsl_0 := 10^{\frac{10\cdot\log(G_A)-0}{10}}$ (Main Beam Gain) $10\cdot\log(Gsl_0) = 43.01$

$\theta bw_0 := .85$ deg. (Main Beam HPBW)

$\phi pa_0 := 0$ deg. (Main Beam Pointing Angle)

$Gsl_1 := 10^{\frac{10\cdot\log(G_A)-24}{10}}$ (1st Sidelobe Gain)

$\theta bw_1 := .429$ deg. (1st SL HPBW)

$\phi pa_1 := 1.25$ deg. (1st SL Pointing Angle)

$Gsl_2 := 10^{\frac{10\cdot\log(G_A)-32}{10}}$ (2nd Sidelobe Gain)

$\theta bw_2 := .536$ deg. (2nd SL HPBW)

$\phi pa_2 := 2.2$ deg. (2nd SL Pointing Angle)

$Gsl_3 := 10^{\frac{10\cdot\log(G_A)-32}{10}}$ (3rd Sidelobe Gain)

$\theta bw_3 := 1.$ deg. (3rd SL HPBW)

$\phi pa_3 := 24.5$ deg. (3rd SL Pointing Angle)

$Gsl_4 := 10^{\frac{10\cdot\log(G_A)-32.5}{10}}$ (4th Sidelobe Gain)

$\theta bw_4 := .643$ deg. (4th SL HPBW)

$\phi pa_4 := 3.125$ deg. (4th SL Pointing Angle)

$Gsl_5 := 10^{\frac{10\cdot\log(G_A)-32.5}{10}}$ (5th Sidelobe Gain)

$\theta bw_5 := 18.5$ deg. (5th SL HPBW)

$\phi pa_5 := 4.285$ deg. (5th SL Pointing Angle)

$Gsl_6 := 10^{\frac{10\cdot\log(G_A)-34}{10}}$ (6th Sidelobe Gain)

$\theta bw_6 := 1.$ deg. (6th SL HPBW)

$\phi pa_6 := 26.5$ deg. (6th SL Pointing Angle)

$\sigma_0 := 0.01$ (Ground reflection coefficient = -20 dB)

Calculations:

A high PRF radar exhibits ambiguous range. As such the clutter power received competing with the target is the power received from all the ambigous ranges. Therefore, targets at a far range will compete with close range, mid-range and far range clutter. Mathematically, the range can be broken into sections of length equal to the unambigous range.

$R_{un} := \frac{c}{2 \cdot PRF}$ m. (Unambiguous range.) $R_{un} = 1.43 \cdot 10^3$ m.

nseg = 35 (Number of segments the unambiguous range is divided into.)

$segL := \frac{R_{un}}{nseg}$ m. (Segment length) segL = 40.82 m.

$m_r = 1 .. floor\left(\frac{R_{max}}{R_{un}}\right)$ (Unambiguous range length index.) $floor\left(\frac{R_{max}}{R_{un}}\right) = 104$

$n_r = 1 .. nseg$ (Range index within each unambiguous range length segment.)

$cR_{m_r,n_r} := \left[\left(m_r - 1\right) \cdot R_{un}\right] + \left(n_r \cdot segL\right)$ m. (Range for clutter calculations which will be equated with the target range.)

$HT_{m_r,n_r} := HA - \left[cR_{m_r,n_r} \cdot \sin\left(\theta_T \cdot \left(\frac{2 \cdot \pi}{360}\right)\right)\right]$ m. (Target altitude above ground. *Clutter range is equal to range of target from antenna.*)

SEP = the physical seperation between the target and clutter point

The antenna, target and clutter point form a plane. The radius from the antenna to the target and clutter point = cR. The physical separation between the target and clutter point can be calculated by:

$$\sin\left[\frac{\phi ps_{n_{SL}}}{2} \cdot \left(\frac{2 \cdot \pi}{360}\right)\right] = \frac{\left(\frac{SEP\left(n_{SL}, m_r, n_r\right)}{2}\right)}{cR_{m_r,n_r}}$$

or

$$SEP\left(n_{SL}, m_r, n_r\right) := 2 \cdot cR_{m_r,n_r} \cdot \sin\left[\frac{\phi ps_{n_{SL}}}{2} \cdot \left(\frac{2 \cdot \pi}{360}\right)\right]$$ m. (separation between target and clutter patch)

When viewed from above, the apparent angle between the clutter patch and the target with the antenna at the vertex is a function of :

$$\theta tilt(n_{SL}, m_r, n_r) := if\left(n_{SL} > 0, asin\left(\frac{HT_{m_r,n_r}}{SEP(n_{SL}, m_r, n_r)}\right), 0\right) \text{ rad.}$$

(Since the separation is fixed by range and sidelobe angle, an argument greater than one would indicate the invalidity of the sidelobe causing clutter return for a target of the indicated range and height.)

$$\theta app(n_{SL}, m_r, n_r) := if\left(n_{SL} > 0, if\left(\left|\frac{HT_{m_r,n_r}}{SEP(n_{SL}, m_r, n_r)}\right| < 1, \psi s_{n_{SL}} \cdot \cos(\theta tilt(n_{SL}, m_r, n_r)), 0\right), 0\right) \cdot deg.$$

The tilt angle is the angle subtended by the ground and the line between the clutter patch and target.

The apparent distance from the antenna to the clutter point when viewed from above is a function of:

$$\theta G_{m_r,n_r} := if\left(\frac{HA}{cR_{m_r,n_r}} < 1, asin\left(\frac{HA}{cR_{m_r,n_r}}\right), \frac{\pi}{2}\right) \text{ rad.}$$

$$Rcp_{m_r,n_r} := cR_{m_r,n_r} \cdot \cos(\theta G_{m_r,n_r}) \text{ m.}$$ (apparent distance from antenna to the clutter patch when viewed from above.)

For the pulsewidth limited case, the main beam ground clutter return may be calculated as follows. The intersection of the ground and main beam forms a hyperbola.

$$a := HA \cdot \cot\left(\frac{2 \cdot \pi}{360} \cdot \frac{\theta bw_0}{2}\right)$$ (Half length of the major axis which is the seperation between origin which is the antenna location and the hyperbola vertex which is the closest ground point which is illuminated by the main beam.)

$b := HA$ (Half length of the minor axis.)

In rectangular coordinates, assuming the center is the origin, the equation for a hyperbola is given as:

$$\frac{x^2}{a^2} - \frac{y^2}{b^2} = 1$$

$$y_{T_{m_r,n_r}} := b \cdot \sqrt{\frac{(Rcp_{m_r,n_r})^2}{a^2} - 1} \text{ m.}$$ (Y axis extent of hyperbola assuming target along x axis.)

$$\gamma_{m_r,n_r} := 2 \cdot atan\left(\frac{y_{T_{m_r,n_r}}}{Rcp_{m_r,n_r}}\right) \text{ rad.}$$ (Azimuth angular coverage of ground clutter patch of main beam.)

$$mbAcp_{m_r,n_r} := if\left(\frac{HA}{cR_{m_r,n_r}} < 1, if\left(Rcp_{m_r,n_r} > a, \frac{c \cdot \tau_{comp}}{2 \cdot \cos(\theta G_{m_r,n_r})} \cdot \frac{\gamma_{m_r,n_r}}{2 \cdot \pi} \cdot Rcp_{m_r,n_r}, 0\right), 0\right)$$

For the pulsewidth limited case, a single illuminated patch size is given by:

$$Acp(n_{SL}, m_r, n_r) := if\left[\left(\frac{HT_{m_r,n_r}}{SEP(n_{SL}, m_r, n_r)}\right) < 1, \left[\frac{\left(\frac{c \cdot \tau_{comp}}{2}\right)}{\cos(\theta G_{m_r,n_r})} \cdot cR_{m_r,n_r} \cdot \theta bw_{n_{SL}} \cdot \left(\frac{2 \cdot \pi}{360}\right)\right], 0\right] \quad m^2$$

There will be two identical patches based on antenna sidelobe symmetry. Therefore, the total clutter patch area for a sidelobe pair can be described by:

$$Acp(n_{SL}, m_r, n_r) := if\left[n_{SL} > 0, if\left[\left(\frac{HT_{m_r,n_r}}{SEP(n_{SL}, m_r, n_r)}\right) < 1, \frac{c \cdot \tau_{comp} \cdot cR_{m_r,n_r} \cdot \theta bw_{n_{SL}}}{\cos(\theta G_{m_r,n_r})} \cdot \left(\frac{2 \cdot \pi}{360}\right), 0\right], mbAcp_{m_r,n_r}\right]$$

The ground reflectivity varies as a function of terrain, structures, ground conductivity, ground dielectric constant, frequency, grazing angle and vegetation. There have been numerous studies documented to determine the average ground clutter reflection coefficient. For Ku band, a generous reflection coefficient is 0.01 or -20 dB.

$\sigma_o := .01$

Therefore, for the sidelobes considered, the total effective ground clutter RCS may be described by:

$$\sigma c_{m_r,n_r} := \sigma_o \cdot \sum_{n_{SL}} Acp(n_{SL}, m_r, n_r) \quad m^2$$

The total power returned to the receiver from the clutter patches may be computed using the radar range equation. Since each sidelobe pair corresponds to different gain levels, the total effective ground clutter calculated above must be modified in the range equation.

The clutter returns from all the ambiguous ranges must be folded into the clutter power received for the first unambiguous range segment. Beyond that segment, the clutter power competing with the target energy will be equivalent for each following unambiguous range length segment.

$$mnPc_{RX_{n_r}} := \frac{P_t \cdot \lambda^2 \cdot \sigma_o}{(4 \cdot \pi)^3} \cdot \sum_{n_{SL}} (Gsl_{n_{SL}})^2 \cdot \sum_{m_r} if\left[cR_{m_r,n_r} > R_{min}, \frac{Acp(n_{SL}, m_r, n_r)}{(cR_{m_r,n_r})^4}, 0\right] \quad W.$$

$$Pc_{RX_{kr}} := mnPc_{RX_{floor}\left[\left(\frac{R_{kr}}{R_{un}} - floor\left(\frac{R_{kr}}{R_{un}}\right)\right) \cdot nscg + 1\right]}$$

$$Pc_{RX_{tr}} := if\left(Pc_{RX_{tr}} > 0, 10 \cdot \log\left(\frac{Pc_{RX_{tr}}}{.001}\right), -200\right) \quad dBm$$

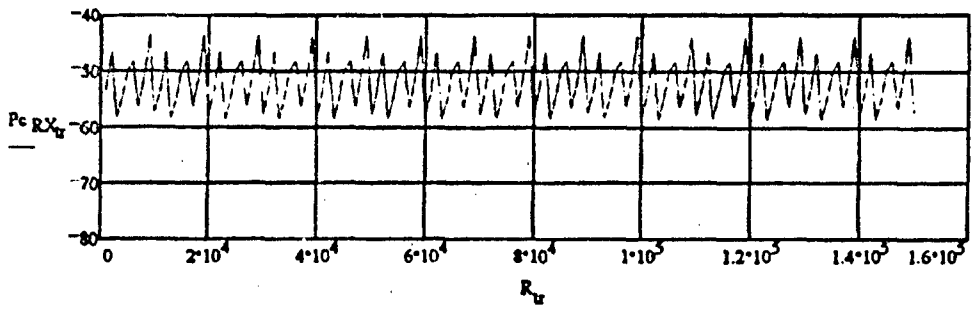

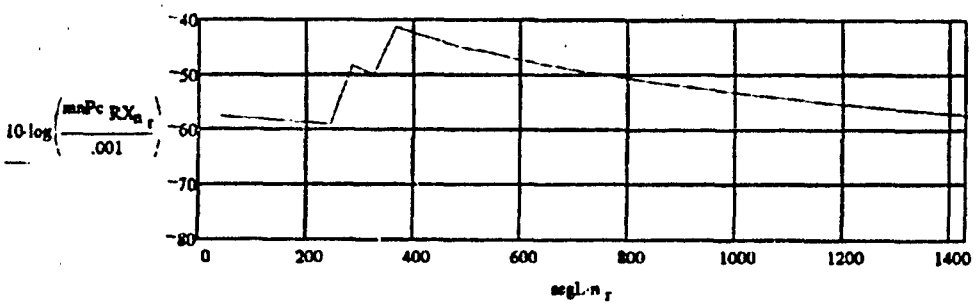

Derivation of Spurious False Target Power Levels

Spurious signals in a radar of sufficient magnitude will appear as false targets. The spurious signals may be caused by a variety of sources such as transmitter harmonics, transmitter spurious signals, transmitter amplitude and phase variations over the pulse bandwidth, I/Q detector phase and amplitude imbalances, linear frequency modulation (LFM) non-linearities, etc. Once the effects of I/Q imbalances and windowing are known, the transmitter spurious signals can be specified to be below the maximum acceptable level. Transmitter harmonics are filtered. The pulse bandwidth will only be a small percentage of the transmitter bandwidth. Variations over the pulse bandwidth will be negligible. The spurs resulting from LFM non-linearities may be accounted for by the SAW device manufacturer.

This example considers a clutter signal and a target signal at the minimum doppler frequency which is 65 dB below the clutter signal. The minimum doppler frequency is the lowest doppler frequency detectable following clutter blanking. Thus, this is the worst case clutter and target return acceptable to the radar. The composite signal is broken into in-phase and quadrature components. The "unwindowed" spectrum is calculated, and then a 65 dB Taylor window is applied to the received pulses after clutter attenuation of 30 dB to reduce leakage of target doppler into adjacnt bins.

Assumptions:

$\phi := 5$ deg. (Maximum phase mismatch between I and Q channels)

$A := .5$ dB (Maximum amplitude mismatch between I and Q channels)

$A := 10^{\frac{A}{20}}$ $A = 0.9441$ (Convert to linear)

Calculations:

Frequency of the clutter (Hz): $f0 := \frac{PRF}{N} \cdot 0.$ Hz $f0 = 0$ Hz

Frequency of the target (Hz): $f1 := \frac{PRF}{N} \cdot 3.5$ Hz $f1 = 3.17 \cdot 10^{3}$ Hz

Signal to Clutter Ratio After Clutter Attenuation: $SCR := ClutFiltRej - SubClutVis$ $SCR = -65$ dB

Relative linear mag: $m1 := 10^{\frac{SCR}{20}}$ $m1 = 5.6234 \cdot 10^{-4}$

$i := 0..N-1$ $t_i := \frac{i}{PRF}$

$f_i := \cos(2 \cdot \pi \cdot f0 \cdot t_i) + m1 \cdot \cos(2 \cdot \pi \cdot f1 \cdot t_i)$ $g_i := \left(\cos\left(2 \cdot \pi \cdot f0 \cdot t_i - \frac{\pi}{2} - \frac{\pi \cdot \phi}{180}\right) + m1 \cdot \cos\left(2 \cdot \pi \cdot f1 \cdot t_i + \frac{\pi}{2} + \frac{\pi \cdot \phi}{180}\right)\right) \cdot A$

$h_i := f_i + (0 - i) \cdot g_i$

$H := cfft(h)$ (Compute the FFT of the unwindowed I&Q data)

$M := \text{floor}\left(\frac{f0}{\frac{PRF}{N}}\right)$ $\quad max := |H_M|$

(Compute the magnitude of this FFT and normalize the magnitude spectrum by the maximum value which is H_M in this case.)

$H_i := \text{if}\left(\frac{|H_i|}{max} < 10^{-10}, -210, 20 \cdot \log\left(\frac{|H_i|}{max}\right) - ClutFiltRej\right)$

Now apply a Taylor window to the I&Q data to set the appropriate sidelobe level (SLL)

$SLL := -SCR - MinSIR \quad SLL = 65$

$nbar := 10$ (Number of sidelobes held at the desired level.)

$RR := 10^{\frac{SLL}{20}} \quad A := \frac{\text{acosh}(RR)}{\pi}$ (Calculate constant related to desired sidelobe level.)

$$\sigma := \frac{nbar}{\sqrt{A^2 - \left(nbar - \frac{1}{2}\right)^2}}$$ (Scaling factor)

$m := 1..nbar - 1 \quad n := 0..nbar - 1 \quad n1 := 1..nbar - 1$ (Indices for calculation of Taylor coefficients)

$$F_n := \frac{((nbar-1)!)^2 \cdot \prod_m \left[1 - \frac{n^2}{\sigma^2 \cdot \left[A^2 + \left(m - \frac{1}{2}\right)^2\right]}\right]}{(nbar - 1 + n)! \cdot (nbar - 1 - n)!}$$

$x := 0, 1..\frac{N}{2} - 1$ (Taylor coefficient index)

$L := N - 1$ (Total length of the number of time samples)

$$Taylor_x := \frac{1}{2 \cdot x} \cdot \left[F_0 - 2 \cdot \sum_{n1} F_{n1} \cdot \cos\left[\frac{n1 \cdot \pi \cdot \left(x + \frac{1}{2}\right)}{\left(\frac{L}{2}\right)}\right]\right]$$ (Calculate the Taylor coefficients.)

$$\eta := \frac{1}{F_0 + 2 \cdot \sum_{n1} (F_{n1})^2} \quad \eta = 0.63 \quad 20 \cdot \log(\eta) = -4.08 \text{ dB}$$ (Efficiency of the Taylor weighting)

$W_x := \text{Taylor}_{\left(\frac{N}{2}-1\right)-x}$ $W_{\left(\frac{N}{2}\right)+x} := \text{Taylor}_x$ (Assign the appropriate Taylor coefficient to each time sample.)

$hw_i := f_i \cdot W_i + (0 - i) \cdot g_i \cdot W_i$ (Weight the target samples with the Taylor coefficients.)

$HW := \text{cfft}(hw)$ (Compute the FFT of the windowed I&Q data

$max := |HW_M|$ $max = 1.71$ $M = 0$

$HW_i := \text{if}\left(\frac{|HW_i|}{max} < 10^{-10}, -210, 20 \cdot \log\left(\frac{|HW_i|}{max}\right) - ClutFiltR_{i,j}\right)$ (Compute the normalized magnitude in dB of this FFT)

$HW_4 = -94.46$ dB	$HW_{112} = -99.57$ dB	$H_4 = -99.19$ dB	$H_{112} = -119$ dB
$HW_5 = -100.53$ dB	$HW_{111} = -101.08$ dB	$H_5 = -108.71$ dB	$H_{111} = -122.41$ dB
$HW_6 = -105.46$ dB	$HW_{110} = -105.48$ dB	$H_6 = -113.12$ dB	$H_{110} = -123.82$ dB

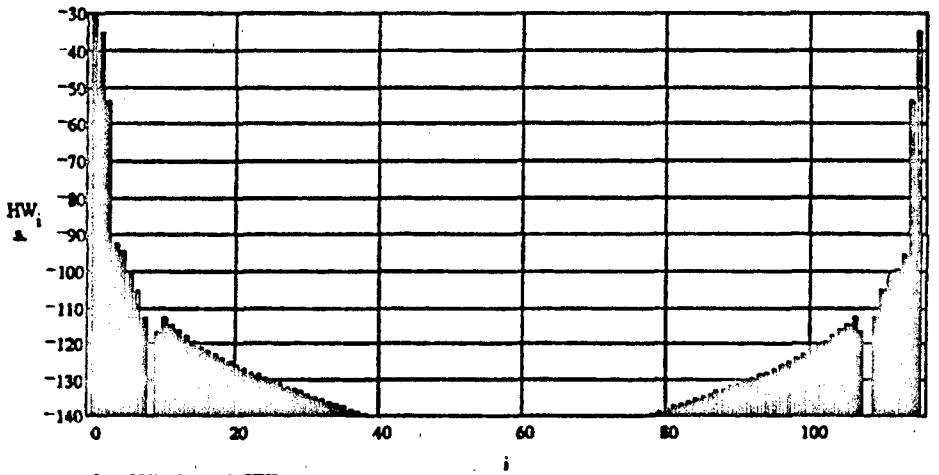

▲ Windowed FFT response

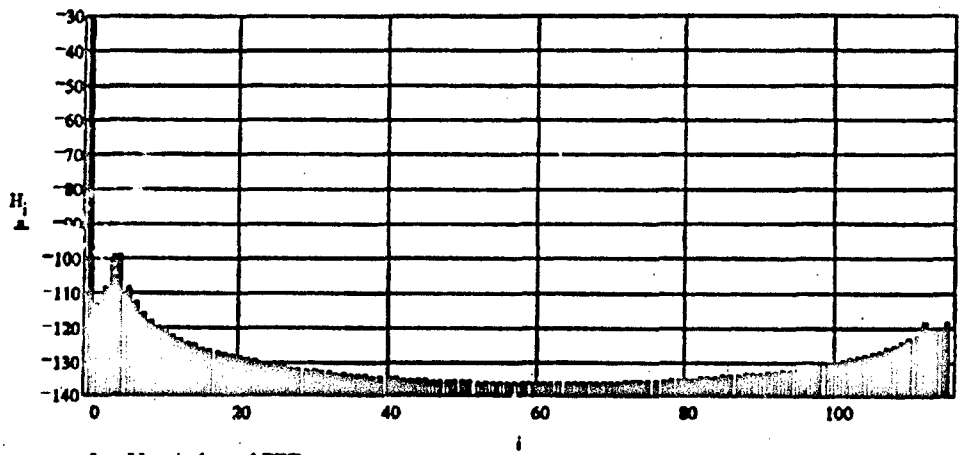

▲ Unwindowed FFT response

The above windowed FFT response indicates the ability to see the target in the clutter and I/Q imbalances after clutter blanking. The target is minimal and at the lowest useable doppler frequency after clutter attenuation.

Derivation of System Phase and Clutter Spectral Leakage Noise Floor

To optimize the receiver design, the clutter noise floor of the system should be specified such that it is a minimum number of dB below the achieveable thermal noise floor. 10 to 15 dB is typical. The clutter noise floor will be the result of the phase noise of the oscillators used in upconversion / downconversion chain of the radar as well as supply voltage ripple in the transmitter. The objective is to design the system so that the phase noise of the worst case oscillator is the limiting factor on the system's clutter phase noise. Usually it is the highest frequency oscillator. In some cases, a multiple stage upconversion scheme is used so that low frequency oscillators with superior phase noise performance can be used to arrive at the transmit frequency.

The analysis is started by modeling the phase noise envelope of the worst phase noise oscillator. A Bode plot of the oscillator skirt can be drawn using poles to mark the knee points in the curve. The Bode plot approach is used to derive a plot of L(f), the phase noise spectral density, which is defined as the ratio of the single sideband phase noise power per Hertz relative to the carrier power. The plot will be used to also set the maximum allowable total noise contributions from the other components in the exciter / transmitter chain.

Assumptions:

$n_1 := 1$ (Phase Noise pole order. 1 => 20 dB/decade, 0.5 => 10 dB/decade, ...)

$f_{c1} := 10$ Hz (Phase Noise carrier offset frequency)

$dBL1 = -75$ dBc/Hz (Maximum allowable phase noise magnitude @ fc1)

$n_2 = 0.0625$ (Phase noise pole order. 1 => 20 dB/decade, 0.5 => 10 dB/decade, ...)

$f_{c2} = 10000$ Hz (Phase Noise carrier offset frequency)

$dBL2 = -135$ dBc/Hz (Maximum allowable phase noise magnitude @ fc2)

$f_{break} := 10000$ (L(f) break frequency)

Calculations:

$f = 10, 1000 .. \frac{B_{comp}}{2}$ Hz (Phase noise skirt frequency range of interest)

$$f_{3dB1} = \frac{f_{c1}}{\sqrt{\left(\frac{1}{10^{\frac{dBL1}{10}}}\right)^{\frac{1}{n_1}} - 1}}$$ (Flicker phase noise 3dB frequency)

$$L_1(f) := \left[\frac{1}{1+\left(\frac{f}{f_{3dB1}}\right)^2}\right]^{n1}$$ (Flicker noise average power per Hertz relative to carrier)

$$f_{3dB2} := \frac{f_{c2}}{\sqrt{\frac{1}{\left(10^{\frac{dBL2}{10}}\right)^{\frac{1}{n2}}}-1}}$$ (White phase noise 3dB frequency)

$$L_2(f) := \left[\frac{1}{1+\left(\frac{f}{f_{3dB2}}\right)^2}\right]^{n2}$$ (White noise average power per Hertz relative to carrier)

$L(f) := if(f<10000, L_1(f), L_2(f))$ (Oscillator phase noise average power per Hertz relative to the carrier power, dBc/Hz)

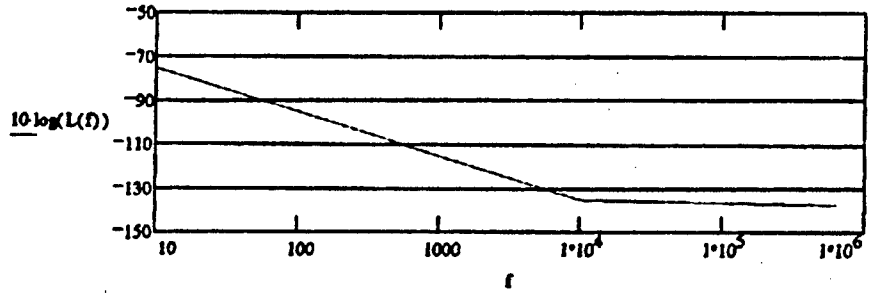

When a signal returns from a target and is downconverted by the same oscillator, some of the phase noise of the oscillator will be canceled due to correlation. This effect is known as the range correlation effect. The improvement in the phase noise skirt of the output waveform can be modeled for a given range delay. In this example, the transmitter is the largest contributor to the transmitted noise floor level and thus the range correlation effect does not apply.

$$M := \frac{B_{comp}}{PRF} \quad \text{(number of spectral lines contained with pulsewidth's spectral mainlobe)}$$

$$\Delta f := \frac{PRF}{N} \quad \text{(bandwidth of an FFT bin in Hertz)}$$

$$m := 1 .. \frac{M - 1}{2} \quad \text{(clutter spectral line index)}$$

$$kk := 1 .. \frac{N - 2}{2} \quad \text{(FFT bin index)}$$

First, the average noise power is computed relative to the carrier in an FFT bin's bandwidth which results from the clutter spectral line at the fundamental carrier frequency.

$Pcarrier_{kk} := \Delta f \cdot L(kk \cdot \Delta f)$ dBc (Average upper sideband phase noise power resulting from the carrier)

$Pcarrier_{N-kk} := Pcarrier_{kk}$ dBc (Average lower sideband phase noise power resulting from the carrier)

Next, the average power relative to the carrier in a bin's bandwidth which results from the replicas of the clutter spectral lines to the left (or negative frequencies) of the fundamental carrier frequency is added.

$$Pneg_{kk} := \sum_{m} \Delta f \cdot L(kk \cdot \Delta f + m \cdot PRF) \cdot \left[\frac{\sin\left[\pi \cdot \left[\frac{m \cdot PRF}{\left(\frac{B_{comp}}{2}\right)}\right]\right]}{\pi \cdot \left[\frac{m \cdot PRF}{\left(\frac{B_{comp}}{2}\right)}\right]} \right]^2$$

$$Pneg_{N-kk} := \sum_{m} \Delta f \cdot L((N - kk) \cdot \Delta f + (m - 1) \cdot PRF) \cdot \left[\frac{\sin\left[\pi \cdot \left[\frac{m \cdot PRF}{\left(\frac{B_{comp}}{2}\right)}\right]\right]}{\pi \cdot \left[\frac{m \cdot PRF}{\left(\frac{B_{comp}}{2}\right)}\right]} \right]^2$$

Finally, the average noise power relative to the carrier contribution from the replicas of the clutter spectral lines to the right (or positive frequencies) of the fundamental carrier is added. Again, the noise power is calculated in a bandwidth of an FFT bin.

$$Ppos_{kk} = \sum_{m} \Delta f \cdot L((N - kk)\cdot\Delta f + (m - 1)\cdot PRF)\cdot \left[\frac{\sin\left[\pi\cdot\left[\frac{m\cdot PRF}{\left(\frac{B_{comp}}{2}\right)}\right]\right]}{\pi\cdot\left[\frac{m\cdot PRF}{\left(\frac{B_{comp}}{2}\right)}\right]} \right]^2$$

$$Ppos_{N-kk} = \sum_{m} \Delta f \cdot L(kk\cdot\Delta f - m\cdot PRF)\cdot \left[\frac{\sin\left[\pi\cdot\left[\frac{m\cdot PRF}{\left(\frac{B_{comp}}{2}\right)}\right]\right]}{\pi\cdot\left[\frac{m\cdot PRF}{\left(\frac{B_{comp}}{2}\right)}\right]} \right]^2$$

$$Pnoise_{kk} = Pcarrier_{kk} - Pneg_{kk} + Ppos_{kk}$$

$$Pnoise_{N-kk} := Pcarrier_{N-kk} - Pneg_{N-kk} + Ppos_{N-kk}$$

$$kk = 0..N-1$$

$$Pnoise_{kk} := if\left(Pnoise_{kk} < 10^{-15}, 10^{-15}, Pnoise_{kk}\right)$$

Decimation of the sampled waveform into range bins coherently aliases the phase noise in the kk^{th} doppler bin with the kk^{th} doppler bin of each PRF line within the pulse bandwidth. Decimation also coherently aliases the signal in the kk^{th} doppler bin with the kk^{th} doppler bin of each PRF line. Therefore, the signal to clutter phase noise ratio in each doppler bin remain unchanged through the decimation process.

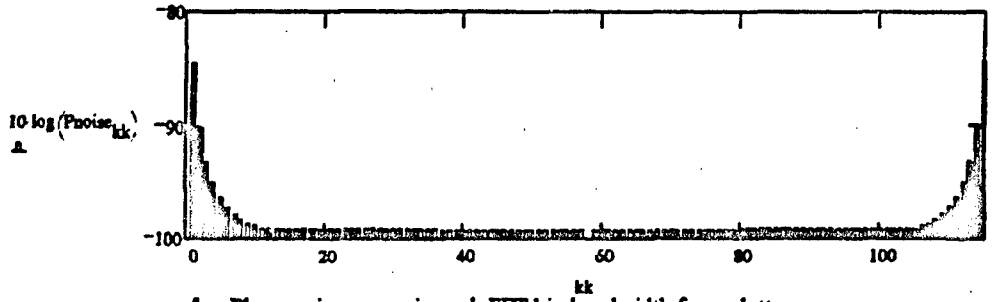

▲ Phase noise power in each FFT bin bandwidth from clutter

The subclutter visibility is also dependant upon the window applied to the range samples. A 65 dB Dolph window can be applied to clutter return samples that have been previously clutter noth attenuated by 30 dB to calculate the "windowed" spectrum. Based on the above clutter phase noise calculation and the following "windowed" clutter calculation, a total subclutter visibility may be specified.

Frequency of the clutter (Hz): $f0 := \frac{PRF}{N} \cdot 0 \quad Hz \quad f0 = 0$

$i := 0..N-1 \qquad t_i := \frac{i}{PRF}$

$f_i := \cos(2 \cdot \pi \cdot f0 \cdot t_i)$ (In phase clutter signal.) $\quad g_i := \cos\left(2 \cdot \pi \cdot f0 \cdot t_i + \frac{\pi}{2}\right)$ (Quadrature clutter signal)

$h_i := f_i + (0 + i) \cdot g_i$

$H := cfft(h)$ (Compute the FFT of the unwindowed I&Q data)

$M := floor\left(\frac{f0}{\frac{PRF}{N}}\right) \qquad max := |H_M|$

(Compute the magnitude of this FFT and normalize the magnitude spectrum by the maximum value which is H_M in this case)

$H_i := if\left(\frac{|H_i|}{max} < 10^{-10}, -210, 20 \cdot \log\left(\frac{|H_i|}{max}\right) - ClutFiltRej\right)$

Now apply the Dolph window to the I&Q data.

$hw_i := f_i \cdot W_i + (0 - i) \cdot g_i \cdot W_i$

$HW := cfft(hw)$ (Compute the FFT of the windowed I&Q data)

$max := |HW_M|$

$$HW_i := if\left(\frac{|HW_i|}{max} < 10^{-10}, -210, 20\cdot\log\left(\frac{|HW_i|}{max}\right) - ClutFiltRej\right)$$ (Compute the normalized magnitude in dB of this FFT)

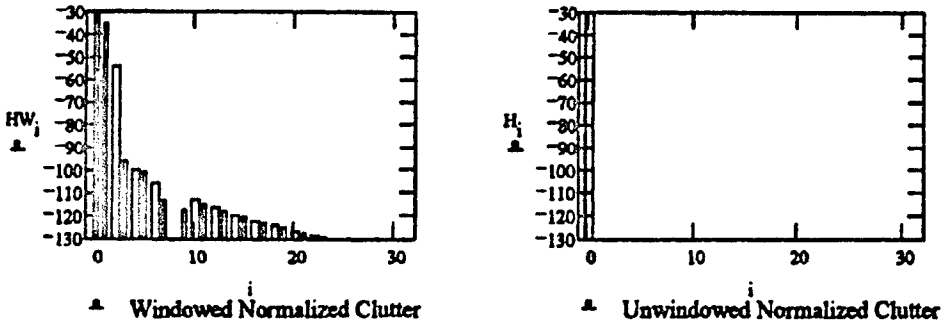

Comparing the previously calculated normalized clutter phase noise and the windowed normalized clutter, the subclutter visibility after clutter blanking may be safely specified as 95 dB. Therefore, any in band spurious signals from the transmitter and SAW devices must be less than the carrier in decibels by the sum of the required subclutter visibility and the minimum signal to interference ratio.

$SubCVis_{-i} := -SubClutVis$

$SubCVis_{RX_{tr}} := Pc_{RX_{tr}} - SubClutVis$ (Visibility relative to the calculated received clutter power.)

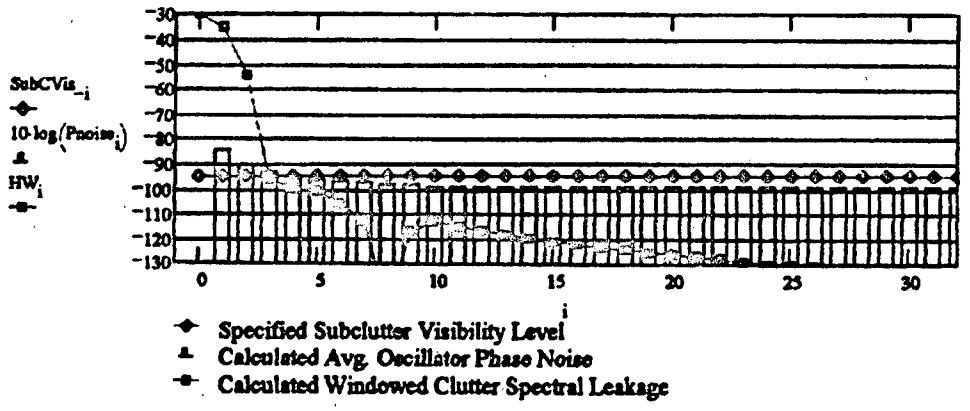

The above graph compares the specified subclutter visibility level, the calculated average oscillator phase noise and the window effects on the clutter. The maximum allowable phase noise from the components in the exciter chain may be specified to be 10 dB below the transmitter phase noise versus frequency. Therefore, the total transmitter noise including the noise contributions of phase, thermal, jitter and acoustic sources must be no greater than -85 dBc/Hz at 10 Hz away from the carrier and no greater than -145 dBc/Hz at 10 kHz away from the carrier.

Derivation of Overall System Detection Performance

The graph below exploits the results of all the previous calculations except AGC. The plots shows the expected receiver input levels for the 100 square meter target, the 1 square meter target and the calculate clutter return with its respective phase noise. They are compared to the receiver input level that would saturate the A/D converter and the minimum detectable signal.

$AGC_{low_{tr}} := Pmax_{RX} - 10$ dBm (Threshold of AGC operation)

$AGC_{hi_{tr}} := Pbig + 10$ dBm (Upper minimum limit of AGC operation)

$AGC := (Pbig - Pmax_{RX}) + 20$ $AGC = 49.63$ dB (Minimum required dynamic range of AGC with a 20 dB safety margin.)

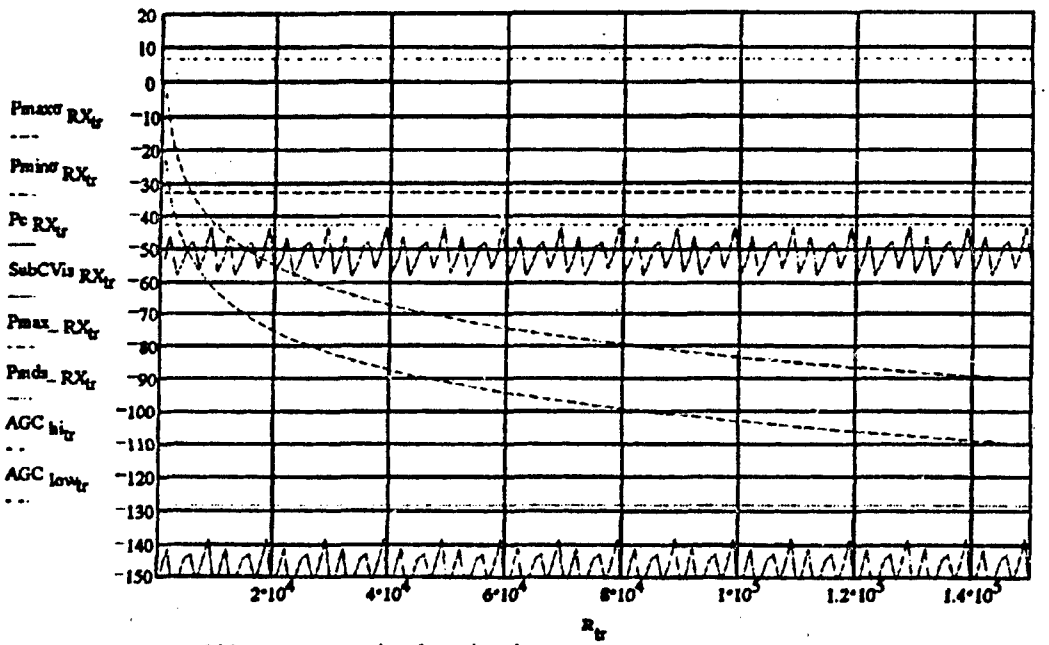

- 100 sq. m. target signal receiver input vs. range
- 1 sq. m. target signal receiver input vs. range
- Calculated received clutter power
- Specified visibility relative to clutter power received
- Maximum receiver input to match A/D saturation level
- Minimum detectable signal receiver input level
- Upper minimum limit of receiver AGC operation
- Lower threshold of receiver AGC operation

OVERVIEW ANALYSIS

Developing Computer Model of Post-Processing Functions

- Performs Post-Processing for Simulated Target-Radar Engagement
- Kalman Filtering Used as Baseline Approach to Target Tracking
- Modified Chinese Remainder as Baseline for Range Resolving

Purpose of Model

- Determine Computational Requirements for RTRS Post-Processor
- Workbench for Adjusting System Parameters to Maintain Track
- Evaluation / Selection of Range Resolve Algorithm

MODEL GEOMETRY
Scientific Research Corporation
Tgt1
Z = 20'
Radar
R1=(0,0,0)
R=0 N=(0,0,1)
Tgt1
V
Y
X
Radar
April 28, 1993
Progress Review - page 01

TRACK FILES

Track Files Maintained by Model

- Two State Azimuth Track
- Two State Elevation Track
- Two State Ambiguous Range Tracks
- Three State Unambiguous Range Track

RANGE RESOLVE ALGORITHM

Limitations of the Chinese Remainder Theorem

- ♦ Modified Chinese Remainder Can be Applied to any Arbitrary PRF
  - - Sacrifice Unambiguous Range When Using Common Factors
- ♦ CRT Algorithm Imposes Artificial Range Bins on Problem
  - - Bin Straddling Leads to an Aliased Measurement of Range
- ♦ Requires Convergence of Kalman Track to Perform

CHINESE REMAINDER THEOREM (CRT)

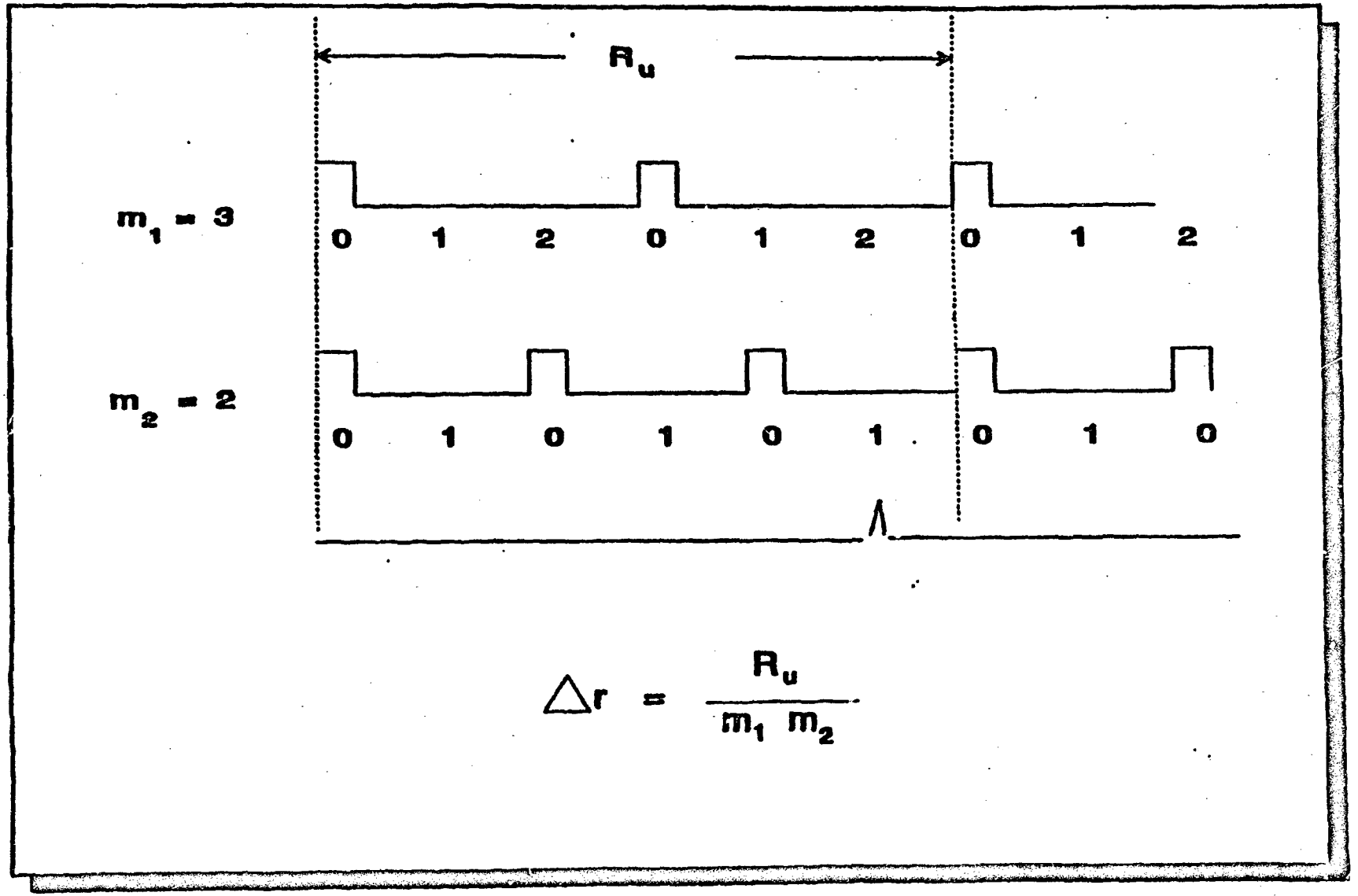

CRT WITH COMMON FACTORS

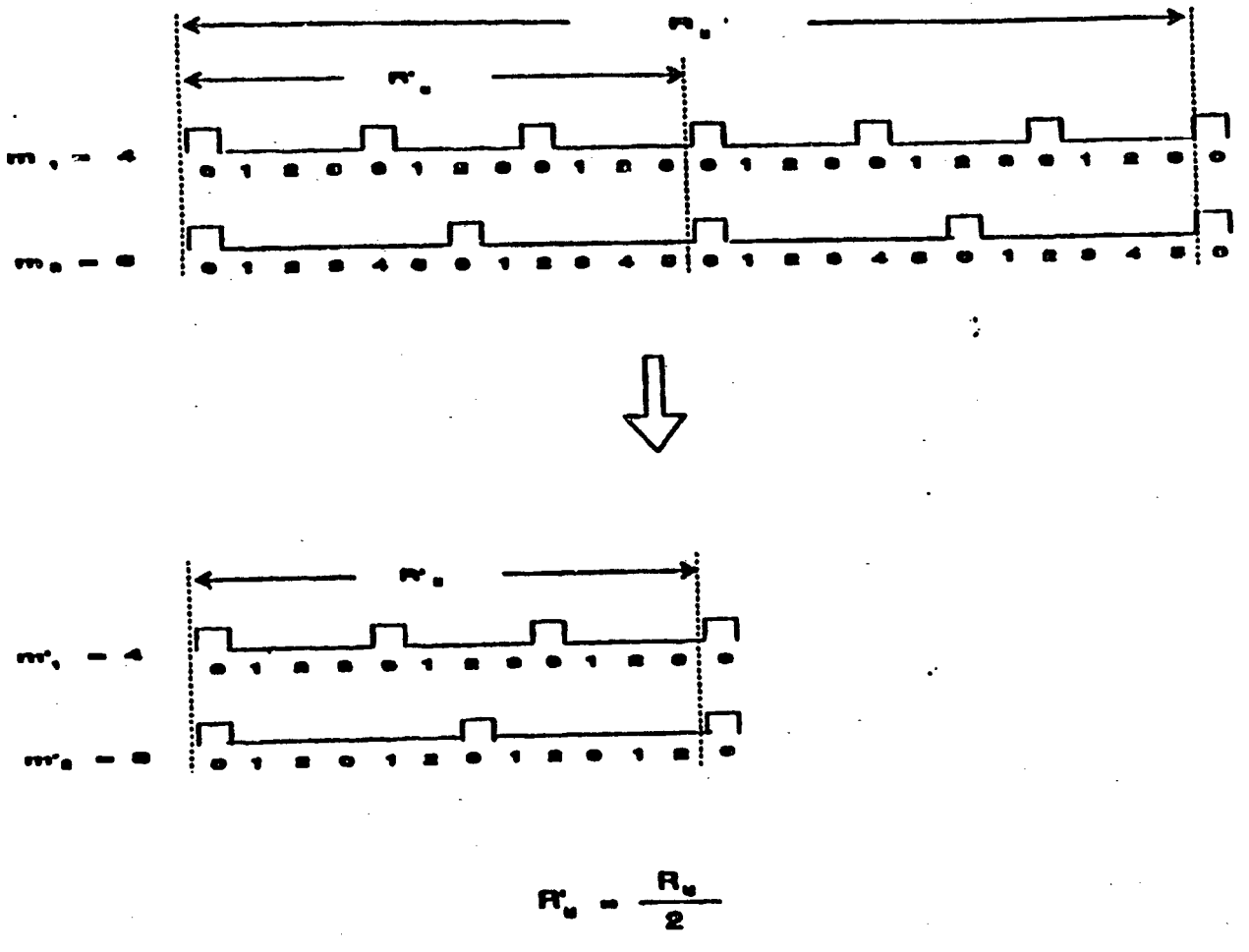

$$R'_u = \frac{R_u}{2}$$

SUMMARY OF CURRENT ANALYSIS

- Kalman Tracking can be Tailored to Emulate a Variety of Trackers
- CRT Range Resolve Algorithm Works, However, it has Limitations
- Evaluating Alternative Range Resolve Algorithms
- Analysis Will Lead to Specification of Post-Processor for RTRS

OVERVIEW OF PRESENTATION

- Define Tracking Subsystem Requirements and Functions in Each Mode
- Present Requirements from Threat Documents
  - Requirements which Drive Post-processor Sizing
  - Parameters Necessary for Simulation
- Discuss A Tracker Baseline
- Summary and Future Work

KEY TRACKER REQUIREMENTS

- Key System-Level Requirements:
  - Support Acquisition and Track
  - Support Manual Initiation of Tracks
  - Simulate Multiple Threats - Current and Future
- Requirements Influence Tracking Subsystem Design:
  - Software Design
    - Highly Modular
    - Algorithm Toolbox
  - Hardware Design
    - Adequate Margin for System Growth

TRACKING SYSTEM FUNCTIONS

1. SEARCH - Tracking System Idle

2. ACQUISITION

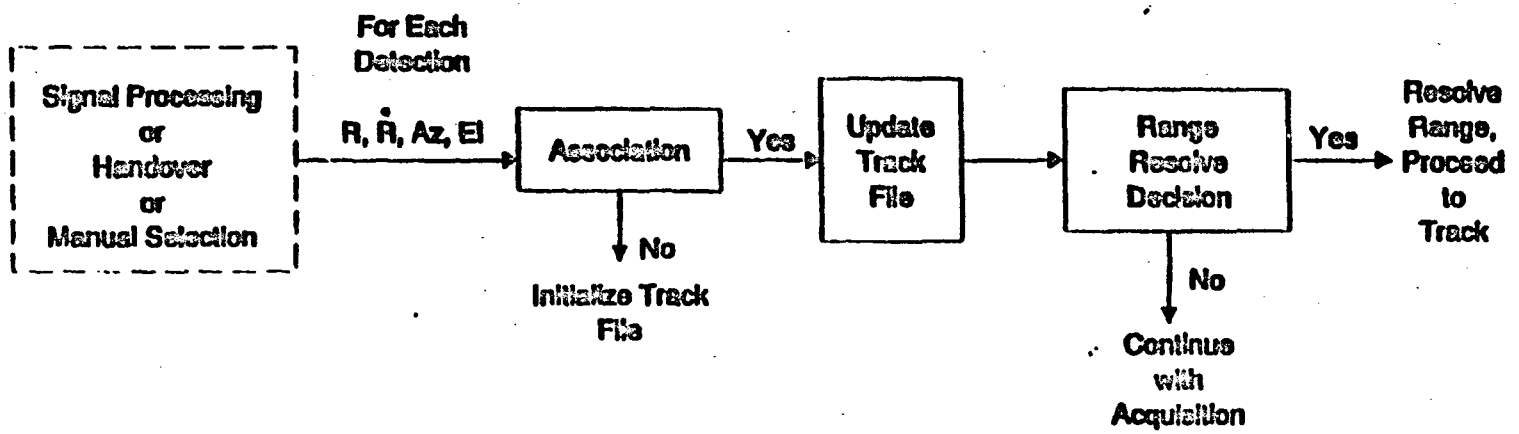

TRACKING SYSTEM FUNCTIONS (CONT)

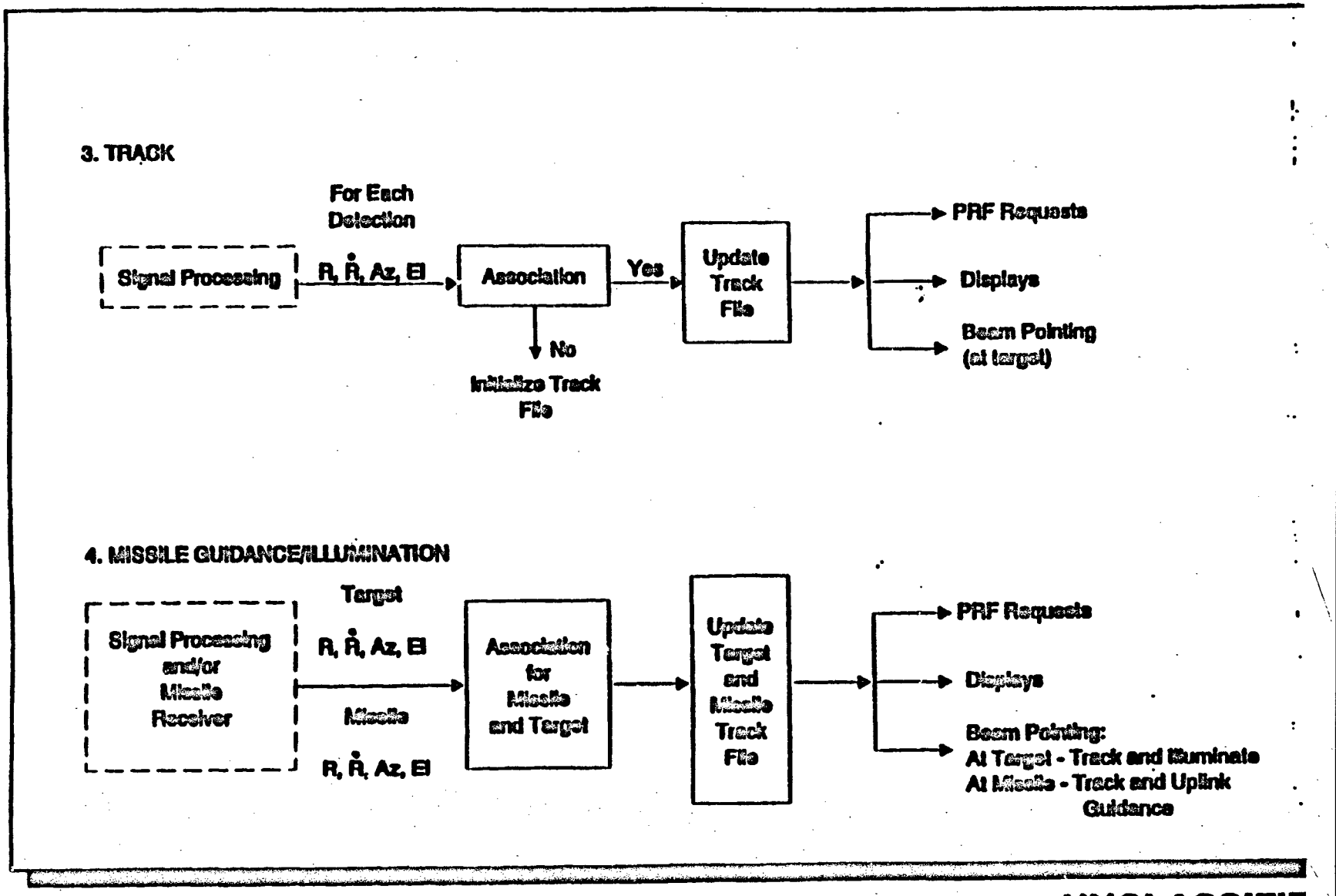

UNCLASSIFIE

UNCLASSIFIED

SRC Scientific Research Corporation

TOP LEVEL REQUIREMENTS

Classified Slides Previously Provided to the Government

UNCLASSIFIED

TRACKING SUBSYSTEM EVENTS

Classified Slides Previously Provided to the Government

UNCLASSIFIED

SRC Scientific Research Corporation

TIMING REQUIREMENTS

Classified Slides Previously Provided to the Government

UNCLASSIFIED

MEASUREMENT ERROR (1 σ)

Classified Slides Previously Provided to the Government

SRC Scientific Research Corporation

ECCM CAPABILITIES

Classified Slides Previously Provided to the Government

ECCM CAPABILITIES (CONT)

Classified Slides Previously Provided to the Government

UNCLASSIFIED
TRACKER BASELINE
Scientific Research Corporation
Track File Maintenance
Measurement Model
Target Model
Association
Track Initialization
Acquisition Processing (Ambiguous Range)
Track Processing (Unambiguous Range)
UNCLASSIFIED
11/23/93 Quarterly Progress Review

SRC Scientific Research Corporation

TRACKER BASELINE

- Track File Maintenance
  - Drop
  - Merge
- Measurement Generation Model
  - Timing and Control Information
  - Target Motion Model
  - False-Alarm Model
  - Measurement Variance Information

SRC Scientific Research Corporation

TRACKER BASELINE

- Association Function
  - Inputs: Detection package from signal processing
  - Outputs: Detection/Track File Pairings
  - The association function consists of:
    - Extrapolate
    - Preselect
    - Chi-squared cost function
    - Arbitration

SRC Scientific Research Corporation

TRACKER BASELINE

Association Functions

- Extrapolate
  - Extrapolate 2-state trackers for Az, El, Doppler, and Ambiguous range for the current PRF to the current time
  - Since each of these trackers has the form

$$\begin{bmatrix} x(k) \\ \dot{x}(k) \end{bmatrix}$$

the extrapolation simply has the form

$$\begin{bmatrix} x(k+1) \\ \dot{x}(k+1) \end{bmatrix} = \begin{bmatrix} x(k)+T*\dot{x}(k) \\ \dot{x}(k) \end{bmatrix}$$

where T is the time since the last update.

TRACKER BASELINE

Association Functions (Continued)

- Preselect
  - Preselect provides a coarse means of eliminating unlikely detection/track file pairings
  - Form an MxN matrix where
    M is the number of detections
    N is the number of active track files
  - For each of the possible MxN pairings, determine whether the difference between extrapolated quantities and detection values exceeds a threshold.
  - This difference is calculated for Az, El, Doppler, and Ambiguous Range

SRC Scientific Research Corporation

TRACKER BASELINE

♦ Preselect (Continued)

♦ For example, with three detections and five active track files, the preselect procedure might produce a matrix of the form

	1	2	3	4	5
1	X	X	1	1	X
2	1	X	X	X	1
3	X	1	1	X	X

where 1 denotes a possible association

SRC Scientific Research Corporation

TRACKER BASELINE

Association Functions (Continued)

- Chi-squared cost function
  - For each pairing which passes the preselect function, a chi-squared cost function is calculated
  - The function returns a number which is a weighted distance function
  - Given a detection y and a track file estimate z, where

$$y=\begin{bmatrix} az \\ el \\ r \\ d \end{bmatrix}, \quad z=\begin{bmatrix} \hat{az} \\ \hat{el} \\ \hat{r} \\ \hat{d} \end{bmatrix}$$

SRC Scientific Research Corporation

TRACKER BASELINE

♦ Chi-squared cost function (Continued)

the chi-squared cost function is calculated as

$$(z-y)^T*(H^TPH+R)^{-1}*(z-y)$$

where H and R are the measurement matrix and measurement variance, and P is the filter covariance matrix

♦ Continuing the previous example, the chi-squared function would give a matrix of the form

	1	2	3	4	5
1	X	X	11.8	4.2	X
2	23	X	X	X	3.8
3	X	4.5	15	X	X

SRC Scientific Research Corporation

TRACKER BASELINE

Association Functions (Continued)

- Arbitration
  - The arbitration function
    (1) Searches the table for the lowest score, and makes the appropriate association
    (2) Eliminates the track file and measurement just associated from further consideration
    (3) Repeats this procedure
  - In the example above, arbitration assigns an association between
    Measurement 2 and Track File 5
    Measurement 1 and Track File 4
    Measurement 3 and Track File 2

SRC Scientific Research Corporation

TRACKER BASELINE

Mode Selection Function

- The mode selection function is performed once per detection
- If a detection did not associate with a track file, track initialization mode is invoked
- For those detections which associate with track files, the track file state is examined:
  - If Range Resolve has not been successfully accomplished for the given track file, the track file is processed in acquisition mode
  - If Range Resolve has been successfully accomplished for the given track file, the track file is processed in tracking mode

TRACKER BASELINE

Alpha-Beta Filters

♦ The two-state alpha-beta filters maintain estimates of x and $\dot{x}$, where x may be azimuth, elevation, ambiguous range, or doppler

♦ Given the extrapolated track file values for x_k and $\dot{x}_k$ and a measurement y_k, the alpha-beta filter's estimate is given by

$$\underline{x}_k = x_k + \alpha(y_k - x_k)$$

$$\underline{\dot{x}}_k = \dot{x}_k + \beta(y_k - x_k)/T$$

where T is the time between updates

♦ Given a value for α, an optimal** beta can be computed as

$$\beta = \alpha^2 / (2-\alpha)$$

**Benedict and Bordner, 1962

TRACKER BASELINE

Alpha-Beta-Gamma Filters

♦ The three-state alpha-beta-gamma filter maintains estimates of x, $\dot{x}$, and $\ddot{x}$ where x is unambiguous range

♦ Given the extrapolated track file values for x_k, $\dot{x}_k$, and $\ddot{x}_k$ and a measurement y_k, the alpha-beta-gamma filter's estimate is given by

$$\underline{x}_k = x_k + \alpha(y_k - x_k)$$

$$\underline{\dot{x}}_k = \dot{x}_k + \beta(y_k - x_k)/T$$

$$\underline{\ddot{x}}_k = \ddot{x}_k + \gamma(y_k - x_k)/T^2$$

where T is the time between updates

SRC Scientific Research Corporation

TRACKER BASELINE

Kalman Filters

♦ Extrapolation:

$$\tilde{x}_{k+1} = Ax_k, \qquad \tilde{P}_{k+1} = AP_kA^T + e^2Q$$

♦ Measurement update

$$K_k = \tilde{P}_kH^T\left(H\tilde{P}_kH^T + R\right)^{-1}, \qquad P_k = (I - K_kH)\tilde{P}_k, \qquad x_k = \tilde{x}_k + K_k(y_k - H\tilde{x}_k)$$

where

A is the plant matrix
P_k is the state covariance matrix
Q is the process noise
H is the measurement matrix
R is the measurement variance
y_k is the measured quantity

SRC Scientific Research Corporation

TRACKER BASELINE

Kalman Filters

- In the two-state case, the equations can be explicitly written out and grouped to avoid numerical instabilities
  - This method is documented in the SRC Memorandum, "Three Simple, Robust Two-State Kalman Filters," JKB-93-05
- For the three-state filter, a numerically stable algorithm is used: the UDU^T filter
  - In this method, the covariance matrix is factored as $P=UDU^T$ where U is unit upper triangular and D is diagonal
  - The method is from G.J. Bierman, Factorization Methods for Discrete Sequential Estimation

SRC Scientific Research Corporation

TRACKER BASELINE

Range Resolve Algorithm

♦ This method is derived and documented in SRC Memorandum JKB-93-09A, "A Range Resolve Methodology for Pulse Doppler Radars"

♦ Method uses the difference between ambiguous ranges so it is not a function of range bins

♦ Problem Statement: Given two PRIs P_1 and P_2 and ambiguous ranges R_1 and R_2, find the smallest unambiguous range which would give these ambiguous ranges.

♦ Offline computations:

(1) Find the product of the mutual prime factors of P_1 and P_2, denoted by F_{12}

(2) Define $P_1'=P_1/F_{12}$, $P_2'=P_2/F_{12}$

(3) Find the "magic number" S_{12} such that $(S_{12}*P_2) \bmod (P_1) = 1$, where $1 \le S_{12} < P_1$

Scientific Research Corporation

TRACKER BASELINE

Range Resolve Algorithm

- Real time computations:

  (1) Extrapolate the ambiguous ranges to the same effective time

  (2) Compute $Rc=(R_1-R_2)/dR$, where $dR=c/(2*f_{clock})$. Rc is the difference in clock counts

  (3) Find $D=Rc \bmod P_1'$; if $D<0$, add P_1'

  (4) Find $A=(S_{12}*D) \bmod P_1'$

  (5) Unambiguous range R is $R_2 + A*P_2''*dR$

- Method can easily accommodate a third PRI

TRACKER BASELINE

Range Resolve Algorithm

- Example

  Consider a target with unambiguous range of 2500m.

  Let P_1=120, P_2=110, with clock frequency 12 MHz.

  With these parameters, R_1=1000m and R_2=1125m.

  Offline computations: P_1'=12, P_2'=11, and S_{12}=11.

  Rc=(1000-1125)/25 = -5

  D=-5 mod P_1' = -5, Add P_1' to get D=7

  A=(S_{12}*D) mod P_1' = 5

  Unambiguous range = R_2+A*P_2'*dR = 1125 + 5*11*25 = 2500m

Scientific Research Corporation

MODEL RESULTS

Model Results

♦ A FORTRAN model has been developed which can simulate an engagement with a single target

♦ The model can accommodate a programmable PRF sequence, accounts for eclipsing effects, and performs range resolve using a threat-based algorithm

♦ Simulations were run to determine time to achieve range resolve using the following parameters:

A target with initial range of 1 mile was flown on a crossing trajectory.

Threat-based frame time, subframe time, pulse repetition frequencies, and measurement variances were used.

A Kalman tracker was used.

SRC Scientific Research Corporation

TRACKER DESIGN

Model Results

Twenty runs were completed, each with initial range increasing by 0.5 range bin. This scenario ensures seeing eclipsing effects.

Results:

- "Fast" Timing Scheme: For 75% of the runs, range resolve was completed within two major frames
  For the remaining 25% of the runs, eclipsing effects dictated that three to six major frames be used before successful range resolve

Scientific Research Corporation

SUMMARY

Current Work:

- Investigated In-house Documents
- Expanded Model to Include Threat Waveform Timing, Measurement Variances, and Range Resolve Algorithm

Future Work:

- Additional Information: Documents Requested
  Contact with Analysts
- Continue with Modeling for Other Threats: Range Resolve
  Tracker
  Algorithms
- Monitor Host Resource Requirements

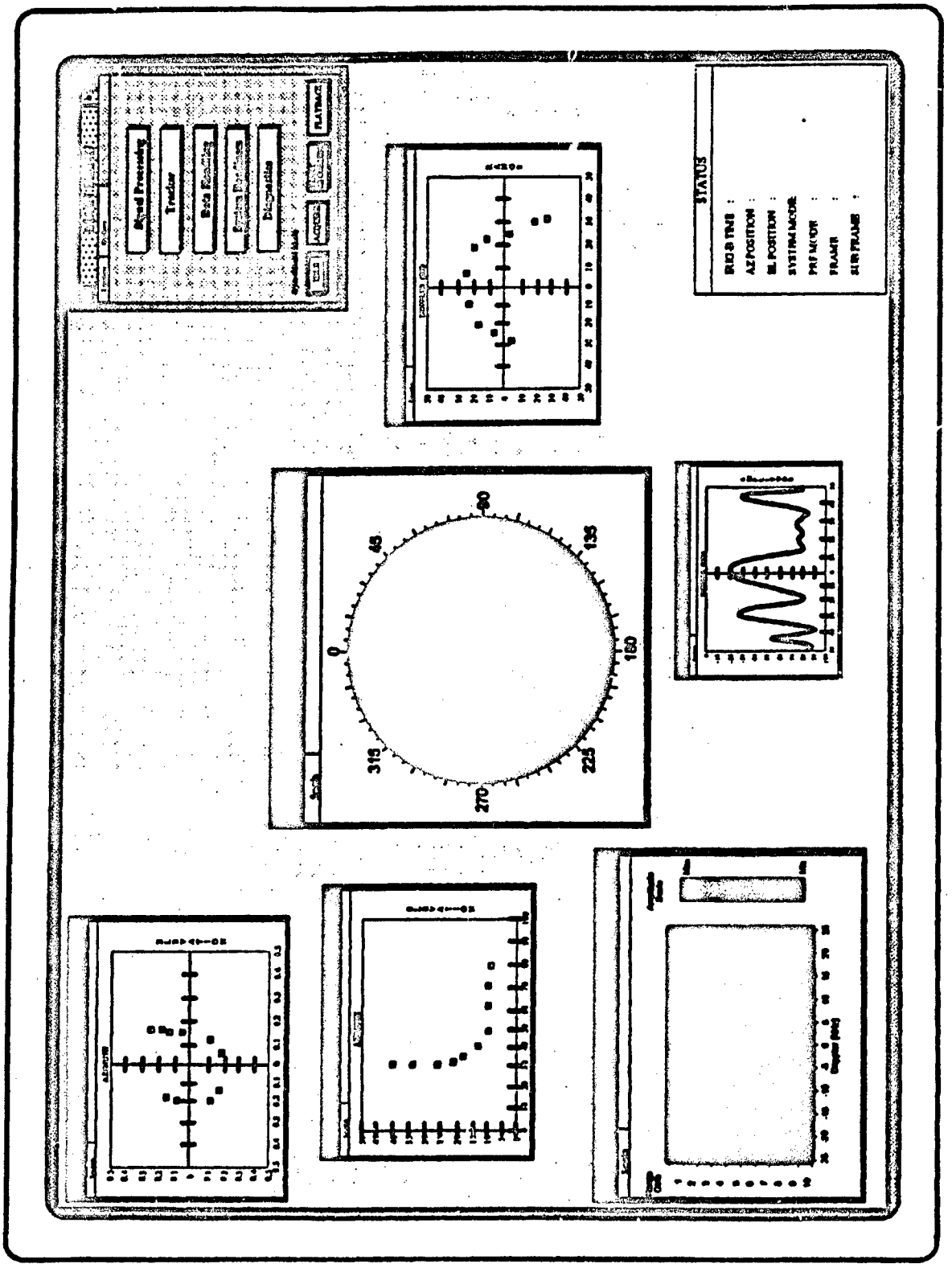
Signal Processing
Tracker
Beta Emitting
Diagnostics
STATUS
90
45
135
0
180
315
225
270

AMPLITUDE - RANGE - DOPPLER

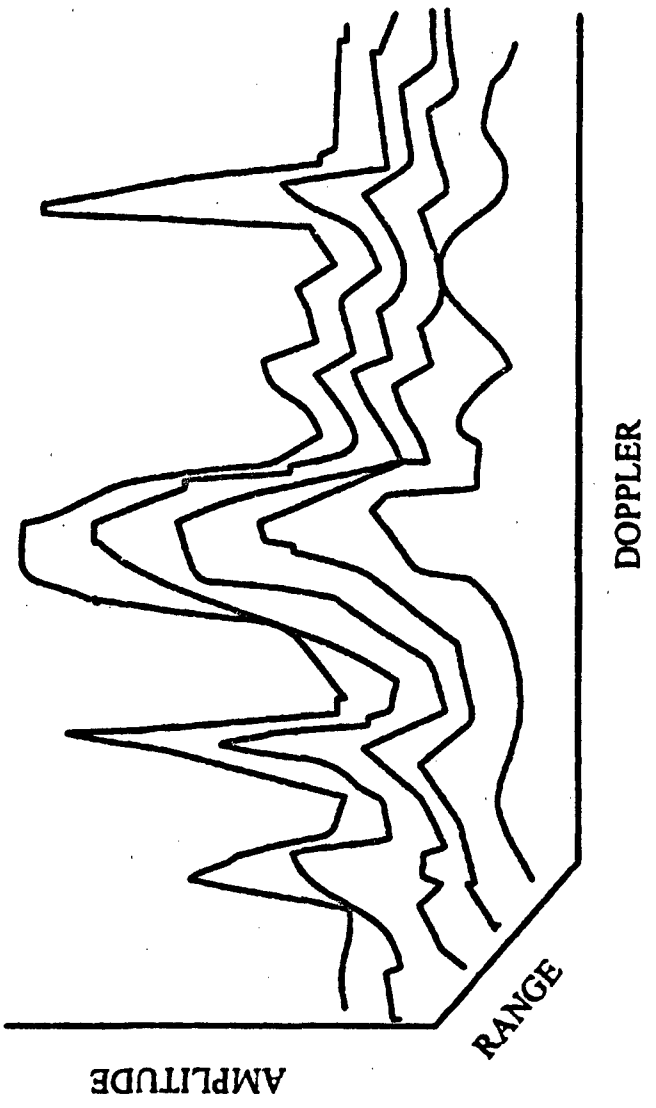

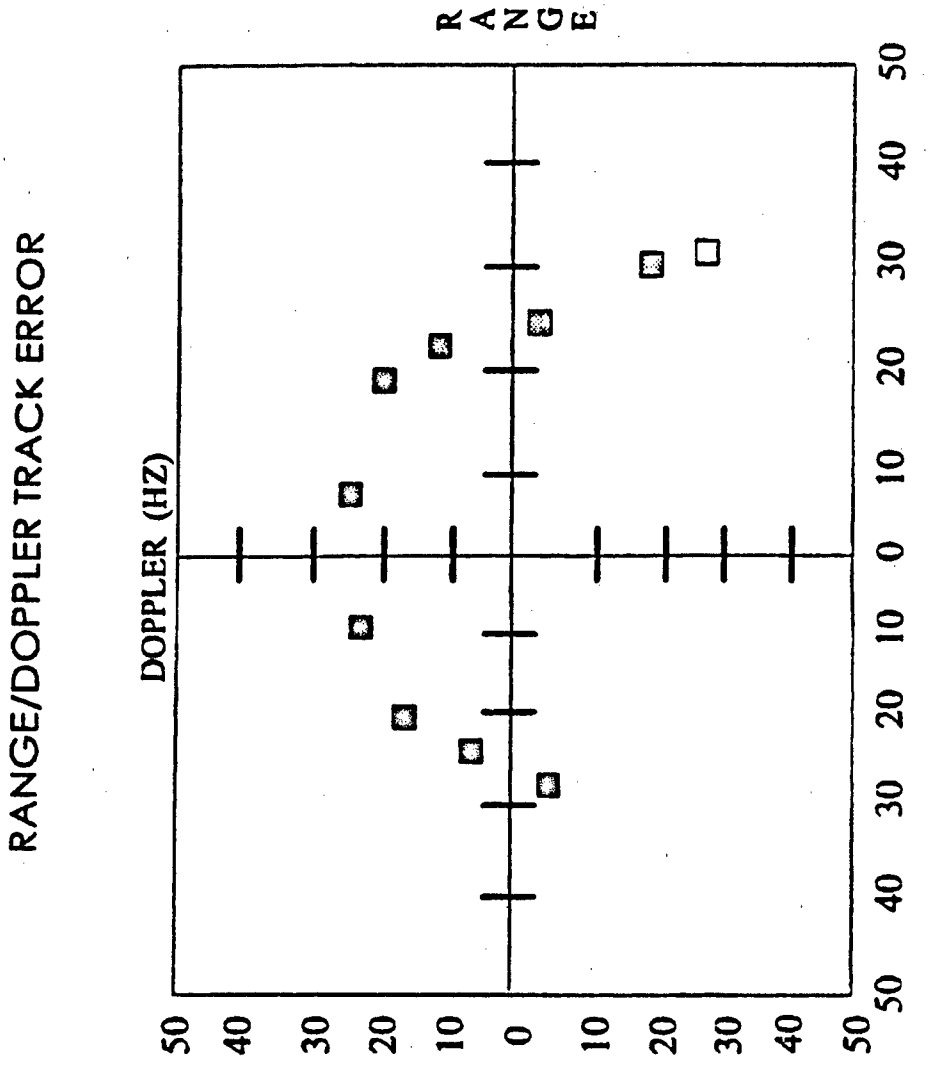
RANGE/DOPPLER TRACK ERROR
RANGE
DOPPLER (HZ)
50
40
30
20
10
0
10
20
30
40
50

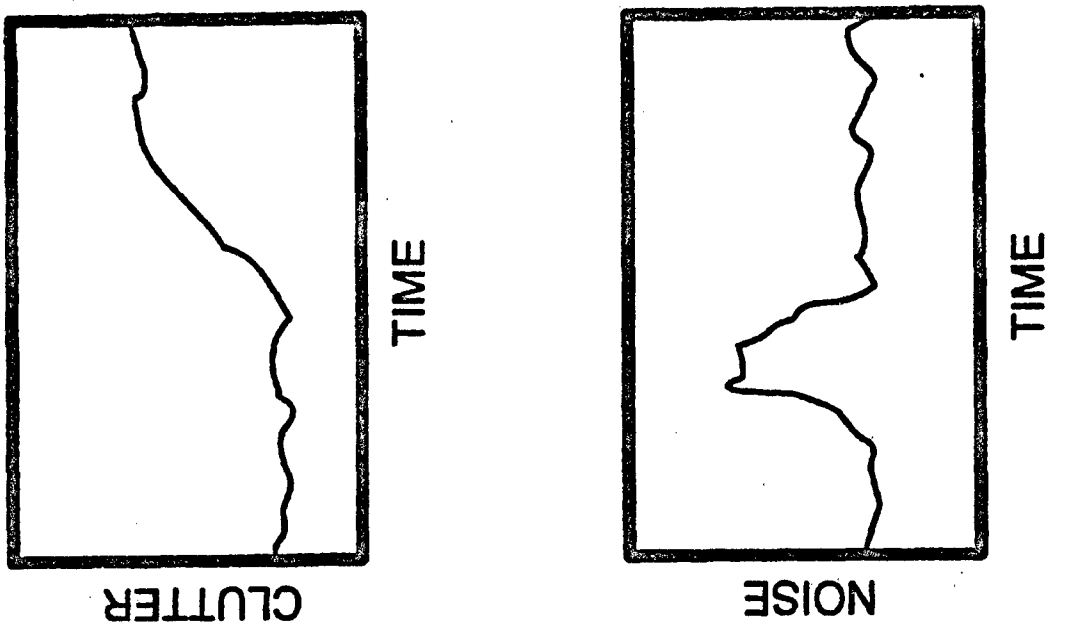

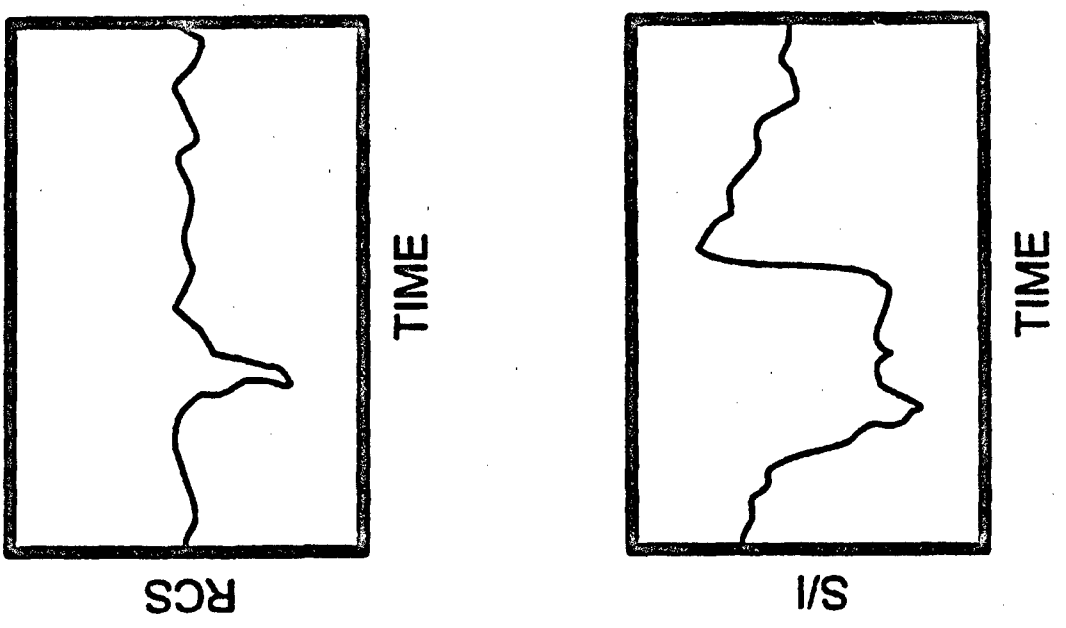

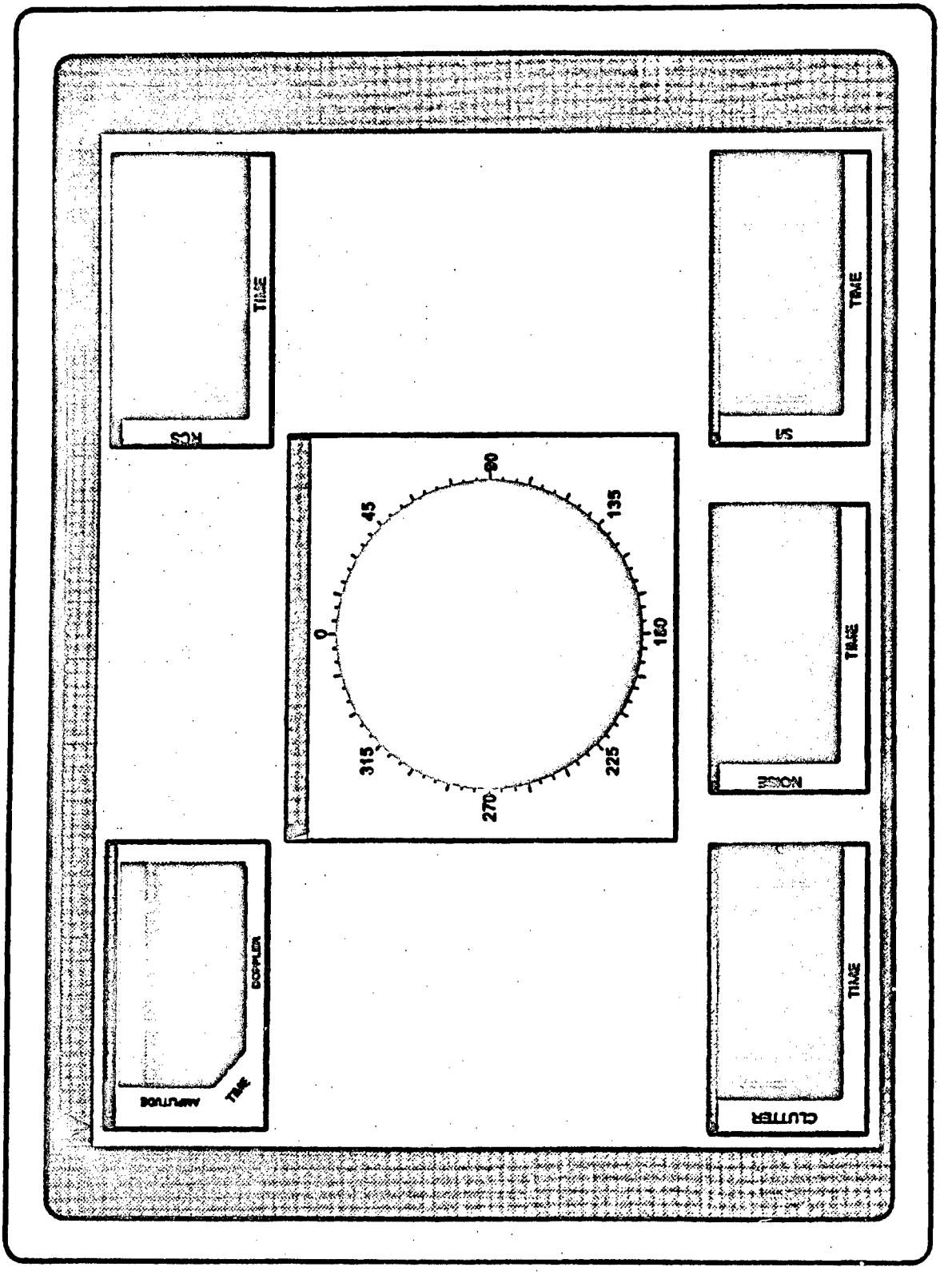
TIME
RCS
TIME
VS
90
45
135
0
180
315
225
270
TIME
NOISE
DOPPLER
AMPLITUDE
TIME
TIME
CLUTTER

AMPLITUDE - DOPPLER

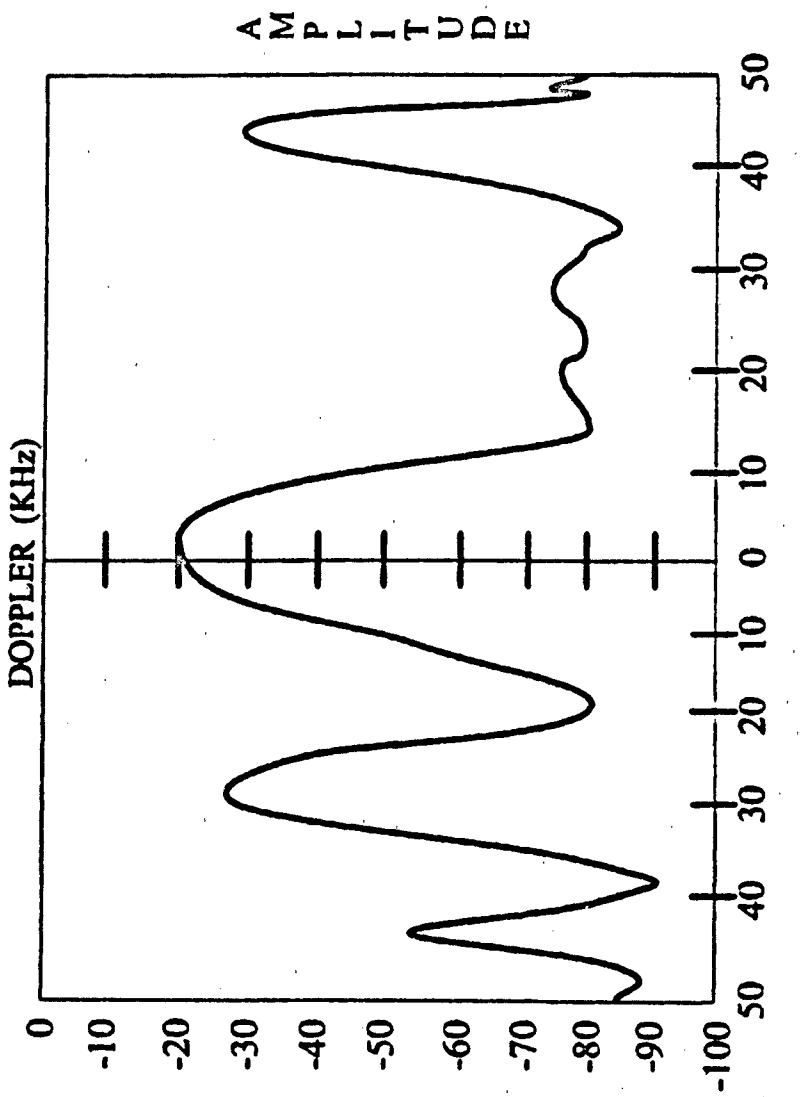

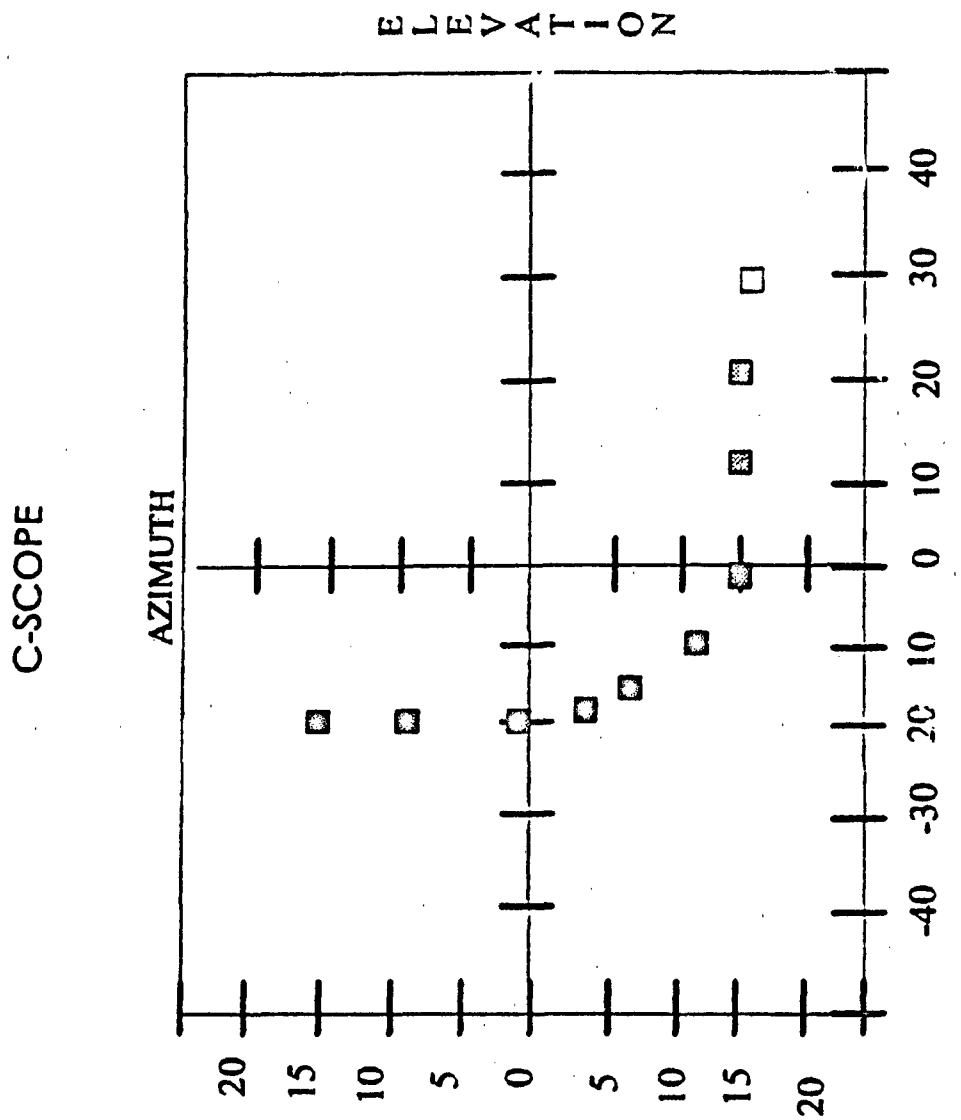
C-SCOPE
AZIMUTH
ELEVATION
20
15
10
5
0
5
10
15
20
40
30
20
10
0
10
20
-30
-40

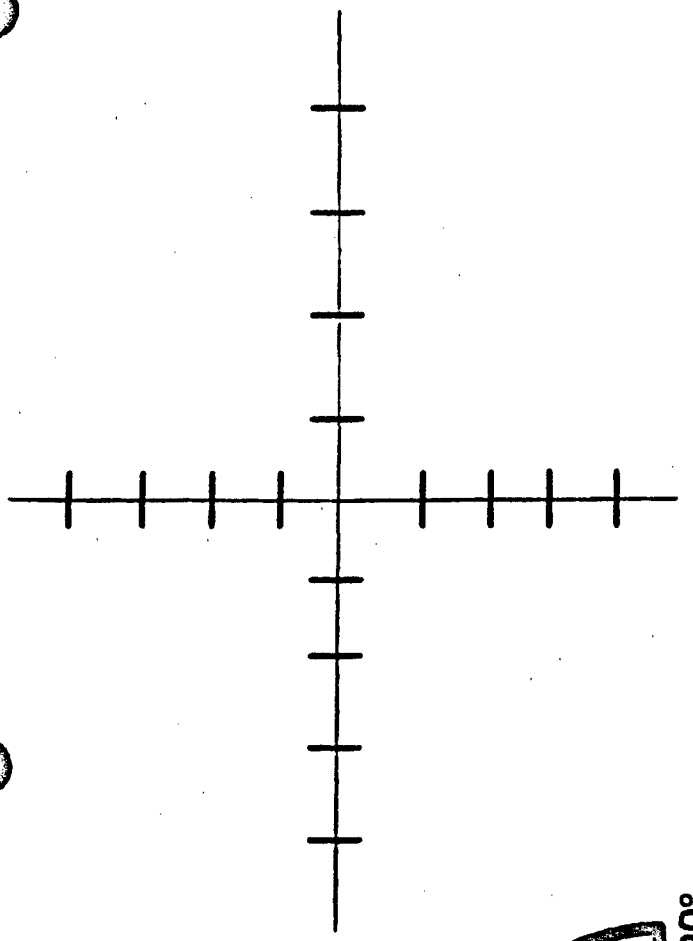

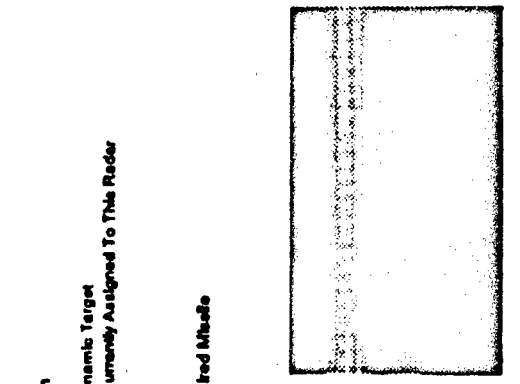

Tracked Target
Autonomous Detection
C² Handover of TBM
C² Handover of Aerodynamic Target
Other C² Targets Not Currently Assigned To This Radar
Commander's Cursor
Operator's Cursor
Tracked Location of Fired Missile

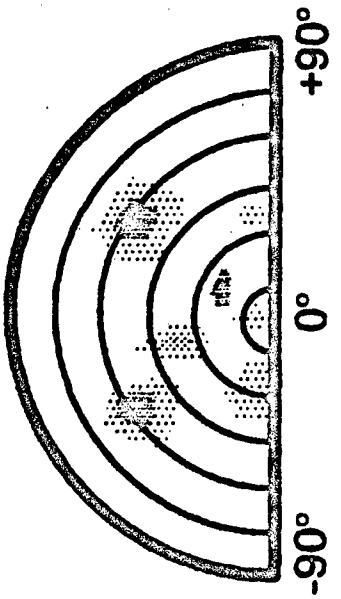

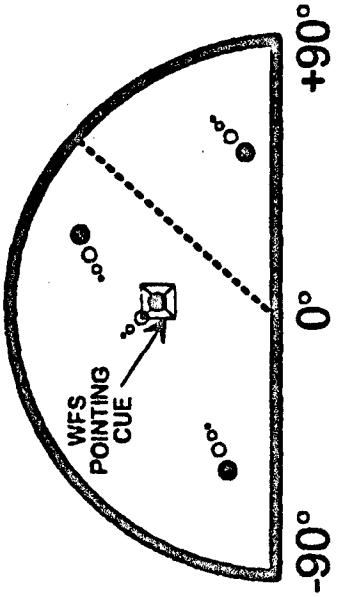

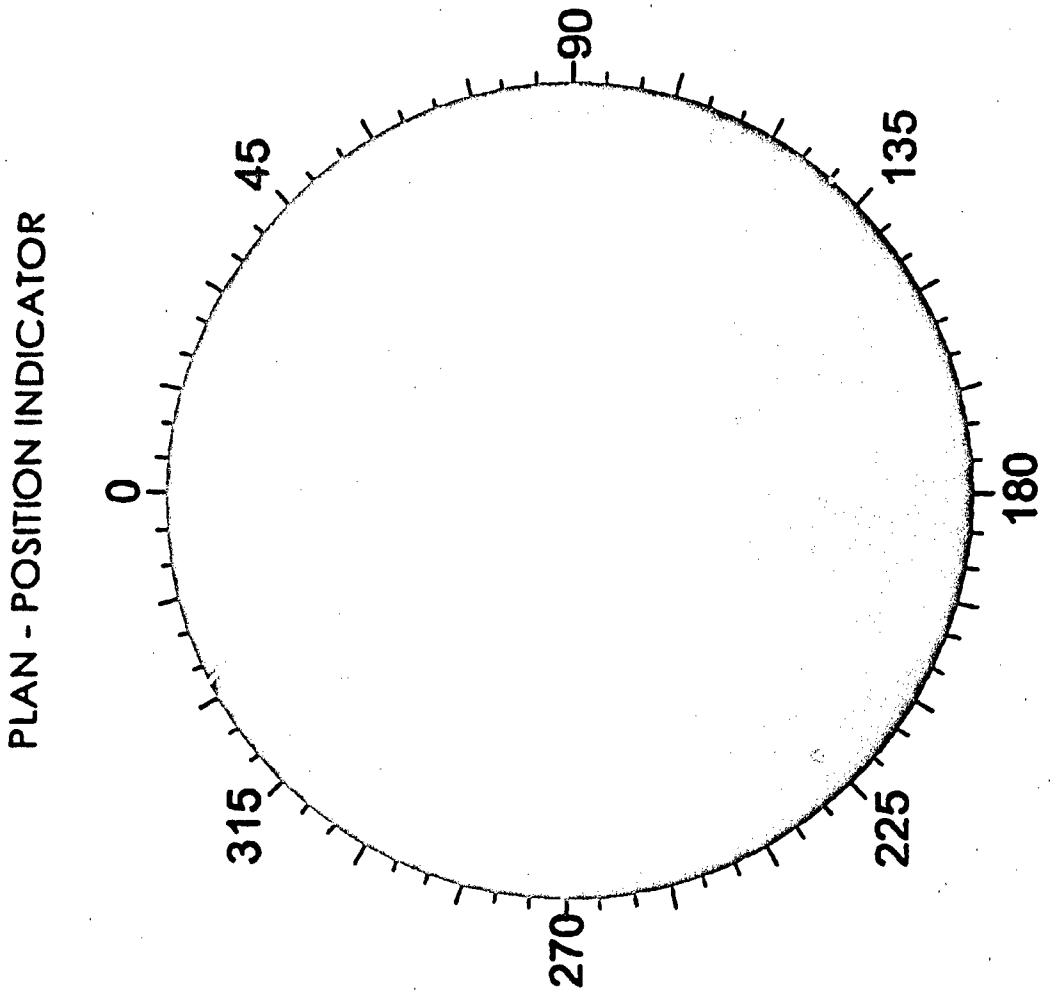
PLAN - POSITION INDICATOR
90
135
45
180
0
315
225
270

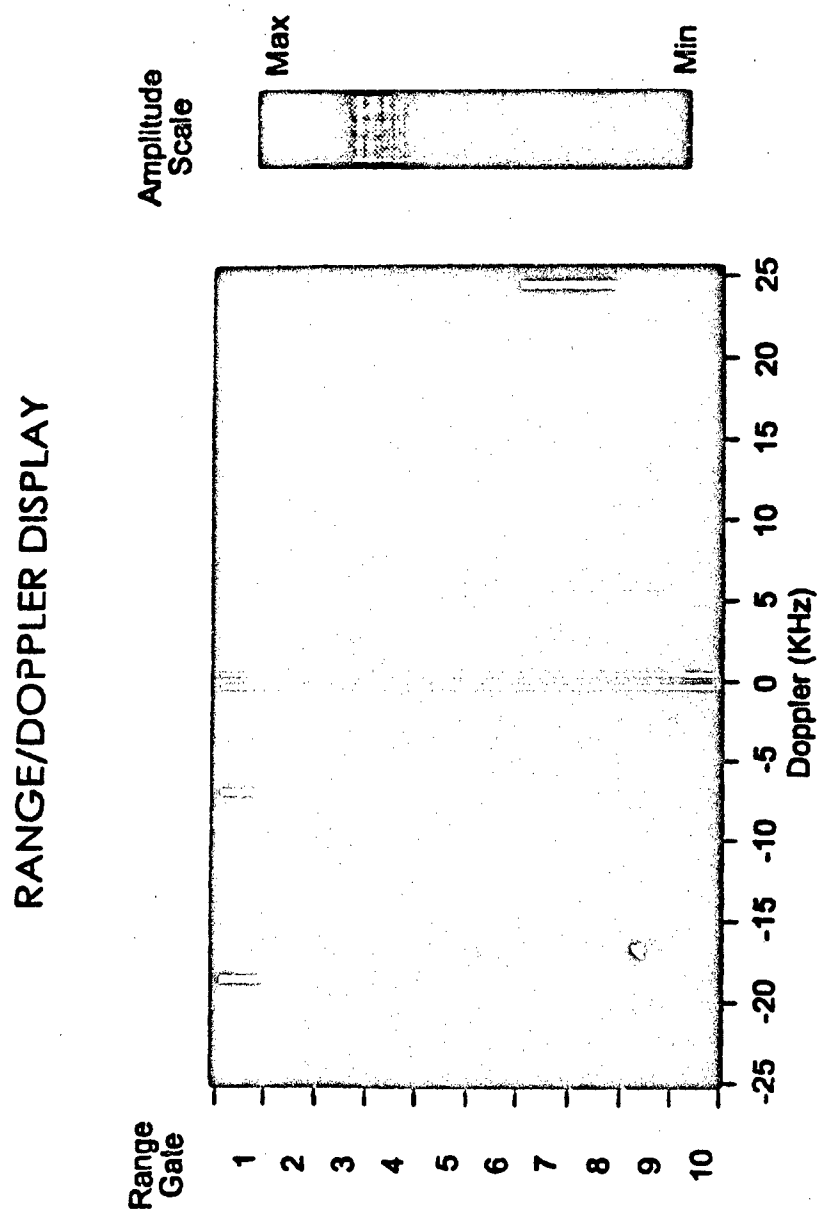
RANGE/DOPPLER DISPLAY
Amplitude Scale
Max
Min
Range Gate
1
2
3
4
5
6
7
8
9
10
Doppler (KHz)
25
20
15
10
5
0
-5
-10
-15
-20
-25

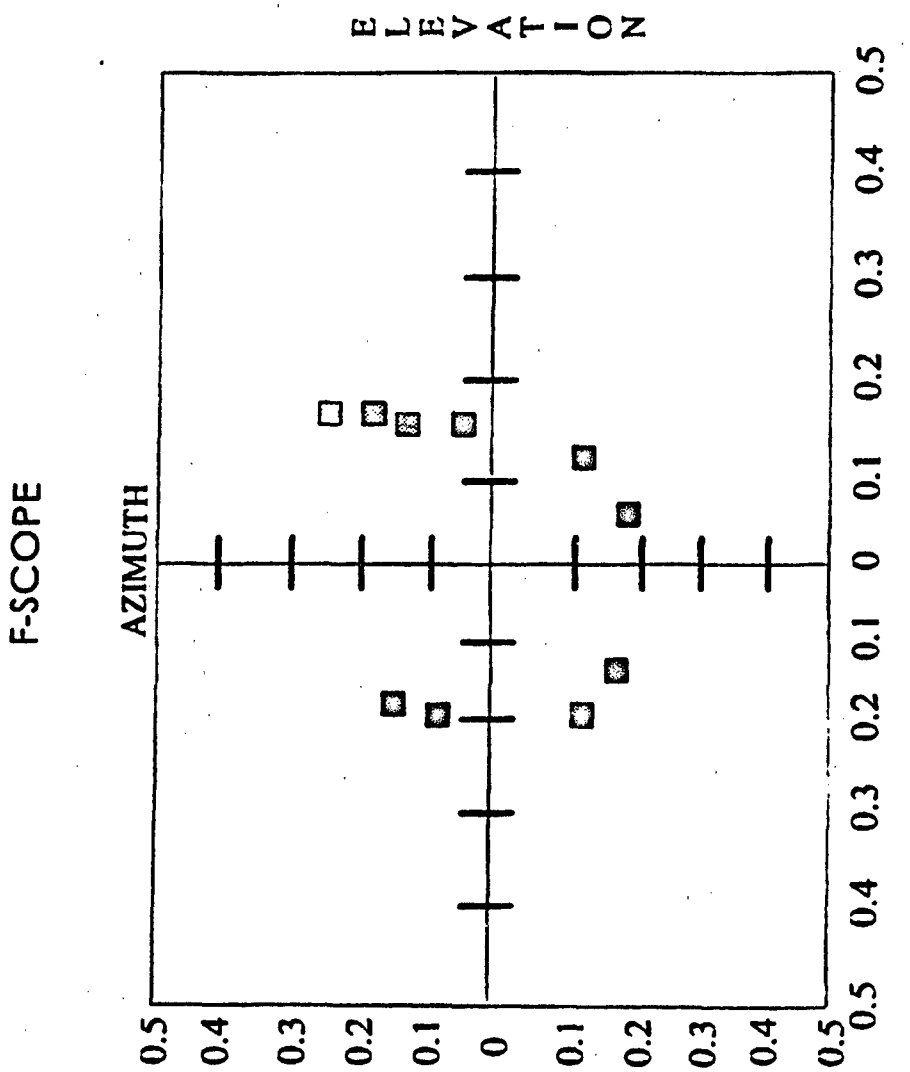
F-SCOPE
AZIMUTH
ELEVATION
0.5
0.4
0.3
0.2
0.1
0
0.1
0.2
0.3
0.4
0.5

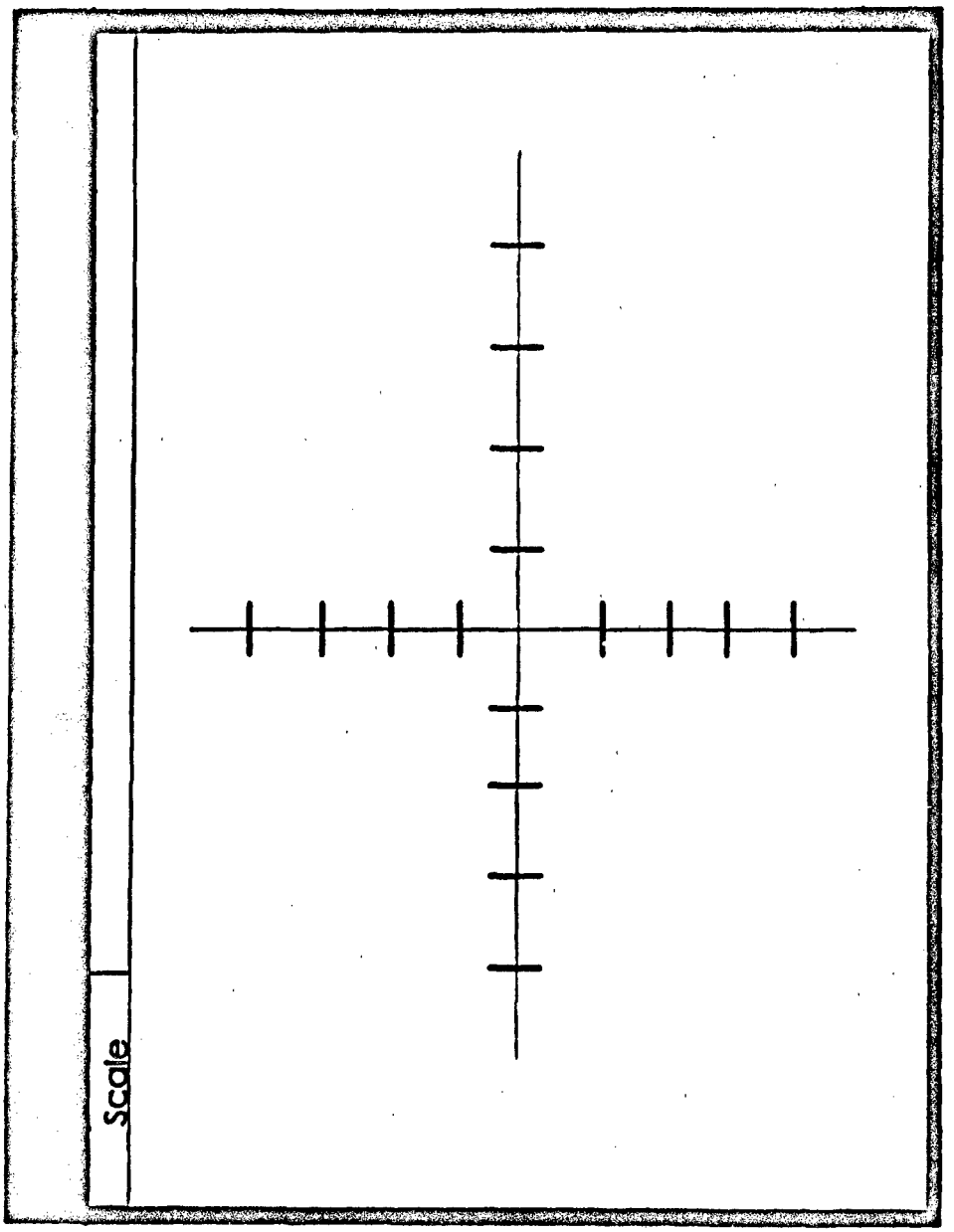

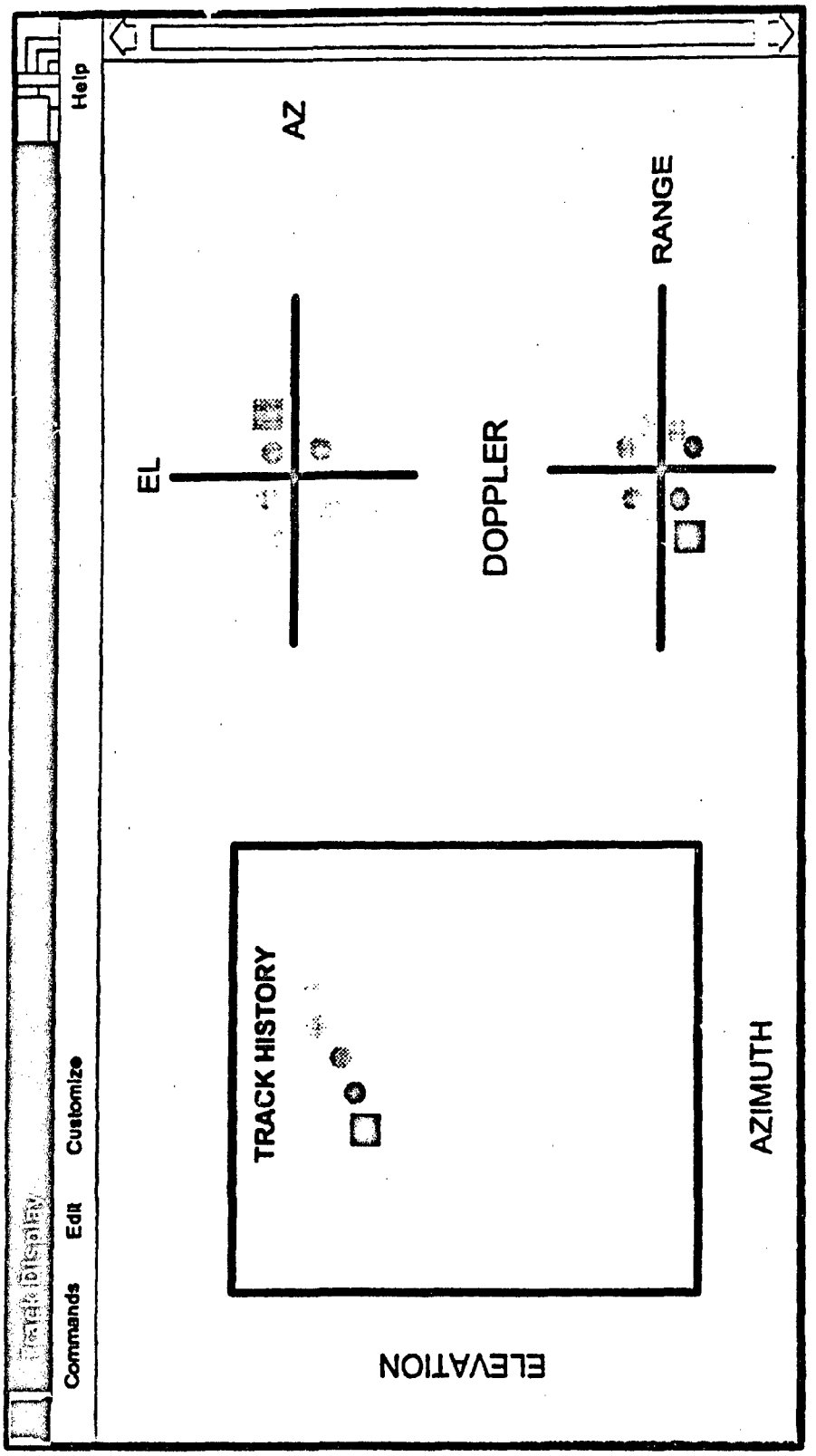
Help
Commands
Edit
Customize
AZ
RANGE
EL
DOPPLER
TRACK HISTORY
ELEVATION
AZIMUTH

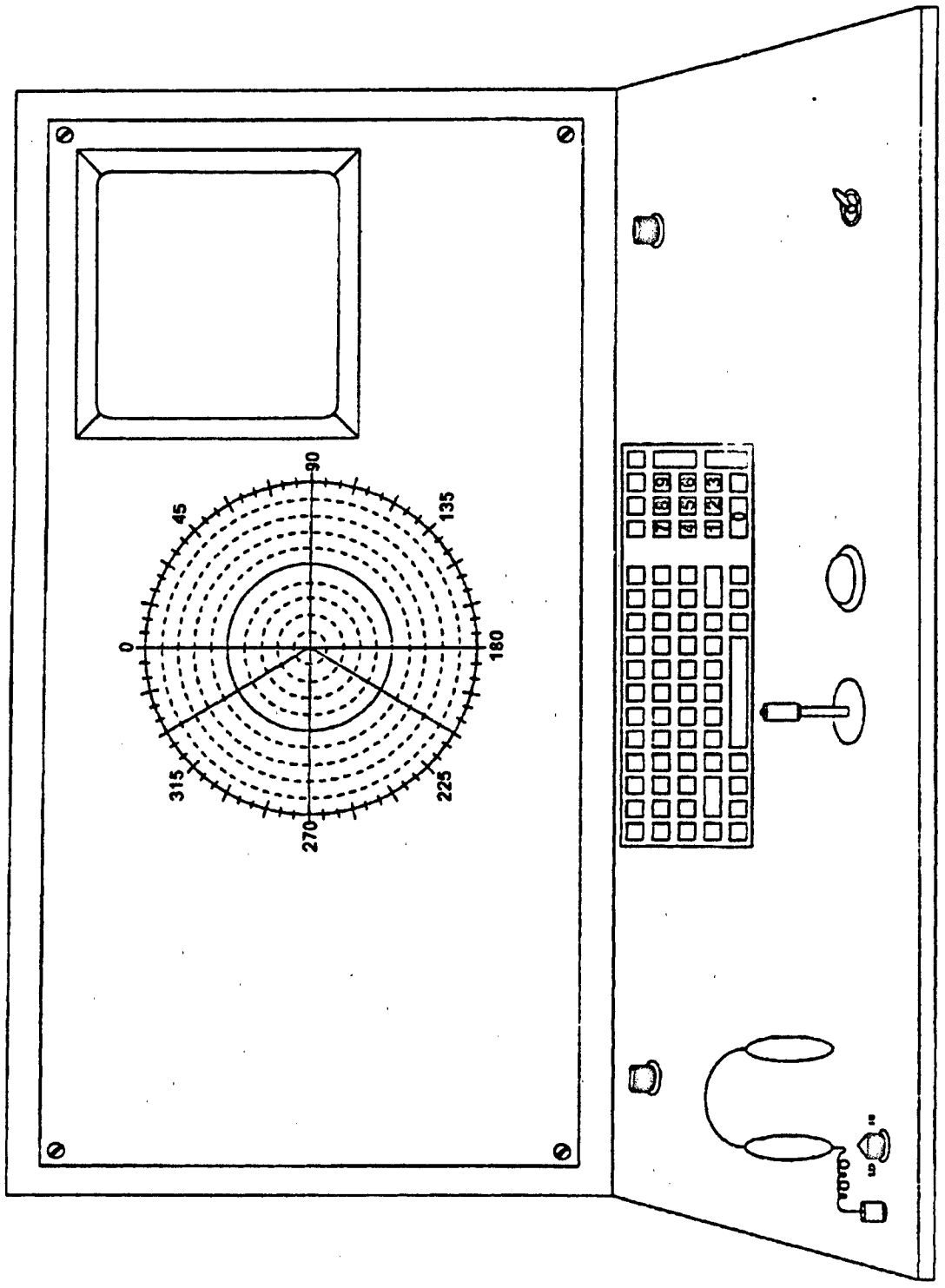

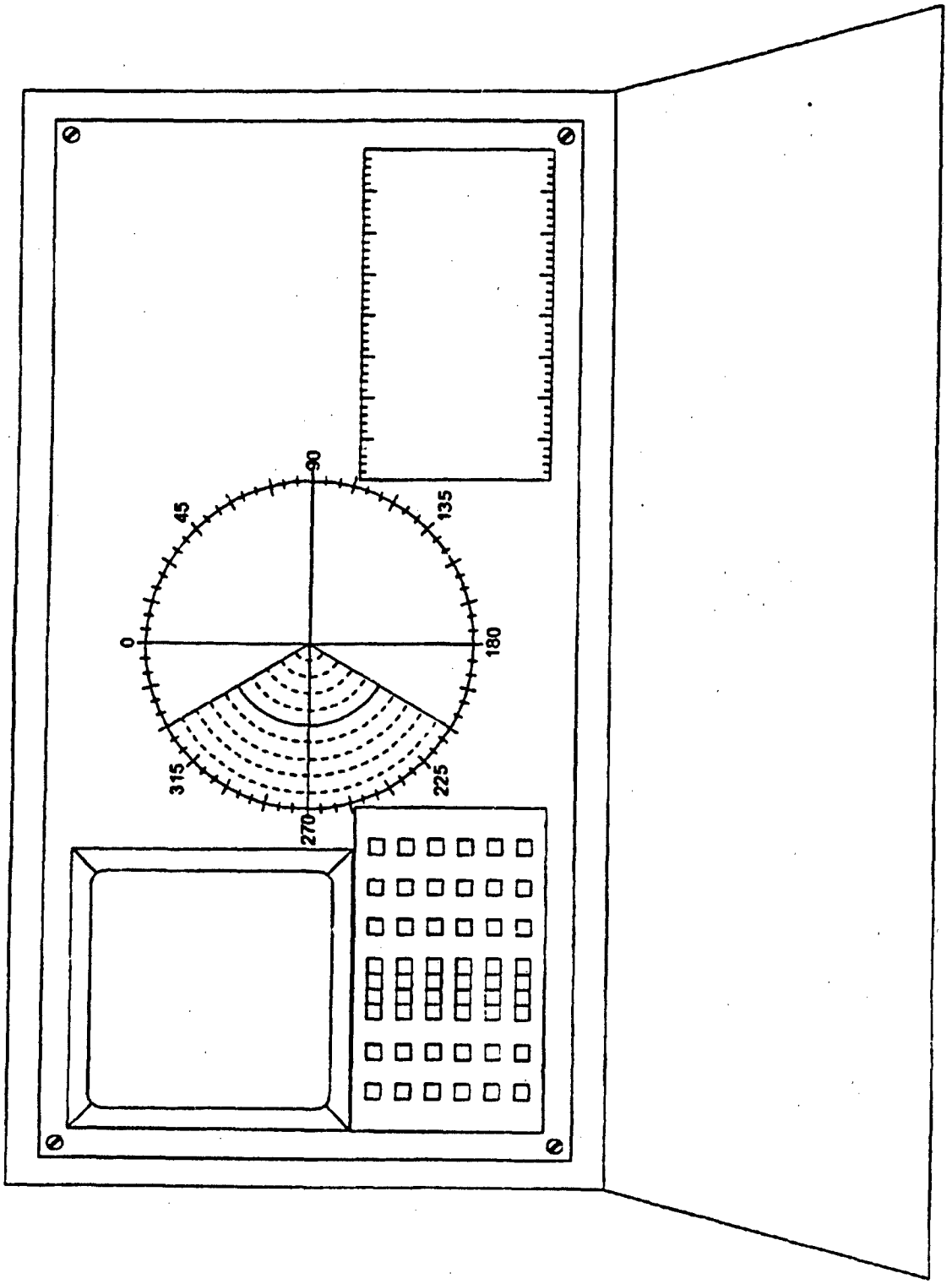

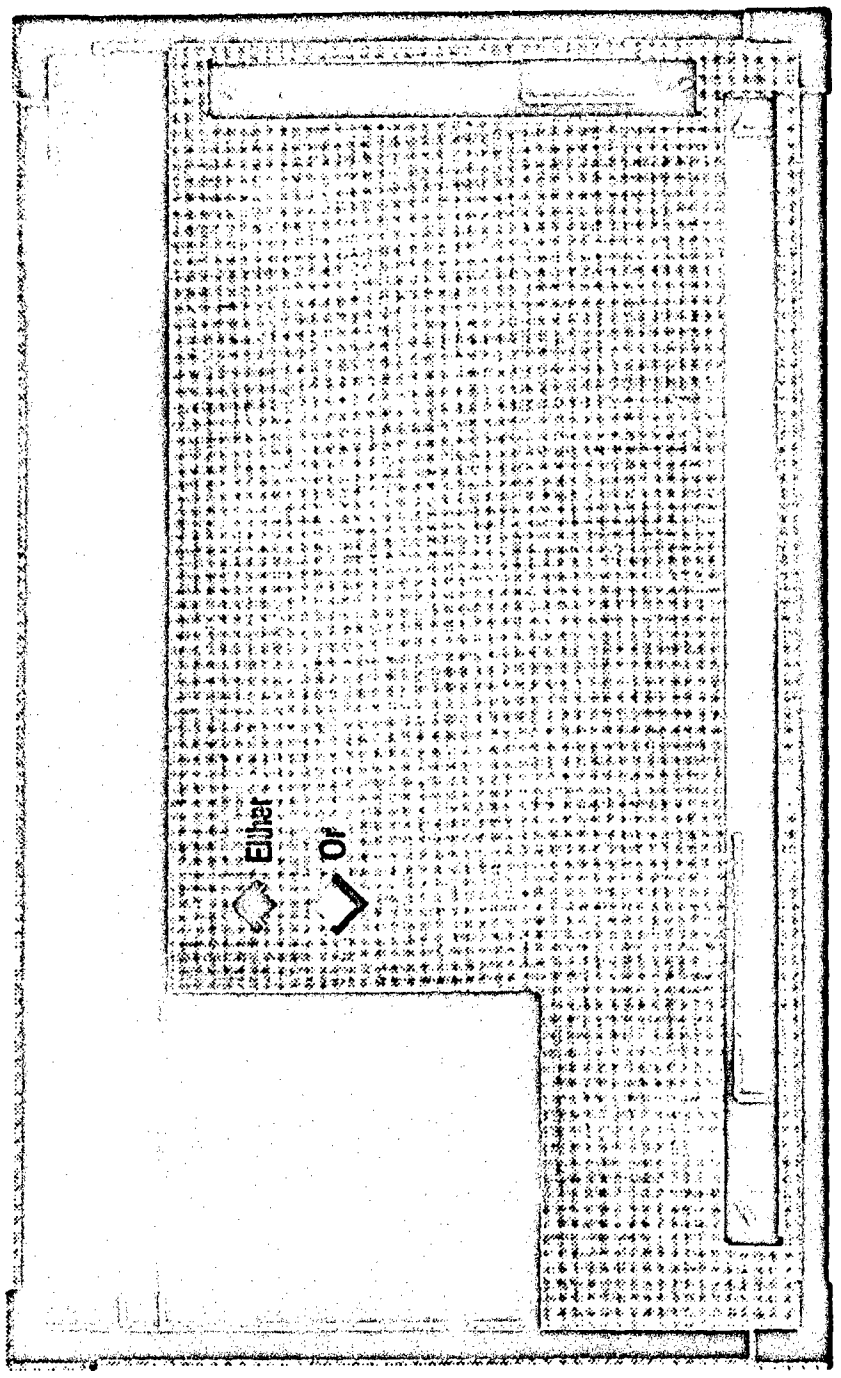

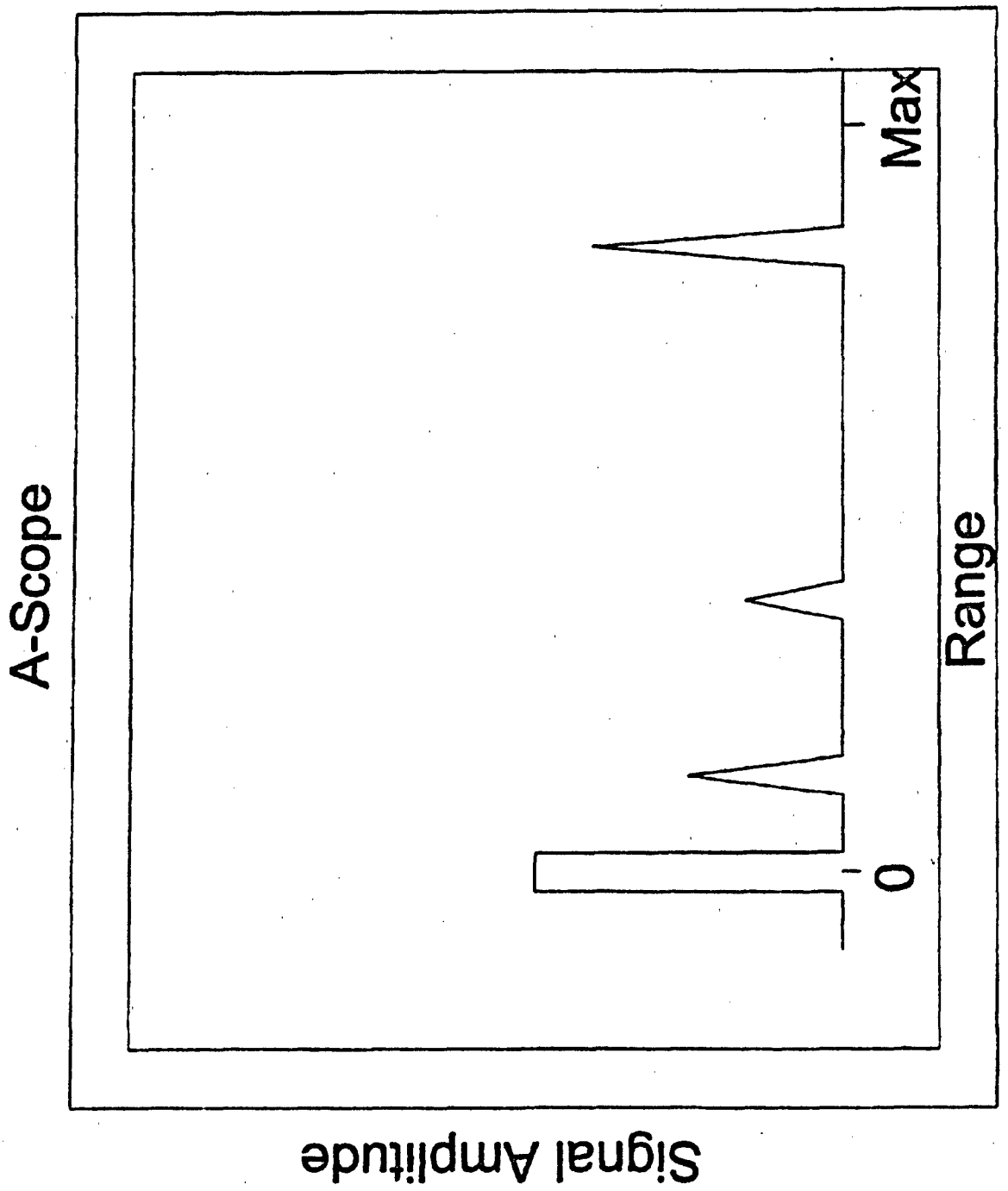

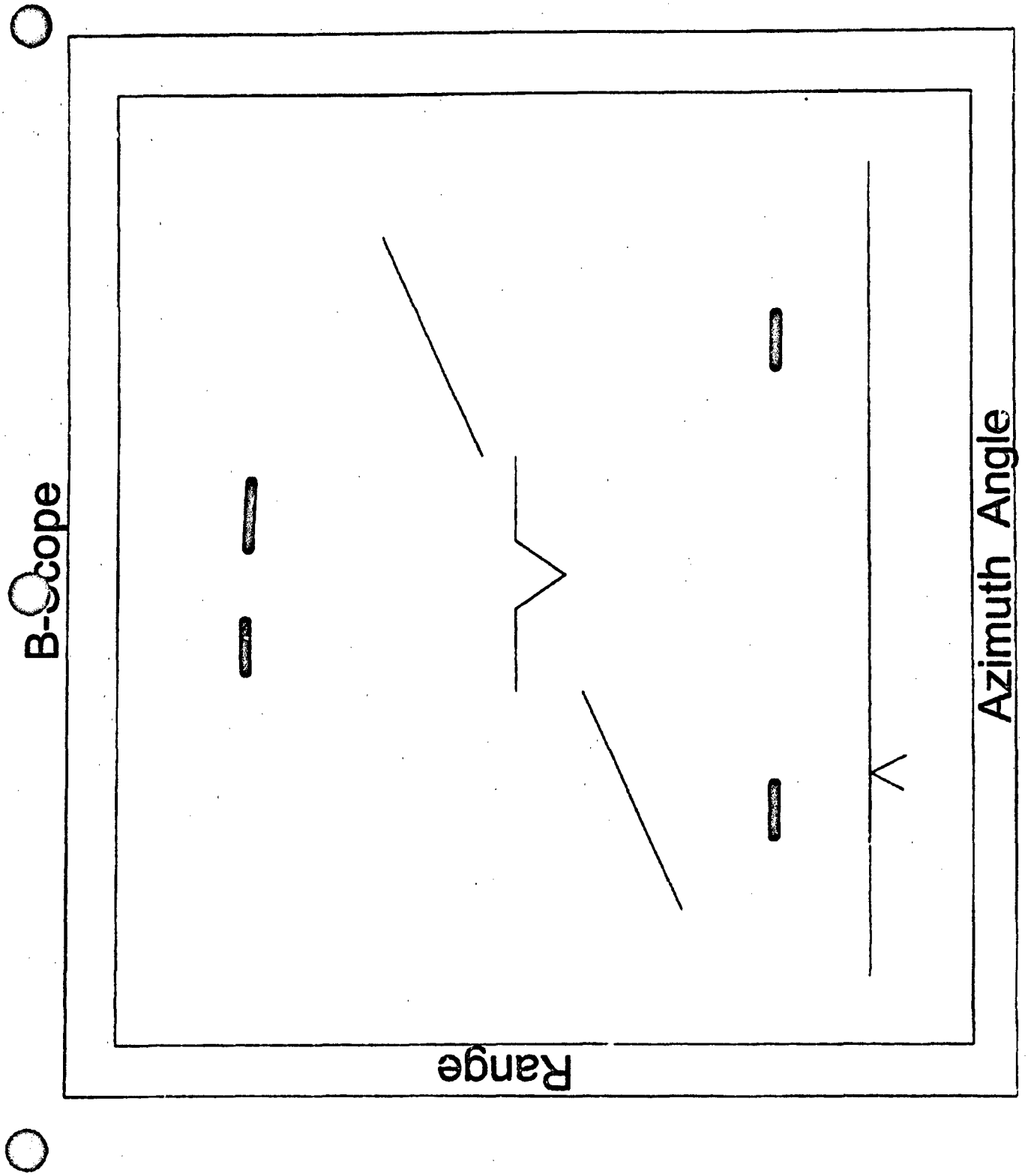

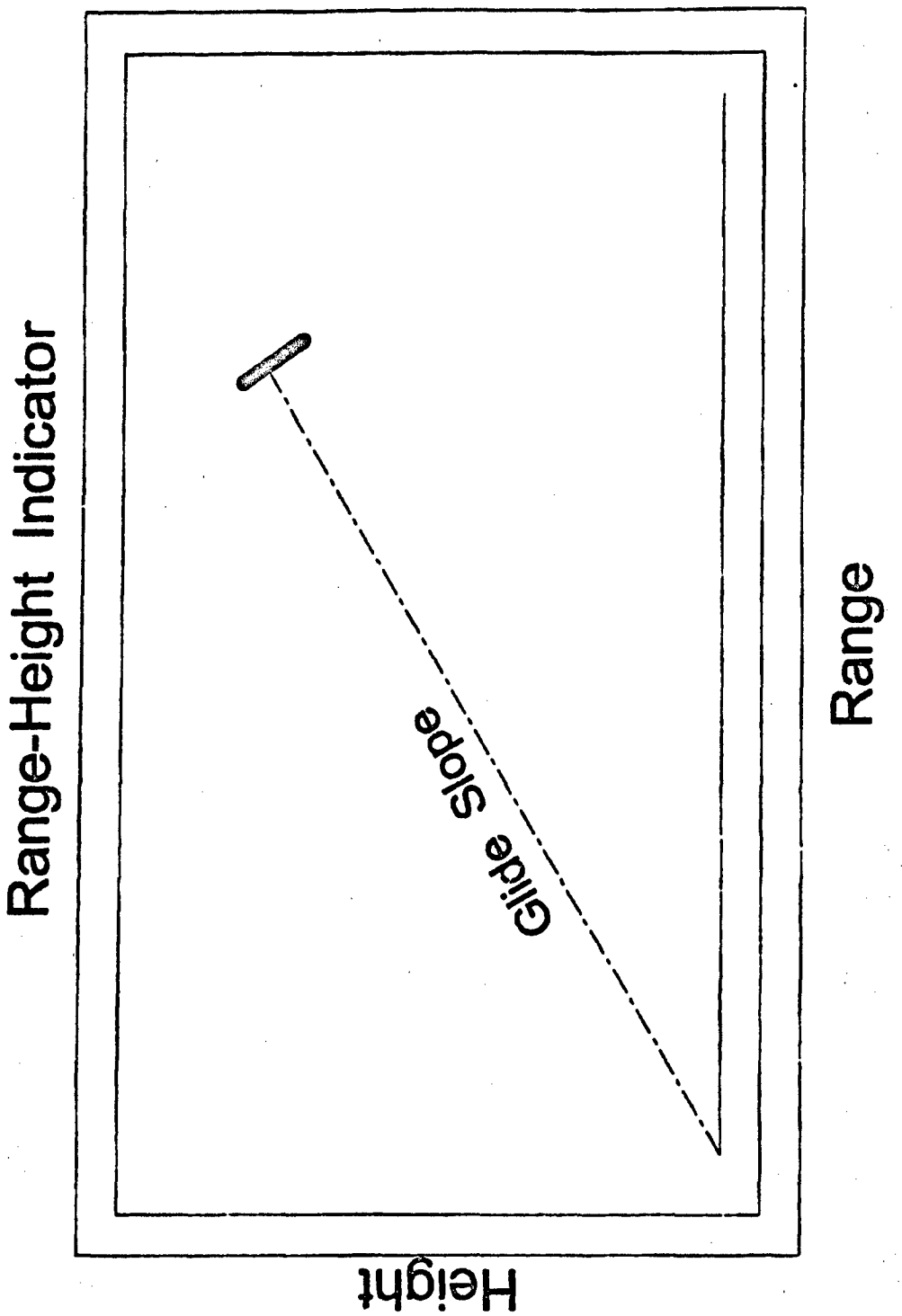

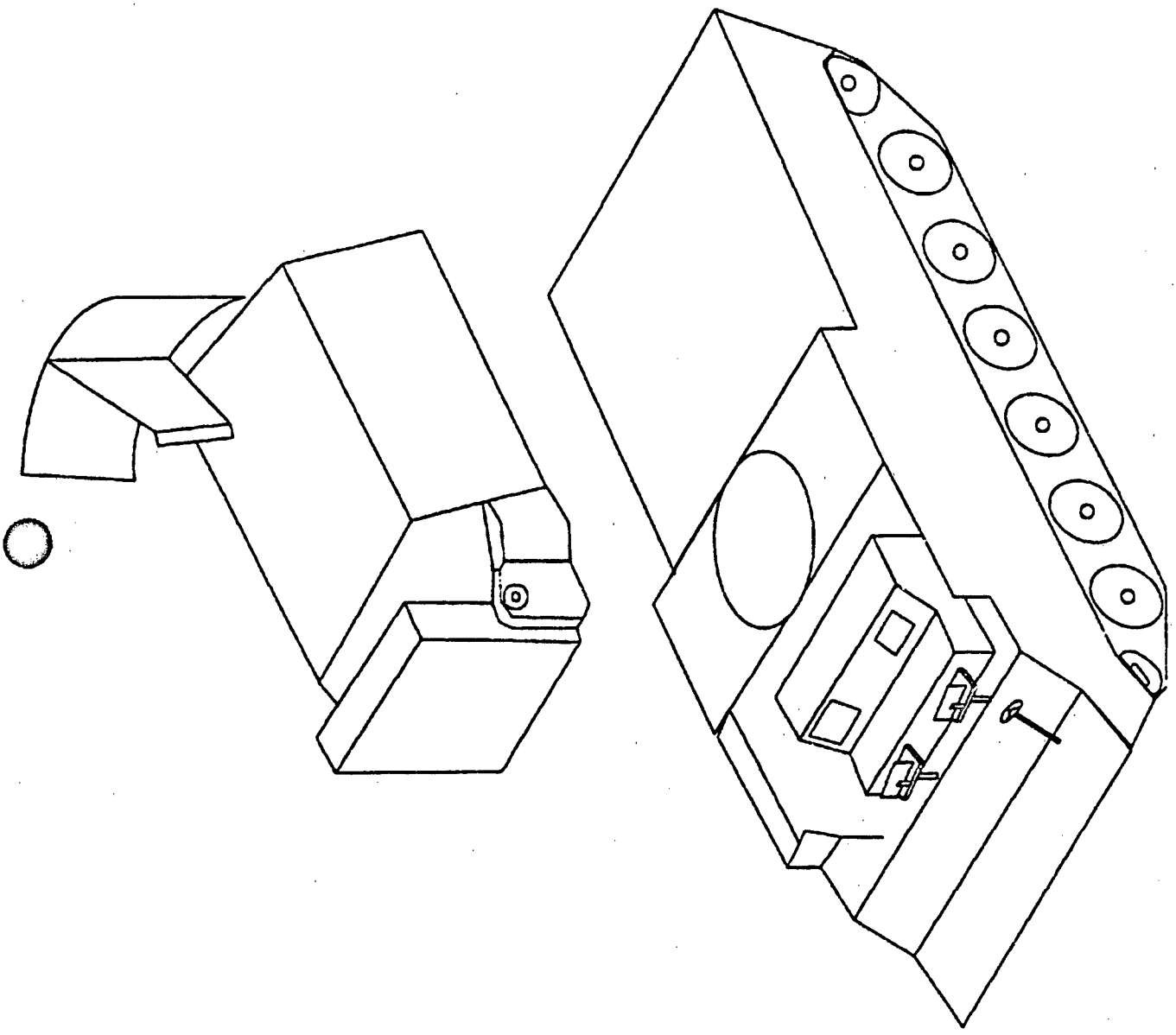

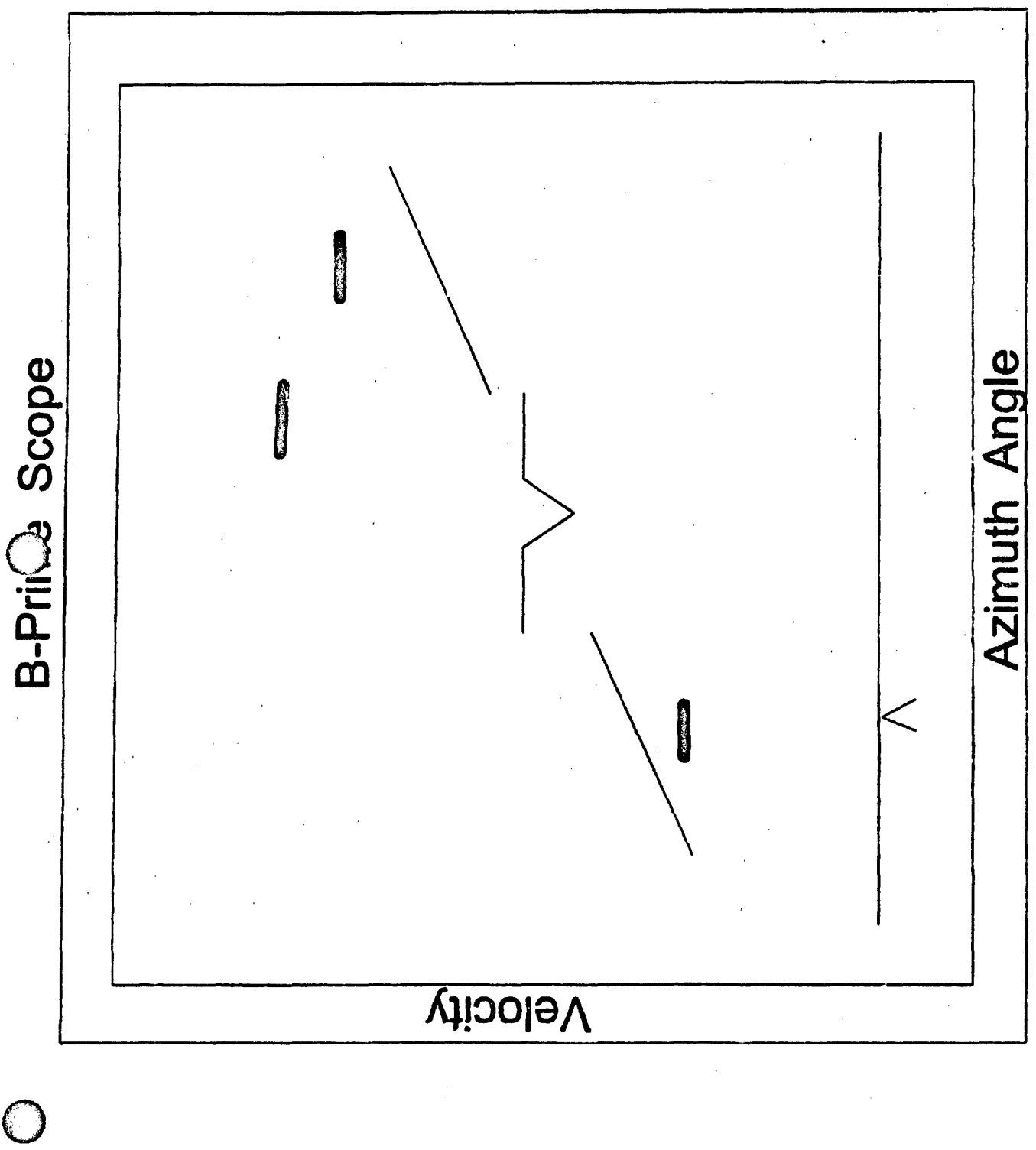
B-Pri Scope
Azimuth Angle
Velocity

DJ-0046C 061193

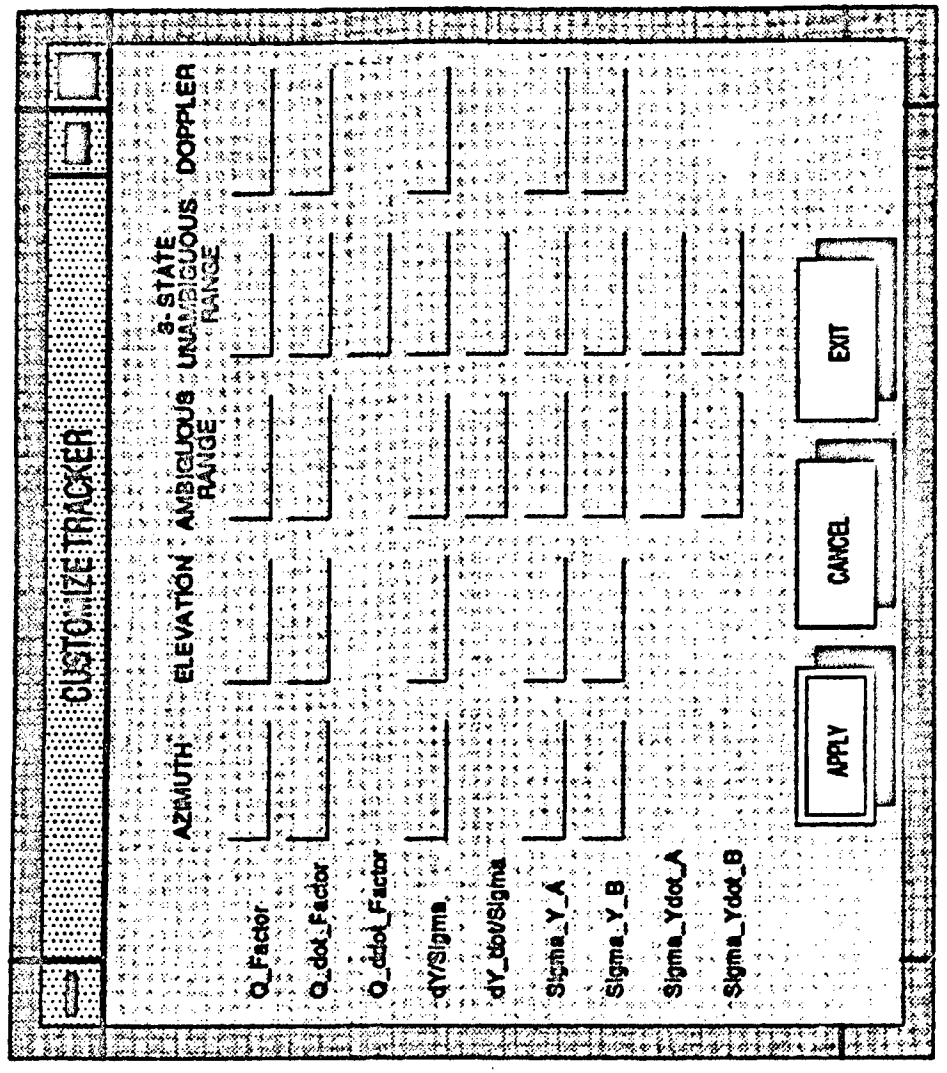
CUSTOMIZE TRACKER
AZIMUTH
ELEVATION
AMBIGUOUS RANGE
3-STATE UNAMBIGUOUS RANGE
DOPPLER
Q_Factor
Q_dot_Factor
Q_ddot_Factor
dY/Sigma
dY_dot/Sigma
Sigma_Y_A
Sigma_Y_B
Sigma_Ydot_A
Sigma_Ydot_B
APPLY
CANCEL
EXIT

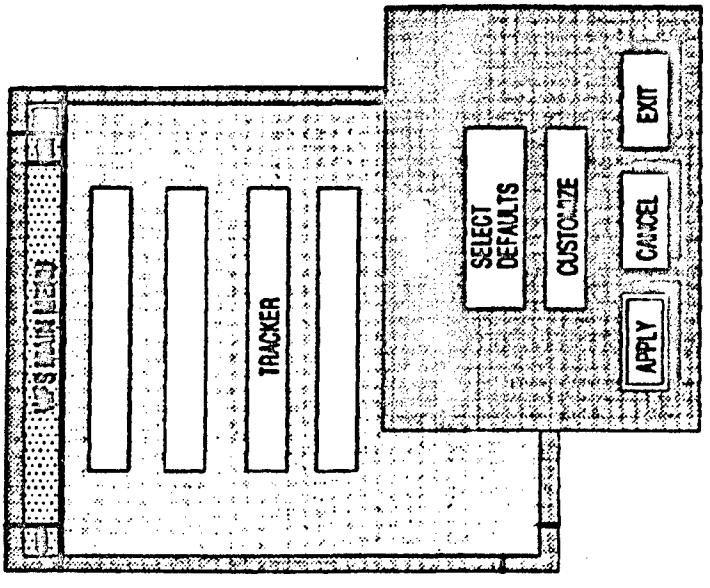
TRACKER
SELECT DEFAULTS
CUSTOMIZE
APPLY
CANCEL
EXIT

* WARNING
ERROR CONTACTING
A/D CONTROLLER or
A/D 0 > 5
ACKNOWLEDGED
* WARNING
FILE DOES NOT EXIST
ON CURRENT DRIVE
ACKNOWLEDGED
FILTER
OK
CANCEL
EXIT
CANCEL
APPLY
Data Handling
A/D CONVERSION
ARCHIVE
PLAYBACK PROCESSED DATA
PLAYBACK RAW DATA
EXIT
CANCEL
APPLY
* WARNING
INSTALL TAPE (DISKS) IN DRIVE(s)
ACKNOWLEDGED
DJ-0045D 071993

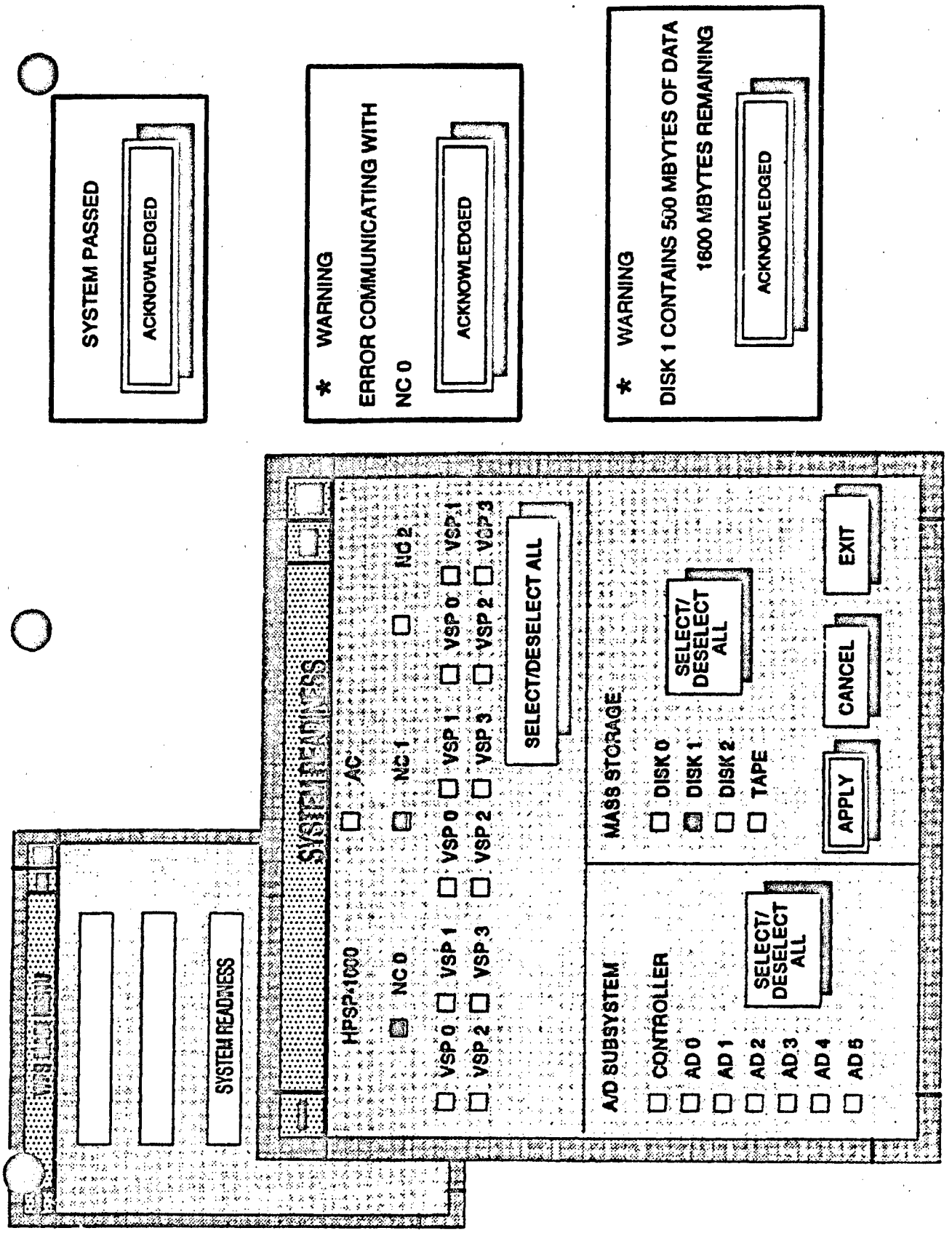
SYSTEM PASSED
ACKNOWLEDGED
* WARNING
ERROR COMMUNICATING WITH
NC 0
ACKNOWLEDGED
* WARNING
DISK 1 CONTAINS 500 MBYTES OF DATA
1600 MBYTES REMAINING
ACKNOWLEDGED
SYSTEM READINESS
HPSP-1000
AC
NC 0
NC 1
NC 2
VSP 0
VSP 1
VSP 2
VSP 3
SELECT/DESELECT ALL
MASS STORAGE
DISK 0
DISK 1
DISK 2
TAPE
SELECT/ DESELECT ALL
APPLY
CANCEL
EXIT
A/D SUBSYSTEM
CONTROLLER
AD 0
AD 1
AD 2
AD 3
AD 4
AD 5
SELECT/ DESELECT ALL

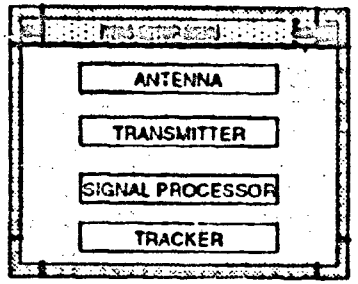
ANTENNA
TRANSMITTER
SIGNAL PROCESSOR
TRACKER

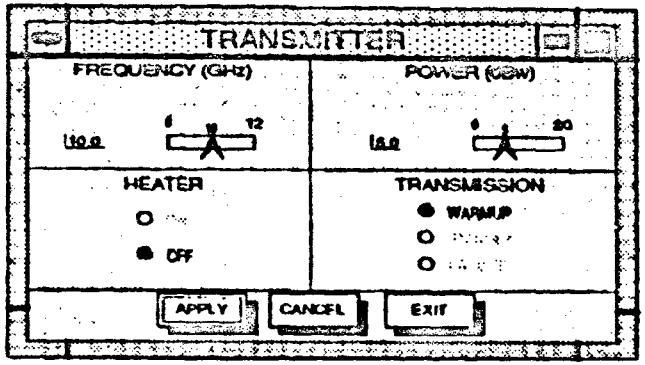
TRANSMITTER
FREQUENCY (GHz)
POWER (dBW)
HEATER
OFF
TRANSMISSION
APPLY
CANCEL
EXIT

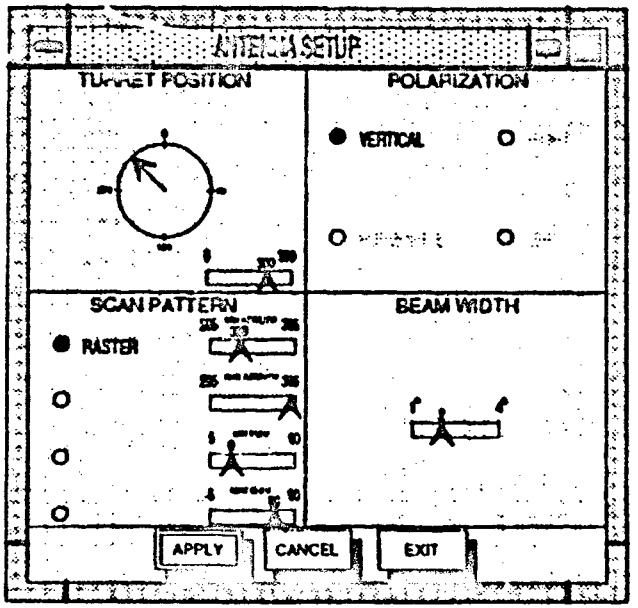
ANTENNA SETUP
TURRET POSITION
POLARIZATION
VERTICAL
SCAN PATTERN
RASTER
BEAM WIDTH
APPLY
CANCEL
EXIT

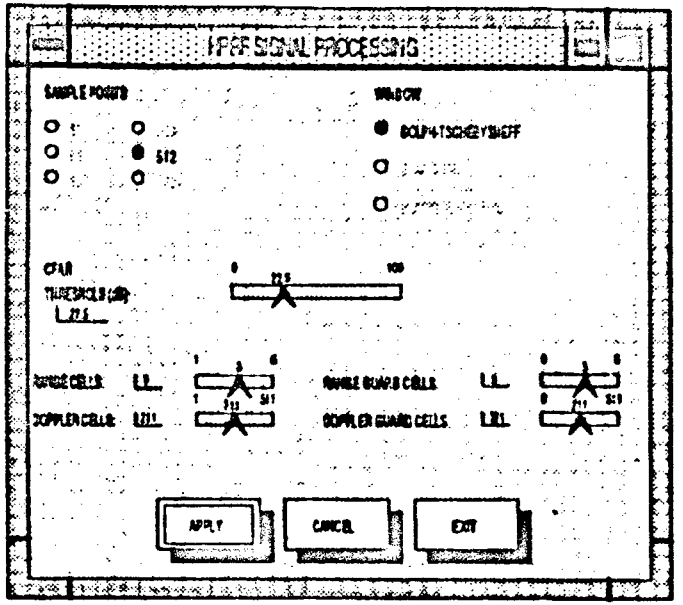
PRF SIGNAL PROCESSING
APPLY
CANCEL
EXIT

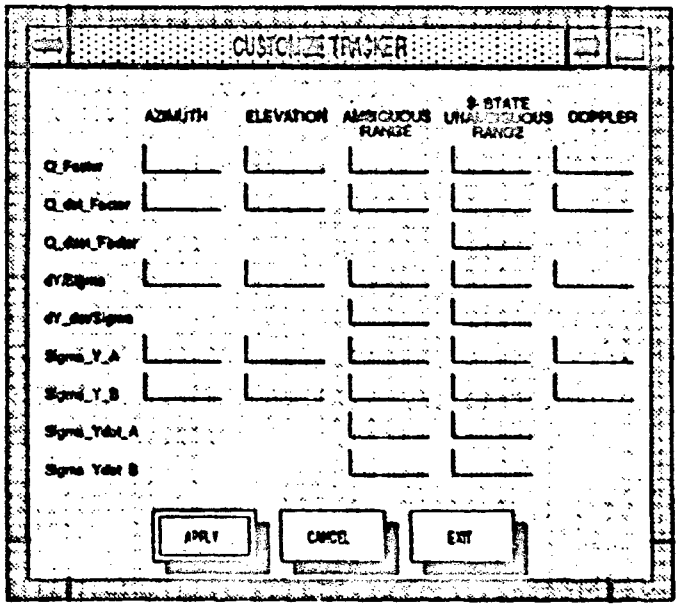
CUSTOMIZE TRACKER
AZIMUTH
ELEVATION
AMBIGUOUS RANGE
UNAMBIGUOUS RANGE
DOPPLER
APPLY
CANCEL
EXIT

TECHNICAL MEMORANDA

TECHNICAL MEMO

To: List
From: J. K. Beard
Date: 23 October 1992
Reference: JKB-92-08
Subject: Capabilities and Limitations of Conventional Computer Architectures

1.0 SUMMARY

There are four broad classifications of conventional computer architectures which include most commercially available computers and microprocessors: Von Neumann (conventional), Harvard (digital signal processor), vectorized (supercomputer), and distributed (systolic, pipelined FFT, etc.). The Von Neumann is the most versatile but the least efficient. The others are much faster in their application areas, but are not as suitable for general purpose computing.

2.0 THE FOUR CONVENTIONAL ARCHITECTURES

Computer architectures are an art and a science, and as such cannot be truly bound by arbitrarily defining a few bins into which all must fall. Observation of the field reveals that nearly all commercially available computers and computer chips do fall into four broad categories. The is one major counterexample that proves the rule, the TI TMS320Cx0 series. A fifth category, hard-wired processors, is also discussed, and its relationship with the other categories.

Generally speaking, efficiency is the average percentage of transistors or gates in a processor that is functioning productively during execution of a program. Speed is obtained by obtaining a higher efficiency, and also by having more gates in the architecture. To obtain very high speeds, the organization of the gates must be directed toward a narrow range of application areas. This means that there exists a tradeoff between speed and flexibility in selection of architectures.

2.1 The Von Neumann Architecture

2.1.1 General definition. The Von Neumann architecture is the conventional architecture we are accustomed to seeing in most mainframes, minicomputers, and microcomputers. This architecture is characterized by a large general purpose memory and a central processor, with the programs and data sharing the memory. The processor itself has a limited amount of memory for data array indexing and address calculation, and for intermediate products of arithmetic expression evaluation. Each instruction must be fetched from memory and does just one thing (this is the "Von Neumann Bottleneck"). Examples are microprocessor chips such as the 8080, 6502, 6800 series, Z80, 680x0 series, and 80x86 series. Other examples are most computers built until very recently, including the IBM 1401 and 1620 series, the CDC 1604 and 3200 series, the

Univac 1108 series, and nearly all minicomputers such as the Honeywell 516 series, DEC PDP-11 and VAX series.

2.1.2 CISC and RISC variants. The complex instruction set (CISC) designation has been given to existing computer types whose assembly language or machine level instructions were designed for ease of programming. The examples given above have CISC instruction sets.

In recent years, a new philosophy has been discovered which seems more efficient in implementation, although it is not obvious on the face of it. A reduced instruction set (RISC) CPU will be able to operate as fast as a CISC doing the same things with the same registers and data paths, if the simpler instructions can be strung together to perform the same operations as each CISC instruction in the same time. An example of this is the 8080 as compared to the Z80; the Z80 is far easier to program because of its extra high-level instructions, but it is no faster than an 8080. In addition, having lower-level instructions available guarantees that you can string them together to do just about anything as efficiently as possible, so that RISC instruction sets are more versatile than CISC instruction sets.

Other properties that characterize RISC instruction sets are (1) a large number of registers available for arithmetic and indexing, and (2) the ability to execute any instruction in one clock cycle. A CISC processor may have four to 16 registers for indexing and arithmetic, whereas a RISC processor will have 32 to 1024 or even more. Examples of RISC instruction sets are the i860, i960, Motorola 88000, MIPS R2000 and R3000 chip sets, and others. RISC computers include the Sun RISCStation and many other high-end workstations, the IBM RISC 6000 series PC's, many of the new Hewlett Packard workstations, the new DECStation desktop minicomputers, and the new RISC DEC computers (distinguished from the VAX series by the use of DEC or ALPHA in place of VAX in their designation).

The RISC instruction set philosophy results in higher efficiency because its smaller number of instructions results in a higher percentage of its architecture operating during any given instruction. Higher speeds result because the total amount of time required to perform a specific operation is equal to or better than that of a comparable CISC instruction set.

2.2 Vectorized Architectures

Massive computational problems such as heat transfer, nuclear reactor modeling, finite element analysis for design of buildings, bridges, and automobiles, and many other applications usually reduce to large linear algebra problems when implemented as computer programs. Research on ways to build computers to work these problems focussed on the vector dot product as the fundamental computation in linear algebra. Computers which performed the FORTRAN operations

C=0.

```
DO I=1,N
  C=C+A(NA+N1*I)*B(NB+N2*I)
  END DO
```

in a single microcoded instruction were designed. The number N is the vector length, NA and NB are address offsets, and N1 and N2 are the strides of the vectors A and B. The weakness of this architecture is that, although it will do very well on benchmarks related to its intended purpose such as LINPACK (Jack Dongarra's linear algebra utility package benchmarks, originally out of Argonne National Laboratories and now out of Oak Ridge National Laboratory), it is far less efficient for other things such as general purpose short programs with no vector arithmetic, such as the Whetstone benchmarks.

Examples of vectorized architectures are all the Cray machines and most supercomputers by CDC, IBM, NEC, Hitachi, Siemens and others.

2.3 Harvard Architecture

The Harvard architecture was originally developed as a way to add programmability and flexibility to hard-wired digital signal processors. The Harvard architecture is characterized by (1) a separate memory for instructions and for data, usually with different word lengths, and (2) execution of every instruction the processor is capable of in every clock cycle. Typically, a Harvard architecture machine uses a 128-bit wide instruction word, a 32-bit complex integer data word, and pipelines both instruction prefetches and data block fetches, as well as its arithmetic instructions. Nearly all Harvard architecture processors are used for digital signal processing and execute an entire radix two or radix four FFT butterfly in a single clock cycle. A radix two FFT butterfly is an operation, using complex arithmetic, of the form

```
ZT=Z(J)*(COS_THETA,SIN_THETA)
Z(J)=Z(I)-ZT
Z(I)=Z(I)+ZT
```

where the angle THETA is constant over ranges of I and J but varies during the FFT. A radix four butterfly is similar, but the operations are done in two steps, each of which involves two radix two butterflies where THETA is $\pi/2$, and three other complex multiplies are used to prepare the data for storage. The data flow in the architecture usually involves two register files, one which receives data from main memory in buffered and pipelined memory block fetches, and the other which holds data that is stored back to memory in similarly buffered and pipelined stores. This register file configuration, with its pipelined access to general memory, is necessary to remove the memory access timing as a restriction on arithmetic speed. The ALU performs real or complex multiply adds from either register file and ROM data containing sines and cosines, filter weights, and other fixed data.

The architecture is usually expanded to allow two real multiply-adds in place of each complex multiply-add, so that convolution filtering and most other digital signal

processing algorithms may be processed efficiently.

Examples of the Harvard architecture, or variants of it, are the Hughes VSP signal processing chip set used in the HPSP-1000, a similar chip set used in the signal processing board for the Hughes airborne radar signal processor for the ATF program, the Analog Devices 2100 and 21000 series chip sets, the AT&T DSP3 chip set, and others.

2.4 Distributed Architectures

Distributed architectures are a set of categories in themselves. Most commercial offerings of distributed processing are either pipelined FFTs or systolic processors.

Pipelined FFTs are usually in the form of a set of identical cards, each of which performs the computations of an FFT. The Cooley-Tukey radix 2 or radix 4 is usually used, but there do exist Winograd FFTs in this class. For clock rates on the order of 10 MHz, an input data point and an output data point, both complex, are obtained for each clock cycle.

Systolic processors are usually matrices of identical processors with a grid of interconnections. Commercial offerings of systolic processors such as N Cube, Systolic Systems, and others have been seen for several years. Most major system vendors have internal systolic processor development efforts, also.

2.5 Hard-Wired Architectures

Hard-wired processing is still used when maximum speed and efficiency is absolutely necessary, such as space applications, ultra-high speed problems such as real-time image processing, some missile seekers, and EW receivers. Processors of this type were the technological ancestor of Harvard architecture processors. They represent the highest efficiency but the least flexibility of any architecture type.

3.0 ADVANTAGES AND LIMITATIONS

3.1 The Von Neumann Architecture

The Von Neumann architecture was developed to solve the problem of interfacing instructions in memory to digital hardware, and the instructions were designed to be easy to use. The CISC instruction set philosophy was part of the paradigm for this reason until very recently. Compiler code generators and optimizers for CISC instruction sets can be shown to be near the optimum for the available hardware for wide classes of program flow configurations. For RISC instruction sets, compilers are more difficult to write and optimizers are still as much an art as a science, but more efficient use of hardware results in faster benchmarks for a given chip complexity and clock speed.

The major disadvantage of Von Neumann architectures is the "Von Neumann

Bottleneck," which is the limitation of one CPU action per instruction. Lack of parallelism means all of the hardware not being used in the current instruction is idle, so that speeds per gate of CPU hardware is low.

3.2 Vectorized Architectures

Computers using vectorized architectures approach their maximum peak design speeds only with vast linear algebra problems, such as 1000 by 1000 matrix operations. For scalar operations, speeds reflecting about 10% of their maximum peak speeds are not unusual.

3.3 Harvard Architecture

Harvard architecture processors use all of their hardware in every instruction in some applications, and therefore have the highest speeds for a given clock rate and complexity of CPU hardware. However, the scope of applications for which this holds true is very narrow, including primarily FFTs and various types of digital filtering.

Floating point instructions have appeared in recent versions; the wider bus widths required to accommodate complex floating point data have not yet followed. The result is that floating point speeds are a factor of two to four slower than fixed point arithmetic in the best of the floating point chip sets. An architecture which can process two real fixed point multiply-adds in a clock cycle will have a 32 bit bus width and can process one floating point multiply-add per clock cycle.

The complex data flows associated with architectures optimized for 16 bit fixed point FFTs involve internal register files. Use of internal CPU register files is very inefficient for operations such as squaring floating point numbers or computing functions such as sines, cosines, logarithms, and exponential. Often such architectures have little or n provision for division, even with floating point. Therefore, use of Harvard architectures for operations not related to FFTs and digital signal processing algorithms varies from inefficient to impossible.

3.4 The TI TMS320 Family

An interesting maverick architecture is the Texas Instruments TMS320 series. This chip has what TI calls a modified Harvard architecture, in which program and data memory are shared. The instruction width is sufficiently narrow that much of the chip must lie dormant during many instructions, but the result is a simple enough instruction set so that compiler code generation is not impossible. The data flow is pipelined and operates on memory data like a Von Neumann architecture, not on register files like Harvard architectures. The result is a chip which approaches the speeds of Harvard architecture digital signal processing chip sets, but can do it with floating point arithmetic as well as fixed point arithmetic. Compilers for the C programming language, Ada, and others are available from TI for cross-compiler platforms, and reasonably efficient (i.e., usable) code results from use of these compilers. The TMS320C60 series, which is due

for introduction shortly, will probably knock on the door of fixed point Harvard architecture chip sets, and do it with floating point arithmetic and C or Ada source code.

3.5 Distributed architectures

Distributed architectures can have very high speeds. Recent offerings by Intel are in the supercomputer range. The high speeds are obtained by distributing the processor in parallel across the processors as well as in serial, so that massive parallelism is obtained. A pipelined FFT is an example of a systolic architecture which is not programmable. This illustrates the critical problem in systolic architectures: problems which were not foreseen in the design may be difficult or impossible to implement efficiently.

3.6 Hard-wired architectures

Hard-wired architectures are the extreme in the tradeoff between speed and efficiency on one hand and versatility on the other. Full efficiency is obtained by a good design, with little or no flexibility in performing different problems.

4.0 CONCLUSIONS

At this time, a maximum efficiency real-time processor will necessarily use a Harvard architecture or hard-wired signal processor for best cost-effectiveness for high-speed digital signal processing. Once the data is past a detection thresholding operation, the data rate is smaller by orders of magnitude, and slower processors can be used for post-detection processing such as tracking. RISC architectures are the most cost-effective here because these processors offer the best efficiency available in chip-level processors.

The TI TMS320 chip set series can be used if floating point signal processing is necessary, or if the speeds obtainable with these chips is acceptable. In another generation or two, chips in this TI series may be capable of competing with fixed point digital signal processors using Harvard architectures. These processors have the additional advantage that they may reasonably be used for post-detection processing, unlike Harvard architecture processors.

Other alternatives to Harvard architectures are RISC chip sets like the i860, i960, MIPS 3000, etc. Software support for these chips is even better than for the TI chips, but speeds are lower.

TECHNICAL MEMORANDUM

To: List
From: J. K. Beard
Date: 21 December 1992
Reference: JKB-92-13A
Subject: Subclutter Visibility in Pulse Doppler Radars

1.0 SUMMARY

Meeting a specified subclutter visibility requirement in a pulse Doppler radar is distinct from the same design requirement in surveillance radars because dwells on the target are single pulse trains of limited length. Requirements for a high degree of subclutter visibility raise issues not seen in older systems. Two methods are examined for achieving high subclutter visibility, one using analog range gating and one using digital range gating.

Revision A, which expanded on the equations derived in the appendices and corrected a minor arithmetic error, was issued on January 5, 1992.

2.0 PROBLEM STATEMENT

Subclutter visibility is defined as the noise floor in the range-Doppler map computed in the signal processor, relative to the total clutter power. The number of bits in the analog to digital converter (A to D) is defined as the dynamic range bottleneck. This reduces the problem for analysis purposes to determining the dynamic range in the range-Doppler map as a function of the number of bits in the A to D.

Two signal processor baselines are analyzed here:

1. Analog range gating at I.F., followed by quadrature demodulators. The outputs of the quadrature demodulators are low pass filtered to remove the PRF lines, and high pass filtered to lower the clutter power into the A to D. This signal is provided to dual A to D converters to provide a complex digital signal for the FFT. A windowed FFT is used to prevent the clutter from splattering into the clear Doppler region.

2. A quadrature demodulator is used at I.F. This two-channel analog signal is provided to dual A to D converters and is digitized at the rate of two complex samples per range gate. The two samples are added to provide a single data point for each range gate. This digital range gated signal is provided to a windowed FFT.

The analog range gating baseline uses an analog clutter notch filter. This analog clutter notch filter must be allowed to settle or its ringing will limit subclutter visibility. However, this allows the subclutter visibility to be broken up into two parts: the clutter notch attenuation and the FFT window sidelobe attenuation. The linking parameter is the proportion of the dwell time

allocated to settling for the clutter filter and for the FFT dwell.

A clutter notch is not used in the digital range gating baseline on the grounds that such a narrow-band filter may cause range sidelobes. It may be argued that a clutter notch has little phase delay outside its stopband, and that a clutter notch could be used at I.F. or baseband without causing significant range sidelobe problems. This possibility is beyond the scope of this report and is not discussed further here.

3.0 BASELINES

3.1 Analog Range Gating

3.1.1 The design equations. The design is formulated by defining tradeoffs between the clutter notch, the number of bits in the A to D, and the FFT dwell time.

The analog range gate baseline uses a clutter filter to lower the dynamic range of he clutter into the A to D. The settling time of an n-pole filter with a band edge at f_0 for a subclutter visibility requirement of S (power ratio) is about (see Appendix).

$$t_s = \frac{n(10 \cdot \log_{10} S)}{85.73 f_0} \qquad (1)$$

A certain amount of dwell is necessary in a high PRF system to wait for returns from maximum range targets. This dwell is

$$t_{RMAX} = \frac{2R_{MAX}}{c} \qquad (2)$$

and may be concurrent with the clutter notch filter settling time because the clutter will be dominated by the first time around returns. A balanced design will match these times as closely as possible.

A 100 nmi system has a t_{RMAX} of 1.24 ms. This settling time for a 2 pole filter requiring 100 dB of subclutter visibility would require that the clutter notch be about 2 kHz wide.

3.1.2 Noise floor analysis. The A to D LSB noise is assumed to be the sensitivity limit here. If the clutter notch attenuates the clutter power by a factor of S_1 and the A to D has N bits, the noise floor, broad band, will be down from the clutter power (as reduced by the clutter notch) by a factor of (see Appendix)

$$\text{Noise floor} = \frac{2}{3} \cdot 2^{-2N}. \tag{3}$$

The FFT will have a noise bandwidth which is determined by the PRF, which is the sample rate into the FFT, and the spectral window used. A 512 weight 100 dB window is given in the Appendix. This example shows a window broadening factor for noise bandwidth of 1.9441, which will be used here. The noise floor in the FFT bin is then

$$\text{FFT noise floor} = \frac{2 \cdot 1.9441}{3N_{FFT}} \cdot 2^{-2N} \tag{4}$$

which, when set equal to the required subclutter visibility power ratio S_1/S and solved for the number of bits N in the A to D, gives us

$$N = \frac{10\log_{10}S - 10\log_{10}S_1 - 10\log_{10}N_{FFT} + 1.126}{6.02} \tag{5}$$

The number given by Equation ? must be recognized as an ultimate minimum. Any realistic system must use an A to D with at least 2 more bits to achieve the A to D dynamic range required and allow a few dB margin.

3.2 Digital Range Gating

3.2.1 The design equations. The block diagram of this alternative uses no clutter notch, because the transient response of any filter which precedes the range gating may give rise to range sidelobes. The use of two samples per range gate and adding the samples does not change the dynamic range equations. Therefore, using a value of S_1 of 1 in the above design equations will give the number of bits necessary when digital range gating is used.

3.2.2 Noise floor analysis. The noise floor analysis is identical to that used above when a value of 1 is used for S_1. Since no clutter filter is used, no settling time is necessary in this design. The number of bits required in the A to D is

$$N = \frac{10\log_{10}S - 10\log_{10}N_{FFT} + 1.126}{6.02} \tag{6}$$

If a clutter notch attenuation of 40 dB is used in the analog range gate approach, the A to D requirement will be smaller by 6.6 bits.

4.0 CONCLUSIONS

Conclusions require that numerical values of parameters be used the results compared to available A to D modules. Table 1 below summarizes a case where 100 dB of subclutter visibility is required and a 40 dB clutter notch is used with the analog range gated system.

Table 1. Design Example

Parameter	Value
Subclutter visibility requirement	100 dB
Clutter notch attenuation	40 dB
No. of points in FFT	512
Ideal/practical A to D requirement	5.7/8 bits
Ideal/practical digital range gate A to D	12.3/14 bits

For the example given, the 40 dB clutter notch gives a 6.6 bit advantage to the A to D requirements in favor of the analog range gating. In addition, the analog range gated system must be sampled at the PRF for a number of channels equal to the number of range gates processed, while the digital range gated system must sample at twice the I.F. bandwidth. Therefore, a simpler, lower cost system is produced using the analog range gating system.

Analog Devices sells a 14 bit 10 MHz A to D, the AD 9014, which apparently meets the dynamic range requirement of 13 bits, ideal equivalent. This means that the digital range gated system is feasible. It is likely that such a system would be higher in cost than the analog range gating approach. Use of this technique would depend on whether a system performance advantage was obtained which was worth the extra cost.

5.0 APPENDICES

5.1 Dynamic Range in A to D Outputs from Quadrature Demodulators

A digital word of N bits will have a peak value of 2^{N-1}-1 and a noise power or σ^2 from rounding of 1/12 the least significant bit (LSB) squared. For a complex signal, the maximum peak sine wave will have a peak value of about 2^{N-1}, and the noise will be twice that seen in a single word. Therefore, the maximum dynamic range of a sine wave to LSB noise is, as a power ratio,

$$SNR_{MAX} = \frac{3}{2} \cdot 2^{2N} \quad \text{(ideal)}. \tag{7}$$

Actual A to D converters usually have about 1.5 bits less dynamic range than is predicted by the ideal equation. The dynamic range figures guaranteed on the data sheet will give a worst case. In critical applications, the A to D should be tested against its dynamic range specification as part of the acceptance procedure.

5.2 Noise Bandwidth of a 100 dB 512 Point Spectral Window

A windowed FFT is a digital filter bank. Each filter in the filter bank is a simple convolution filter operating on complex data with complex coefficients.

Conventional window functions are real convolution filters with a low pass frequency response. The frequency response of each FFT bin is an exact replica of the frequency response of the window, but shifted to the center frequency of the FFT bin. Each filter in the digital filter bank has the same noise bandwidth. Therefore, the FFT filter bank is characterized by a single number for noise bandwidth which applies for all FFT bins.

We can use an analogy with the perfect rectangular passband filter to define the noise bandwidth in terms of the window weights as follows. Consider a complex data stream sampled at a rate of f_s. Since each filter in the digital filter bank has the same frequency response shape, they all have the same noise bandwidth. We can use an analogy with the perfect rectangular passband filter to define the noise bandwidth in terms of the window weights as follows.

Consider a complex data stream sampled at a rate of f_s. The unambiguous or Nyquist frequency range is $-\frac{1}{2}f_s$ to $+\frac{1}{2}f_s$. If white noise of variance 1.0 is sampled, the resulting data stream is white, or uncorrelated, but is bandlimited over a bandwidth of f_s, so that the power spectral density is $1/f_s$. Therefore, if this data is passed through a perfect rectangular bandshape filter with passband insertion loss 0 dB and bandwidth B, the variance of its output will be B/f_s.

The zero frequency FFT bin is a low pass filter. Its weights are real, and are the same as the window weights. The output of the zero frequency FFT bin for input consisting a simple DC signal of amplitude 1.0 is the sum of its weights. The output of the zero frequency bin to the white noise data stream of rms amplitude 1.0 is the sum of the square of its weights. By analogy with the perfect rectangular bandpass filter, the noise bandwidth of the window B_n can therefore be given in terms of its weights w_i be equating ratio of the passband peak to the variance of white normalized noises:

$$\frac{B_n}{f_s} = \frac{\sum_{i=1}^{N} w_i^2}{\left(\sum_{i=1}^{N} w_i\right)^2}. \tag{8}$$

Here, we introduce a noise bandwidth broadening factor β, given by

$$\beta = N\frac{\sum_{i=1}^{N} w_i^2}{\left(\sum_{i=1}^{N} w_i\right)^2}. \tag{9}$$

The noise bandwidth is given by

$$B_n = \beta\frac{f_s}{N}. \tag{10}$$

Cauchy's Inequality can be used to show that β has a minimum value of 1, which is achieved when all the w_i are equal. This is the rationale for calling β the noise bandwidth broadening factor. The noise bandwidth for any window is easily found from β using Equation (10), which in turn is easily found from the window weights using Equation (9).

A 512-point Dolph-Chebychev window designed for 100 dB equiripple sidelobes is shown as Figure 1 below. Other output from the program which designed this window, including β, is shown below in Table 2.

Table 2. Dolph-Chebychev Window Design

Parameter	Value
3 dB Broadening Factor	1.8419
Noise Bandwidth	1.9441 f_s/N
Peak FFT Crossover Scalloping Loss	-8.783 dB

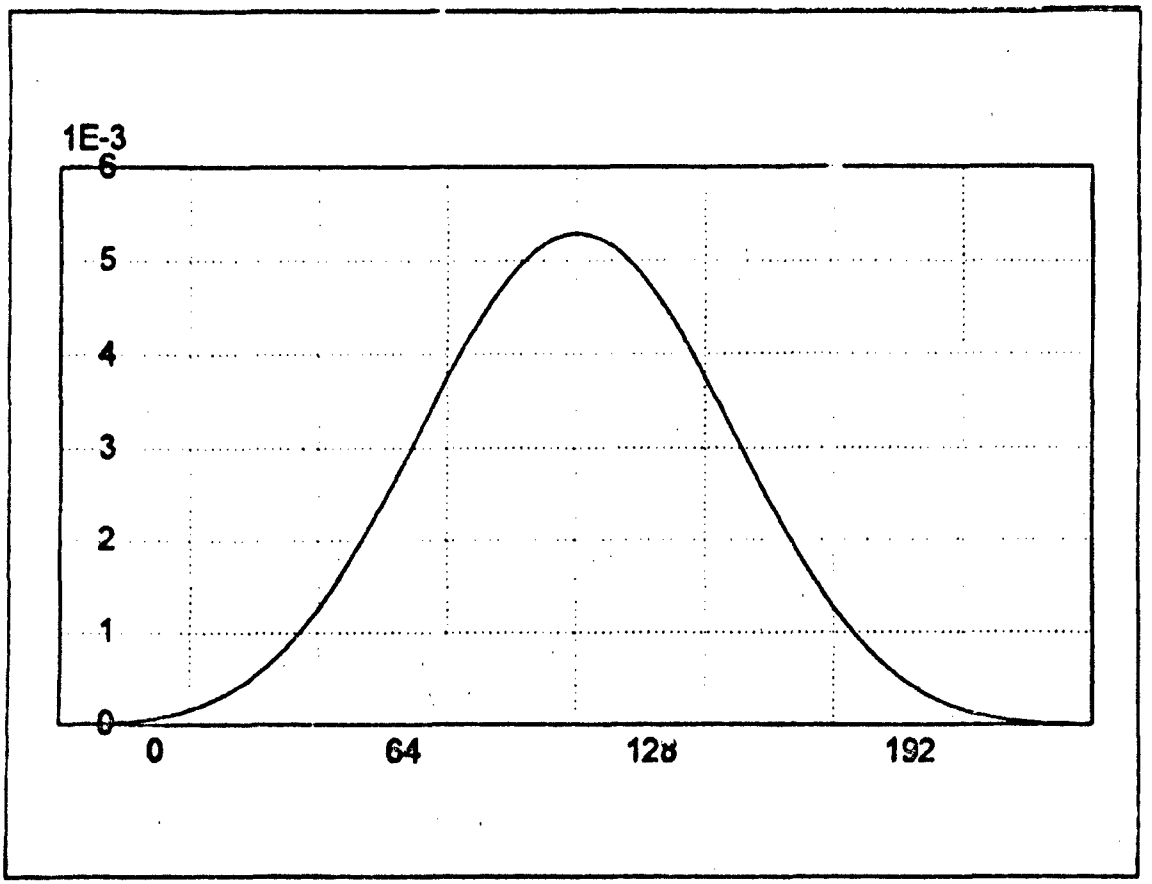

Figure 1. 100 dB, 512 Weight Dolph-Chebychev Window

5.3 Settling Times for Analog Filters

For the purposes of this report, Butterworth high pass filters will be used as an analysis baseline. The driving parameter of this analysis is the highest Q seen in the filter poles Butterworth filters have a very moderate Q for their selectivity. If other filters such as elliptic filters which have higher Q's are used, those filters will have much slower settling times than are predicted by this analysis.

The transfer function for an n-pole high pass Butterworth filter is, in terms of Laplace transforms,

$$|H(s)|^2 = \frac{\left(\frac{s}{js_0}\right)^{2n}}{1+\left(\frac{s}{js_0}\right)^{2n}} \qquad (11)$$

where $s_0/2\pi$ is tne passband limit. From Equation (11), the poles are s_0 times the $2n^{th}$ roots of 1; that is, they are evenly spaced on a circle of radius s_0, and the angular separation between them is π/n.

Only the stable poles are taken when H(s) is found. The settling time is estimated from the transient response from the highest Q pole pair. The exact location of the poles is easily found by drawing a circle on the complex s plane and noting that the imaginary axis always bisects an arc of the circle between two of the roots. The highest Q pole pair are those in the left half plane closest to the imaginary axis. The angular separation of this pole from the imaginary axis is $\pi/2n$. Therefore, this pole pair is given by the roots of

$$s^2 + 2\zeta s s_0 + s_0^2 = 0, \quad \zeta = \frac{1}{2Q} = \sin\phi, \quad \phi = \frac{\pi}{2n}. \tag{12}$$

The Laplace transform of the dominant term in the step response of the filter is of the form

$$F(s) = \frac{s + a}{s^2 + 2\zeta s_0 s + s_0^2} \tag{13}$$

which corresponds to the step response

$$f(t) = \exp(-\zeta s_0 \cdot t) \cdot \left[\frac{1}{\cos(\zeta)} \cos\left(\sqrt{1-\zeta^2}\, s_0 \cdot t + \zeta\right) + a \cdot \sin\left(\sqrt{1-\zeta^2}\, s_0 \cdot t\right) \right]. \tag{14}$$

The exponential term is the envelope of the transient response, which defines the settling of the filter. Taking $20 \cdot \log_{10}$ of the envelope term gives us

$$\text{Envelope} = -8.69 \zeta s_0 \cdot t \quad \text{dB} \tag{15}$$

which can be approximated by

$$\text{Envelope} \approx \frac{85.73}{n} \cdot f_0 t \quad \text{dB}. \tag{16}$$

This means that if the filter edge is at 1000 Hz and a two pole filter is used, the filter settles at about 43 dB per millisecond. A four pole filter would settle at about 21.5 dB per millisecond. A four pole, 5,000 Hz filter would settle at 107 dB per millisecond.

TECHNICAL MEMORANDUM

To: List
From: J. K. Beard
Date: 12 April 1993
Reference: JKB-93-04
Subject: A 14-Bit A to D Gives a 100 dB Noise Floor in the WFS Signal Processor Upgrade

1.0 SUMMARY

The Waveform Simulator (WFS) Signal Processor Upgrade signal processing baseline uses Burr Brown ADS 615 BH A to D converters. Simulations of the current signal processing baseline show that, when the A to D forms the noisc floor for the system and the window weighting sidelobe suppression is greater than about 110 dB, **these 14-bit A to D converters provide a noise floor over 100 dB below total clutter** power in FFT bins more than about 1000 Hz from the cutter spectral center. The signal processing baseline has been simulated and the noise floor has been verified as being over 100 dB below the total clutter power.

An SRC analysis[1] has been presented which predicts the performance of the signal processing baseline. Another analysis by Dynetics[2] uses a different signal processing baseline which does not allow a noise floor of 100 dB, primarily because it uses a 90 dB Dolph-Chebychev window which limits clutter attenuation to 90 dB. For the Dynetics signal processing baseline, the SRC simulation shows the same performance, but with the single change to a 120 dB Dolph-Chebychev weighting window, the modified Dynetics signal processing baseline produces a noise floor over 100 dB below the clutter.

A 16 bit version of the Burr Brown ADS 615 A to D converter should be available in time for delivery of the WFS Signal Processor Upgrade. **Using this unit will put the A to D noise floor below the transmitter phase noise.** This plug-in replacement is recommended for the WFS if additional dynamic range is desired. A 23 bit A to D is available and should be considered in future radars when it is desired to provide dynamic ranges far in excess of limits imposed by any obtainable transmitter phase noise.

2.0 PROBLEM STATEMENT

A Dynetics report[2] appears to conflict with results which have been used to proceed with the design of the WFS Signal Processor Upgrade. The relevant system parameters used for analysis are a 10 GHz center frequency, a 1μs pulse and range gate, a 100 kHz PRF, and a dwell of 512 pulses. The signal processing baseline for the WFS Signal Processor Upgrade is:

1. The use of selected ADS 615 BH A to D converters (for 80 dB SNR performance),

2. Complex 14 bit sampling of the output of a quadrature demodulator at a data rate equal to two samples per range gate, (a 16 bit upgrade should be available before delivery to MIT/LL),

3. Presumming the two samples in each range gate and forming one complex sample per range gate (as part of the corner-turning or range gating operation),

4. The use of a 120 dB Dolph-Chebychev window weighting, and

5. A 512-point FFT.

The signal processor baseline given in the Dynetics report differs from the baseline used in the WFS Signal Processor Upgrade in two respects:

a. The window used in the Dynetics report is a 90 dB Dolph-Chebychev window weighting instead of a 120 dB Dolph-Chebychev window.

b. The sampling used in the Dynetics report is one complex sample per range gate instead of two.

Because the only source of substantial clutter attenuation in the signal processing baseline concept is in the window weighting, selection of any window with less than 100 dB selectivity, as was done in (a) above, will prevent any possibility of achieving 100 dB of clutter attenuation. The use of two samples per range gate achieves about 2 dB of processing gain; this is not critical to the central issue of 100 dB of clutter attenuation. It is necessary to show:

i. The Dynetics report, although correct in the prediction of the signal processing baseline used there, is not directly relevant to the signal processing baseline actually used in the WFS Signal Processor Upgrade, and

ii. The signal processing baseline in the WFS Signal Processor Upgrade does achieve 100 dB of clutter attenuation.

This has been done by building a general signal processor simulation and reproducing the results seen in the Dynetics report[2], then changing the window to a 120 dB Dolph-Chebychev window, and showing that 100 dB of clutter attenuation is achieved. A small additional gain is achieved by using two samples per range gate.

3.0 SIMULATION AND ANALYSIS

3.1 Overview

SRC simulated the WFS Signal Processor Upgrade baseline in the configuration described in Section 2 above. Most parameters were left as variables for the purposes of comparative analysis. These variables included clutter amplitude and frequency, signal amplitude and frequency, A to D word length, A to D dynamic range, dithering, the number of samples per range gate, the sidelobe attenuation of the Dolph-Chebychev window, the number of points in the FFT, and other parameters. The pulse shape is Gaussian, which is the impulse response of a Gaussian IF filter shape whose bandwidth is approximately matched to a range gate. The simulation uses 32 bit IEEE floating point arithmetic, which is the same arithmetic used in the signal processor of the WFS Signal Processor Upgrade, the Hughes HPSP-1000.

3.2 Transmitter Phase Noise

Current practice in transmitter design will produce real-world transmitters capable of phase noise 135 dB below the carrier 10 kHz away from the center frequency. Phase noise generally decreases as the measurement point moves farther away from the carrier.

A Doppler of 10 kHz is a good point for evaluation of capability against low observable targets, because it corresponds to 290 kts range rate at 10 GHz. Targets moving much faster than this will produce aerodynamic and thermal wakes whose radar cross section (RCS) will rival that of the target itself. Lower Doppler will be closer to the carrier, where the transmitter has higher phase noise.

The noise bandwidth of each FFT bin is about 400 Hz (including a broadening factor of about 2 due to window weighting). This means that the transmitter noise floor in an FFT bin will be 109 dB below the clutter. Assuming that another 10 dB is possible in future transmitters, the transmitter noise floor would be, at the very lowest, about 120 dB below the clutter. Using the 16 bit A to D (which, as shown in Section 3.3.6 below has a noise floor 112 dB below the clutter) as a reference point, this corresponds to the noise floor from a 17 bit A to D. Even noting that noise at IF will not be uncorrelated in the range gate presum as A to D noise is, it is clear that 16 bits is near the point of diminishing returns for A to D word length. A 23 bit A to D is available from Hewlett Packard (see Section 3.3.7 below). Using this A to D will entirely remove the A to D from the position of system dynamic range bottleneck.

The -109 dB transmitter noise level was arrived at as -135 dB in a 1 Hz band, plus 27 dB for a 512 point FFT, minus 3 dB for window broadening, plus 2 dB for the two sample presum for each range gate.

3.3 The Simulations

3.3.1 The Basic Case

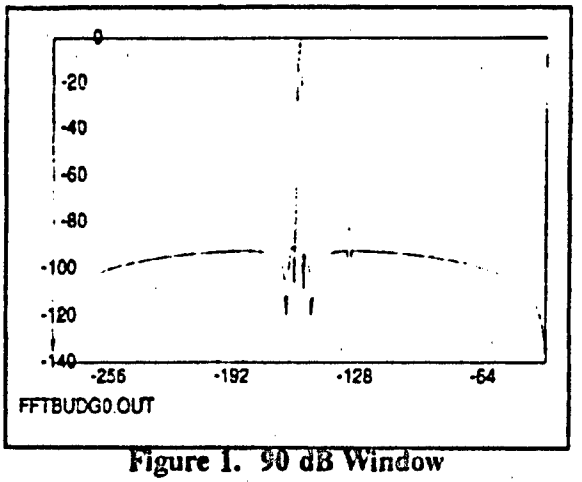

Figure 1. 90 dB Window

The basic case is 0 dB clutter at DC with a -80 dB signal centered in FFT bin 50. A plot of FFT output for this case is shown in Figure 1. A 90 dB Dolph-Chebychev window is used, as in the Dynetics report[2]. The figure effectively shows the output of the spectrum analyzer in the WFS Signal Processor Upgrade. The apparent gradual variation in the window frequency response shape is an artifact of the parameters used. The frequency response of a 512 point Dolph-Chebychev window has 511 lobes, and the plot looks at the output of 512 FFT bins. Therefore, what is shown in Figure 1 is a Moire pattern, which does not show the equiripple character of the window at 90 dB.

3.3.2 Adding Simple Quantization

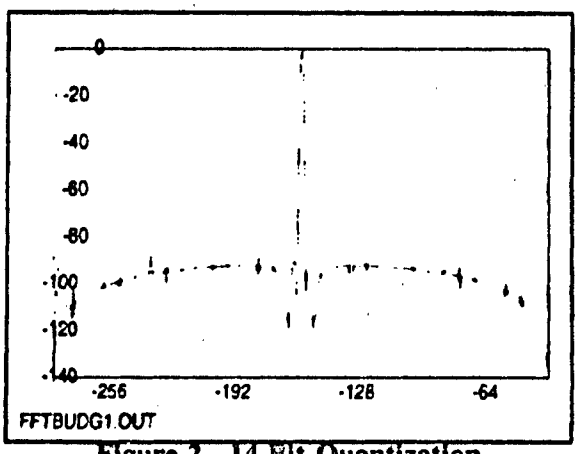

Figure 2. 14 Bit Quantization

A perfect 14 bit A to D was modeled as simple quantization. The result is shown in Figure 2. Again, a 90 dB Dolph-Chebychev window is used as in the Dynetics report[2]. Spurious effects appear over the spectrum analyzer output. Several of these, including a line seen at bin -251, have an amplitude of -90 dB, which is the suppression level of the Dolph-Chebychev window used.

3.3.3 Noise Dithering

Most high resolution A to D converters (10 bits or more) are self-dithering, in that sufficient internal electromagnetic interference (EMI) occurs so that the LSB and possibly the next bit up will "dance". This will allow signals weaker than an LSB in amplitude to be represented stochastically in the digitized output so that they can be brought out in signal processing such as an FFT. If the A to D selected is so clean that this does not occur, a small amount of noise or other dithering signal may be added to the input to achieve the same effect. The result of this is that a noise floor appears in the digitized output which is higher than predicted by the quantization error alone. This spurious noise is primarily white, but contains tonal lines to some degree.

The white portion is specified in A to D data sheets as the signal to noise ratio

(SNR) specification. The amplitude of the tonal lines in a 1 Hz band is specified in the spurious-free dynamic range (SFDR) specification. Integration times on the order of 1 second are required to measure these tonal lines. For use in radars with dwell times of a few milliseconds, the SNR specification is principally of interest. Figure 3 shows the output of the spectrum analyzer for a 14-bit A to D with an SNR specification of 78 dB. As before, only a 90 dB Dolph-Chebychev window is used as in the Dynetics report[2]. Although the FFT will have 24 dB gain against this noise, the spectrum analyzer is sampling the peaks of the Dolph-Chebychev window at -90 dB with noise effects added.

Figure 3 is the last figure shown here showing results reproduced from the Dynetics report[2]. This figure is used there to conclude that the noise floor (which is effectively the clutter attenuation) as limited by the A to D converter is at about a -90 dB level. The SRC simulation shows that, for the Dynetics signal processing baseline, the average noise level is at only -94.5 dB relative to the clutter power. However, the noise seen at the -90 dB level is noise riding on the sidelobes of the 90 dB Dolph-Chebychev window.

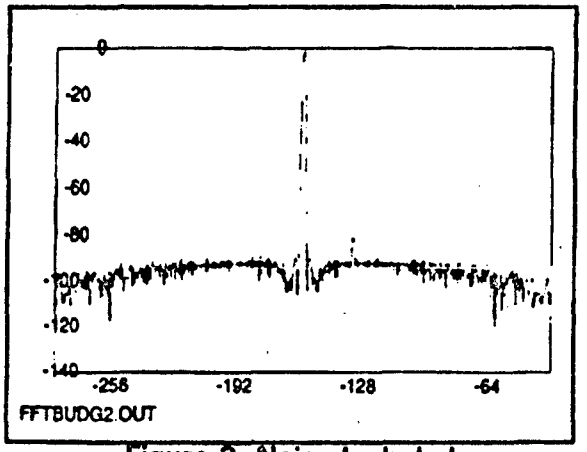

Figure 3. Noise Included

3.3.4 Using a 120 dB Window Weighting

Figure 4 shows the spectrum analyzer output with nothing changed from the Dynetics baseline except the window side lobe level, which has been increased to 120 dB. The simulation shows that the average noise level is now about 101.5 dB below the clutter power. This is not unexpected, because the A to D noise level was at -78 dB and the FFT gain is about 24 dB. The noise now has the appearance of Rayleigh noise, and we are indeed looking at the resulting system noise floor in Figure 4.

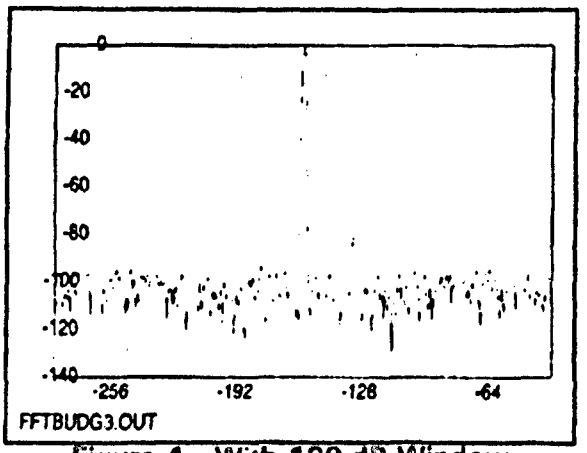

Figure 4. With 120 dB Window

The signal shown in Figure 4 is centered in a range and Doppler bin so that no scalloping loss is included. Range gate mismatch losses are seen to be small, and the signal appears at the -80 dB level.

3.3.5 Including the Presum

The WFS Signal Processor Upgrade baseline includes sampling twice per range gate and summing these samples before performing the window weighting and FFT operations. The spectrum analyzer output for this case is shown in Figure 5. Note that the clutter has gone up 6 dB, the signal has gone up 5 dB, and noise has gone up 3 dB. The total SNR gain is about 2 dB. The simulation shows the noise floor is at -98.5 dB, while the clutter is at +6 dB; **the noise floor is 104.5 dB below the clutter power.**

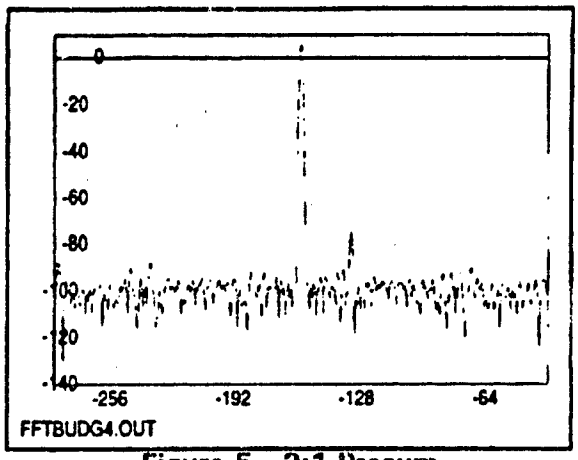

Figure 5. 2:1 Presum

TECHNICAL MEMORANDUM

To: List
From: J. K. Beard
Date: 3 May 1993
Reference: JKB-93-05
Subject: Three Simple, Robust Two-State Kalman Filters

1.0 SUMMARY

Very simple two-state trackers are used as the underlying basis of tracker subsystems in a wide variety of applications. These basic trackers perform basic system functions, such as angle tracking, Doppler tracking, or ambiguous range tracking with Doppler data. More sophisticated trackers are used for unambiguous range tracking and other estimation functions.

A simple two state adaptive Kalman filter is presented here. The final form of the filter is so simple that distinction between this filter and an alpha-beta tracker is academic. The states are position and velocity, and the measurement is position, velocity, or both. Crucial algebraic representations in the computation of the covariance matrix and the Kalman gain make all computations additions and divisions, making covariance collapse and other problems known in Kalman filters impossible. The Kalman filter is adaptive in that the plant noise is made proportional to squared measurement error; the author has found this to be a simple method of ensuring robustness in a wide range of Kalman filters. The update of the Kalman filter depends on whether position, velocity, or both are available as measurements. All three forms are presented here.

Critical portions of the development of these trackers were developed by the author prior to any application in 1981 and were adapted to the forms presented here on personal time. Therefore, the designs presented here are proprietary to SRC.

2.0 PROBLEM STATEMENT

Tracker subsystems are usually based on a simple set of two state trackers which support essential functions such as beam pointing which are necessary to sustain tracking. Other more sophisticated estimators are used to support system functions such as estimation of target position where accuracy is the principal requirement. The basis trackers must above all be robust. Simplicity of implementation is also important so that this basic support function consumes a minimum of system resources.

Alpha-beta trackers are often used for this purpose. A Kalman tracker is presented here which is as simple as an alpha-beta tracker and is easily applied to a wider variety of applications. Most alpha-beta literature specializes on range tracking of aircraft and do not treat use of range rate as a measurement[1 pp 21-25]. Even in aircraft tracking, Kalman trackers usually perform much better because they account for variations in signal to noise ratio (SNR) and other effects neglected in alpha-beta trackers[1, p. 29]. In any case, the method presented here is as simple in implementation as an alpha-beta tracker.

3.0 THE KALMAN FILTER

3.1 General theory. The Kalman filter[2] is presented in many different forms, which vary in whether the system being tracked or the tracker itself is represented by a differential equation (the continuous system or filter) or a difference equation (the discrete system or filter). The case presented here uses a discrete system and filter, as is the case in most computer-based trackers used in system engineering. Nonlinearities in the system are handled by the use of extensions. The concept is based on assuming a model of the system being measured, with some noisiness in the model, a model of the measurements, an initialization of the tracker, and estimation theory. The resulting Kalman filter equations[2 p. 188, modified] are given as the equations in Table I.

3.2 The simple two state case. The equations in Table I are used to develop a tracker design by defining the matrices Φ, H, Q, P(0), and the initial state vector $\underline{x}(0)$, and implementing the initialization, extrapolation, and update equations. The matrix R is taken from the signal to noise ratio and an analysis of the measurement method.

Initialization is taken from the first one or two measurements. The method is minimum variance or maximum likelihood. Initialization cannot be complete until position is available in at least one measurement. Initialization is complete in one measurement if both position and velocity are available. There are five cases where initialization occurs in two measurements. The total of seven cases is summarized in Table II below. Very simple special case initialization equations are possible in all but one case.

3.3 The Kalman Update. The Kalman update is subject to simplifications for all three combinations of measurements. These special cases are given below in Table III. Note that there are no subtractions in any of the Kalman gain or covariance matrix update equations, so that covariance collapse cannot occur. A final safety check, bounding the determinant D to be nonnegative, will prevent any possibility that any of these Kalman filters will ever become unstable in implementation.

3.4 Adaptive Plant Noise. In Table III, the plant noise matrix Q is defined in terms of normalized measurement error. In particular, the measurements are translated into a chi-square random variable which is used to multiply the undefined constants q_{11} and q_{22}. When both position and velocity are available, then,

$$\text{Cov}\{\underline{y} - \underline{h}(\hat{\underline{x}})\} = H \cdot \bar{P} \cdot H^T + R, \quad [H \cdot \bar{P} \cdot H^T + R]^{-1} = \frac{1}{D + \sigma_2^2 \cdot \bar{p}_{11} + \sigma_1^2 \cdot \bar{p}_{22}} \begin{bmatrix} \bar{p}_{22} + \sigma_2^2 & -\bar{p}_{12} \\ -\bar{p}_{12} & \bar{p}_{11} + \sigma_1^2 \end{bmatrix}$$

Table I. Generic Kalman Filter Equations

MODEL OF STATE VECTOR

$$\frac{d\underline{x}}{dt} = \underline{f}(\underline{x}) + \underline{w}; \quad \underline{x}(t(-)) = \underline{x}(-), \quad \mathrm{Cov}\{\underline{w}\} = Q$$

MODEL OF MEASUREMENTS

$$\underline{y} = \underline{h}(\underline{x}) + \underline{v}; \quad \mathrm{Cov}\{\underline{v}\} = R$$

INITIALIZATION

$$\underline{x}(-) = \underline{x}(0), \quad P(-) = P(0)$$

EXTRAPOLATION TO CURRENT TIME

$$\underline{\hat{x}} = \Phi \cdot \underline{x}(-), \quad \frac{d\Phi}{dt} = F\Phi, \quad F = \frac{\partial \underline{f}(\underline{x})}{\partial \underline{x}}$$

$$\hat{P} = \Phi \cdot P(-) \cdot \Phi^T + Q$$

THE KALMAN GAIN

$$K = \hat{P} H^T \cdot [H \cdot \hat{P} \cdot H^T + R]^{-1}, \quad \text{where} \quad H = \frac{\partial \underline{h}(\underline{x})}{\partial \underline{x}}$$

UPDATE USING MEASUREMENT DATA

$$\hat{x} = \hat{x} + K \cdot (y - h(\hat{x}))$$

$$P = (I - K \cdot H) \cdot \hat{P}$$

$$= (I - K \cdot H) \cdot \hat{P} (I - K \cdot H)^T + K \cdot R \cdot K^T$$

$$= [\hat{P}^{-1} + H^T \cdot R^{-1} \cdot H]^{-1}$$

TIME VARYING DEPENDENCIES

The functionals $\underline{f}(\underline{x})$, $\underline{h}(\underline{x})$, and the matrices Φ, H, R, and Q may be time varying.

Table II. Initialization with One or Two Measurements

NOTATION

Measurements at times t_1 and t_2, current time is t_2, $T = t_2 - t_1$

Position measurement: $y_i = y_{i1}$, $R_i = \sigma_{i1}^2$, $H_i = [1 \ -(t_2 - t_i)]$

Velocity measurement: $y_i = y_{i2}$, $R_i = \sigma_{i2}^2$, $H_i = [0 \ 1]$

Both in measurement: $y_i = \begin{bmatrix} y_{i1} \\ y_{i2} \end{bmatrix}$, $R_i = \begin{bmatrix} \sigma_{i1}^2 & 0 \\ 0 & \sigma_{i2}^2 \end{bmatrix}$, $H_i = \begin{bmatrix} 1 & -(t_2 - t_i) \\ 0 & 1 \end{bmatrix}$

ALGORITHM

$$y = \begin{bmatrix} y_1 \\ y_2 \end{bmatrix}, \quad H = \begin{bmatrix} H_1 \\ H_2 \end{bmatrix}, \quad R = \begin{bmatrix} R_1 & 0 \\ 0 & R_2 \end{bmatrix}$$

$$P^{-1}(0) = H^T \cdot R^{-1} \cdot H = H_1^T \cdot R_1^{-1} \cdot H_1 + H_2^T \cdot R_2^{-1} \cdot H_2$$

$$\hat{x}(0) = P(0) \cdot H^T \cdot R^{-1} \cdot y$$

ONE MEASUREMENT--POSITION AND VELOCITY

$\hat{x}(0) = y_1$, $P(0) = R_1$, current time is t_1

TWO MEASUREMENTS--POSITION, POSITION

$$\hat{x}(0) = \begin{bmatrix} y_{21} \\ \dfrac{y_{21} - y_{11}}{T} \end{bmatrix}, \quad P(0) = \begin{bmatrix} \sigma_{21}^2 & \dfrac{\sigma_{21}^2}{T} \\ \dfrac{\sigma_{21}^2}{T} & \dfrac{\sigma_{11}^2 + \sigma_{21}^2}{T^2} \end{bmatrix}$$

TWO MEASUREMENTS--POSITION, VELOCITY

$$\hat{x}(0) = \begin{bmatrix} y_{11} + y_{22} \cdot T \\ y_{22} \end{bmatrix}, \quad P(0) = \begin{bmatrix} \sigma_{11}^2 + \sigma_{22}^2 \cdot T^2 & \sigma_{22}^2 \cdot T \\ \sigma_{22}^2 \cdot T & \sigma_{22}^2 \end{bmatrix}$$

Table II (continued). Initialization with One or Two Measurements

TWO MEASUREMENTS--POSITION, POSITION AND VELOCITY

$$P(0) = \frac{\sigma_{21}^2}{\sigma_{11}^2 + \sigma_{21}^2 + \sigma_{22}^2 \cdot T^2} \cdot \begin{bmatrix} \sigma_{11}^2 + \sigma_{22} \cdot T^2 & \sigma_{22} \cdot T \\ \sigma_{22} \cdot T & \sigma_{22} \cdot (1 + \frac{\sigma_{11}^2}{\sigma_{21}^2}) \end{bmatrix}, \quad \hat{x}(0) = P \begin{bmatrix} \frac{y_{11}}{\sigma_{11}^2} + \frac{y_{21}}{\sigma_{21}^2} \\ -\frac{y_{11} \cdot T}{\sigma_{11}^2} + \frac{y_{22}}{\sigma_{22}^2} \end{bmatrix}$$

TWO MEASUREMENTS--VELOCITY, POSITION

$$\hat{x}(0) = \begin{bmatrix} y_{21} \\ y_{22} \end{bmatrix}, \quad P(0) = \begin{bmatrix} \sigma_{21}^2 & 0 \\ 0 & \sigma_{12}^2 \end{bmatrix}$$

TWO MEASUREMENTS--VELOCITY, POSITION AND VELOCITY

$$\hat{x}(0) = \begin{bmatrix} y_{21} \\ \frac{\sigma_{22}^2 \cdot y_{12} + \sigma_{12}^2 \cdot y_{22}}{\sigma_{12}^2 + \sigma_{22}^2} \end{bmatrix}, \quad P(0) = \begin{bmatrix} \sigma_{21}^2 & 0 \\ 0 & \frac{\sigma_{12}^2 \cdot \sigma_{22}^2}{\sigma_{12}^2 + \sigma_{22}^2} \end{bmatrix}$$

where D is the determinant of the extrapolated covariance matrix. A chicken-and-egg problem arises here: the plant noise matrix Q is used in computing the extrapolated covariance matrix, and we are computing Q at this point in the implementation.

In practical cases, the squared measurement error can be used and complications involving the extrapolated covariance matrix are unnecessary. Therefore, it is necessary to define a method for computing e^2 which is not dependent on the extrapolated covariance matrix. A method which has been found sufficient is

$$e^2 = (y_1 - \hat{x}_1)^2 + (y_2 - \hat{x}_2)^2 \cdot T^2$$

where T is the time since the last update. If either the position or velocity measurement is not available, simply omit that term in the equation. This is the recommended method. More elaborate methods have not been found to be more productive.

Table III. Special Case Updates

EXTRAPOLATION AND NOTATION, ALL CASES

$$Q = e^2 \cdot \begin{bmatrix} q_{11} & 0 \\ 0 & q_{22} \end{bmatrix}, \quad e^2 = (\underline{y} - \underline{h}(\hat{\underline{x}}))^T \cdot [H \cdot \bar{P} \cdot H^T + R]^{-1} \cdot (\underline{y} - \underline{h}(\hat{\underline{x}})) \text{ (see Sections 3.4, 3.5)}$$

$$\bar{P} = \Phi \cdot P(-) \cdot \Phi^T + Q = \begin{bmatrix} \bar{p}_{11} & \bar{p}_{12} \\ \bar{p}_{12} & \bar{p}_{22} \end{bmatrix}$$

$$D = \bar{p}_{11} \cdot \bar{p}_{22} - \bar{p}_{12}^2$$

POSITION MEASUREMENT

$$K = \frac{1}{\sigma_1^2 + \bar{p}_{11}} \begin{bmatrix} \bar{p}_{11} \\ \bar{p}_{12} \end{bmatrix}, \quad P = \frac{\sigma_1^2}{\sigma_1^2 + \bar{p}_{11}} \begin{bmatrix} \bar{p}_{11} & \bar{p}_{12} \\ \bar{p}_{12} & \bar{p}_{22} + \frac{D}{\sigma_1^2} \end{bmatrix}$$

VELOCITY MEASUREMENT

$$K = \frac{1}{\sigma_2^2 + \bar{p}_{22}} \begin{bmatrix} \bar{p}_{12} \\ \bar{p}_{22} \end{bmatrix}, \quad P = \frac{\sigma_2^2}{\sigma_2^2 + \bar{p}_{22}} \begin{bmatrix} \bar{p}_{11} + \frac{D}{\sigma_2^2} & \bar{p}_{12} \\ \bar{p}_{12} & \bar{p}_{22} \end{bmatrix}$$

BOTH POSITION AND VELOCITY MEASUREMENTS

$$K = \frac{1}{1 + \frac{\bar{p}_{11}}{\sigma_1^2}\cdot\sigma_2^2 + \frac{\bar{p}_{22}}{\sigma_2^2}\cdot\sigma_1^2} \begin{bmatrix} \frac{\bar{p}_{11}}{\sigma_1^2} + \frac{D}{\sigma_1^2\cdot\sigma_2^2} & \frac{\bar{p}_{12}}{\sigma_2^2} \\ \frac{\bar{p}_{12}}{\sigma_1^2} & \frac{\bar{p}_{22}}{\sigma_2^2} + \frac{D}{\sigma_1^1\cdot\sigma_2^2} \end{bmatrix}$$

$$P = \frac{1}{1 + \frac{\bar{p}_{11}}{\sigma_1^2}\cdot\sigma_2^2 + \frac{\bar{p}_{22}}{\sigma_2^2}\cdot\sigma_1^2} \begin{bmatrix} \bar{p}_{11} + \frac{D}{\sigma_2^2} & \bar{p}_{12} \\ \bar{p}_{12} & \bar{p}_{22} + \frac{D}{\sigma_1^2} \end{bmatrix}$$

3.5 Tuning the Kalman Filter--Adaptive Plant Noise. Tuning the Kalman filter is done by adjusting the adaptive plant noise is accomplished by setting the constants q_{11} and q_{22}. Any non-negative value, including zero, is allowable. In general, setting these constants determines a tradeoff point between accuracy and robustness of the tracker. The smaller these constants are, the more closely the Kalman filter will track--so long as the constant velocity model implicit in its formulation is followed by the measurements. If significant state acceleration is seen in the measurements, the value of q_{22} should be used to provide the artifice of modeling acceleration as noise in the velocity state. Some general points are usually valid in the selection of q_{11} and q_{22}.

1. Determine starting values for q_{11} and q_{22}. Examine the nature of the quantity being tracked and attempt to formulate some realistic values for the elements of Q in terms of noise in the state propagation of the real system. Examination of the mean value of e^2 for the steady-state tracker condition will give you a starting point for a definition of q_{11} and q_{22}.

2. Model the tracker and vary the values of q_{11} and q_{22} to examine the performance of the tracker. Keeping q_{11} small or zero while using q_{22} to tune for robustness will give best overall accuracy, but increasing q_{11} will give a more rapid response of the tracker when the measurements exhibit a sudden acceleration.

3. Setting q_{11} to zero is often the best policy. Plant noise from the q_{22} term will propagate to p_{11} through the covariance extrapolation equation. However, setting q_{22} to zero will force p_{22} to be monotonically decreasing, and the covariance matrix will eventually become singular. Therefore, q_{22} should never be set to zero.

4. Allow some access to q_{11} and q_{22} through system integration and deployment to allow fine tuning the tracker as a wider range of experience with real conditions is obtained.

Variation of q_{11} and q_{22} with conditions is obviously a direction which may be pursued. Better tuning of the filter will result in a better accuracy-robustness tradeoff. However, it is important to keep sight of the main purpose of this type of tracker: robust support of underlying system functions. Therefore, robustness within relatively broad accuracy limits is the purpose of this type of tracker, not accuracy of estimation. It is best to use this type of tracker to support basic system functioning, but to use more sophisticated overlaying estimation methods for actual estimation problems such as target position estimation and support of fire control.

This type of adaptive feedback into the Kalman gain was originally developed

from early academic attempts to estimate the Q matrix as part of the state vector[2 pp 316-320][3, 4, 5, 6, 7]. These early academic methods were not adaptable to simple, efficient implementations such as those given here. Adding complexity to the tracker should be examined very carefully, and should probably be avoided unless necessary to meet real system requirements.

4.0 CONCLUSIONS

The two state Kalman filter implementations as given in the tables are applicable to many systems where this type of tracker forms the basis of a tracking subsystem. The initialization, extrapolation, and update as given are very simple and robust, so that these trackers can form the basis of modules which support basic system functions such as beam pointing, tracking Doppler, or tracking ambiguous range. These trackers are known to perform well with minimum latency and use of system resources.

5.0 REFERENCES

[1] "Multiple-Target Tracking with Radar Applications," Samuel S. Blackman, Artech House (1986).

[2] "Applied Optimal Estimation," A. Gelb, Ed., MIT Press (1974).

[3] R. K. Mehra, "On the Identification of Variances and Adaptive Kalman Filtering," IEEE Trans. on Automatic Control, Vol. AC-15, No. 2, April 1970, pp. 175-184.

[4] I. M. Weiss, "A Survey of Discrete Kalman-Bucy Filtering with Unknown Noise Covariances," AIAA Guidance, Control and Flight Mechanics Conference, Paper No. 70-955, Santa Barbara, California, August 1970.

[5] R. K. Mehra, "On-Line Identification of Linear Dynamic Systems with Applications to Kalman Filtering," IEEE Trans. on Automatic Control, Vol. AC-16, No. 1, February 1971, pp. 12-21.

[6] P. D. Abramson, Jr., "Simultaneous Estimation of the State and Noise Statistics in Linear Dynamic Systems," Ph. D. Thesis, Massachusetts Institute of Technology, TE-25, May 1968.

[7] T. Kailath, "An Innovations Approach to Least Squares Estimation--Part I: Linear Filtering in Additive White Noise," IEEE Trans. on Automatic Control,

Vol. AC-13, May 1968.

TECHNICAL MEMO

To: List
Date: 19 May 1993
Subject: ADC Subsystem Interface to HPSP-1000

From: Michael Emry
Reference: MLE-93-02

1.0 Introduction

Data transfers in the Waveform Simulator Signal Processor Upgrade (WFS SPU) system between the Pentek 4261A A/D Converter and the HPSP-1000 will exit the 4261A through the parallel port and enter the HPSP-1000 through the DIO module. This document outlines the specifications of the parallel port on the 4261A and the DIO module on the HPSP-1000 as they pertain to the interface that will be used on the WFS SPU system.

2.0 Pentek 4261A A/D Converter

The Pentek 4261A A/D Converter provides a parallel port which serves as an interface between the A/D converter and a general purpose device. The port is accessible through a front panel 50-pin IDC flat ribbon cable connector. It utilizes single ended TTL to send 16 data bits and 2 handshake control lines. Both control lines, DAV and NRFD, are active low signals. Data Available (DAV) is set low by the 4261A when it has placed valid output data on the parallel port data lines. Not Ready For Data (NRFD) is set low by the receiver indicating that it is accepting the output data. NRFD is then set high by the receiver when the data has been loaded and it is ready for more data. This triggers DAV high until more valid output data is available on the port data lines. The maximum output rate of the data transfer for the 4261A is 10 MHz. Operation of the two control lines is shown in the diagram on the attached page 20 from the Pentek 4261A A/D Converter Operating Manual.

Pentek Technical Support has stated two characteristics of the control lines on the 4261A parallel port that are significant to the WFS SPU system interface. They state that the DAV line is triggered by the rising edge of the sampling clock of the A/D, assuming that the NRFD line is not still low, in an attempt to maintain an output rate equal to the system input rate. This is inconsistent with the Pentek 4261A Operating Manual which suggests that the output of the parallel port on the 4261A is designed to be independent of the input to allow for the delivering of the data in bursts. Both sources agree that the average output rate must equal or exceed the average input rate or input data will be lost.

Pentek Technical Support has also stated that the 4261A is triggered solely by the rising edge of the NRFD line and the location of the falling edge is not significant to the operation of the parallel port. The WFS interface configuration is dependent on this characteristic of the parallel port. A look at the attached page 20 from the Operating

Manual suggests that as long as NRFD remains low for a minimum time, t_w = 30 ns, the 4261A will be able to recognize that the data has been read and bring DAV high.

3.0 HPSP-1000

The Data I/O Module (DIO) on the HPSP-1000 is designed as the main sensor interface for the signal processor. It should be used for transfers that require high average data rates and a simple control handshake interface.

The DIO contains 4 16-bit parallel ports or external DMA ports. Each port is accessible through a 50-pin D connector on the rear of the HPSP-1000 rack. These ports can also be accessed through the 40-pin flat ribbon cable connections found immediately on the back on the HPSP-1000 chassis. The ports are currently configured for differential TTL signals. However all of the data and control lines are terminated with a resistor network. The resistor networks can be selected to provide single ended TTL connections as well as allow for inverted signals by swapping the differential lines. A diagram showing the possible configurations of the resistor networks are shown in the attached Figure 2.4.3 from the HPSP-1000 External Interface Description, page 11.

The DIO can perform data transfers in both synchronous and asynchronous mode of operation. Synchronous operation requires an external clock and can transfer data at rates up to 1/2 the HPSP-1000 system clock or 8 MHz. Asynchronous operation requires a simpler handshaking interface but can only transfer data at 1/4 the HPSP-1000 system clock or 4 MHz. Data transfers on the WFS SPU system will be done using asynchronous operation.

In asynchronous mode the DIO uses two active high control lines, EXT_RDY and DIO_RDY. External Ready (EXT_RDY) indicates that valid data is present on the port data lines. DIO Ready (DIO_RDY) indicates that the data has been received. DIO_RDY goes active and inactive in response to EXT_RDY, typically lagging by 150 ns. Operation of the two control lines is shown in the attached Figure 3.1.3-3 from the HPSP-1000 External Interface Description, page 31.

4.0 WFS SPU System Interface

The WFS SPU system will be able to achieve its necessary data transfer rates by using the DIO in the asynchronous mode of operation. Handshaking can be accomplished by connecting the DAV line from the 4261A with EXT_RDY on the DIO. It will be necessary to invert this line on the DIO card. The NRFD line on the 4261A will be connected to the DIO_RDY line on the DIO. This line will not need to be inverted, but both control lines and the 16 data lines will have to be configured for single ended TTL on the DIO card.

While this configuration appears to be the most practical for the WFS SPU system, there

are several areas of concern. The physical cable connection will be complex. In order to transfer data from 2 A/D's to one DIO module, there will be 2 50-pin IDC flat ribbon cables running from the front of the A/D Converter chassis to 4 50-pin D connectors at the back of the HPSP-1000 rack. This will involve a custom made interface box and approximately 12 feet of ribbon cable for every 2 A/D boards and DIO module. The WFS SPU system will have 3 such connections.

There is also a concern with the use of single ended TTL lines to transfer data at high rates over long cables. Hughes recommends against using single ended TTL signals at data rates over 2 MHz, due to problems with noise and crosstalk. The WFS SPU system will be operating at that rate and on cables in excess of 6 feet in length. If the interface is not capable of operating in this configuration, the lines can be shortened by bypassing the 50-pin D connectors on the back of the HPSP-1000 rack and connecting to the 40-pin IDC socket connections on the rear of the HPSP-1000 itself. While this may make it difficult to access the back of the HPSP-1000, it will shorten the data lines by several feet. A final more complex solution would involve adding a digital board, possibly in the A/D Converter chassis that would provide circuitry to change the single ended TTL lines to chip driven differential TTL signals.

This configuration also is limiting in that it does not provide an easy way to improve data rates to a speed over 4 MHz. The DIO is capable of transfer rates of 8 MHz if synchronous transfer rates are used. In order to utilize synchronous transfer rates the entire interface would have to be replaced. A synchronous interface would have to include an external clock source and more complex handshaking. It would probably require a separate digital board. Increased speed would also encourage more problems with the single ended lines.

Complete testing of the previously described interface will require preparing 4 components of the transfer path.

1) Software for the A/D Converter Subsystem that will allow the A/D to simulate collection and output data through the parallel port. This has been completed.

2) Collection code for the DIO module will also need to be written to collect data and place it into global memory.

3) The cable connection will have to be designed and custom built to correctly interface the parallel port on the 4261A and the DIO module.

4) The DIO card will need to be studied and the on board resistor network terminated for single ended TTL and for inverted signals. Hughes Technical Support said that this could be done but was unable to offer specifics.

5.0 References

[1] Pentek 4261A A/D Converter Operating Manual

[2] Hughes Programmable Signal Processor Engineering Notebook, Books 6-7

[3] Mark Lee, Pentek Technical Support

[4] Dennis Reagle and Chris Bodette, Hughes Technical Support

TECHNICAL MEMO

To: List
Emry
Date: May 19 1994
Subject: WFS SPU A/D Characterization

From: Michael L.
Reference: MLE-94-01

1.0 Introduction

The A/D Subsegment of the Waveform Simulator Signal Processor Upgrade (WFS SPU) is a VME chassis that contains 7 Pentek Model 4261A A/D converter boards (1 board is a spare unit) and the accompanying hardware and software required to control, monitor, and interface these boards. As part of the WFS SPU program, each of the 7 Pentek 4261A boards will be characterized and its performance specifications verified and documented. The characterization of each board is designed to measure standard A/D performance specifications within the scope of the WFS SPU program.

The characterization is divided into three separate tests. The first test is a measurement of the performance of the board with a full scale input. This test will calculate Signal-to-Noise Ratio (SNR) and effective number of bits (Meff). It will also estimate the Spurious Free Dynamic Range (SFDR) and the average noise floor that the A/D boards will provide within the WFS SPU program. The second test will examine the performance of the board with a grounded input. This test will calculate the DC offset of the board and estimate the average noise floor of the A/D board with a grounded input. The third test is a histogram analysis of the board at an input amplitude greater than the full scale amplitude of the A/D board. This test will verify that the board has no missing codes and demonstrates good Differential Linearity Error (DLE).

Additionally, this document outlines the interaction between Pentek and SRC that led to the final prototype version of the Model 4261A that will be used in the WFS SPU program. It outlines the test equipment, data collection methods, and the procedures of each of the three tests. Results of the tests on the prototype board (SN #9401008) are also included. These measurements provide the performance benchmark for the 7 units that will be purchased by SRC for use in the WFS SPU system. As they become available, these 7 units will be tested and their specifications recorded in an appendix to this document.

2.0 Pentek 4261A A/D Converter

The Pentek Model 4261A A/D converter board is a single 6U VMEbus compatible analog to digital converter. The standard unit uses the Burr-Brown ADC603 A/D

Converter and Sample & Hold, a 10 MHz 12-bit A/D converter chip. The board has two identical memory buffers, each consisting of 1 Mega-samples of FIFO storage, a VMEbus interface, and a parallel output port. The board supports internal and external triggering and sampling. The input impedance is 50 Ohm resistive and accepts a full scale analog signal input voltage of +/- 1.0 Volts or full signal amplitude of 10.0 dBm.

The Model 4261A is designed to allow plug-in replacement of any of Burr-Brown's 46 pin A/D converter chips. The prototype board tested and documented in this memo houses a Burr-Brown ADC614 KH converter. This converter is a 14-bit, 5.12 MHz A/D Converter and Sample & Hold. According to Burr-Brown performance specifications this chip achieves 74 dB typical SNR and 82 dB typical SFDR.

The original A/D subsegment design used Pentek Model 4261A's with the Burr-Brown ADS615 chip. This chip is a 10 MHz, 14-bit A/D Converter and Sample & Hold. Pentek provided SRC with a Model 4261A containing this part. SRC tested the performance of the board and the results indicated SNR from 55 dB to 60 dB. The testing was conducted at various input sampling frequencies as described in Section 4.1 of this memo. This accounts for the 6 dB range in SNR values.

Since the performance was well below those specified, Pentek made some modifications to the board. They replaced the Burr-Brown OPA620 Op-amp on the A/D module daughter-card, compensated the new part with a 10 pf capacitor to reduce oscillation, added an amplifier termination of 100 Ohms, and reduced the input bandwidth. SRC testing on the board after the changes were implemented showed SNR in the range of 59-64. It was also during this time period that SRC became aware of potential problems relating fo Burr-Brown's supply and support of the ADS615 A/D converter and decided to replace the part with the Burr-Brown ADC614 A/D converter. The ADC614 is a 5 MHz, 14-bit A/D Converter and Sample & Hold. Pentek shipped a 4261A board with the ADC614 part and SRC test results indicated SNR in the range of 62-67 dB. Pentek also provided SRC with a KH grade ADC614 to replace the JH grade part in the board. Burr-Brown specifications stated that the KH grade part would perform 1-2 dB better than the JH grade part. Test results indicated no difference between the two grades of the A/D converter chip.

Pentek proposed a new layout for the A/D module daughter-card on the Model 4261A. The new layout utilized improved component placement and more extensive ground planning around the OPA620 Op-amp. A 2.5 MHz, 3-pole Butterworth low pass filter was added between the OPA640 and the ADC614. SRC performance testing indicated SNR greater than 70 dB for all sampling rates below the maximum rate of 5.000 MHz. The results of the testing of this prototype board (SN #9401008) are included in this document. This board is considered the final prototype version and it is understood that all 7 boards supplied by Pentek for the WFS SPU program will meet or exceed the specifications documented in this report.

3.0 Test Setup

The characterization of the Model 4261A A/D converter board requires the use of the A/D subsegment hardware of the WFS SPU system. The A/D subsegment includes an Electronics Solutions VME Power Cage II with decoupled backplane, a Motorola162 Embedded Controller with PDOS operating system and 712A/B/AM Transition Module, and the Pentek Model 4261A A/D Converter. The equipment external to the VME chassis includes a 50 Ohm termination, a Fluke 6082A Signal Generator, and a personal computer with ethernet card. The 50 Ohm termination and the Fluke 6082A Signal Generator are used as input signals for the A/D converter. This signal generator was chosen because of its low noise performance. The Fluke 6082A provides phase noise of -137 dBc/Hz at 20 kHz offset from carrier. The personal computer has a Microtec C Cross Compiler, FTP (File Transfer Protocol) capabilities, and MATLAB.

The diagnostic software was developed on the personal computer with the Microtec Compiler and downloaded across ethernet with FTP to the Motorola 162 Controller in the VME chassis. The diagnostic software initializes the A/D boards for collection with internal trigger, internal sampling clock, and output going to VME backplane. Sampled data is collected in the data buffers, downloaded across the VME backplane to a RAM file on the Motorola 162 Controller, and transferred to the personal computer across ethernet with FTP. A utility program on the personal computer alters the data file into a format compatible with MATLAB. Once in this format, MATLAB is used to process, analyze, and plot the sampled A/D data.

4.0 Test Procedure and Data Analysis

As explained in the Introduction, the characterization is divided into three separate tests: Full Scale Input, Grounded Input, and Histogram Analysis. Details concerning the test procedures and data analysis methods for each buffer follow in this section. Test results for the prototype board are found in Section 5.0. As the 7 boards that will be a part of the WFS SPU system become available, they will be characterized in an identical manner and the results appended to this memo.

4.1 Full Scale Input Test

Measurements are taken at five different pairs of sampling frequencies (Fs) and input frequencies (Fin). Since the Model 4261A internal, divide by N clock, is 10.000 MHz, all sampling frequencies are integer multiples of 10.000 MHz. The exact input frequencies were chosen to phaselock Fs and Fin and center the input signal in one frequency bin to reduce spectral leakage. The five pairs of frequencies were chosen to demonstrate the performance of the full range of the A/D. The amplitude is set to approximately -.5 dB full scale to provide an input signal that is not clipped. Due to slight variations in the gain of the A/D board due to the filter added by Pentek, full scale on the A/D converter is between 10.8 dBm and 11.8 dBm.

For each frequency pair, 4096 data samples are collected. The set of data will hereafter be referred to as a run. Eight 512-point FFT's were performed on the data and a 120

dB Dolph-Chebyshev window is applied. The FFT size and window are consistent with the signal processing on the WFS SPU system. The frequency data is adjusted for window broadening and normalized for full scale input at 0 dB. The frequency data is also reduced by 2 dB to account for the summing of two samples per range bin that occurs in the WFS SPU system.

SNR is calculated by dividing the RMS sum of the peak signal by the RMS sum of the noise. For this test the noise does not include DC (5 bins), the fundamental peak signal (9 bins), the first 4 harmonics (7 bins each), and the two highest spurs (5 bins each). These bins account for 20.0 % of the total frequency spectrum. The RMS sum of the noise is multiplied by a factor of 20.0 % to achieve a more accurate SNR measurement. The noise floor is the average of the bins used in the noise sum calculation. SFDR is the difference between the fundamental peak signal and the second highest spur, excluding harmonics. Meff is determined from SNR.

4.2 Grounded Input Test

By placing a 50 Ohm termination load on the input of the A/D board the board is characterized for a grounded input. Data was collected at the sampling frequencies of 1.000, 2.000, 3.333, and 5.000 MHz. The data is windowed and processed identically to the data collected in the full scale test. For each sampling rate, DC offset and average noise floor are calculated.

4.1 Histogram Analysis Test

The Fluke 6082A Signal Generator is used to inject a sinewave with an input frequency of 0.977 MHz and at sampling rates of 5.000 MHz and 3.333 MHz. In order to assure that all the output codes are tested, the input signal is set to an amplitude of +.5 dB full scale. One million samples are collected at each sample rate and a utility program on the personal computer creates a histogram output file. The histogram data file shows the number of samples that fell in each of the possible output codes for the A/D converter. For a 14-bit A/D converter there are 2^14 or 16384 possible output codes.

Differential Linearity Error (DLE) is a measure of how each code bin varies in size with respect to the ideal. Mathematically, DLE is the ratio of the actual probability of the nth code occurring to the theoretical probability of the nth code occurring. Instead of a mathematical calculation of DLE, the data was analyzed for missing codes. Additionally, a visual analysis of the histogram output will show data that approximates the standard probability function for a sinewave.

5.0 Test Results

The results of the testing and characterization effort on the Pentek prototype board (SN #9401008) are included in this section. The results of all runs for each test are tabulated and displayed in this section. Graphical plots are labeled by the run number and follow

the tabulated results.

5.1 Full Scale Input Test

Run	filename	Fs (MHz)	Fin (MHz)	SNR (dB)	Meff (bits)	SFDR (dB)	noise floor (dB)
5.1.1	proto01a.dat	5.000	2.305	60.18	9.70	-74.91	-84.41
5.1.2	proto02a.dat	3.333	0.977	71.34	11.56	-81.91	-95.15
5.1.3	proto03a.dat	3.333	0.117	71.25	11.54	-81.71	-95.20
5.1.4	proto04a.dat	2.000	0.977	70.81	11.47	-81.63	-94.62
5.1.5	proto05a.dat	1.000	0.117	73.52	11.92	-82.20	-97.46

Figure 5.1.1: FFT Spectral Response of File PROTO01A.DAT

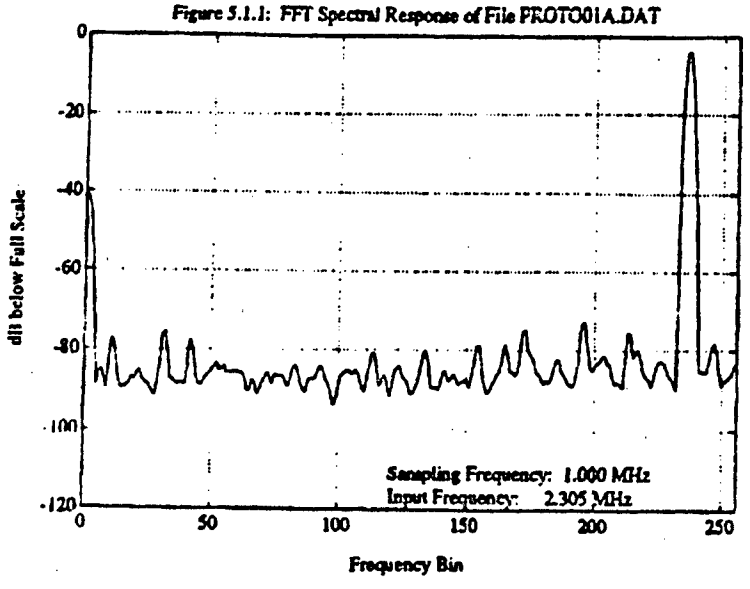

Figure 5.1.2: FFT Spectral Response of File PROTO02A.DAT

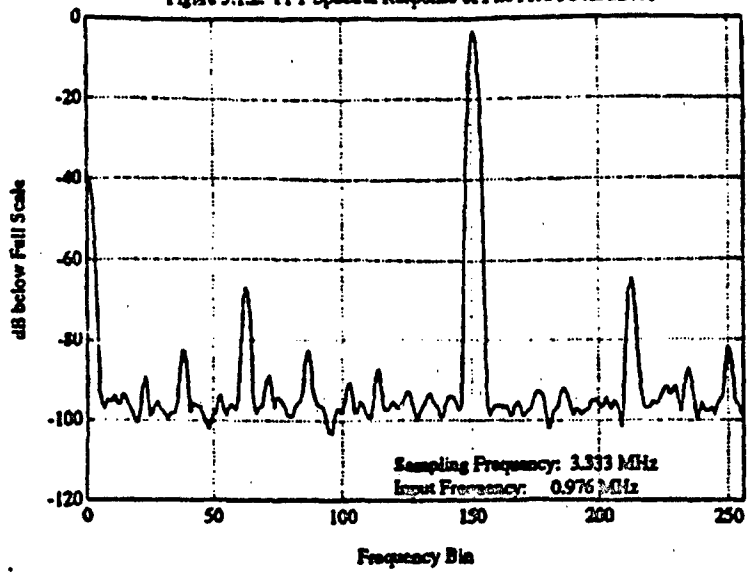

Figure 5.1.3: FFT Spectral Response of File PROTO03A.DAT

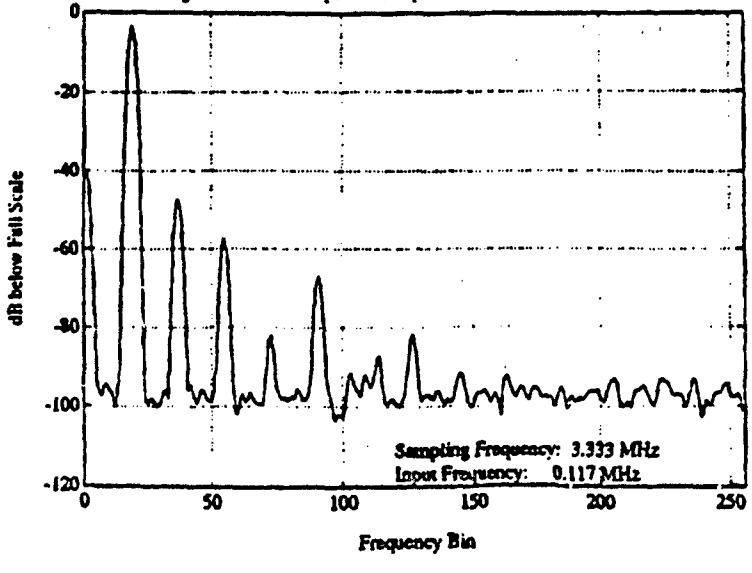

Figure 5.1.4: FFT Spectral Response of File PROTO04A.DAT

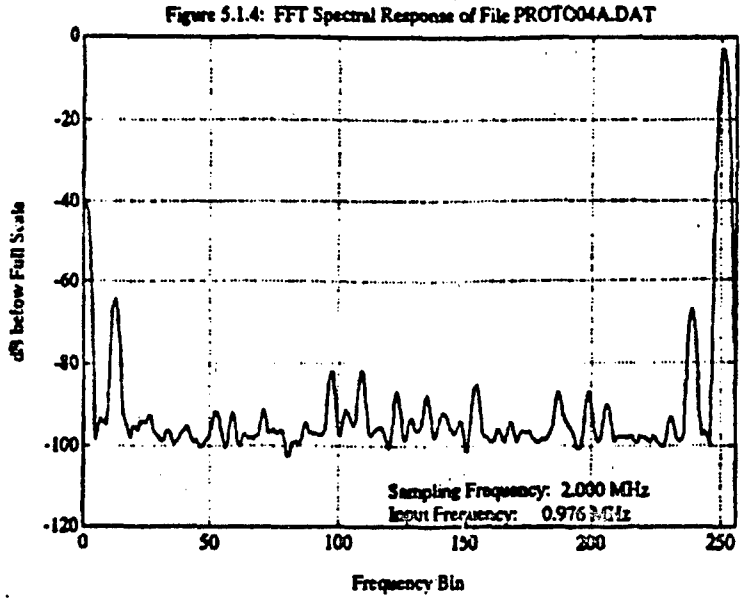

Figure 5.1.5: FFT Spectral Response of File PROTO05A.DAT

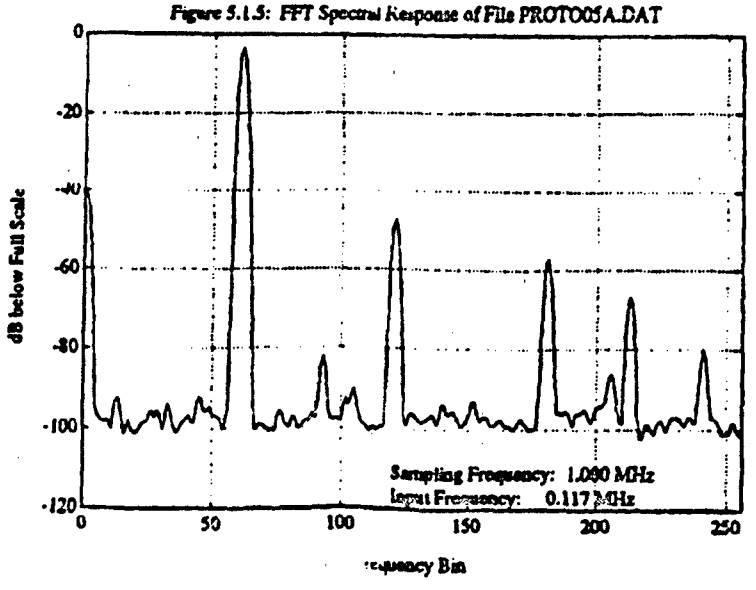

5.2 Grounded Input Test

Run	filename	Fs (MHz)	DC offset (counts)	noise floor (dB)
5.2.1	proto06a.dat	5.000	-47.12	-97.41
5.2.2	proto07a.dat	3.333	-46.57	-98.88
5.2.3	proto08a.dat	2.000	-47.82	-99.97
5.2.4	proto09a.dat	1.000	-48.14	-101.03

Figure 5.2.1: FFT Spectral Response of File PROTO06A.DAT

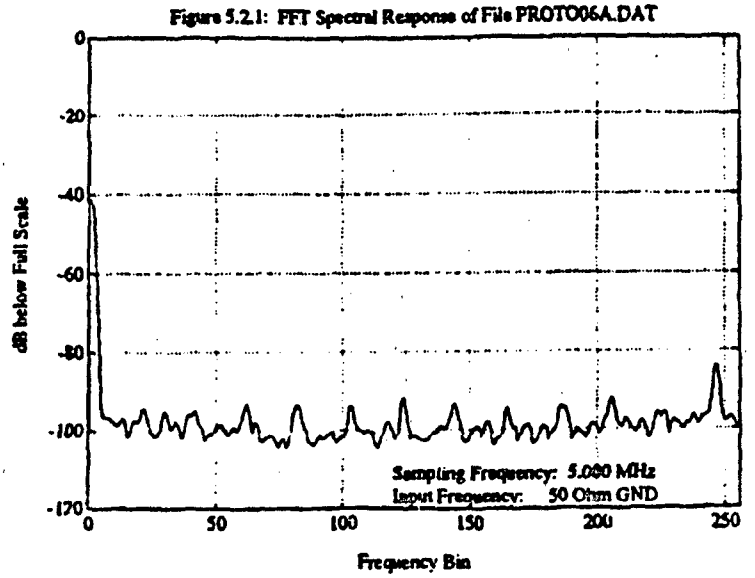

Figure 5.2.2: FFT Spectral Response of File PROTO07A.DAT

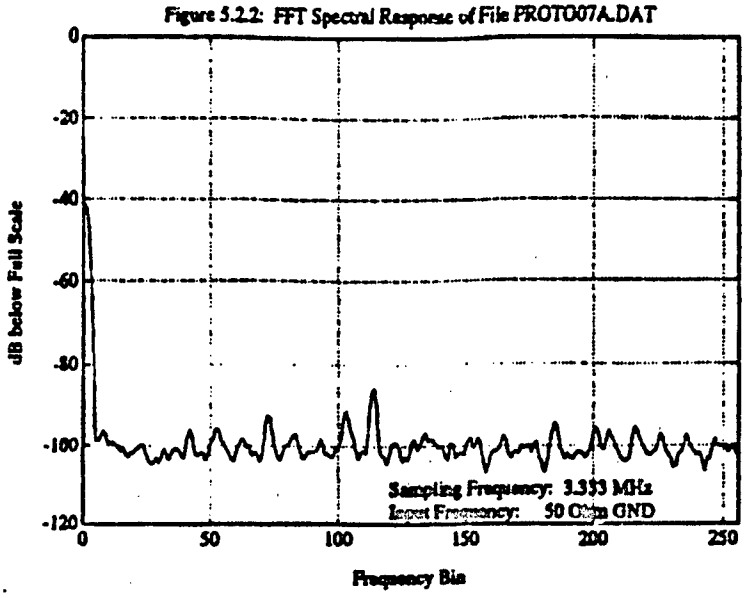

Figure 5.2.3: FFT Spectral Response of File PROTO08A.DAT

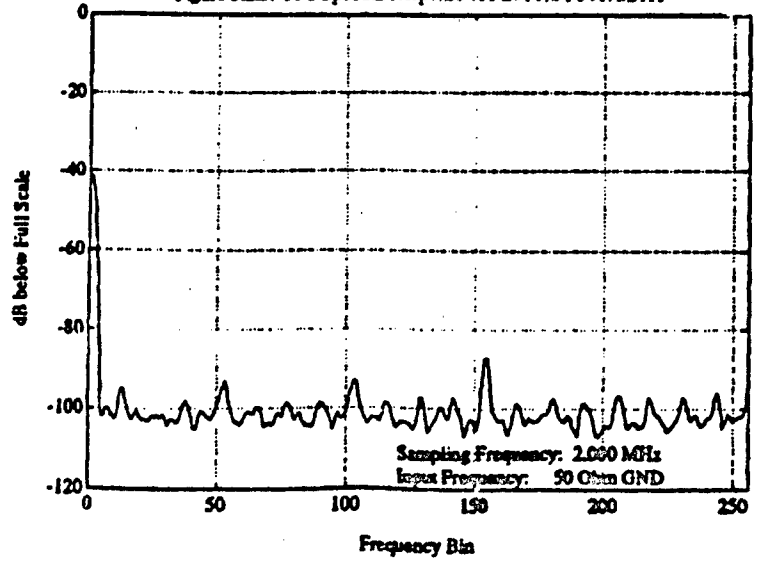

Figure 5.2.4: FFT Spectral Response of File PROTO09A.DAT

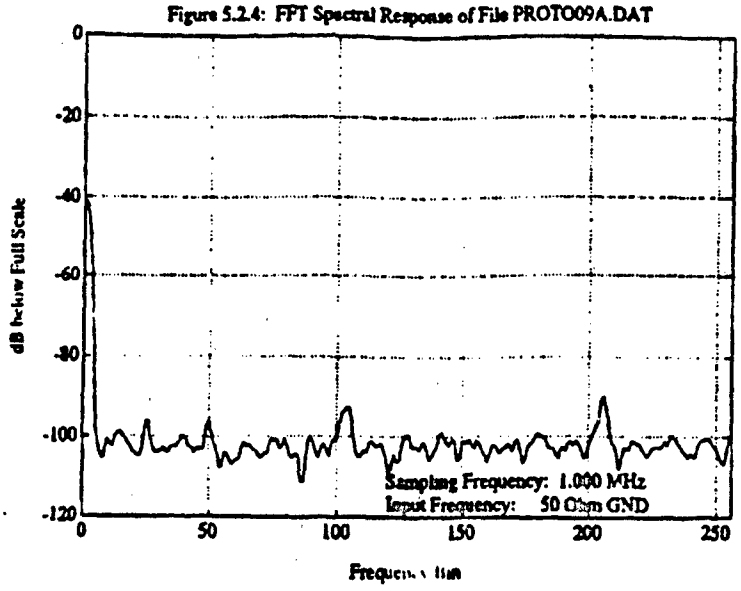

5.1 Histogram Analysis

Run	filename	Fs (MHz)	Fin (MHz)	Amplitude (dBm)
5.3.1	proto10a.dat	5.000	0.977	11.0
5.3.2	proto11a.dat	3.333	0.977	11.0

Figure 5.3.1: Histogram Output at 5.000 MHz

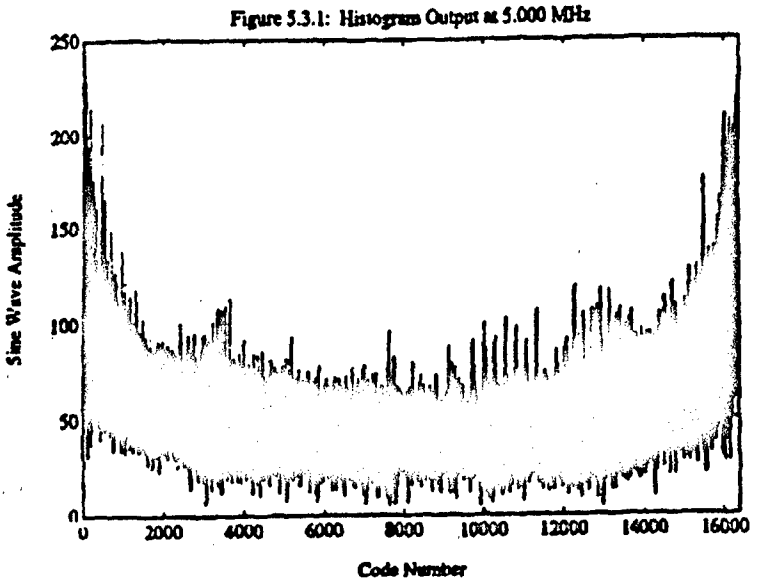

Figure 5.3.2: Histogram Output at 3.333 MHz

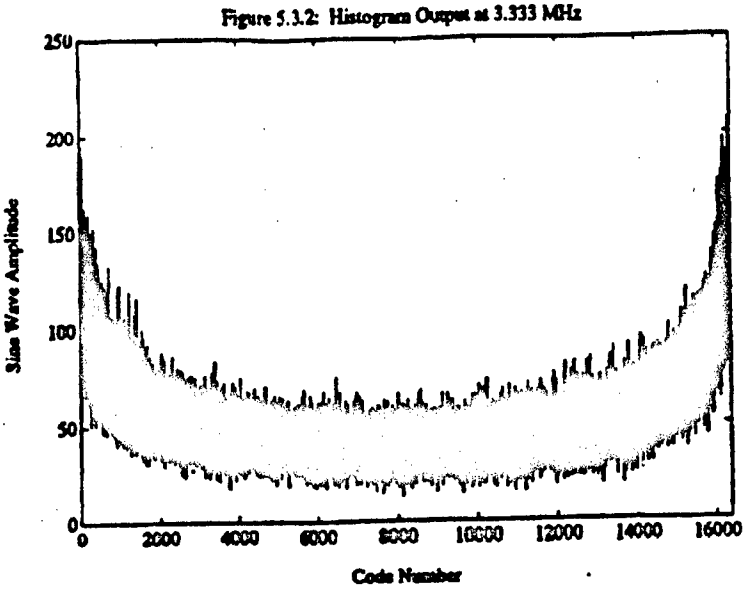

TECHNICAL MEMORANDUM

To: List
From: J. K. Beard
Date: 5 June 1993
Reference: JKB-93-06
Subject: Description of the Tracker CSC for Pulse Doppler Radars

1.0 SUMMARY

The purpose of this memo is to provide a brief description of the target tracker CSC and its functions. The system is a generic ground based pulse-Doppler radar with an electrically steered array (ESA) used for target engagement and surface-to-air missile (SAM) fire control.

2.0 THE TRACKER CSC

The ESA forms pencil beams which are steered at one of several targets sequentially. The radar timing is organized about a major frame time of about 100 milliseconds. All of the targets in track are illuminated once each major frame. Each time a target is illuminated, one or more pulse Doppler bursts is transmitted. The received signals are used with three channel monopulse processing to support a robust, high performance target track. The target track data is used to support ESA beam steering, missile fire control, and missile guidance.

The Tracker CSC is hosted in a processor closely linked with the signal processor. The signal processor provides target detection data, including ambiguous range, ambiguous Doppler, chirp rate of the pulses in the burst (if the pulses are chirped), the burst parameters (including maximum ambiguous range and Doppler, bandwidth, etc.), and target angles as found from monopulse processing. The output of the Tracker CSC is a data block from which beam steering angles are taken for use in the ESA beam steering controller for the next dwell on each target, another data block for use in displays and controls, and signals or interrupt lines signaling that these data blocks are ready and valid.

The central data base of the Tracker CSC is an array of track files. One track file is assigned to each target in track. Each track file is a data structure. Typical contents of this data structure are shown below in Table I. Note that the key parameter in the track file is an indicator of its state, which determines the actions taken by each Tracker CSC Function. The Tracker CSC Functions are Association, Initialization, Update, Range Resolve, Drop Track, and System Interface. Each of these CSC Functions is described below.

Table I. Typical Track File

Block	Variables	Purpose
1	Track File State	0-Unused, 1-Initialized, 2-One Hit 3-Established, 4-Range Resolved
2	Times	First Hit, Last Hit times, etc.
3	Quality Indicators	No. of hits, No. of misses, etc.
4	Azimuth Track	Kalman filter data block
5	Elevation Track	Kalman filter data block
6	Doppler Track	Kalman filter data block
7	Ambiguous PRF Track 1	Kalman filter data block
8	Ambiguous PRF Track 2	Kalman filter data block
9	Ambiguous PRF Track 3	Kalman filter data block
10	Ambiguous PRF Track 4	Kalman filter data block
11	Ambiguous PRF Track A	Kalman filter data block
12	Ambiguous PRF Track B	Kalman filter data block
13	Ambiguous PRF Track C	Kalman filter data block
14	Ambiguous PRF Track D	Kalman filter data block
15	Unambiguous Range Track	Kalman filter data block
16	Missile Track	Kalman filter data block, etc.
17	Display Data	As appropriate
18	Subframe Allocation	As required
19	Second Tracker	As required

3.0 Descriptions of Tracker Functions

Each of the Tracker CSC Functions described below is done sequentially after each target dwell. All of the functions operate on the track files using data from the signal processor, except System Interface, which maintains the data blocks used to support beam steering and the displays and controls.

3.1 Association

At the time the Tracker CSC is invoked, the only data available is target detection data and the track file data. The first operation is to determine which track files correspond to which target detections. This operation is the association of returns to tracks, or simply Association.

The association problem and its solutions are well known [1]. For this type of radar, less than 20 targets are tracked and less than 20 returns are usually detected on each dwell. Even with these relatively small numbers, simplifications of the sorting process are appropriate. The association logic is as follows:

a. **Preselect by target angle.** Examine the azimuth track for each active track file, extrapolated to current time. If the difference between the predicted and measured azimuth exceeds a preselected threshold (typically about a beamwidth), no association exists for this return and this track file. Repeat for elevation. The threshold for elevation preselection is independent from that used for azimuth.

b. **Preselect by Doppler.** Examine the Doppler track, extrapolated to current time. If the Doppler difference is more than about three standard deviations of the extrapolated Doppler track, association again fails.

c. **Preselect by range.** Examine the ambiguous range track for this track file for the PRF used in this dwell, extrapolated for current time and taken modulo the maximum unambiguous range for this PRF. If the difference exceeds a reasonable threshold, association fails.

This process is invoked for each return for all active track files. More detailed checking is done during the track update process. Each return that has been associated with an existing track file is flagged as having been used.

In the event that no detections occur in a dwell steered at a target in track, the preselection in angle process will be used to select the appropriate track file or files and the "miss" counter will be incremented in the track quality data blocks of these track files.

3.2 Initialization

3.2.1 Automatic Initialization. Detected targets that have not been associated with an existing track file are used to initialize a new track file. An unused track file data structure in the track file array is initialized by setting the track file state appropriately and initializing the angle, Doppler, and ambiguous range track for the PRF used in the dwell.

3.2.2 Manual Initialization. Operator initialization of a track file may be done by designation of target angles, Doppler, PRF, and ambiguous range. An unused track file data structure is used and initialized as appropriate with the data available.

3.3 Update

3.3.1 Two state Kalman filters. The same state Kalman filter, with application-dependent tuning, is used to update azimuth track, elevation track, and Doppler track. This adaptive Kalman filter uses states congruent to the measurement and its time derivative, such as angle and angle rate. The ambiguous range track is updated with a slightly different version which accepts range rate measurements as well as range measurements.

The two state Kalman filters use adaptive plant noise, in which the diagonal plant noise term corresponding to time derivative is scaled with the square of the measurement error. This provides an adaptive mechanism which allows maximum accuracy for well-behaved targets with maximum robustness of track for ill-behaved targets. Innovative algebraic mechanisms are used to prevent any possibility of covariance collapse, so that maximum possible robustness is achieved with a very simple tracker.

In some instances, Doppler measurement data is invalid or unavailable. In this case, the ambiguous range track for the PRF used is updated with the appropriate Kalman filter without a Doppler measurement, and the Doppler track data is not updated.

In other instances, range measurement data is invalid or unavailable, but Doppler measurement data is available. A special third two state Kalman filter is available for updating the ambiguous range tracks for occasions when this occurs.

3.3.2 Three state Kalman filter. If the range ambiguity has been resolved earlier in the track history, the track file state is set to indicate that a three state range tracker has been initialized. Range ambiguity data appropriate to the PRF used in the dwell is used to correct the ambiguous measured range, and this data is used with Doppler data to update the three state range tracker.

The three state Kalman filter uses adaptive plant noise. The diagonal noise terms corresponding to range rate and range acceleration are scaled by squares of the measurement errors in range and Doppler. This provides maximum accuracy with maximum robustness for any target, as with the two state Kalman filters.

When a constant velocity target is tracked for an extended period, the three state range tracker would be liable to covariance collapse due to extremely small variance of range acceleration. This is sometimes prevented by placing significant plant noise in the range acceleration state, at the expense of tracker accuracy. The three state range tracker does not use inappropriate plant noise to prevent covariance collapse. Instead, a UDUT square root Kalman filter[2] is used for this tracker.

3.3.3 Track update failure. When, during the execution of a track file update, data checks reveal that the detection should not be associated with the track file or that the update data is otherwise invalid, the update will fail. The "miss" counter is incremented

in the track quality data block, a software flag is set, the "used" flag in the signal processor data set is reset, and update is abandoned. Such detection data is used to initialize new tracks. Whenever the track update does not fail, the "miss" counter is reset to zero.

3.4 Range and Doppler Resolve

Doppler ambiguity resolution is performed by examining ambiguous range track; the range rate from two dwells will nearly always allow accurate resolution of Doppler ambiguity for high PRF. Doppler for PRFs that are too low to be useful in this operation are simply discarded. Doppler ambiguity resolution is repeated every dwell for any track file for which range ambiguity resolution has not been accomplished.

Range ambiguity resolution requires that the ambiguous range tracks from at least two and usually three PRFs converge so that range track accuracy is considerably better than a range gate. Range resolve in reasonably short periods requires that Doppler data be used in the range tracks.

The ambiguous ranges from several tracks are extrapolated to the same effective point in time, called the range resolve epoch. The variances of these ranges at the range resolve epoch are thresholded according to the range resolve algorithm applicable for the PRF combination and the feasibility of successful range resolve is evaluated. If the range variances are sufficiently small, range resolve proceeds; otherwise, range resolve is abandoned for this track file.

Range resolve is done by evaluating the differences in ambiguous ranges in terms of the differences in maximum unambiguous range for each PRF pair involved. Modulo arithmetic is used in a final equation which yields the unambiguous target range, effective at the range resolve epoch. This information, along with range rate from the Doppler track, to initialize the three state range tracker. The state of the track file is changed to indicate that range resolve has been accomplished.

3.5 Drop Track

The track quality indicators are scanned and tracks for which the "miss" count is too high, or for which the last update was too long ago, are dropped. Tracks are dropped by resetting the track file state to zero, to indicate that the track file data structure is unused and is available for use with new track initiations.

Track files are examined by pairs to ensure that more than one track file has been assigned to the same target. Screening is done by using target angle, ambiguous range, and Doppler data from one track file and scanning down the remainder of the track files using comparison logic similar to that used in Association. In the event that two track files are found which are tracking the same target, the target quality indicators are examined and the best track file is retained and the other is dropped.

Efficiency in scanning the track files can be assured by scanning the track state indicators. In the event it is deemed that efficiency requires that the track files be compact, track file data structures will be sorted when tracks are dropped to keep them all in a contiguous block.

3.6 System Interface

A system data block is maintained for use by the beam steering controller. Steering data is provided, effective at the next dwell time, for each subframe with sufficient lead time to ensure that data latency requirements are met for operation of the beam steering controller.

Another data block is maintained for use by the displays and controls. This data block includes target display identifiers, target position and velocity, and other identifiers such as high closing Doppler and other operator alert signals. Other data not serviced by this function, such as the real or complex range-Doppler map from the signal processor may be used by the displays and controls, is identified by pointers or other data in this data block.

The System Interface function services the system communication data blocks by processing data from the track files as appropriate. Beam steering data is kept in sine space in the angle track files so that this processing operation for beam steering simply amounts to extrapolation of angle data to the major frame subframe slot allocated to the target being tracked. This is done even if a "miss" has been recorded for this target. Data for the displays and controls is formatted with a minimum of processing for use by the displays and controls functions.

Whenever the operations of storing new data in a system data block begin, a software or hardware "data block busy" signal will be set. At the completion of the data storage operation, the data flag will be set to "data valid."

4.0 CONCLUSIONS

A simple description of the Target Track CSC for a pulse Doppler engagement radar has been described.

5.0 REFERENCES

[1] "Multiple Target Tracking with Radar Applications," S. Blackman, Artech House (1986).

[2] "Factorization Methods for Discrete Sequential Estimation," G. J. Bierman, Academic Press (1977).

TECHNICAL MEMORANDUM

To: List
From: J. K. Beard
Date: 30 July 1993
Reference: JKB-93-09A
Subject: A Range Resolve Methodology for Pulse Doppler Radars

1.0 SUMMARY

A fast method has been found for performing the range resolve function using ambiguous ranges from multiple pulse repetition frequencies (PRFs). The method is applicable to PRIs which share prime factors in common. Requirements on tracker accuracy are relaxed in proportion to the product of prime factors shared between PRIs, so that shared factors are a requirement for practical application for closely spaced PRFs. The method, its derivation, examples, and a simulation are given in this report. This memo was revised and reissued on 10 August 1993.

2.0 PROBLEM STATEMENT

2.1 The Range Resolution Problem

Pulse-Doppler radars often use high PRFs so that target Doppler is unambiguous. When a radar return from a target is detected, it is impossible to determine from which transmitted pulse the energy originated. This is the range ambiguity problem inherent in the pulse-Doppler radar system concept.

Range ambiguities are resolved by chaining PRFs and observing differences in apparent, or ambiguous, target range. If the target range does not change, the target return is from the transmitted pulse just preceding the return. If the target return appears at different ranges for different PRFs, then the target return is from a previous pulse. The range ambiguity resolution problem is determining which transmitted pulse originated the energy for a given return.

2.2 System Engineering Tradeoffs

In selecting a set of PRFs for a pulse-Doppler design, it is important that the PRFs for each class of modes be kept as close as possible so that the signal processing can be kept as similar as possible for the different PRFs. This means that the tracker performance does not vary as the PRFs are changed to prevent a target from falling into a blind range. Also, range resolve is done early in the track history, so that tracker accuracy is limited to approximately one range gate. Therefore, the tracker accuracy requirement of the range resolve algorithm should be matched to the bandwidth of the radar.

The bandwidth of the radar, for unmodulated pulse train bursts, is approximated by one over the pulse length used in the bursts. Thermal consideration in final amplifiers limit the duty cycle in the bursts (or the average power in the bursts), which is kept as high as possible because this parameter maps directly into the signal to noise ratio. Therefore, the duty cycle remains nearly constant over PRF changes. The number of non-overlapping range gates, including the blind range, is approximately the reciprocal of the duty cycle. Since one of the parameters in the range resolution methodology design to the number of range gates, duty cycle interacts with the range resolve methodology.

The number of pulses in a burst is not the dwell time. A wait time of $(2 \bullet R_{MAX}/c)$ is necessary to wait for returns to begin coming in from the longest range targets. Processing begins at the end of this wait time through the end of the burst. This processing time determines the energy on the target during the burst, and the Doppler resolution of the radar is proportional to one over the processing time.

Tracker performance is determined by range accuracy, Doppler accuracy, and revisit time. The number of dwells between revisit times is the limit of independent targets a phased array may consider independently; this is the beam occupancy limit.

A single system clock crystal is usually used in pulse-Doppler radars so that receiver design deals only with the lines of one oscillator and its harmonics; this oscillator frequency is usually selected in terms of the minimum display granularity of the system. System clocks of 10 to 15 MHz, corresponding to system granularities of 65 to 100 nanoseconds or 10 to 15 meters, are common. PRIs are selected as integers multiples of the system granularity. This means that design of the range resolve methodology interacts with selection of the system clock frequency.

In summary, requirements on the range resolve design are determined from the requirements on a phased array radar, posed in terms of maximum range requirements, peak and average power available, and tracker performance requirements. A range resolve methodology is selected within the constraints of number theory, using system clock frequency as a free parameter, to meet system requirements in terms of allowable tracker accuracy, maximum range, the number of independent target tracks, the number of PRFs, the number of range gates, and the system clock frequency.

3.0 RESOLVING RANGE AMBIGUITY

3.1 The Method

The method, as presented here, is applied to two PRFs. The method is nested to apply it to three or more PRFs. The results of combining the first two PRFs is used as data which is taken as inputs from a virtual PRF which is much lower, and this data is used with data from a third PRF.

The problem statement is: given two pulse repetition intervals (PRIs) in terms of clock counts for a common system clock P_1 and P_2, and ambiguous ranges from PRFs corresponding to these PRIs, find the smallest range that would result in these observed ambiguous ranges.

As part of the radar mode setup, some offline computations are performed to set up the range resolve methodology. These steps are:

1. Find the prime factors of the two PRIs P_1 and P_2,
2. Find the mutual prime factors of P_1 and P_2, F_{12}, and find the mutually prime virtual PRIs $P'_1=P_1/F_{12}$ and $P'_2=P_2/F_{12}$,
3. Define the context granularity as the system clock rate divided by F_{12},
4. Define the "magic number" S_{12} from P'_1 and P'_2.

Real time computations, done as part of the tracker functions when range resolve is to be executed, are:

a. Extrapolate the two tracker ambiguous range position states to the same effective time (selected to minimize the variance of $R_1 - R_2$ as used in the next step),

b. Find the difference in the ambiguous ranges $R_1 - R_2$, rounded to the nearest number of "context clock" counts, $(Rc_1 - Rc_2) = (R_1 - R_2)/dR$, where $dR=c/(2 \bullet f_{clock})$.

c. Find $D = (Rc_1 - Rc_2) \bmod (P'_1)$; if $D<0$ add P'_1,

d. Find $A_2 = (S_{12} \bullet D) \bmod (P'_1)$ (this step may be skipped if $S_{12} = 1$), and

e. Find the unambiguous range $R_{12} = R_2 + A_2 \bullet P_2 \bullet dR$.

Note that the difference between ambiguous ranges is used, so that the method is not a function of arbitrary "range bins" as are older methods using the classical Chinese remainder theorem[1]. However, note that the tracker accuracy requirement, defined by the rounding in step (b) above, requires that the difference between two ambiguous ranges be accurate within a "bin" of $F_{12} \bullet dR$. This means that F_{12} should be approximately one range bin, or pulse width, in terms of clock ticks. This means that P'_1 and P'_2 should be approximately equal to the number of range gates.

In most applications, combinations of PRFs can be found such that S_{12} is 1 for useful PRF combinations. When this is done, step (d) above is redundant with step (c) and is omitted.

Practical application nearly always requires that more than two PRFs be used in resolving range ambiguity. This is done by nesting the method. This process is described in the next section.

3.2 More than Two PRFs

Adding PRFs is simple. The process is as follows:

i. Select two PRFs and apply the method as described above, including defining the effective PRI corresponding to the combination of P_1 and P_2, $P_{12} = F_{12} \bullet P'_1 \bullet P'_2$,

ii. Take the range rate and effective time for R_{12} as those of R_2, so that a complete set of virtual ambiguous range tracker states is defined for the results of combining PRF 1 and PRF 2,

iii. Take the ambiguous range tracker states for PRF 3 and combine it with the virtual tracker states defined for PRFs 1 and 2 and reapply the method.

For the new set of common factors F_{23} is computed from P_{12} and P_3, as is the new "magic number" S_{23}. The value of S_{23} is dependent on the order of the PRFs selected in application of the method, and that some simplification can be achieved if the order of the PRFs is selected such that S_{23} is 1. Examination of the possibilities shows that there are six ways that three PRFs can be combined. All should be examined in development of a methodology to be applied in an actual system.

The minimum value of F that is used throughout the process determines the requirements on tracker accuracy. Estimates of tracker accuracy available from the track file data should be used to ensure that range resolve can be accomplished with high confidence before proceeding. Also, the ambiguous range tracks should be continued and range resolve checked for several "hits" to ensure correct range resolve is accomplished.

3.3 Derivation of the Method

Ambiguous ranges from each PRF are, in terms of the system clock ticks,

$$Rc_i = (R) \bmod (P_i \cdot dR), \quad dR = \frac{c}{2 \cdot f_{clock}} \tag{1}$$

which can be restated in terms of products and remainders as

$$\left.\begin{aligned} R &= R_1 + A_1 \cdot P_1 \cdot dR,\ 0 \le A_1 < P_2, \\ R &= R_2 + A_2 \cdot P_2 \cdot dR,\ 0 \le A_2 < P_1. \end{aligned}\right\} \tag{2}$$

The integers A_1 and A_2 are unknown. Determination of either A_1 or A_2 resolves the range ambiguity.

Subtracting the two forms given in Equation (2) and rearranging terms gives

$$Rc_1 - Rc_2 = A_2 \cdot P_2 - A_1 \cdot P_1 \tag{3}$$

where Rc_1 and Rc_2 are the ambiguous ranges given in clock ticks,

$$\left.\begin{aligned} Rc_1 &= \frac{R_1}{dR}, \\ Rc_2 &= \frac{R_2}{dR}. \end{aligned}\right\} \tag{4}$$

Taking both sides of Equation (3) modulus P_1 gives

$$D = (A_2 \cdot P_2) \bmod (P_1) \tag{5}$$

where D is given by

$$D = (Rc_1 - Rc_2) \bmod (P_1), \text{ if } D < 0 \text{ then add } P_1 \text{ to } D. \tag{6}$$

Writing the modulus relationship in Equation (5) in terms of a product and remainder gives

$$A_2 \cdot P_2 = D + k \cdot P_1,\ 0 \le k < P_2. \tag{7}$$

The range resolve problem has now been reduced to finding A_2 from D in

Equation (7). Three "brute force" methods have been demonstrated by simulation:

- Step k from 0 to (P_2 - 1) in Equation (7), stop when (D + k•P_1) mod (P_2) is zero. Then, find $A_2 = (D + k \bullet P_1)/P_2$.
- Use the first approach to build up a lookup table of $A_2(D)$.
- Step A_2 from 0 to (P_1 - 1), finding D for each case, to build up the lookup table.

However, a more elegant method is available which does not need a lookup table, and which does not require a search for k in the real time processing.

The basic intuition is achieved by taking both sides of Equation (7) modulus P_2,

$$(D + k \cdot P_1) \bmod (P_2) = 0. \tag{8}$$

We can find a value of k which satisfies Equation (8), by using a constant S_x such that

$$(S_x \cdot P_1) \bmod (P_2) = -1, \quad 1 \le S_x < P_2 \tag{9}$$

so that a value of k which satisfies Equation (8) can always be found as

$$k = S_x \cdot D. \tag{10}$$

Then, A2 can be found from

$$A_2 = \left(\frac{D + D \cdot S_x \cdot P_1}{P_2} \right) \bmod (P_1). \tag{11}$$

Given the thinking shown in Equations (8) through (11), a "magic number" S can be found as follows. First, find S_x by stepping from 1 to (P_2 - 1) and check Equation (9), looking for (P_2 - 1) as the result of the modulus operation because (P_2 - 1) is equal to (-1) modulus (P_2). Since P_1 and P_2 are mutually prime, S_x will always exist. The "magic number" S is given by

$$S = \frac{S_x \cdot P_1 + 1}{P_2} \tag{12}$$

and A_2 is found from

$$A_2 = (D \cdot S) \bmod (P_1). \tag{13}$$

A final insight is available from examination of Equation (12):

$$(S \cdot P_2) \bmod (P_1) = 1, \quad 1 \le S < P_1. \tag{14}$$

Since P_1 and P_2 are mutually prime, S always exists and is unique. S can be found directly from Equation (14) by simply stepping test values from 1 to (P_1 - 1) and testing the modulus.

4. EXAMPLES

Five examples are summarized below. Each uses three PRFs and a system clock of 14.990 MHz for a system granularity of 66.7 nanoseconds or 10 meters. The PRIs were selected by examining prime factorizations of integers from 100 to 150 and exploring combinations based on numbers which have prime factors from 5 to 15.

4.1 PRIs of 153, 152, and 144 clock ticks

The PRIs correspond to PRFs of 104.1 kHz, 98.6 kHz, and 98.0 kHz. Table 4.1-1 gives the tracker tolerance in meters. The extra two rows and columns correspond to use of two PRIs in one iteration of the method. As discussed above, the tracker tolerance is equal to the product of the factors common to the PRIs, multiplied by the system granularity of 10 meters. Therefore, symmetry about the main diagonal is seen in the table. Entries where all the prime factors of one or both of the PRIs are common to both are not viable, and are shaded in the table.

Table 4.1-1. Tracker Tolerance, Meters

PRI 2 -> / PRI 1	153	152	144	2448	2736
153		10	90		90
152	10		80	80	
144	90	80			
2448		80			1440
2736	90			1440	

Note that the smallest number in the table is the system granularity of 10 meters, but combinations of PRFs can be found which give system granularities of 80 and 90 meters. Tracker accuracies of 8 or more clock ticks are obtainable early in a track history, while tracker accuracies of a single clock tick are difficult under any circumstances.

The "magic number" needed in implementation is given for each possible combination of PRFs in Table 4.1-2. Note that this table is not symmetrical; the magic number depends on the order in which the PRIs are taken.

Table 4.1-2. Magic Number

PRI 2 -> / PRI 1	153	152	144	2448	2736
153		152	16		8
152	1		18	10	
144	1	1			
2448		145			9
2736	161			9	

Note that the magic number can be 1 if the lowest PRF is taken second in the first iteration of the method, but that the magic number is not 1 for the second iteration. The ratio of the highest to lowest PRF is 1.0625 for this design. The total unambiguous range for this PRF combination is 46512 clock ticks, 465 km, or 251 nautical miles.

4.2 PRIs of 144, 143, and 132 clock ticks

The PRIs correspond to PRFs of 113.6 kHz, 104.8 kHz, and 104.1 kHz. Table

4.2-1 gives the tracker tolerance in meters. As discussed above, the tracker tolerance is equal to the product of the factors common to the PRIs, multiplied by the system granularity of 10 meters. Therefore, symmetry about the main diagonal is seen in the table. Entries where all the prime factors of one or both of the PRIs are common to both are not viable, and are shaded in the table.

Note that the smallest number in the table is the system granularity of 10 meters, but combinations of PRFs can be found which give system granularities of 110 and 120 meters. Tracker accuracies of 11 or more clock ticks are obtainable early in a track history, while tracker accuracies of a single clock tick are difficult under any circumstances.

Table 4.2-1. Tracker Tolerance, Meters

PRI 2 -> / PRI 1	144	143	132	1584	1716
144		10	120		120
143	10		110	110	
132	120	110			
1584		110			1320
1716	120			1320	

The "magic number" needed in implementation is given for each possible combination of PRFs in Table 4.2-2. Again, this table is not symmetrical; the magic number depends on the order in which the PRIs are taken.

Table 4.2-2. Magic Number

PRI 2 -> / PRI 1	144	143	132	1	1716
144		143	11		11
143	1		12	10	
132	1	1			
1584		133			1
1716	12			12	

Note that the magic number can be 1 throughout the implementation if the PRIs are taken in the order 132 and 144, resulting in an equivalent PRI of 1584, then 143 and

1584. The ratio of the highest to the lowest PRF is 1.091 for this design. The total unambiguous range for this PRF combination is 20592 clock ticks, 206 km, or 111 nautical miles.

4.3 PRIs of 133, 132, and 126 clock ticks

The PRIs correspond to PRFs of 119.0 kHz, 113.6 kHz, and 112.7 kHz. Table 4.3-1 gives the tracker tolerance in meters. Again, the tracker tolerance is equal to the product of the factors common to the PRIs, multiplied by the system granularity of 10 meters, and symmetry about the main diagonal is seen in the table. Entries where all the prime factors of one or both of the PRIs are common to both are not viable, and are shaded in the table.

Note that the smallest number in the table is the system granularity of 10 meters, but combinations of PRFs can be found which give system granularities of 60 and 70 meters. Tracker accuracies of 6 or more clock ticks are obtainable early in a track history, while tracker accuracies of a single clock tick are difficult under any circumstances.

Table 4.3-1. Tracker Tolerance, Meters

PRI 2 -> / PRI 1	133	132	126	2394	2772
133		10	70		70
132	10		60	60	
126	70	60			
1330		60			1260
2772	70			1260	

The "magic number" needed in implementation is given for each possible combination of PRFs in Table 4.3-2. Note that this table is not symmetrical; the magic number depends on the order in which the PRIs are taken.

Table 4.3-2. Magic Number

PRI 2 -> / PRI 1	133	132	126	1330	2772
133		132	18		6
132	1		21	15	
126	1	1			
1330		127			13
2772	271			7	

Note that the magic number can be 1 in the first iteration of the method, but not in the second. The ratio of the highest to the lowest PRF is 1.056 for this design. The total unambiguous range for this PRF combination is 52668 clock ticks, 527 km, or 284 nautical miles.

4.4 PRIs of 121, 120, and 110 clock ticks

The PRIs correspond to PRFs of 136.3 kHz, 124.9 kHz, and 123.9 kHz. Table 4.4-1 gives the tracker tolerance in meters. Again, the tracker tolerance is equal to the product of the factors common to the PRIs, multiplied by the system granularity of 10 meters, and symmetry about the main diagonal is seen in the table. Entries where all the prime factors of one or both of the PRIs are common to both are not viable, and are shaded in the table.

Note that the smallest number in the table is the system granularity of 10 meters, but combinations of PRFs can be found which give system granularities of 100 and 110 meters. Tracker accuracies of 10 or more clock ticks are obtainable early in a track history, while tracker accuracies of a single clock tick are difficult under any circumstances.

Table 4.4-1. Tracker Tolerance, Meters

PRI 2 -> / PRI 1	121	120	110	1210	1320
121		10	110		110
120	10		100	100	
110	110	100			
1210		100			1100
1320	110			1100	

The "magic number" needed in implementation is given for each possible combination of PRFs in Table 4.4-2. Note that this table is not symmetrical; the magic number depends on the order in which the PRIs are taken.

Table 4.4-2. Magic Number

PRI 2 -> / PRI 1	121	120	110	1210	1320
121		120	10		10
120	1		11	1	
110	1	1			
1210		111			1
1320	11			11	

Note that the magic number can be 1 throughout the implementation if the PRIs are taken in the order 110 and 121, resulting in an equivalent PRI of 1210, then 120 and 1210. The total unambiguous range for this PRF combination is 14520 clock ticks, 206 km, or 78.4 nautical miles.

4.5 PRIs of 105, 104, and 100 clock ticks

The PRIs correspond to PRFs of 149.9 kHz, 144.1 kHz, and 142.8 kHz. Table 4.5-1 gives the tracker tolerance in meters. The tracker tolerance is equal to the product of the factors common to the PRIs, multiplied by the system granularity of 10 meters, as before, and symmetry about the main diagonal is seen in the table. Entries where all the prime factors of one or both of the PRIs are common to both are not viable, and are shaded in the table.

Note that the smallest number in the table is the system granularity of 10 meters, but combinations of PRFs can be found which give system granularities of 40 and 50 meters. Tracker accuracies of 4 or more clock ticks may be obtainable early in a track history, while tracker accuracies of a single clock tick are difficult under any circumstances.

Table 4.5-1. Tracker Tolerance, Meters

PRI 2 -> / PRI 1	105	104	100	2100	2600
105		10	50		50
104	10		40	40	
100	50	40			
2100		40			1000
2600	50			1000	

The "magic number" needed in implementation is given for each possible combination of PRFs in Table 4.5-2. Note that this table is not symmetrical; the magic number depends on the order in which the PRIs are taken.

Table 4.5-2. Magic Number

PRI 2 -> / PRI 1	105	104	100	2100	2600
105		104	20		4
104	1		25	21	
100	1	1			
2100		101			17
2600	421			5	

Note that the magic number can be 1 throughout the implementation if the PRIs are taken in the order 100 and 105, resulting in an equivalent PRI of 2100, then 104 and 2100. The ratio of the highest to the lowest PRF is 1.05 for this design, an exceptionally low value. The total unambiguous range for this PRF combination is 54600 clock ticks, 206 km, or 295 nautical miles.

5.0 CONCLUSIONS

The methodology presented is simple and straightforward. Interaction with system engineering tradeoffs is direct and simple. Implementation is simple and straightforward, as is illustrated in a simulation attached as an Appendix. Several examples were given and developed, using a sample system clock corresponding to a straw-man system granularity of 10 meters. Results from the examples are summarized in Table 5.0-1.

Table 5.0-1. Summary of Examples

PRIs	Ratio	ΔR, ticks	Smallest P'	R_{MAX}/R_{AMBI}	All S=1?
153, 152, 144	1.0625	8	16	304	NO
144, 143, 132	1.091	11	11	143	YES
133, 132, 126	1.056	6	18	396	NO
121, 120, 110	1.100	10	10	120	YES
105, 104, 100	1.050	4	21	520	NO

Several generalizations can be made from the examples. First, all of them follow the pattern of the largest two PRIs differ by 1, with the spread being approximately ΔR and the number of range gates (or the smallest P') is slightly less than the PRI/ΔR. Second, the tighter the PRFs are grouped, the larger the number of range gates (as given by the smallest P' in the table) tends to be. Also, grouping the PRFs too tightly makes keeping the requirements on tracker accuracy low. However, the maximum unambiguous range is increased when the PRFs are grouped more tightly, the tracker accuracy requirements are increased, and the number of range gates is increased.

Simulation has revealed the limitations of the technique. The maximum peak error in $(R_i - R_j)$ cannot exceed one half the tabulated value of ΔR. In addition, if the input ranges are in the wrong ambiguity, the inputs to the algorithm are invalid; this can happen if the true target range is near zero or maximum ambiguous range and tracker errors cause the apparent target position to be on the other side of the ambiguity discontinuity. For example, if the unambiguous range is 50.01 km and the range ambiguity is 1 km, the ambiguous range is .01 km or 10 meters. If the tracker error is -20 meters, the tracker will report the ambiguous range as .99 km, not .01 km, for an error in ΔR of nearly 1 km. This can be easily sensed by avoiding attempting range ambiguity resolution when the ambiguous range as reported by the tracker is dangerously near either zero or maximum unambiguous range.

In conclusion, the methodology is well adapted to pulse-Doppler radar design. Its implementation and use are well defined. Its application is simple and efficient. It has no significant deficiencies in implementation or application.

6.0 REFERENCES

[1] "Radar Handbook," Merrill Skolnik, Editor, McGraw-Hill (1970), p. 19-16. A later edition is now available.

10.0 APPENDIX

A FORTRAN listing of three subprograms, *rresolv*, *isok*, and *doext*, follows. These subprograms were used in a simulation of the examples which verified the range resolve capability and the tolerance on tracker accuracy. Extrapolation to a time between the last track file update times is included in the module *isok*.

```
      subroutine rresolv(r,rdot,pri,ff,varnc,s23,teff,isdone,runamb) !Res
range
C Inputs:
* r(3)          Three ambiguous ranges, given in floating point clock ticks
* pri(3)        The three PRI's corresponding to the ambiguous ranges
* ff(3)         Factors between PRI's ((1)<->(1,2); (2)<->(1,3); (3)<->(2,3))
* varnc(3,2)    Standard deviations of the three ranges
* s23           Magic number for second pass
* teff(3)       Effective times for the three ambiguous range tracks
C Outputs:
* isdone  Logical flag indicating success or failure
* runamb  Unambiguous range (undefined when isdone=.FALSE.)
      implicit none
      double precision r(3),rdot(3),varnc(3,2),teff(3),t13,t23,r13,
     &  runamb
      integer i,j,ff,pri(3),ff(3),pri13,pritot,one,s23
      logical isok,isdone
      data one /1/
*
C Begin by performing checks
C First check is PRF 1 vs. PRF 3
      i=3
      j=1
      isdone=isok(teff,varnc,i,j,ff(2),t13) !Three sigma limit
      if(isdone) then !Second test if first test passed
        i=3
        j=2
        isdone=isok(teff,varnc,i,j,ff(3),t23)
        end if
      if(isdone) then !Executed if both tests passed
        i=3
        j=1
        call doext(teff(i),teff(j),t13,r(i),r(j),rdot(i),rdot(j),
     &    pri(i),pri(j),ff(2),one,r13,pri13) !New extended RRA
        i=2
        j=1 !Use teff, rdot from 2nd of two PRI's used above
        call doext(teff(i),teff(j),t23,r(i),r13,rdot(i),rdot(j),
     &    pri(i),pri13,ff(3),s23,runamb,pritot)
        end if
      return
      end
*
      logical function isok(teff,varnc,i,j,ff,tchk)
*Inputs:
* teff(3)      Effective times of last update
* varnc(3,2)   Variances of position, velocity states
* i            Pointer to first time & variance
```

```
* j           Pointer to second time & variance
* ff          Common factors between PRI i and PRI j
*Outputs:
* tchk        Time at which variance of (Ri - Rj) is minimized
*Returned value:  .TRUE. if (Ri - Rj) is three-sigma within range tolerance
      implicit none
*
      double precision teff(3),varnc(3,2),tchk,t1,t2,v1,v2,
     &  vdot1,vdot2,var,width,varmax
      integer i,j,ff
      double precision dr_clk
      common /dr_clock/ dr_clk
*
      t1=teff(i)
      t2=teff(j)
      v1=varnc(i,1)
      v2=varnc(j,1)
      vdot1=varnc(i,2)
      vdot2=varnc(j,2)
      var=v1+v2+2.*vdot1*vdot2*(t1-t2)**2
      width=ff*dr_clk
      varmax=(width/6.)**2 !Three sigma limit
      if(var.gt.varmax) then
        isok=.FALSE.
      else
        isok=.TRUE.
        tchk=(vdot1*t1+vdot2*t2)/(vdot1+vdot2)
        end if
      return
      end
*
      subroutine doext(te1,te2,tdo,r1,r2,rdot1,rdot2,
     &  priA,priB,ff,s,rout,priout) !New extended RRA
*Inputs, all except first in integer clock ticks:
* te1         Effective time of first r, rdot
* te2         Effective time of second r, rdot
* tdo         Effective time at which range resolve is done
* r1          First range
* r2          Second range
* rdot1       First rdot
* rdot2       Second rdot
* priA        First PRI
* priB        Second PRI
* ff          Prime factors in common between PRIA and PRIB
* s           Magic number
*Outputs:
* rout        Unambiguous range
* priout      Effective PRI of unfolded range using PRIA and PRIB
*NOTES:
* 1.  PRI1>PRI2, no mutual prime factors, are necessary conditions
* 2.  The "magic number" is assumed to be 1; select the PRIs to achieve this
      implicit none
*
      double precision te1,te2,tdo,r1,r2,rdot1,rdot2,rout,r1e,r2e,delta
      integer pria,prib,ff,pri1,pri2,ia2,priout,p12,s
      double precision dr_clk
      common /dr_clock/ dr_clk
*
      pri1=pria/ff !Eliminate common factors in PRIs
      pri2=prib/ff
      r1e=(r1+rdot1*(tdo-te1))/dr_clk !Extrapolate to time "tdo"
      r2e=(r2+rdot2*(tdo-te2))/dr_clk !  and convert to clock cycles
      delta=(r1e-r2e)/(dble(ff)) !Quantize to local clock cycles
      p12=idnint(delta) !Round
```

```
ia2=mod(p12,pri1) !Find (A2*PRI2) mod (PRI1)
if(ia2.lt.0) ia2=ia2+pri1
if(s.ne.1) ia2=mod(s*ia2,pri1) !Magic number, if necessary
rout=r2+ia2*prib*(dr_clk)
priout=pri1*prib
return
end
```

TECHNICAL MEMORANDUM

To: List
From: J. K. Beard
Date: 4 August 1993
Reference: JKB-93-13
Subject: Quadrature Demodulation in Digital Pulse Doppler Radars

1.0 SUMMARY

The interface between the receiver and the signal processor is a quadrature demodulator and a pair of A to D converters, plus associated drivers and buffering hardware. A pulse-Doppler radar will use a variety of waveforms. These waveforms will change every few milliseconds. This data acquisition interface must ether serve for all of the waveforms or change whenever a waveform change demands a different interface.

The focus of this report is definition of a procedure for specification of quadrature demodulators for digital pulse-Doppler radars. These filters are two matched low pass filters. The drivers for these specifications are amplitudes of undesired or spurious signals in the signal processor output. These undesired signals arise from negative frequency images due to I/Q channel mismatch in the quadrature demodulation process, aliasing of out of band signals, and feed-through of undesired mixer outputs. Specifications include passband width, phase and amplitude matching requirements in the passband, stopband attenuation, and minimum stopband frequency.

A methodology is defined here for specifying a quadrature demodulation interface which is the same for all pulse-Doppler waveforms. The methodology is integrated in specification of sample rate for each PRF. Waveforms from low and medium pulse repetition frequencies (PRFs) are oversampled, and the samples in each range gate are summed; this has the effect of allowing the same I.F. bandwidth, quadrature demodulator, and approximate sample rate for all PRFs.

2.0 PROBLEM STATEMENT

In general, pulse-Doppler radars use pulse bursts, or well defined intervals where a burst of identical pulses is transmitted at a constant PRF. The standard pulse-Doppler waveform uses unmodulated pulses at a single frequency. Signal processing consists of a range gated spectrum analyzer. The sequence of operations in the data acquisition, range gating, and spectrum analysis process are:

- **Quadrature demodulation** is performed first. This operation consists of downconversion of signals at the last I.F. to baseband with two mixers using two exciter signals 90 degrees apart in phase.

- **Clean-up filtering** on the mixer outputs serves two purposes. The unwanted mixer

outputs are removed, leaving video signals at baseband, and a band limited signal is made available for sampling by the A to D converter.

- **Sampling and Analog to Digital Conversion** provides digital signals for use in the digital signal processor. The sample rate should provide adequate sampling to the analog signal bandwidth as defined by Nyquist's criteria for complex signals.

- **Digital range gating** demultiplexes received data for each pulse into about 12 channels, each representing data corresponding to a range gate.

- **Summation of samples in each range gate** provides a single complex number as data for each range gate.

- **Spectral window weighting** using Dolph-Chebychev, Kaiser-Bessel, Taylor, or other high performance spectral window weighting provides clutter attenuation in the spectrum analyzer.

- **The FFT** provides an efficient method of applying the spectral window amplitude weighting to produce an array of complex convolution digital filters, each of whose frequency response is a shifted replica of the spectral window frequency response.

The parameters used in each part of this process depend on the parameters of the transmitted signal. A pulse-Doppler radar will use low (Doppler ambiguous), high (range ambiguous) or medium (both range and Doppler ambiguous) PRFs, depending on the needs of the radar in the mission timeline. These waveforms will all be at approximately the maximum rated duty cycle of the transmitter so that maximum average power can be transmitted in all modes. Therefore, the pulse width will be larger and the required I.F. bandwidth will be smaller for lower PRFs. Variations on elementary pulse-Doppler waveforms such as frequency jump burst (FJB) or the use bursts of linear frequency modulated pulses (LFMOP) at low PRF are not specifically addressed here.

The receiver and quadrature demodulator are usually specified and designed to provide for the widest bandwidth transmitted. The quadrature demodulator cleanup filter is matched to the I.F. bandwidth. Lower I.F. bandwidths are effectively accomplished in the digital system by oversampling the pulses at lower PRFs and summing samples taken in each range gate.

3.0 PHASE AND AMPLITUDE MATCHING

The quadrature demodulator consists of two mixers followed by two low pass clean up filters. Exciter signals 90 degrees apart in phase are required for the two mixers. The effects of phase and amplitude mismatch are treated in the literature[1] and are summarized here.

Consider the transfer function at a Doppler shift f_D to be z_I in the in phase or I channel and z_Q in the quadrature or Q channel. The desired outputs of the mixers, e_I and e_Q for a signal of amplitude e_o, are, after the clean up filters,

$$\left.\begin{aligned} e_I &= e_o \cdot (1 + a_I) \cdot \cos(\omega_D t + b_I) \\ e_Q &= e_o \cdot (1 + a_Q) \cdot \sin(\omega_D t + b_Q) \end{aligned}\right\} \quad (1)$$

where the transfer functions z_I and z_Q are characterized as

$$\left.\begin{aligned} z_I &= (1 + a_I) \cdot \exp(jb_I) \\ z_Q &= (1 + a_Q) \cdot \exp(jb_Q). \end{aligned}\right\}$$

The signal to be processed can be characterized as e_P and is given by

$$e_P = \frac{z_I + z_Q}{2} \cdot e_o \cdot \exp(j\omega_D t) + \frac{z_I - z_Q}{2} \cdot e_o \cdot \exp(-j\omega_D t). \quad (3)$$

Note that the desired signal is proportional to $(z_I + z_Q)$ while an undesired negative frequency image is proportional to $(z_I - z_Q)$.

Significant simplification is obtained by treating the amplitude mismatch as a single parameter a and the phase mismatch as a single parameter b. Common errors in the transfer functions are then characterized as system block insertion gain and phase. The transfer functions are then simply

$$\left.\begin{aligned} z_I &= \sqrt{1 + a} \cdot \exp\left(j\frac{b}{2}\right) = z, \\ z_Q &= \frac{1}{\sqrt{1 + a}} \cdot \exp\left(-j\frac{b}{2}\right) = \frac{1}{z}. \end{aligned}\right\} \quad (4)$$

The significant parameter to specify is how far down the negative frequency image relative to the desired signal. This ratio r is

$$r = \frac{z - \frac{1}{z}}{z + \frac{1}{z}} = \frac{z^2 - 1}{z^2 + 1} = \frac{(1 + a)\cdot\exp(jb) - 1}{(1 + a)\cdot\exp(jb) + 1} \approx \frac{a + jb}{2}. \tag{5}$$

Relationships between amplitude mismatch in dB AM and phase mismatch in degrees PM are

$$\left.\begin{aligned} AM &= 20\cdot\log_{10}(1 + a), \quad a = 10^{\frac{AM}{20}} - 1 \\ PM &= \frac{180}{\pi}\cdot b, \quad b = \frac{\pi}{180}\cdot PM. \end{aligned}\right\} \tag{6}$$

A specified level of negative frequency image rejection in dB, S, is related to r by

$$S = -10\cdot\log_{10}(|r|^2). \tag{7}$$

Assuming that amplitude mismatch dominates, S and AM are related by

$$10^{-\frac{S+6}{20}} = 10^{\frac{AM}{20}} - 1 \tag{8}$$

which, with the assumption that AM is small, is well approximated by

$$AM = 17.37\cdot 10^{-\frac{S}{20}} \text{ dB (b negligable), where } \frac{40}{\log_e 10} \approx 17.37 \tag{9}$$

A similar development assuming that phase mismatch dominates leads to

$$PM = 114.6\cdot 10^{-\frac{S}{20}} \text{ degrees (a negligable), where } \frac{360}{\pi} \approx 114. \tag{10}$$

Equation (5) shows that the effects of amplitude and phase mismatch contribute to negative frequency image amplitude by a root sum of squares rule. This fact and Equations (9) and (10) can be used together to develop and evaluate specifications for phase and amplitude matching.

4.0 PASSBAND AND STOPBAND FREQUENCY LIMITS

The low pass filters in the quadrature demodulator perform the functions of suppressing unwanted mixer outputs and providing a bandlimited signal for sampling by the A to D converter. Its performance as an antialiasing filter requires that its stopband begin where unwanted signals would otherwise alias into the processing band after sampling. Its performance in the radar requires that its passband include signals to be processed. Therefore, its passband limit is defined by the pulse bandwidth, and its stopband limit is defined by the sample rate as the lowest frequency for which an out of band signal would alias into the signal band.

Since the pulse bandwidth is proportional to the PRF when the duty cycle is held constant, the driver for the I.F. bandwidth is the pulse width used for the highest PRF. The passband frequency limit is half the I.F. bandwidth. The sample rate at the A to D should exceed the I.F. bandwidth to satisfy the Nyquist criteria.

An important concept in specifying low pass filters is the shape factor. The shape factor SF is the ratio of the lowest stopband frequency f_{ST} to the highest passband frequency f_P,

$$SF = \frac{f_{ST}}{f_P} < 1. \tag{11}$$

For high performance in matching filters in pairs, it is important to keep the shape factor significantly larger than 1. This is particularly important if passband flatness, stopband attenuation, or other requirements add difficulty to the realization of the filters.

Pulse-Doppler radars often base their timing and control (T&C) on a single clock frequency to minimize the number of lines in the equipment. All PRFs and pulse widths are counted down from this clock frequency f_C. If the number of clock counts in the range gate used in PRF i is n_i and the number of samples per range gate is N_i, the sample rate f_{Si} is

$$f_{Si} = \frac{N_i f_C}{n_i}. \tag{12}$$

The criteria for the stopband edge f_{ST} to prevent frequencies in the stopband from aliasing into the processing band is

$$f_{ST} < f_{Si} - \frac{B}{2} \tag{13}$$

where B is the I.F bandwidth as defined by the narrowest pulse width used. Equation (13) links a lower limit on allowable sample rate with an upper limit on f_{ST}.

If only one sample per range gate is used at the highest PRFs, the shape factor of the filters is driven toward 1. If two samples per range gates are used at the highest PRFs, the shape factor is bounded above by 3, leading to more practical filter specifications. This also means that the sample rate is always approximately 2B complex, or about twice that required by the Nyquist criteria for the I.F. bandwidth. This is accomplished by increasing N_i with n_i so that f_s as defined by Equation (12) is held above the limit given by Equation (13) but no higher than necessary. To keep the hardware which provides the sample clock simple, the values of N_i selected for the lower PRF modes is varied.

5.0 STOPBAND ATTENUATION

A requirement for the stopband attenuation can be determined by examining the system frequency response for tones near the transmitted frequency. The stopband attenuation requirements near the point defined by the shape factor is driven by the following factors:

- First, the low pass filters between the mixers used in the quadrature demodulator and the A to D converters are the antialiasing clean-up filters. Any noise or spurious signals which appear at the outputs of the mixers must be dealt with by these filters. A minimum of 20 dB should be used to control the system noise figure. Higher attenuations may be necessary to handle signals introduced by EMI.

- Second, the stopband attenuation has the effect of adding to the adjacent channel selectivity obtained by the last I.F. stage of the receiver. This filter and the I.F. filter working together determine this important system ECCM characteristic.

- Third, and most importantly, this filter is the only major attenuation for unwanted mixer outputs. These unwanted signals appear at the last I.F. frequency and its harmonics, so that the stopband attenuation requirements can be relaxed by using a double balanced mixer to reduce signals at the last I.F. frequency and by raising the last I.F. to make this and the double frequency signals farther from the passband. The total attenuation of these signals should be large enough to make them undetectable, which will require attenuations of over 100 dB at these frequencies. This attenuation can be met by specifying rolloff so that the required attenuations are met at the I.F. frequency and its harmonics.

The system frequency response reveals the place of these filters. Examining the output of the signal processing as a tone is swept slowly across the receiver I.F. bandwidth, the place of the stopband attenuation of the quadrature demodulation filters in adjacent channel rejection is revealed. At the lower PRFs, signals in the I.F. bandwidth are chopped by the range gating process and converted to lines which are ambiguous with target Doppler lines, which can cause false detections. In a system

which uses analog range gating, these unwanted signals are unattenuated unless the receiver I.F. bandwidth varies with the PRF. In the digital range gating system baseline presented here, these lines are attenuated by the summation of samples over a range gate. This is shown as follows.

The summation of N_i samples over the range gate provides a low pass filter response. This is seen from the Z transform representation of the transfer function G(z) of this filter,

$$G(z) = \frac{1 - z^{N_i}}{1 - z}. \tag{14}$$

This filter clearly has zeros uniformly placed around the unit circle at intervals of $2\pi/N_i$ except for $z = 1$. The bandpass of this filter is matched to the pulse width by definition, since it is a block averager over the pulse width. This provides a bandwidth matching function for the system without varying the I.F. bandwith with pulse width in the receiver. This keeps overall system processing gain as high at the lower PRFs as at the highest PRF.

The simple block averager used in summing samples in a range gate serves to attenuate unwanted signals and to provide optimal processing gain at all PRFs. At the expense of a dB or two of processing loss and additional requirements on computational resources, a finite impulse response (FIR) low pass filter can be designed using the Parks and McClellan procedure[2]. This is probably not advisable unless strong rejection of signals which appear in the I.F. bandwith at high PRFs is required at medium or low PRF, or if it is necessary to "square off" the passband to prevent attenuation of high Doppler signals at low PRF.

6.0 CONCLUSIONS

A digital pulse-Doppler data acquisition baseline which uses digital range gating with a sample rate which is held to about the same value for all PRFs is postulated. The number of samples per range gate rises as the PRF decreases and the size of each range gate increases, requiring summation of samples over each range gate. This allows the use of a single receiver I.F. bandwidth while the system bandwidth decreases with PRF due to the low pass filtering effect of the summation over the range gates.

Specifications of phase and amplitude matching in terms of negative frequency image magnitude is treated in Section 3. The tradeoffs and design procedure are well summarized by Equations (9) and (10), with background supplied by Equations (4) and (5).

Specification of stopband attenuation is determined by requirements in rejection of unwanted mixer outputs at the I.F. frequency and its harmonics, and the fact that these low pass filters work with the receiver I.F. filters to achieve total system adjacent channel rejection. Rejection of signals in the receiver I.F. band at medium and low PRFs is discussed in Section 4. Considerations related to unwanted mixer outputs and adjacent channel rejection are discussed in Section 5.

Specification of the passband bandwidth is fairly straightforward, but the stopband edge specification is less obvious. The tradeoffs and design equations are discussed in Section 4. A design procedure is summarized below.

- Define the number of samples per range gate at the highest PRF N_{MIN}. A value of 2 is suggested, although 1 is a viable number with some compromises in adjacent channel rejection.

- Define the I.F. bandwidth by matching it to the narrowest pulse width. For a system clock of f_C and a pulse width countdown of n_{MIN}, the I.F. bandwidth B is

$$B = \frac{f_C}{n_{MIN}}. \tag{15}$$

- Define the sample rate (complex) for the highest PRF f_{SX},

$$f_{SX} = \frac{N_{MIN} \cdot f_C}{n_{MIN}}. \tag{16}$$

- Define the sample rates for the other PRFs f_{Si} to allow for digital range gating and simple countdowns from the master system clock f_C, but keeping the sample rate close to f_{SX} by varying the number of pulses per range gate N_i.

$$f_{Si} = \frac{N_i f_C}{n_i} \approx f_{SX}. \tag{17}$$

- Determine the shape factor SF of the low pass cleanup filters from the minimum sample rate f_{SMIN},

$$SF < \frac{2 \cdot f_{SMIN}}{B} - 1. \tag{18}$$

- Set the passband bandwidth to B/2 and the stopband to SF•B/2.

This process will usually be an iterative design procedure because the shape factor, hardware A to D sampling clock countdown, passband matching specifications, and stopband attenuation requirements all interact. Also, attenuation of high Doppler targets at low or medium PRF by the summation of samples in a range gate should be checked.

7.0 REFERENCES

[1] "Coherent Radar Performance Estimation," James A. Scheer and James L. Kurtz, Editors, Chapter 3: "Effects of I/Q Errors," pp 61-68.

[2] "Theory and Application of Digital Signal Processing," Lawrence R. Rabiner and Bernard Gold, Prentice-Hall (1975) pp 187-204.

6 SRC **TECHNICAL MEMORANDUM**

To: List
From: J. K. Beard
Date: August 20, 1993
Reference: JKB-93-10
Subject: Digital Range Gating in Pulse-Doppler Radars

1.0 SUMMARY

Digital range gating in pulse-Doppler radars provides versatility and programmability without complex analog hardware. In addition, clutter data is available in the digital signal processor. Although dynamic range requirements at the A to D converter are greater than in analog range gated systems using a clutter notch, the current state of the art in A to D technology makes digital range gating a simpler and more practical choice for most new system configurations. This and other design and implementation issues in digital range gating are identified and discussed.

2.0 PROBLEM STATEMENT

Airborne pulse-Doppler systems have used digital range gating for many years. However, ground based pulse-Doppler systems differ in that the ground clutter is much greater, and the Doppler of ground clutter is confined to near zero frequency. Analog range gating allows a clutter notch to be used, so that the higher clutter levels are attenuated prior to the A to D converter. However, complex analog hardware is necessary to support the analog range gate and clutter notch. In particular, the clean-up filter following the analog range gate must have a programmable cutoff frequency to follow significant changes in pulse repetition frequency (PRF).

The analog range gate with clutter notch scheme has one other significant disadvantage relative to digital range gating: the clutter notch filter must be allowed to settle[1]. The clutter attenuation in the digital range gating scheme is in the spectral window used in the FFT. The tradeoff is the use of an analog filter with poles versus the use of a convolution filter (the spectral window) which has no poles. The result is that the digital range gating scheme allows use of a greater portion of the burst for processing.

A difficulty with the digital range gating scheme is that the sample rate, like the analog range gate timing, must be coherent with the PRF so that the ground clutter appears at the same phase and range for every pulse in the burst. If this rule is not strictly followed, the ground clutter will be smeared over the Doppler, reducing the sensitivity of the radar. The relationships determining the sample rate are developed and implementation of sample clock timings are discussed.

3.0 DIGITAL RANGE GATING

3.1 The Analog Range Gate System Concept

A pulse-Doppler radar signal is essentially a burst of pulses, generally at a PRF high enough so that some range ambiguity exists. Ground clutter is received with a resolution consistent with the pulse width. The clutter spectrum therefore has a bandwidth equal to that of the transmitted pulse. Also, the clutter repeats in time at a repetition frequency equal to the PRF, so the clutter spectrum is repeated across the receiver bandwidth at frequency intervals equal to the PRF. These repeated clutter spectra in the receiver bandwidth are called clutter lines. The number of clutter lines in the received spectrum is approximated by one over the duty cycle of the burst.

A processing filter matched to a target would have an impulse response which was a replica of the return pulse, at the same Doppler, but with the time variable reversed. Processing which approximates this matched filter is gating the receiver output synchronously with the PRF, matching the time extent of the returned pulse, followed by a spectrum analyzer which integrates over the time of the burst. This is a gated spectrum analyzer, and is the fundamental pulse-Doppler radar signal processor.

Examining the signal processing scheme in the frequency domain reveals that range gating effectively undersamples the pulse bandwidth, but, since the sample rate is the same as the PRF, all the clutter lines are aliased to the zero frequency clutter line. In addition, analog range gating is a chopping operation, and chopping the receiver output introduces splatter lines which are also periodic in frequency at intervals separated by the PRF. A low pass filter which restricts bandwidth to ½ the PRF will eliminate the splatter while preserving all information which is passed by the range gate. This clean up filter also is an antialiasing filter for the A to D converter which follows. Use of a quadrature demodulator requires that two channels be used, but the ambiguity between positive and negative Doppler shifts is resolved by the relative phase of signals ir the in-phase and quadrature channels.

Following the clean up filter, the power spectrum of a ground based radar is dominated by the ground clutter, which is confined to the region near DC. A high pass filter (called a "roughing filter" in some references) at this point will dramatically reduce the power at this point without significantly affecting the signal. This reduces the headroom required at the A to D converter, so that less bits are necessary. The disadvantage of using a clutter notch is that the high Q low frequency poles of such a filter will ring, and it is necessary to wait for the filter to settle before beginning processing the burst. The clutter notch settling time encroaches on the coherent processing interval (CPI).

3.2 The Digital Range Gate System Concept

When the range gating is done digitally, the output of the quadrature demodulator is sampled. The receiver output is sampled for each pulse in the burst in exactly the same manner. Data that would have been in an analog range gate is sampled at the same point in time, so that range gating can be accomplished exactly as in analog range gating.

The method for accomplishing digital range gating is to store the digitized data in a raster or rectangular matrix format. The data from each pulse in the burst is stored in a row, and each range gate is represented by a column of the matrix. The FFT is done across the columns of the matrix. The data after the FFT is a range-Doppler map. This data buffer is sometimes called a "corner-turning buffer."

The number of samples per range gate is a design parameter. If only one sample per range gate is used, the sample rate is minimized and a workable system concept results. If more than one sample per range gate is used, processing losses are reduced by about 2 dB[2]. A simple presum of two samples per range gate will obtain nearly all gains possible with negligible impact on requirements for processor resources. Other processing options are available, such as overlap or redundancy in range gate processing, which will further reduce processing losses. However, the A to D rate increases in direct proportion to the number of samples per range gate. Of course, signal processor resource requirements are directly proportional to redundancy in range gate processing.

3.3 A to D Clock Timing

It is not a hard requirement is that the sample rate be a multiple of the PRF. However, it is necessary that the timing of the A to D clock be coherent with the clock used to count down the pulse repetition interval (PRI). If the sample rate is not a multiple of the PRF, it is absolutely necessary that the counter for the A to D clock be reset each pulse so that the samples fall in the same timing pattern for each pulse in the burst. The design equations for the A to D clock timing are different for these two cases and are treated separately.

The variables and notation used in the design equations are:

f_C = clock rate

P_i = PRI countdown for PRF number i

p_i = pulse width clock count for PRF number i

N_G = number of samples per range gate

(1)

3.3.1 Sample Rate Not a Multiple of the PRF

In this case, the design equations are very simple. The sample rate is given by

$$f_s = \frac{N_G \cdot f_C}{p_i}. \tag{2}$$

Implementation is simple; a master clock of $N_G \cdot f_C$ is divided by P_i. Since the sample rate is not a multiple of the PRF, the samples will fall on a different place from pulse to pulse unless the A to D clock counter is reset as each pulse is transmitted.

3.3.1 Sample Rate a Multiple of the PRF

Here, we have a little more complex tradeoff. We begin by defining the sample rate as approximately N_G samples counts per p_i clock counts as before,

$$f_S \approx \frac{N_G \cdot f_c}{p_i}, \tag{3}$$

but we adjust the sample rate slightly so that the samples fall on the same place every pulse:

$$f_S = k \cdot f_i, \quad f_i = \frac{f_C}{P_i}. \tag{4}$$

The multiplier k is given by

$$k \approx \frac{N_G \cdot P_i}{p_i}. \tag{5}$$

The simplest way to arrive at k is to round the value given by Equation (5). Then, the sample rate is given by Equation (4).

Implementation generally requires that f_C be multiplied to a much higher master A to D clock than when the A to D clock counter is reset every pulse. This is illustrated by the example given in Table I below. In the table, f_C is 12 MHz, N_G is two, and the duty cycle is held constant by a change in p_i as the PRF changes.

Table I. Sample Clock Examples

P_i	p_i	k	f_S, no reset	f_S, reset
121	9	27	324 MHz/121	24 MHz/9
120	9	27	324 MHz/120	24 MHz/9
118	9	26	312 MHz/118	24 MHz/9
110	8	27	324 MHz/110	24 MHz/8

4.0 CONCLUSIONS

Examining the table, it is clear that the preferable arrangement is to reset the A to D sample clock counter each pulse. If this is not done, the master countdown for the A to D clock will be a large multiple of the master system clock f_C. It is possible use the same k and to avoid generating this high frequency in implementation but, in any case, implementation of the A to D clock is more complex when it is reset only once per burst than when it is reset each pulse.

5.0 REFERENCES

[1] J. K. Beard, "Subclutter Visibility in Pulse-Doppler Radars," SRC Technical Memorandum JKB-92-13A, 21 December 1992.

[2] J. K. Beard, "A 14-Bit A to D Gives a 100 dB Noise Floor in the WFS Signal Processor Upgrade," SRC Technical Memorandum JKB-93-04, April 12, 1993.

TECHNICAL MEMORANDUM

To: List
From: J. K. Beard
Date: August 23, 1993
Reference: JKB-93-11A
Subject: A Doppler Resolve Methodology for Pulse Doppler Radars

1 SUMMARY

A fast method has been found for performing the Doppler resolve function using ambiguous Dopplers from multiple pulse repetition frequencies (PRFs). The method is applicable to pulse repetition intervals (PRIs, the PRI defined as equal to one over the PRF) which, when given in terms of ticks of a single master system clock from which all the PRFs are counted down, share prime factors in common. Requirements on tracker accuracy are relaxed in proportion to the product of prime factors shared between PRIs, so that shared factors are a requirement for practical application for closely spaced PRFs. The method, its derivation, and examples are given in this report. The method given here is adapted from the range resolve methodology reported earlier[1].

2 PROBLEM STATEMENT

2.1 The Doppler Resolve Problem

Pulse-Doppler radars transmit RF energy as bursts of pulses characterized by a pulse type (usually unmodulated, but sometimes a chirp) and a burst duration. If a PRF is too low, target Doppler can be ambiguous. This is because the radar data is sampled at the PRF rate, and the PRF undersamples the target Doppler, aliasing it. The degree of aliasing represents an ambiguity in the target Doppler. This is the Doppler ambiguity problem inherent in the pulse-Doppler radar system concept.

In pulse-Doppler radars, PRFs are loosely categorized as low, medium, or high. Low PRFs are those low enough so that, for the application at hand, range is unambiguous. Medium PRFs are those for which range is ambiguous, but not high enough so that Doppler is unambiguous. High PRFs are those which are high enough that Doppler is unambiguous. Pulse-Doppler radars often use low or medium PRFs for search and acquisition so that target Doppler is ambiguous.

Doppler ambiguities are resolved by chaining PRFs and observing differences in apparent, or ambiguous, target Doppler. If the target Doppler does not change with PRF, the target Doppler is less than half the PRF and is unambiguous. If the target return appears at different Doppler for different PRFs, then the true Dopplers differ from each ambiguous Doppler by integer multiples of the respective PRFs. Doppler ambiguity is resolved by determining these integer multiples.

2.2 System Engineering Tradeoffs

In selecting a set of low or medium PRFs for a pulse-Doppler design, it is important that the PRFs for each class of modes be varied over a significant range so that a target cannot fall into a blind range or Doppler for more than one PRF. Also, Doppler resolve is done early in the track history, so that tracker accuracy is limited to approximately two over the dwell time (one over the dwell time with a factor of two for processing losses).

The dwell time of the radar, for unmodulated pulse train bursts, is approximated by the length used in the bursts, minus a lead time. A wait time of $(2 \bullet R_{MAX}/c)$ is necessary to wait for returns to begin coming in from the longest range targets. Processing begins at the end of this wait time and continues through the end of the burst. This processing time, called the coherent processing interval (CPI), determines the energy on the target during the burst, and the Doppler resolution of the radar is inversely proportional to the CPI.

Tracker performance is determined by range accuracy, Doppler accuracy, and revisit time. The number of dwells between revisit times is the limit of independent targets a phased array may consider independently; this is called the beam occupancy limit. Thus CPI is traded off against the revisit time and the number of simultaneous target tracks.

A single system clock crystal is usually used in pulse-Doppler radars so that receiver design deals only with the tonal lines of one oscillator and its harmonics; this oscillator frequency is usually selected in terms of the minimum display granularity of the system. System clocks of 10 to 15 MHz, corresponding to system granularities of 65 to 100 nanoseconds or 10 to 15 meters, are common. PRIs are selected as integers multiples of the system granularity. This means that design of the Doppler resolve methodology interacts with selection of the system clock frequency. It should be noted that design of a range resolve methodology at high PRF interacts with these same parameters.

In summary, requirements on the range and Doppler resolve designs are determined from the requirements on a phased array radar, posed in terms of maximum range requirements, peak and average power available, and tracker performance requirements. Range and Doppler resolve methodologies are selected within the constraints of number theory, using system clock frequency as a free parameter, to meet system requirements in terms of allowable tracker accuracy, maximum range, the number of independent target tracks, the number of PRFs, the number of range gates, and the system clock frequency.

3 RESOLVING DOPPLER AMBIGUITY

3.1 The Method

The method, as presented here, is applied to two PRFs. Although in most practical cases this use of three PRFs is not required, the method is easily nested to apply it to three or more PRFs. The results of combining the first two PRFs is used as data which is taken as inputs from a virtual PRF which is much lower, and this data is used with data from a third PRF.

The problem statement is: given two pulse repetition intervals (PRIs) in terms of clock counts for a common system clock P_1 and P_2, and ambiguous Dopplers from PRFs corresponding to these PRIs, find the smallest Doppler that would result in these observed ambiguous Dopplers.

As part of the radar mode setup, some offline computations are performed to set up the Doppler resolve methodology. These steps are:

1. Find the prime factors of the two PRIs P_1 and P_2, From these sets of prime factors, find the greatest common multiple (GCM) of P_1 and P_2, F_{12}, and find the mutually prime virtual PRIs $P'_1=P_1/F_{12}$ and $P'_2=P_2/F_{12}$,

2. Define the context granularity as the system clock rate divided by F_{12}, $f'_C = f_C/F_{12}$,

3. Define the "magic number" S_{12} such that $(S_{12} \bullet P'_2) \bmod (P'_1) = 1$.

Real time computations, done as part of the tracker functions when Doppler resolve is to be executed, are:

a. If the range rate is changing significantly between updates, extrapolate the two tracker ambiguous Doppler position states to the same effective time (selected to minimize the variance of $f_1 - f_2$ as used in the next step),

b. Find the difference in the ambiguous Dopplers $f_1 - f_2$, rounded to the nearest number of "context Doppler bins," $(fb_1 - fb_2) = (f_1 - f_2)/df$, where $df = f'_C/(P'_1 \bullet P'_2)$.

c. Find $E = (fb_1 - fb_2) \bmod (P'_2)$; if $E<0$ add P'_2,

d. Find $B_2 = (S_{12} \bullet E) \bmod (P'_2)$ (this step may be skipped if $S_{12} = 1$ because, in this case, $B_2 = E$), and

e. Find the unambiguous Doppler $f_{12} = f_2 + B_2 \bullet P_1 \bullet df$

Note that the tracker accuracy requirement, defined by the rounding in step (b)

above, requires that the difference between two ambiguous Dopplers be accurate within a "bin" of df, and that the maximum unambiguous Doppler ambiguity range is $F_{12} \bullet F_C/(P_1 \bullet P_2)$. This means that F_{12} should be at least $(2 \bullet P_1 \bullet P_2)/(f_C \bullet CPI)$ but less than f_C/f_{MAX}, where f_{MAX} is the total maximum unambiguous target Doppler range. Note that the product $f_C \bullet CPI$ is the CPI in system clock ticks.

In most applications, combinations of PRFs can be found such that S_{12} is 1 for useful PRF combinations. When this is done, step (d) above is redundant with step (c) and is omitted.

Practical application occasionally requires that more than two PRFs be used in resolving Doppler ambiguity. This is done by nesting the method. This process is described in the next section.

3.2 More than Two PRFs

Nearly always, resolution of Doppler ambiguity can be accomplished using two PRFs. However, when necessary, adding PRFs is simple. The process is as follows:

i. Select two PRFs and apply the method as described above, including defining the effective PRI corresponding to the combination of P_1 and P_2, $P_{12} = F_{12} \bullet P'_1 \bullet P'_2$,

ii. Take the Doppler and effective time for f_{12} as those of f_2, so that a complete set of virtual ambiguous Doppler tracker states is defined for the results of combining PRF 1 and PRF 2,

iii. Take the ambiguous Doppler tracker states for PRF 3 and combine it with the virtual tracker states defined for PRFs 1 and 2 and reapply the method.

For the new set of common factors F_{23} is computed from P_{12} and P_3, as is the new "magic number" S_{23}. The value of S_{23} is dependent on the order of the PRFs selected in application of the method, and that some simplification can be achieved if the order of the PRFs is selected such that S_{23} is 1. Examination of the possibilities shows that there are six ways that three PRFs can be combined. All should be examined in development of a methodology to be applied in an actual system.

The minimum value of F that is used throughout the process determines the accuracy requirements on the ambiguous Doppler trackers. Estimates of tracker accuracy available from the track file data should be used to ensure that Doppler ambiguity resolution can be accomplished with high confidence before proceeding. Also, the ambiguous Doppler tracks should be continued and Doppler ambiguity resolution checked for several "hits" to ensure the Doppler ambiguity resolution is accomplished correctly.

3.3 Derivation of the Method

Ambiguous Dopplers from each PRF are, in terms of the true Doppler f, the PRF f_{Pi}, the system clock frequency f_C, and the PRI in system clock ticks P_i,

$$f_i = (f) \bmod (f_{Pi}), \quad f_{Pi} = \frac{f_C}{P_i} \tag{1}$$

which can be restated in terms of products and remainders as

$$\left.\begin{aligned} f &= f_1 + B_1 \cdot f_{P1},\ 0 \le B_1 < P_2, \\ f &= f_2 + B_2 \cdot f_{P2},\ 0 \le B_2 < P_1. \end{aligned}\right\} \tag{2}$$

To simplify the derivation in this section, we are dealing with the situation after the GCM has already been divided out of P_1, P_2, and f_C; this allows the assumption here that the GCM of P_1 and P_2 is 1.

In Equation (2), the integers B_1 and B_2 are unknown. Determination of either B_1 or B_2 resolves the Doppler ambiguity.

Subtracting the two forms given in Equation (2) and rearranging terms gives

$$fc_1 - fc_2 = B_2 \cdot P_1 - B_1 \cdot P_2 \tag{3}$$

where fc_1 and fc_2 are the ambiguous Dopplers given in FFT bins,

$$\left.\begin{aligned} fc_1 &= \frac{f_1}{df}, \\ fc_2 &= \frac{f_2}{df} \end{aligned}\right\} \tag{4}$$

where df is

$$df = \frac{f_C}{P_1 \cdot P_2}. \tag{5}$$

Taking both sides of Equation (3) modulus P_2 gives

$$E = (B_2 \cdot P_1) \bmod (P_2) \tag{6}$$

where the left hand side E is given by

$$E = (fc_1 - fc_2) \bmod (P_2), \text{ if } E < 0 \text{ then add } P_2 \text{ to } E. \tag{7}$$

The Doppler resolve problem has now been reduced to finding B_2 from E in Equation (6). This can be done using number theory as follows. Writing the modulus relationship in Equation (6) in terms of a product and remainder gives

$$B_2 \cdot P_1 = E + k \cdot P_2, \; 0 \le k < P_1. \tag{8}$$

We need to eliminate k in Equation (8), while extracting B_2 from the left hand side. We accomplish this by proceeding as follows. Multiply Equation (8) by an arbitrary integer S,

$$B_2 \cdot P_1 \cdot S = E \cdot S + k \cdot P_2 \cdot S. \tag{9}$$

Taking this result modulus P_2 eliminates k:

$$(B_2 \cdot P_1 \cdot S) \bmod (P_2) = (E \cdot S) \bmod (P_2). \tag{10}$$

To extract B_2 from the left hand side, we only need define S such that

$$(S \cdot P_1) \bmod (P_2) = 1 \tag{11}$$

to allow B_2 to be found as[2]

$$B_2 = (E \cdot S) \bmod (P_2). \tag{12}$$

Since P_1 and P_2 are mutually prime, S always exists and is unique[3]. S can be found

directly from Equation (12) by simply stepping test values from 1 to (P_2 - 1) and testing the modulus.

4 EXAMPLES

Two examples are given here. One is given with medium PRIs poorly selected for Doppler ambiguity resolution, and a slight modification of these same PRIs is given to show well selected PRIs. Both examples use four PRIs spaced over an octave and separated by factors of about $2^{1/4}$. This spacing gives maximum probability that a target will not fall into blind range and Doppler for more than one PRF at a time, a good design criteria for search and acquisition modes.

4.1 PRI counts of 880, 658, 548, and 440

The first PRI is an exact integer multiple of the last PRI; therefore these are not useful in combination. For a system clock of 15 MHz and a center frequency of 10 GHz, the combinations of 548 and 440 or 880 counts have GCMs of 4, corresponding to a tracker tolerance of 7.5 meters per second, which requires an excessive CPI of about 10 milliseconds. Maximum unambiguous Doppler range is excessive. It is obvious from this analysis that this is a very poor selection of PRIs for Doppler ambiguity resolution. A table of magic numbers S is given below as Table I.

Table I. Magic Numbers, First Example

	880	658	548	440
880		83	104	
658	329		5	109
548	53	323		53
440		166	71	

4.2 PRI Counts of 870, 690, 570, and 450

The PRIs have been adjusted to be multiples of 30 clock ticks, and each pair has a GCM of 30. The same system clock and center frequency of 15 MHz and 10 GHz, respectively, give a worst case tracker tolerance of 750 Hz using Equation (5), corresponding to a realizable CPI of 2.7 milliseconds. The maximum unambiguous Dopplers are 7,500 meters per second for any pair of PRFs. These PRIs are more reasonable for Doppler ambiguity resolution. The magic numbers are listed below as Table II.

Table II. Magic Numbers

	870	690	570	450
870		4	2	14
690	24		5	2
570	26	17		4
450	2	20	14	

5 CONCLUSIONS

Resolution of Doppler ambiguity is easily done at low or medium PRF using two PRFs. PRIs must be selected so that, when the number of system clock counts in each PRI is examined, a large GCM exists to allow tracker accuracy requirements to be met with one or two hits. Use of PRIs whose durations in system clock ticks do not contain a large GCM cannot be easily used to resolve Doppler ambiguity using the methods given here.

It may be possible to achieve resolution of Doppler ambiguity with PRI pairs which do not meet the number theory criteria given here by use of slightly different virtual PRIs, and simply accepting the differences in measured ambiguous Dopplers as errors. This possibility was not explored here.

6 REFERENCES

[1] J. K. Beard, "A Range Resolve Methodology for Pulse Doppler Radars," SRC Technical Memo JKB-93-09A, July 30, 1993.

[2] See Appendix A, First Lemma.

[3] See Appendix A, Second Lemma.

A Appendix

The proofs given here are from classical elementary number theory. They are given in this Appendix because they are critical to the method as given in this report, they are not necessarily intuitively obvious to all readers, and because references on number theory are not readily available to the engineering community.

A.1 First Lemma: Nested Modulus

This simple lemma is stated

$$\left.\begin{aligned}(A\cdot B\cdot C) \bmod (D) &= (A\cdot E) \bmod (D),\\ \text{where}\quad E &= (B\cdot C) \bmod (D)\end{aligned}\right\} \qquad \text{(A-1)}$$

where A, B, C, D and E are nonnegative integers and E is less than D. The modulus operation is defined here as a nonnegative remainder. The proof is accomplished by restating the definition of E in terms of a quotient and a remainder,

$$B\cdot C = E + k\cdot D \qquad \text{(A-1)}$$

and substituting the result into the first term of the equation for the triple product:

$$\left.\begin{aligned}(A\cdot B\cdot C) \bmod (D) &= (A\cdot(E + k\cdot D)) \bmod (D)\\ &= (A\cdot E + k\cdot A\cdot D)) \bmod (D)\\ &= (A\cdot E) \bmod (D).\end{aligned}\right\} \qquad \text{(A-1)}$$

This result shows that, given Equation (11) in the report, Equation (12) follows from Equation (10).

A.2 Second Lemma: Unique Existence of Factor with Product Modulus of 1

This more complex result is stated as follows: there exists a unique S such that, when P and Q are mutually prime (i. e., their GCM is 1), then

$$(S\cdot P) \bmod (Q) = 1, \quad 1 < S < Q. \qquad \text{(A-1)}$$

We begin by generalizing the lemma, by making the right hand side a variable and allowing a value of 0 for S:

$$(S\cdot P) \bmod (Q) = M, \quad 0 \le S < Q. \qquad \text{(A-1)}$$

The generalized lemma is stated: given that the GCM of P and Q is 1, then for each M from 0 to Q-1 there exists a unique S which satisfies Equation (A-5). This is equivalent to a fundamental premise in number theory: that every nonnegative N less than P•Q is uniquely defined by the digits a_1 and a_2 or b_1 and b_2, and that N is returned by the relationships

$$\left.\begin{aligned} N &= a_1 + a_2 \cdot P = b_1 + b_2 \cdot Q, \\ 0 \le a_1 &< P, \quad 0 \le a_2 < Q, \\ 0 \le b_1 &< Q, \quad 0 \le b_2 < P. \end{aligned}\right\} \qquad \text{(A-1)}$$

This fundamental theorem is the root of the Chinese Remainder Theorem. The equivalence to Equation (A-5) is seen by taking (b_1 - a_1) as M, a_2 as S, and taking the equation returning N modulo Q.

The generalized lemma is proved by showing that there are Q distinct values of both S and M. We begin by showing the uniqueness of M for each Q by assuming a contradiction and reducing the contradiction to absurdity. Since Equation (A-5) is a defined arithmetic action (i. e., a nonnegative remainder) then for every S there exists at least one M. Suppose that both M_1 and M_2 satisfy Equation (A-5) for the same S. Then,

$$\left.\begin{aligned} (S \cdot P) \bmod (Q) &= M_1, \\ (S \cdot P) \bmod (Q) &= M_2. \end{aligned}\right\} \qquad \text{(A-1)}$$

Subtracting these two equations shows that

$$M_1 = M_2 = M. \qquad \text{(A-1)}$$

This proves that M is unique for each S. Since there are Q values of S, there are Q values of M (if each value of M is generated by only one value of Q), and that is all of them, since no two are the same. All that remains is to show that each value of M is generated by only one value of Q. We show this, again using reduction to absurdity. If a single value of M is generated by two distinct values of S,

$$\left.\begin{aligned}(S_1 \cdot P) \bmod (Q) &= M \\ (S_2 \cdot P) \bmod (Q) &= M\end{aligned}\right\} \qquad \text{(A-1)}$$

then the difference between these equations shows that

$$((S_1 - S_2) \cdot P) \bmod (Q) = 0, \quad -Q < S_1 - S_2 < Q. \qquad \text{(A-1)}$$

Without loss of generality, we can restate Equation (A-10) as

$$((\Delta S \cdot P) \bmod Q) = 0, \quad 0 < \Delta S < Q \qquad \text{(A-1)}$$

because the value of 0 for ΔS is the one showing $S_1 = S_2$, and reversing the order of the subtraction makes the equation identical for positive and negative values of ΔS. This equation can never hold for ΔS in bounds when the GCM of P and Q is 1, because ΔS•P can never contain all the prime factors of Q so long as ΔS is less than Q. Therefore, for every M there exists a unique value of S which generates M according to Equation (A-5). Therefore, for any S there is a unique M, and for any M there is a unique S. If P and Q had a GCM C greater than one,

$$\left.\begin{aligned}P &= P' \cdot C \\ Q &= Q' \cdot C\end{aligned}\right\} \qquad \text{(A-1)}$$

then there would be only Q' values of M, which would repeat as S increased from 0 to Q - 1; this can be seen by substituting Equation (A-12) into Equation (A-11) because a value of ΔS equal to any multiple of Q' would satisfy Equation (A-11). Therefore, it is necessary that P and Q be mutually prime for S to be unique for each M.

The original lemma is the particular case where M is 1. This case always exists because all Q values of M are represented, and one of them is necessarily 1. The value of 0 for S is excluded in Equation (A-5) because M is always 0 when S is zero. Since a unique S always exists, then the use of Equation (11) in the derivation of the Doppler resolve methodology is legitimate.

TECHNICAL MEMORANDUM

To: List
From: J. K. Beard
Date: 2 September 1993
Reference: JKB-93-12
Subject: Sample Jitter and Skew in Digital Pulse Doppler Radars

1.0 SUMMARY

A digital pulse-Doppler radar does not use analog range gates, but samples the I.F. output directly. The sample rate clock is synchronous with the range gating, so that range gating is performed by demultiplexing the A to D output. As such, the bandwidth at the A to D is much higher in a digital system than in an analog system. Therefore, the sampling jitter and skew requirements are more stringent than in an analog system.

The A to D sampling aperture jitter requirement is examined in terms of a dynamic range specification. A numerical example relevant to WFS is used to show that the A to D jitter requirement is consistent with performances guaranteed for most COTS video A to Ds.

Skew in sample clock between the sum channel and the difference channels will result in errors in the monopulse ratio. The sample skew requirement is examined in terms of specification of the quality of the monopulse ratio. A numerical example relevant to WFS reveals that the sample skew requirement is on the order of 35 picoseconds, which is achievable with care in design and layout of the clock drivers and clock routing in the data acquisition subsystem.

2.0 PROBLEM STATEMENT

In analog pulse-Doppler radars, the I.F. signal is range gated. A filter is used to clean up the outputs of the range gates which has a bandwidth of approximately half the PRF. This is the signal which is digitized when digital spectrum analyzers are used. In digital pulse-Doppler radars, the I.F. signal is digitized, so that the bandwidth of the signal at the A to D is the pulse bandwidth. This bandwidth is higher than that of the analog cleanup filters by a factor of one over the duty cycle of the pulse-Doppler burst, or about an order of magnitude.

The A to D sampling aperture jitter generates noise in proportion to the average slope of the signal at the A to D input. Because of the higher bandwidth at the input of the A to D, the sampling aperture jitter is more likely to be part of the system dynamic range budget than in analog systems. Also, error due to sampling skew between monopulse channels is proportional to bandwidth at the A to D.

3.0 SAMPLE APERTURE JITTER REQUIREMENTS

Jitter in the sampling aperture maps into additive noise. This can be seen by examining the data samples from a sine wave of amplitude e_o, angular frequency ω_s, and RMS aperture jitter σ_C:

$$s_i = e_o \cdot \cos(\omega_s \cdot (t_i + \sigma_C \cdot n_{ci}) + \phi) \tag{1}$$

where t_i is the sample time for sample i, n_c is instance i of a Gaussian random variable (zero mean, unit variance), and ϕ is a uniformly distributed random phase. What happens is that when the sample happens on the slope of the sine wave, the timing jitter maps into voltage in s_i in proportion to the slope at that point. We can analyze this effect by looking at the differential. Defining the ideal sample s_{oi} as a sample identical to s_i but having no jitter, the differential is

$$\delta_i = s_{oi} - s_i = -2 \cdot e_o \cdot \sin(\omega_s \cdot (t_i + \frac{\sigma_c}{2} \cdot n_{ci}) + \phi) \cdot \sin(\frac{\omega_s \cdot \sigma_c}{2} \cdot n_{ci}). \tag{2}$$

If the aperture jitter is small compared to a cycle of signal at frequency ω_s, then the differential is well approximated as

$$\delta_i \approx -e_o \cdot \omega_s \cdot \sigma_c \cdot n_{ci} \cdot \sin(\omega_s \cdot (t_i + \frac{\sigma_c}{2} \cdot n_{ci}) + \phi) \tag{3}$$

and its variance, taking an ensemble over both i and ϕ, is

$$\sigma_{si}^2 = \frac{1}{2}(e_o \cdot \omega_s \cdot \sigma_c)^2. \tag{4}$$

We can now write the ratio of the RMS signal level to the RMS noise floor for aperture this case as

$$SNR = -20 \cdot \log_{10}(\omega_s \cdot \sigma_c), \tag{5}$$

a nice simple result. This number compares with the broadband SNR specification of an A to D converter. For comparison of noise level in a 1 Hz band, the SNR is increased by 10 log of the sampled bandwidth. This is the complex sample rate for quadrature demodulated signals or half the sample rate for real sampled data.

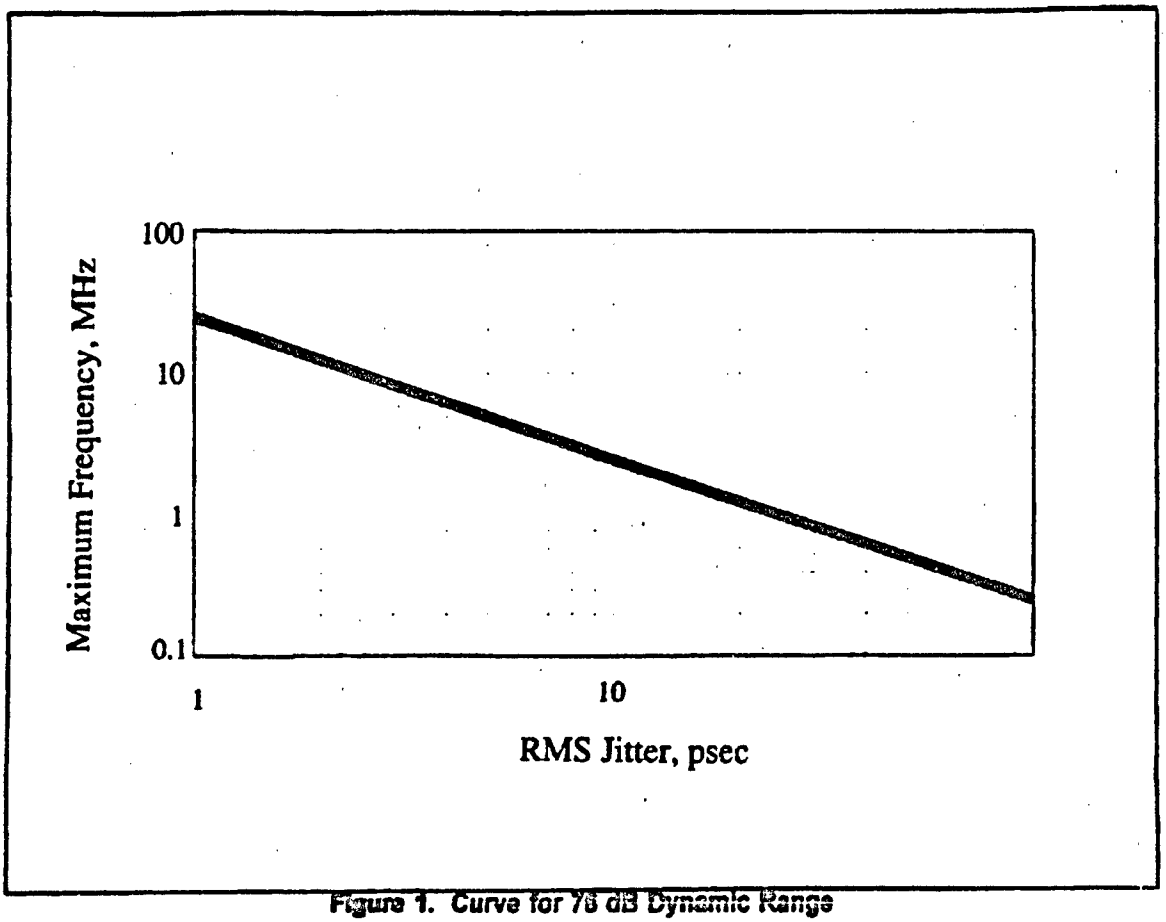

Figure 1. Curve for 76 dB Dynamic Range

For WFS, we might say that the dynamic range at the A to D must be 76 dB to support a 100 dB dynamic range in a 512 point FFT bin, allowing for 3 dB window weighting loss. A curve of the maximum frequency full amplitude sine wave versus the RMS A to D aperture jitter is shown as Figure 1. As can be seen from the plot, aperture jitters of 10 to 20 picoseconds are allowable; this is consistent with performance of the track-and-hold modules associated with commercially available A to D converters for sample rates over 1 MHz and resolutions greater than 12 bits.

4.0 SKEW BETWEEN MONOPULSE CHANNELS

4.1 Description of Phase Monopulse

In order to provide a basis for analysis, a quick derivation of a phase monopulse target angle measurement is given here. The signals at the output of two adjacent array segments with phase centers separated by distance d, from a signal at angle θ toward array segemtn 1 from boresight, are the real parts of

$$\left.\begin{aligned} e_1 &= e_o \cdot \exp(-j \cdot (\omega \cdot t + k \cdot (x + \tfrac{d}{2} \cdot \sin\theta) - \phi)) \\ e_2 &= e_o \cdot \exp(-j \cdot (\omega \cdot t + k \cdot (x - \tfrac{d}{2} \cdot \sin\theta) + \phi)) \end{aligned}\right\} \quad (6)$$

where k is the wavenumber,

$$k \triangleq \frac{2\pi}{\lambda} = \frac{\omega}{c}. \quad (7)$$

The sum and difference channels are given by

$$\left.\begin{aligned} S &= e_1 + e_2 = 2 \cdot e_o \cdot \exp(-j \cdot (\omega \cdot t + k \cdot x + \phi)) \cdot \cos(\tfrac{k \cdot d}{2} \cdot \sin\theta) \\ D &= e_1 - e_2 = -2j \cdot e_o \cdot \exp(-j \cdot (\omega \cdot t + k \cdot x + \phi)) \cdot \sin(\tfrac{k \cdot d}{2} \cdot \sin\theta). \end{aligned}\right\} \quad (8)$$

We know that the the receiver affects these signals primarily by shifting frequency. So, we can represent the output of the quadrature demodulators by the same equations, but ω represents the angular frequency of the Doppler shift, not the RF frequency as at the horns. In addition, we can consider the complex numbers because quadrrature demodulation has been used. With this understanding, the monopulse ratio is

$$\frac{D}{S} = -j \cdot \tan(\tfrac{k \cdot d}{2} \cdot \sin\theta). \quad (9)$$

4.2 Sampling Skew between Monopulse Channels

The signal presented to the A to D converter is a quadrature demodulated video signal. The signal is the return pulse, downconverted to DC so that its center frequency is the target Doppler shift. Its envelope is the pulse shape. Since the pulse duration is nearly always short compared to a period of maximum Doppler (i.e., the pulse bandwidth is much higher than the Doppler shift) then the phase changes little during each pulse period as it is received. Therefore, the principal errors in skew between sum and difference channels is in amplitude due to sampling the pulse envelope at different times.

A Gaussian pulse whose bandwidth B is defined as the two-sigma extent of its Fourier transform has the form

$$p(t) = e_o \cdot \exp(-\tfrac{(\pi \cdot B \cdot t)^2}{2}) \quad (10)$$

and its maximum slope is

$$p'_{MAX} = p'(\frac{1}{\pi \cdot B}) = e_o \cdot \pi \cdot B \cdot \exp(-\frac{1}{2}) \approx 1.9 \cdot e_o \cdot B. \quad (11)$$

This shows that, for a skew of T_{SKEW}, a monopulse error of 0.1 degrees or less maps to the restriction

$$T_{SKEW} < \frac{1}{1092 \cdot B} \quad (12)$$

or, for a bandwidth of 1.5 MHz, T_{SKEW} must be less than 600 picoseconds.

Target Doppler maps 0.1 degrees of monopulse error to the restriction

$$T_{SKEW} < \frac{1}{3600 \cdot f_{DOPPLER}} \quad (13)$$

which is 72 milliseconds for 50 KHz of Doppler shift.

4.3 Sampling Skew between I and Q Channels

Skew between sampling of the I and Q channels of the quadrature demodulator will cause amplitude and phase mismatch which results in negative frequency images of targets. This effect is similar to target images caused by phase and amplitude mismatch in quadrature demodulators. The same analysis given above holds, except that 0.1 degrees of monopulse error maps to a negative frequency image of 55 dB. Therefore, approximately the same skew restrictions apply to skew in sample clocks for quadrature demodulators.

5.0 CONCLUSIONS

The RMS track-and-hold jitter requirement for digital pulse-Doppler radar data acquisition is on the order of 12 picoseconds when clutter attenuation of about 100 dB is required. This is effectively used up by the A to D itself. The clock signal itself should have an RMS phase jitter smaller than 10 picoseconds.

Sampling skew can cause errors in monopulse angle measurement and cause negative frequency images in quadrature demodulators by contributing to amplitude and phase mismatch between the I and Q channels. Skew errors should be kept under 500 picoseconds. This much error can be caused about 4 inches of cable length mismatch.

TECHNICAL MEMO

To: Whom It May Concern
From: Michael L. Emry
Date: 18 May 1993
Reference:
Subject: A/D Testing and Characterization

1.0 INTRODUCTION

This document describes the procedures that will be used to test and record the characteristics of each of the Pentek 4261A 10 MHz, A/D Converters that are a part of the A/D Converters Subsystem of the Waveform Simulation Upgrade project. The complete set of static and dynamic tests will verify that the A/D has been correctly offset, show system harmonics, and determine the following specifications:

SNR	Signal to Noise Ratio
Meff	Effective Numberof Bits
SINAD	Signal to Noise and Distortion
SFDR	Spurious Free Dynamic Range
DLE	Differential Linear Error
THD	Total Harmonic Distortion

2.0 EQUIPMENT LIST

Fluke 6082A Synthesized RF Signal Generator
HP 8656B Signal Generator .1 - 999 MHz
Wavetek 12 MHz Synthesized Function Generator model 23
Kepco Power Supply
2 9th Order Chebyshev .1 dB Low Pass Filters (custom made)
Sinewave to TTL Clock Circuit (custom made)
50 Ohm Termination Load
Mini Circuits ZFSC-2-1 signal combiner
Personal Computer with MATLAB and File Transfer Protocol (FTP) Capabilities

3.0 TEST SETUP

The Fluke 6082A Synthesized RF Signal Generator will be used to generate the external sampling clock for the A/D board. The Fluke 6082A will be set at the sampling frequency of 2 MHz which is consistent with the sampling rate of the Waveform Simulation Upgrade System. The output of the signal generator will run through the Sinewave to TTL Clock Circuit to create a 2 MHz TTL level clock that can be connected to the A/D external clock

input. The TTL clock needs to be connected to the A/D with a 50 Ohm termination load using a T connection at the A/D external clock input.

Software written for the A/D Converters Subsystem allows output data from the A/D's to be dumped to the screen or stored in a binary file. Data written to output files can be downloaded to a PC over ethernet using File Transfer Protocol Software. The file can then be processed using MATLAB. All Discrete Fourier Transforms used in these tests will be 1024 point FFT's processed on MATLAB.

In determining the value of the input frequency used in the tests, there were several factors that came into play. First the input frequency needed to be within the 1 MHz bandwidth used in the WFS project. Secondly this frequency needed to be as fast as possible to produce the worst case harmonics but remain below the Nyquist rate of the sampling clock (Nyquist rate is 1 MHz for this case). Finally in order to reduce the effects of spectral leakage as much as possible, the input frequency needed to be phaselocked to the sampling frequency. This required that the input frequency, (Fin = (m * Fs) / N). N represents the number of points in the FFT, already determined to be 1024. Fs represents the sampling frequency of 2 MHz and m is an integer. The input frequency, Fin was calculated for m = 500 and is equal to 976.563 kHz.

4.0 TEST PROCEDURE

1) System Harmonics

Terminate the input signal to the A/D with a 50 Ohm load. Verify that the offset of the A/D has been adjusted properly so that the A/D output is correct for 0 V. If the offset is not adjusted properly, the A/D should be tuned for an output of 0 V. Once the A/D board is properly tuned, collect data and run an FFT on the data. The frequency domain data will show any miscellaneous system harmonics that are present on the A/D chip.

2) Signal to Noise Ratio
Effective Number of Bits

Using the Kepco Power Supply, inject the minimum level DC signal (approximately -1 V) and collect data. An averaging of the data collected will give the noise floor of the A/D. Repeat the test using a maximum level DC signal (approximately +1 V) to calculate the upper bound of the A/D. From the difference of these values the Signal to Noise Ratio can be determined. The Effective Number of Bits (Meff) can then be calculated from the Signal to Noise Ratio using the formula Meff = (SNR - 1.76) / 6.02.

3) Signal to Noise and Distortion

Spurious Free Dynamic Range

This test will require combining 2 sinewaves and adjusting their amplitudes for a combined input amplitude at the maximum level of approximately 2 Vpp. One sinewave will be generated with a frequency of Fin = 976.563 kHz (m = 500) using the HP 8656B Signal Generator and the second sinewave will be generated with a frequency of 966.797 kHz (m = 495) using the Wavetek 12 MHz Synthesized Function Generator. Each signal will be filtered through an 8th order .1 dB Chebyshev Low Pass Filter to remove harmonics. Inject the combined signal into the A/D, collect data, and run an FFT on the data. The data will show the Signal to Noise and Distortion (SINAD) value. Reduce the amplitudes of the input sinewaves until the spurs are lost in the noise floor. Collect data and run an FFT on the data. Measure the Spurious Free Dynamic Range (SFDR).

4) Differential Linearity Error

Using the HP 8656B Signal Generator inject a sinewave with a frequency of 976.563 kHz (m = 500) and with the maximum level amplitude of approximately 2 Vpp, collect as many samples of data as possible. This will be approximately 1.5 million samples. Create a histogram of the output data with the vertical axis representing analog amplitude and the horizontal amplitude representing the 16384 possible codes from 14-bit conversion. Analyzing the histogram and comparing to the standard parabolic distribution will determine missing states and Differential Linearity Error (DLE).

5) Total Harmonic Distortion

Using the HP 8656B Signal Generator inject a sinewave with a frequency of 976.563 kHz (m = 500) and with the maximum level amplitude of approximately 2 Vpp, collect data and run an FFT on the data. Find the values of the first five harmonics and calculate their magnitude. This will be the value of the Total Harmonic Distortion (THD).

5.0 REFERENCES

[1] Michael W. Johnson, "Test High Speed, High-Resolution A-D Converters", Design Applications, May 10, 1990 pp 95-100.

[2] Robert E. Leonard Jr., "Data Converters: Getting to Know Dynamic Specs", Design Applications, November 8, 1990 pp 89-04.

[3] James L. Kurtz and Robert G. Pauley, "Radar Component and Subsystem Tests", Coherent Radar Performance Estimates, Chapter 15, 1993.

TECHNICAL MEMO

To: List
From: J.K. Beard
Date: 12 August 1992
Reference: JKB-92-08
Subject: A Beam Steering Controller Concept for Phased Arrays

1. SUMMARY

Phased arrays, or electrically steered arrays (ESA's) are used in high-performance tracking radars. The ability to steer the transmit and receive beams electrically allows these radars to track several targets at once without moving the array. An ESA is made up of an RF feed and a large number of phase shifters. On the order of 10,000 phase shifters must be used in an ESA that has a 1° pencil beam and steers over a 60° cone.

A major system problem in operating ESA's is meeting the requirement of driving all the phase shifters. The 10,000 phase shift computations must be accomplished as part of preparing to resteer the beam. A simple methodology is presented here for accomplishing this with three multiplications and two additions per ESA element. The methodology can be cascaded, allowing it to be used for subarrays. The methodology is also adaptable to multiple parallel processors, so that the computation can be done using multiple processors in the beam steering computer or even at the element level.

2. PROBLEM STATEMENT

A beamformer adds the signals received from all the ESA elements. The basic problem of steering the beam in a given direction is finding the phase shift for each element such that of the signal from a given element in phase with the signals from the other elements, performing the necessary computations, and driving the phase shifters to implement the phase shifts.

3. SYSTEM CONCEPT

3.1 Methodology

We will use vector notation because this results in a very simple final result. Consider an ESA with a phase center $\underline{x}_0$. The phase center is the point in space that represents the virtual position of the ESA as an RF reception sensor. For each element i, at position $\underline{x}_i$, we want to determine the phase shift ϕ_i that will put the signal received at that element in phase with the signals from all the other elements. We do this by putting all the elements in phase with a virtual element the array phase center at position $\underline{x}_0$.

The phase shift is found in terms of the difference in path length d_i between an element at position $\underline{x}_i$ and at position $\underline{x}_0$. If a unit pointing vector in the direction of the beam boresight is denoted by $\underline{u}$, then, the vector between positions $\underline{x}_0$ and $\underline{x}_i$ is $(\underline{x}_i - \underline{x}_0)$. The difference in wave propagation path length along $\underline{u}$, d_i, is given by the dot product of the vectors $\underline{u}$ and $(\underline{x}_i - \underline{x}_0)$,

$$(1) \qquad d_i = (\underline{x}_i - \underline{x}_0) \bullet \underline{u}.$$

This relationship is well known [1, p. 11-15] [2, p. 20-16]. Given the differential path length that the phase shifter must account for, we convert to phase by multiplying by the wavenumber:

$$(2) \qquad \phi_i = \frac{2\pi d_i}{\lambda}; \qquad \text{where } \lambda \text{ is the wavelength.}$$

3.2 Spherical Correction

A corporate feed that supplies a planar wave forms an unsteered beam. Applying the phase shifts given by Equation (2) will steer the beam in the direction of the pointing vector $\underline{u}$. However, when an array is fed from a single horn some distance from the array, the phase shifters must deal with a spherical wave and form a beam, as well as steer the beam. These

arrays are aptly called ESA lenses. The correction for the spherical wave is fixed and is simply added to the phase used to steer the beam.

3.3 Temperature Compensation

The accuracy of phase shifters depends on compensating for insertion phase, temperature, frequency, and other factors. Compensation for insertion phase, temperature and frequency is done by correcting ϕ_i, usually by means of a **lookup table** and **interpolation**. Usually, a lookup table is fixed for a given frequency and the temperature is determined by a sensor local to the phase shifter element. This compensation for insertion phase and temperature is sometimes done at the phase shifter element driver, not in the beam steering controller. Different lookup tables are used at different frequencies.

3.4 Binary Phase Shifters

Some ferrite phase shifters are analog in nature. However, most phase shifters are binary, having on-off phase shifts of about 180°, 90°, 45°, 22.5°, etc. The most significant bit nearly always corresponds to 180°. Usually three to five bits of accuracy are used, with four bits being the typical case. The bits for the phase shifter are found by the most significant bits in the fractional part of the quantity $\phi_i/(2\pi)$.

3.5 Subarrays

Most ESA's are built as a collection of subarrays. When the transmitter and receiver are segmented into the subarrays, an opportunity arises to phase correct the phase centers of the subarrays to the conglomerate array phase center. When true time delay binary phase correction is used, all the significant bits of $\phi_i/(2\pi)$ must be used; this approach minimizes pulse edge transients for steered beams and increases the instantaneous bandwidth of the ESA.

4. SUMMARY

4.1 The Phase Shift

An ESA is steered in the direction of a unit pointing vector $\underline{u}$ by phasing the output of the elements before summing in the beamformer. The data flow for implementing this phasing operation for an ESA can be implemented by computing the phase shift in revolutions ψ_i, for each element i:

$$(3) \qquad \psi_i = \frac{(\underline{x}_i - \underline{x}_0) \bullet \underline{u}}{\lambda}.$$

The factor of $1/\lambda$ can be absorbed into $\underline{u}$ as transmitted to the beam steering controller as part of the beam steering command. The phase center $\underline{x}_0$ can be removed from the equation by making $\underline{x}_0$ the origin of the coordinate system in which $\underline{x}_i$ is expressed. This reduces implementation of Equation (3) to a simple dot product, which is three multiplications and two additions.

4.2 Compensation for Spherical Waves, Insertion Phase, Temperature, and Frequency

Spherical correction, insertion phase and temperature compensation can be accomplished by means of a single lookup table. Only the significant bits of ψ_i need be used in the lookup table. When true time delay is not used, only the bits below the binary point are significant. Interpolation can be done using the first few bits of ψ_i and interrogating the lookup table ROM for this value and its increment, then interpolating by using the bits of ψ_i not used in the lookup operation.

Frequency compensation can be implemented by using a separate temperature compensation lookup table for each frequency. If finer resolution is necessary, a lookup table can be used for frequency compensation that is identical to the scheme used for temperature compensation.

4.3 Computing the Phase Shifts and Driving the Phase Shifters

Tradeoffs exist in where the phase shift is computed. The concept presented here is consistent with values of μ/λ being broadcast to the phase shifter drivers at the element level, or the beam steering controller can perform all computations and send phase shifter bits to the elements, or anywhere in between.

5. REFERENCES

[1] "Radar Handbook", Merrill Skolnik, ed., McGraw-Hill (1970)

[2] "Antenna Engineering Handbook," Second Edition, Richards C. Johnson and Henry Jasik, Eds., McGraw-Hill (1984).

JKB-93-01

TECHNICAL MEMO

To: List
Date: 12 August 1992
Subject: An Analysis Model for ESA Point Designs

From: J.K. Beard
Reference: JKB-92-08

1.0 SUMMARY

Attached is a report on an analysis model for prediction of patterns for electrically steered arrays (ESAs). The model produces two dimensional beam patterns in sine space, given element positions and amplitude weightings. If desired, the model will apply a single element pattern which applies to all elements. Element positions are parameterized as positions on a fixed planar rectangular grid; this allows modeling of triangular grids. Modeling of sparse arrays is implicit in the model. The model is also capable of modeling perturbations due to phase shifter errors and weighting errors.

The use of sine space to produce the beam pattern allows a single model run to produce a pattern which applies to all steered beams. This is because beam steering in sine space is a simple translation of the pattern, and the beam pattern is mapped from a unit circle centered on the physical (unsteered) boresight of the antenna. Therefore, the effects of steering can be examined by moving a unit circle around on the pattern and observing the lobes which enter the unit circle. The element pattern moves with the unit circle and is applied multiplicatively on the array pattern.

2.0 EXAMPLE

To test the model, a 0.7 m circular array with equilateral element spacing of 1 wavelength was run with the program. The frequency was 10 GHz and the array had 990 elements.

2.1 RESULTS OF MODEL

The plot in figure B-1 is a unshaded circular aperture. This array uses four bit phase shifters with 0.5 degree 1-σ random insertion phase. The array errors plotted in linear amplitude are shown in figure B-2.

Next an amplitude weighting was applied to the array. Amplitude weighting of the form $(1-(r/radius)^2)^2$ was used. The resultant plot is shown in figure B-3.

The same array was thinned using stochastic thinning. The number of active elements used was 374. Figure B-4 is the plot of combined amplitude weighting and stochastic thinning. Finally, Bickmore-Spellmire Weighting was applied to array. Figure B-5 is the resultant output.

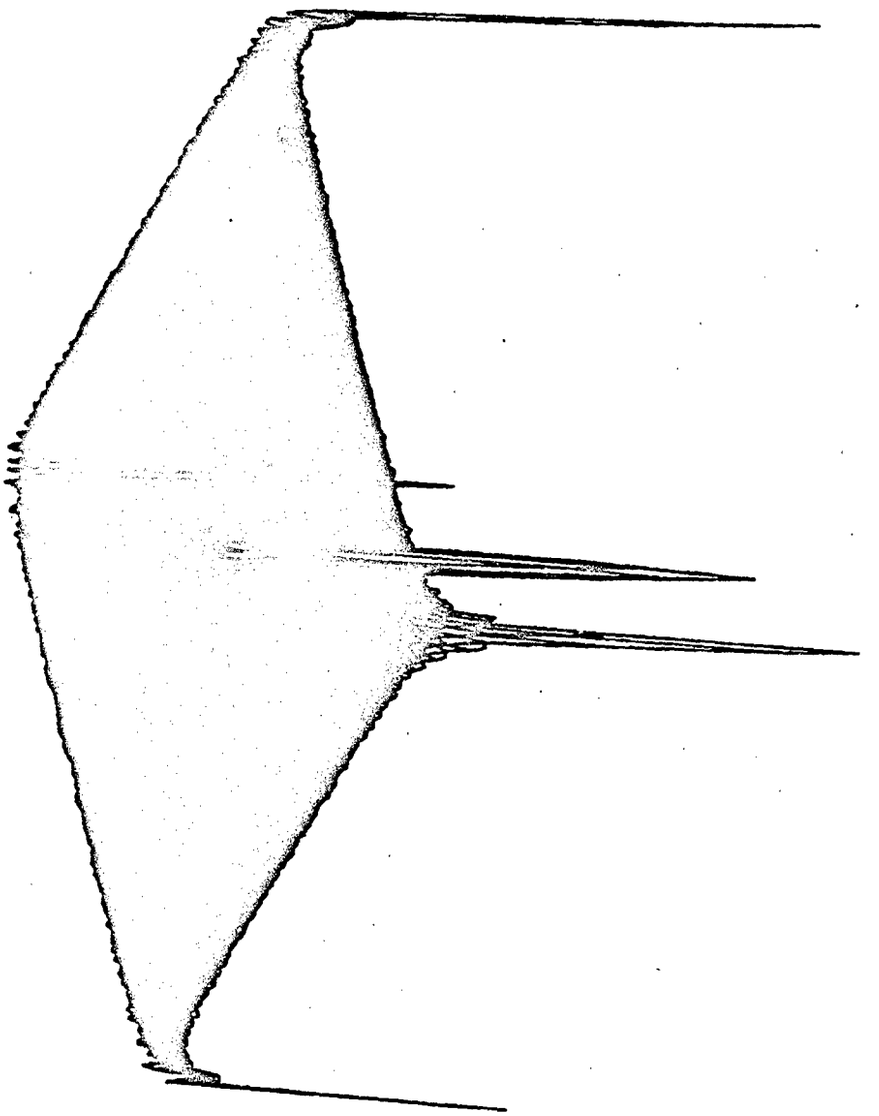

Fig. B-1 Unshaded Circular Aperture.

Fig. B-2 Array Errors.

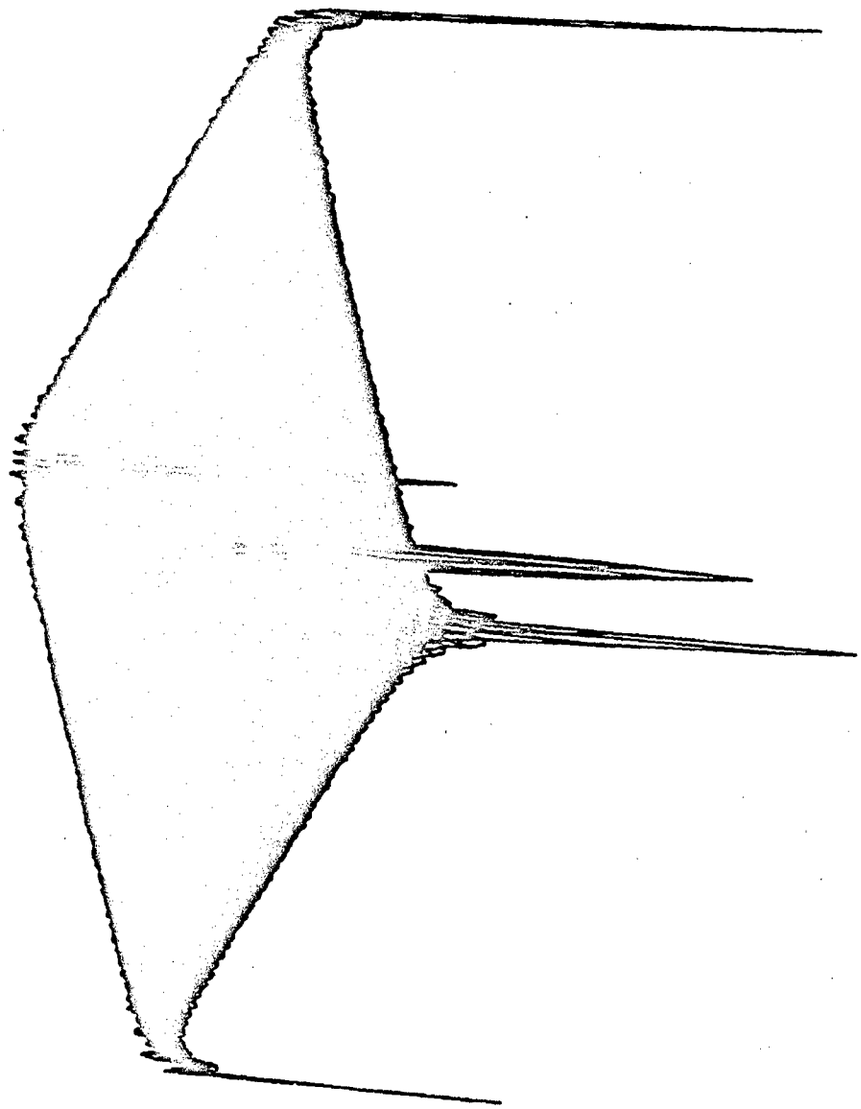

Fig. B-3 $(1-(r/radius)^2)^2$ Weighting.

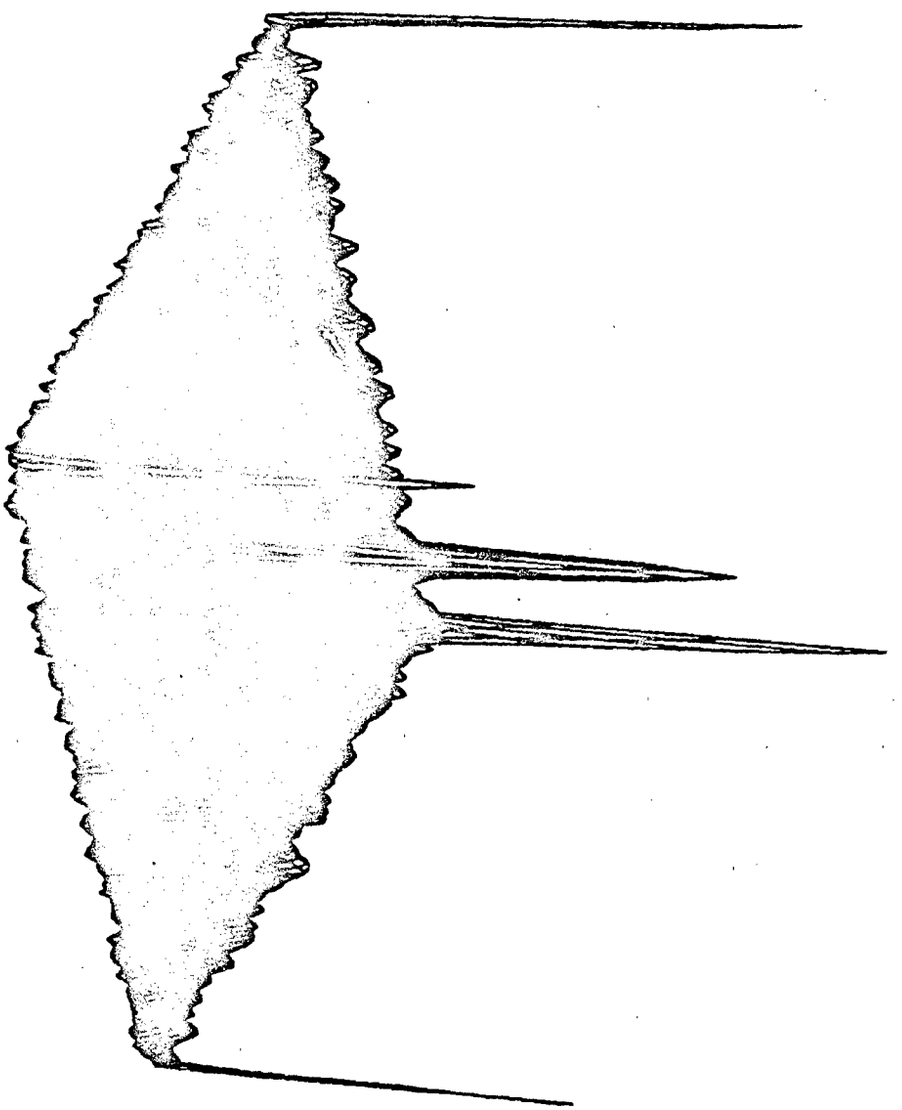

Fig. B-4 Shaded Array With Stochastic Thinning.

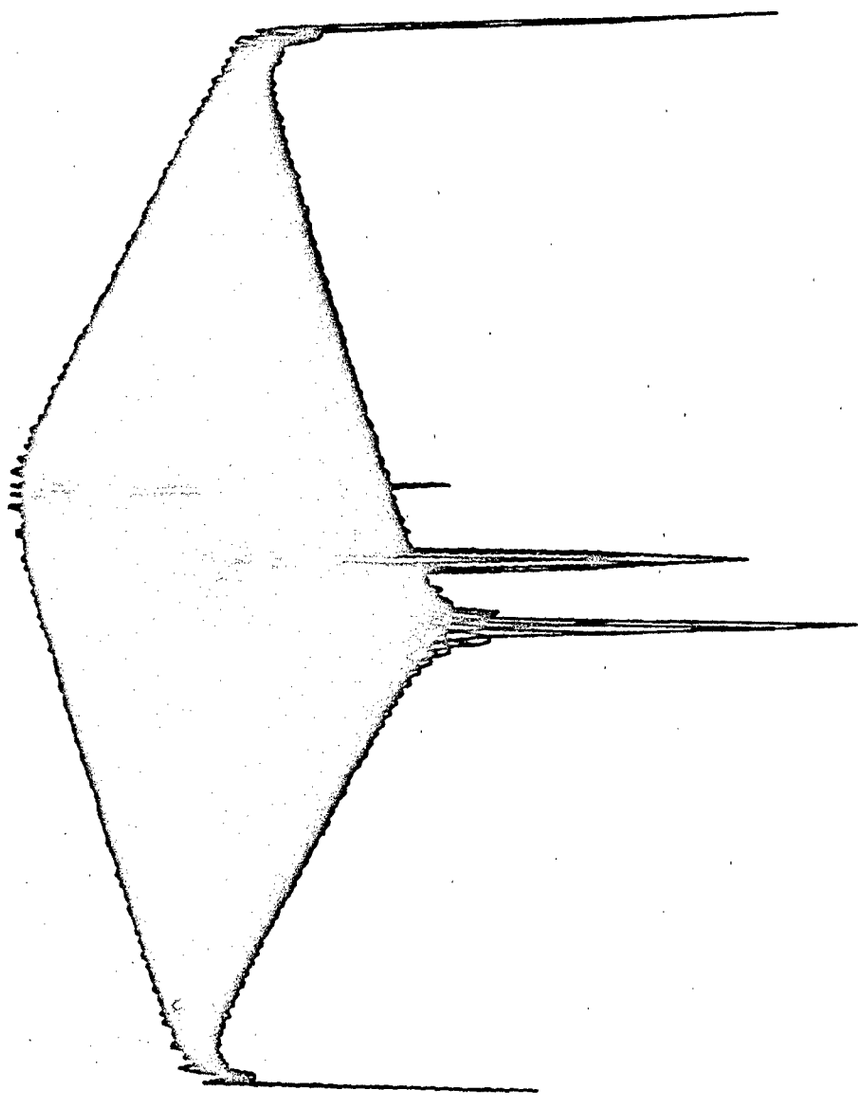

Fig. B-5 Bickmore-Spellmire Weighting.

A BEAM PATTERN MODEL

FOR

ELECTRICALLY STEERED ARRAYS

CONTRACT NO. DASG60-91-C-0118

Prepared by:

SCIENTIFIC RESEARCH CORPORATION
2300 Windy Ridge Parkway, Suite 400 S
Atlanta, Georgia 30339

19 March 1993

TABLE OF CONTENTS

A BEAM PATTERN MODEL FOR ELECTRICALLY STEERED ARRAYS

1 Summary

A model for predicting beam patterns for electrically steered arrays (ESAs) is presented. The array is assumed to be planar, and element positions are assumed to be on a rectangular grid. Triangular grids are modeled by taking alternately odd and even numbered positions in alternate rows, and by adjusting the array spacing.

The model produces two dimensional beam patterns in sine space [1, pp 11-15 through 11-20], given element positions and amplitude weightings. If desired, the model will apply a single element pattern which applies to all elements. Element positions are parameterized as positions on a fixed planar rectangular grid; this allows modeling of triangular grids. Modeling of sparse arrays is implicit in the model. The model is also capable of modeling perturbations due to phase shifter errors and weighting errors.

Sine space is a coordinate system identical to the orthonormal mapping projection, which maps a spherical surface to a plane. A projection plane is defined as the plane of the array, and the origin of the coordinate system is the phase center

of the array. Pointing directions are mapped onto the plane by projecting a unit vector from the origin toward the pointing direction, and projecting its tip to the plane along a line perpendicular to the plane. In this way, the hemisphere in front of the phased array is mapped to a unit circle. Points outside the circle arise mathematically, but do not correspond to real pointing directions. For this reason, the interior of the circle is called the *real space* and the exterior of the circle is called the *imaginary space*.

The use of sine space to produce the beam pattern allows a single model run to produce a pattern which applies to all steered beams. This is because beam steering in sine space is a simple translation of the pattern, and the beam pattern is mapped from a unit circle centered on the physical (unsteered) boresight of the antenna. Therefore, the effects of steering can be examined by moving a unit circle around on the pattern and observing the lobes which enter the unit circle. The element pattern moves with the unit circle and is applied multiplicatively on the array pattern.

2 Applicable Documents

2.1 Government Documents

NONE

2.2 Non-Government Documents

[1] "Radar Handbook," Merrill Skolnik, Editor, Chapter 11, "Array Antennas" by Theodore C. Cheston and Joe Frank.

[2] "Antenna Engineering Handbook," Richard C. Johnson and Henry Jasik, Editors, Chapter 20, "Phased Arrays" by Raymond Tang and Richard C. Burns.

3 The Model

3.1 Analytical Basis and Assumptions

3.1.1 The Beamformer Equation

The far-field beamformer equation is developed as follows. Electromagnetic waves are summed as they pass through a hypothetical plane, which is positioned normal to a line passing through the phase center of the array. Time delay from the phase center to the hypothetical plane is then dropped. The result is the far-field beam pattern, with signal phasing equal to that of the array phase center. Complex arithmetic is used to represent signal phase.

The beam pattern is a linear combination of contributions of each of the elements. This contribution is multiplicatively modified by an element pattern f(d), where d is a unit vector pointing in the direction of a point for which the beam pattern is to be computed. The total beam pattern is [2, pp 20-16 through 20-21]

$$P(\underline{d}) = f(\underline{d}) \bullet \sum_{i_1 i_2} w_{i_1 i_2} \bullet \exp\left(-j\left(\left(\frac{2\pi}{\lambda}\right) \bullet \underline{x}_{i_1 i_2}^T \bullet \underline{d} - \theta_{i_1 i_2}\right)\right) \qquad 1$$

where the subscripts i_1 and i_2 represent element positions along rows and columns in a rectangular grid. The amplitude weights w_{ij} are inputs, and are zero for unused element positions. The phase steering angles θ_{ij} are computed for a desired steering direction $\underline{d}_s$ by

$$\theta_{i_1 i_2} = \left(\frac{2\pi}{\lambda}\right) \bullet \left(\underline{x}_{i_1 i_2}^T \bullet \underline{d}_s\right). \qquad 2$$

The element positions $\underline{x}_{ij}$ are assumed to be in a coordinate system whose x and y axes are in the plane of the array, and whose origin is the phase center of the array $\underline{x}_0$. The phase center $\underline{x}_0$ is the weighted average of element positions,

$$\underline{x}_0 = \frac{\sum_{i_1 i_2} w_{i_1 i_2} \underline{x}_{i_1 i_2}}{\sum_{i_1 i_2} w_{i_1 i_2}}. \qquad 3$$

Taking the element phasing algorithm as given by Equation (2) into account, the beam steering equation is

$$P(\underline{d}) = f(\underline{d}) \bullet \sum_{i_1 i_2} w_{i_1 i_2} \bullet \exp\left(-j\left(\frac{2\pi}{\lambda}\right) \bullet \underline{x}_{i_1 i_2}^T \bullet \left(\underline{d} - \underline{d}_s\right)\right). \qquad 4$$

This result is the beamforming equation. The beam relative intensity P is given in terms of a pointing vector d using the element pattern f(d), the element weights w_{ij}, the element positions $\underline{x}_{ij}$, and the pointing vector $\underline{d}_s$ to account for beam steering. The wavelength λ is included in the equation. The direction cosines are the components of d corresponding to the plane of the array.

3.1.2 Beam Patterns as Fourier Transforms

Our coordinate system has its origin at the array phase center and its x and y axes in the plane of the array. The x axis is horizontal, the z axis points out along the array boresight, and the y axis is in the direction of the z axis crossed into the x axis. This coordinate system is commonly called **array coordinates**. If the array

elements are positioned on a rectangular grid whose horizontal and vertical separations are a_1 and a_2, respectively, then the element positions $\underline{x}_{ij}$ can be given as

$$\underline{x}_{i_1 i_2} = i_1 \bullet a_1 \bullet \underline{e}_1 + i_2 \bullet a_2 \bullet \underline{e}_2 \qquad 5$$

where $\underline{e}_1$ and $\underline{e}_2$ are the unit vectors along the x and y directions, respectively, in array coordinates. The unit vector $\underline{e}_3$ points out along the array axis.

The pointing vector $\underline{d}$ can be quantized in such a way that the complex exponential in the beamformer equation conforms to a discrete Fourier transform (DFT). The quantization is

$$\sin\theta_i = \frac{\lambda}{a_i} \bullet \frac{k_i}{N_i} \qquad 6$$

where i is 1 for the horizontal direction and 2 for the vertical direction. N_1 and N_2 are the number of points in the rectangular grid in the vertical and horizontal direction, respectively, and k_1 and k_2 are new indices which give the output of the two dimensional DFT in terms of the pointing vector $\underline{d}$. The full equation for $\underline{d}$ is

$$\underline{d} = \sin\theta_1 \bullet \underline{e}_1 + \sin\theta_2 \bullet \underline{e}_2 + \sin\theta_3 \bullet \underline{e}_3 \qquad 7$$

where $\sin\theta_3$ is found from

$$(\sin\theta_1)^2 + (\sin\theta_2)^2 + (\sin\theta_3)^2 = 1. \qquad 8$$

Given these variable changes, the beamformer equation is

$$P(k_1, k_2) = f(k_1, k_2) \qquad 9$$

$$\bullet \sum_{i_1=0}^{N_1-1} \sum_{i_2=0}^{N_2-1} w_{i_1 i_2} \bullet \exp(j\theta_{i_1 i_2})$$

$$\bullet \exp\left(j \bullet 2\pi \left(\frac{i_1 \bullet k_1}{N_1} + \frac{i_2 \bullet k_2}{N_2} \right) \right)$$

which is very apparently a two dimensional DFT of the element weights and the phase shifter phases, with the element pattern as a multiplicative factor.

compatibility requirements must be met for MATLAB to access extended memory, such as use of no high memory manager, or use of QEMM or 385MAX instead of HIMEM, the memory manager supplied with MS-DOS.

The array definition module shown in the above listing executes for several minutes for even a small array. Because of this, since the listings above were written, the array definition module was recoded in Microsoft FORTRAN and is executed as a separate module. Using FORTRAN, the array definition process takes only a few seconds.

Microsoft FORTRAN supports compilation for Windows and OS/2 as well as DOS. An attempt was made to compile the array definition segment to define a 2 MB array under Windows, but it was not possible to access extended memory. The program was compiled for OS/2 and executed under an individual's personal copy of OS/2. A project copy of OS/2 is being procured to support this model in future development and use.

4 Results, Conclusions, and Recommendations

The model has been implemented using the simple MATLAB scripts and FORTRAN program given above. The resulting fishnet and contour plots are attached. The beam pattern in sine space is end-around periodic in both directions, so that the plots given can be extended as far as desired.

From the definitions of the element spacing grid given in the program, the extent of the plot in the x direction is 2 and the extent in the y direction is 1.1547, so that the distance of the first grating lobe from the main lobe is 1.1547 in sine space. This means that the array can be scanned only about 9 degrees in some directions before a grating lobe begins to peek over the edge of the array.

The element pattern can be used to suppress the grating lobe to extend the scanning angle. In general, the maximum scanning angle possible without emergence of a grating lobe, using equilateral triangular spacing, requires a reduction in the element grid spacing of 1/1.732 over that given in the example. The array elements will then be three times as dense per unit of area on the array face. If this were done, the plots would appear the same, but the scale factors in sine space as given by Equation 6 will change so that the radius from the main lobe to the nearest grating lobe is 2.0

Listing 1. Main Program

```
clear
%
%Define the array element positions and weightings
%
% weight.mat is a file containing the array elements
load weight1.mat
contour(elements); %Look at array shape
pause
%
%Compute the beam pattern
%
beam_pattern=fft2(elements);      %Compute beam pattern in sine space
%
%Write the outputs
%
xx=abs(beam_pattern)+1.e-10;  %Real nonnegative envelope
w=20*log10(xx);   %Log plots
mesh(xx);       %Fishnet plot in linear amplitude
pause
mesh(w);        %Fishnet plot in dB
pause
contour(w);     %Contour map in dB
```

Listing 2. Array Definition Module

```
      Program Compute

******* This Program defines the element positions and weightings for
******* a model of an ESA Radar.
******* Define variables
      implicit none
      Integer opt
      Real xvert(10),yvert(10),hegs,vegs,width
      Double precision rweights(128,128),qweights(128,128)
      Common /Global/ xvert,yvert,hegs,vegs,width

****** opt - option
****** xvert - x vertices
****** yvert - y vertices
****** hegs - horizontall element grid spacing (meters)
****** vegs - vertical element grid spacing (meters)
****** width - width of octagon
****** rweights - real weights of array
****** qweights - imaginary weights of array

****** Setup defines position of Octagon, options in the program,
****** and element grid spacing.
      Call Setup(opt)

****** Inarray defines the real and imaginary weights of the array
      Call Inarray(rweights,qweights,opt)
```

```
******  Savmatx prepares rweights and qweights to be outputted in a format
******  Matlab can read.
      Call Savmatx(rweights,qweights,opt)

      End


      Subroutine Setup(opt)
      implicit none
      Integer opt
      Real Lambda,FO,CVEL,Side,width,p1,p2,xvert(10),yvert(10)
      Real hegs,vegs,xsize,ysize
      Common /Globel/ xvert,yvert,hegs,vegs,width

******  FO -
******  CVEL - Speed of Light
******  Lambda -
******  xsize - size of octagonal in x direction
******  ysize - size of octagonal in y direction

      FO=10e9    !X-BAND
      CVEL=299792458.  ! Speed of Light
      LAMBDA=CVEL/FO
      HEGS=.5*LAMBDA
      VEGS=SQRT(.75)*HEGS
      width=0.35 !Array width in meters

      xsize=width/hegs !Matrix of element positions; horizontal spacing
      ysize=width/vegs ! "; vertical spacing

******  Displays options for the user and tells the size of the octagon
      print *,'FACTS ABOUT THE ESA MODEL:'
      Print *
      print *,' Present size of Array:                128x128'
      print *,' Horizontal element grid spacing:'
      print 10, hegs
      print *,' Vertical element grid spacing:'
      print 10, vegs
      print *,' Width of Octagon:                     2 meters'
      print *,' Number of elements horizonatally in octagon'
      print 10, xsize
      print *,' Number of elements vertically in octagon'
      print 10, ysize
      print *
      print *
      print *,'This ESA Model provides you with the following options:'
      print *
      print *,'1) Noisy array with the use of Random variables'
      print *,'2) Regular array with use of Random variables'
      print *,'3) Regular array without use of Random variables'
      print *
      print *,'Please enter a selection of 1-3:'
      read *, opt
   10 Format (50x,g15.6)

******  Define positions of Octagon
******  side - Length of side of octagon
******  p1 - position of vertices of octagon
```

```
      side=(width)/(1.+sqrt(2.))
      p1=side/sqrt(2.)
      p2=p1+side
      xvert(1)=p1   !Position of first vertex
      yvert(1)=0
      xvert(2)=p2   !Position of second vertex
      yvert(2)=0
      xvert(3)=width !Position of third vertex
      yvert(3)=p1
      xvert(4)=width !Position of fourth vertex
      yvert(4)=p2
      xvert(5)=p2   !Position of fifth vertex
      yvert(5)=width
      xvert(6)=p1   !Position of sixth vertex
      yvert(6)=width
      xvert(7)=0    !Position of seventh vertex
      yvert(7)=p2
      xvert(8)=0    !Position of eighth vertex
      yvert(8)=p1
      xvert(9)=p1   !Repeat first vertex in ninth position
      yvert(9)=0

    Return
    End

    Subroutine Inarray(rweights,qweights,opt)

    implicit none
    Integer itest,wo,I,J,seed,opt
    Real x,y,xvert(10),yvert(10)
    Real hegs,vegs,mb,rb,cl,rand,gaurand,pi,theta,width
    Double precision rweights(128,128),qweights(128,128),w1
    Common /Global/ xvert,yvert,hegs,vegs,width
    Logical test

    MB=4        !Four bit phase shifters
    pi=4.*atan(1.)
    CL=180./pi   !57.3 radians to degrees conversion factor
    RB=5./cl     !5 degrees one-sigma angle error

****** Initialize Random Number Generator
    Call Getseed(seed)

****** For each possible element position (i,j), find only element
****** positions within octagon.
    do i=1,128
     do j=1,128
      x=(i-1)*hegs
      y=(j-1)*vegs
     If (x.le.width.and.y.le.width) then
      itest=i+j
      itest=itest-(itest/2)*2
      wo=0.
      if (itest.ne.0) THEN
       IF (test(x,y)) then ! skip (i+j) odd for triangular position
        Select Case (opt)
         Case (1)     ! Noisy Array with Random variables
```

```
            theta=rb*gaurand(seed)
            w1=1.+(2.**(-MB))*(rand(seed)-.5)
            rweights(i,j)=w1*cos(theta)
            qweights(i,j)=w1*sin(theta)

            Case (2)     ! Regular Array with Random variables
            theta=rb*gaurand(seed)
            w1=1.+(2.**(-MB))*(rand(seed)-.5)
            rweights(i,j)=w1*cos(theta)-1.
            qweights(i,j)=w1*sin(theta)

            Case (3)     ! Regular Array w/o Random variables
            rweights(i,j)=1
            qweights(i,j)=0

          end select
        endif
      endif
    endif
    enddo
  enddo
  Return
  End

****** Subroutine that prepares array in a format Matlab can read.
  Subroutine savmatx(rweights,qweights,opt)

****** Define variables
  implicit none
  Real xvert(10),yvert(10),hegs,vegs,width
  Double precision rweights(128,128),qweights(128,128)
  Integer*4 type,mrows,ncols,imagf,namlen,wtflg
  Integer opt
  Character name(9)*1
  Common /Global/ xvert,yvert,hegs,vegs,width

****** type -
****** mrows - number of rows in array
****** ncols - number of columns in array
****** imagf - =1 if imaginary numbers are used in array
****** namlen - name of array
****** wtflg - write flag (test for successful export)

  type=0
  mrows=128
  ncols=128
  if (opt.eq.1 .or. opt.eq.2) then
    imagf=1
  endif
  namlen=9
  name(1)='e'
  name(2)='l'
  name(3)='e'
  name(4)='m'
  name(5)='e'
  name(6)='n'
  name(7)='t'
  name(8)='s'
```

```
      name(9)=0

*****  Calls subroutine to actually save arrays in Matlab format
      Call Savemat(type,mrows,ncols,imagf,namlen,name,rweights,
     + qweights,10,wtflg)

      Return
      End

      Subroutine Getseed(seed)

******  Define variables
      Implicit None
      Integer IHOUR,IMIN,ISEC,IHUN,Seed

******  Ihour - Integer for the hour number on computer's clock
******  Imin - Integer for the minute number on computer's clock
******  Isec - Integer for the second number on computer's clock
******  Ihun - Integer for the 1/100th number on computer's clock
******  Seed - Seed for Random number generator

      Call Gettim(Ihour,Imin,Isec,Ihun)

      If (Imin.EQ.0.0) then
        Imin=1.0
      Endif
      If (Isec.EQ.0.0) then
        Isec=1.0
      Endif

      Seed=((Imin*Isec*Ihun)/13)+1

      Return
      End

******  Logical Function to test if a point falls in the octagon
      Logical function test(xe,ye)

******  Define variables
      implicit none
      Integer I
      Real dxv,dyv,dxt,dyt,isit,xe,ye,xv(10),yv(10),a,b,width
      Common /Global/ xv,yv,a,b,width

      test=.true.
      Do i=1,8
        dxv=xv(i+1)-xv(i)
        dyv=yv(i+1)-yv(i)
        dxt=xe-xv(i)
        dyt=ye-yv(i)
        isit=(dxt*(-dyv))+(dyt*dxv)
        if (isit.lt.0) then
          test=.false.
          exit
        endif
      enddo
      return
      end
```

```
****** Function to generate a random number
      Real Function Rand(I)
      implicit none
      integer i,j
      real fac
*
      Data Fac/4.6566129E-10/
      J=ISHFT(I,-18)
      J=IEOR(I,J)
      I=ISHFT(J,19)
      I=ISHFT(I,-6)
      J=IEOR(I,J)
      I=ISHFT(J,-13)
      I=ISHFT(I,27)
      I=ISHFT(I,-1)
      I=IEOR(I,J)
      RAND=i*FAC
      END

****** Gaussian random number generator
      Real function gaurand(seed)
      implicit none
      real x1,x2,r2,r,d,rand,cosang,sinang
      integer seed
      logical oddcall
      save oddcall
      data oddcall/.true./
*
      if(oddcall) then
       do while(.true.) !Find (x,y) in unit circle
        x1=2.*rand(seed)-1. !Start with unit square
        x2=2.*rand(seed)-1.
        r2=x1**2+x2**2
        if(r2.lt.1.) exit !Reject corners; repeat 21% of the time
        end do !repeat
       r=-alog(r2) !Scaled Poisson
       d=sqrt(r2)
       cosang=x1/d
       sinang=x2/d
       gaurand=r*cosang
       oddcall=.false.
      else
       gaurand=r*sinang
       oddcall=.true.
       end if
      return
      end


****** Subroutine borrowed from Matlab to save arrays in a format
****** Matlab can read.
      Subroutine savemat( type, mrows, ncols, imagf, namlen, name,
     $                    rpart, ipart, lunit, wtflg )

c Description of inputs:
c
c     type    - matrix type flag; considering the type flag as a
```

```
c            decimal integer, the ones decimal place is used to
c            indicate numeric or textual interpretation of the
c            matrix data (0 for numeric or 1 for textual);
c            the 1000's decimal place is used to indicate the
c            machine format for the matrix data (0 for Intel 80(2)86
c            based machines, 1 for Motorola 68000 based machines,
c            and 2 for Vax d format). For example, A flag of 1000 indicate
c            numeric data in a 68000 machine format and a flag of
c            1001 indicates textual interpretation of the 68000
c            machine format data.
c     mrows  - number of rows in matrix
c     ncols  - number of columns in matrix
c     imagf  - imaginary flag; 0 for no imaginary part or 1 if the
c            data has an imaginary part
c     namlen - number of characters in matrix name plus 1 (for zero
c            byte string terminator supplied by this routine)
c     name   - character array holding the matrix name. (Be sure
c            character array has room for the zero byte terminator)
c     rpart  - real part of matrix (mrows x ncols double precision
c            elements stored column wise)
c     ipart  - imaginary part of matrix (only used if imagf = 1)
c     lunit  - logical unit number of output file
c
c Description of outputs:
c
c     wtflg  - write flag; 0 = good write, -1 = error during file write
c
c NOTES :
c
c     o THE OUTPUT FILE MUST BE OPENED WITH THE FOLLOWING STATEMENT:
c       open(unit=lunit, file='file_name', form='binary')
c
c     o Be sure that the 4 byte integer option is used when compiling
c       this routine and that SAVEMAT's integer arguments are 4 byte.
c
c     o Be sure to close the file when there are no more
c       matrices to be saved.
c
c     o You may call SAVEMAT multiple times to write multiple matrices
c       onto the output file before closing it.
c
      implicit none
c 20 byte header
      integer  type, mrows, ncols, imagf, namlen
c
c character string for name (length of name plus one)
      character  name(*)*1
c
c double precision data arrays for example
      double precision  rpart(*), ipart(*)
c
c output file logical unit number
      integer lunit
c
c write flag
      integer  wtflg
c
c zero byte needed to terminate variable name
```

```
      integer*1  zerobyte
      integer*4 mn,i
      data zerobyte / 0 /
c
     open (unit=10,file='weight.mat',form='binary')
     lunit=10
      mn =mrows*ncols
c
c  write header
      write(lunit)  type,mrows,ncols,imagf,namlen
c
c  write variable name
      write(lunit)  (name(i),i=1,namlen-1),zerobyte
c
c  write real part of variable
      write(lunit)  (rpart(i),i=1,mn)
c
c  write imaginary part of variable if any
      if (imagf .eq. 1)  write(lunit)  (ipart(i),i=1,mn)
c
c  good write
      wtflg = 0
      return
c
c  error during write
c999    wtflg = -1
      close (10)
      return
      end
*****************************
* The End *
```

TECHNICAL MEMO

To: List
Date: 12 August 1992
Subject: Derivation of Antenna Pedestal Rotation Rate

From: J.K. Beard
Reference: JKB-92-10

1. SUMMARY

The purpose of this derivation is to calculate the maximum mechanical movement requirements of the radar's antenna pedestal. This model assumes that the target is moving in a level flight path with constant velocity. For a target traveling at Mach 1.2 and 1500 m off the deck will require a minimum pedestal azimuth velocity of 16° per second for a target pass distance of 1500m. The results of this model can be used to size minimum velocity requirement for radar pedestals.

2. PROBLEM STATEMENT

The geometry of the problem is the pass-course problem. Suppose a target under track is crossing in front of the radar. The point where maximum angular velocity occurs is when the target's velocity vector is tangential to the radar's boresight at a minimum range from the radar.

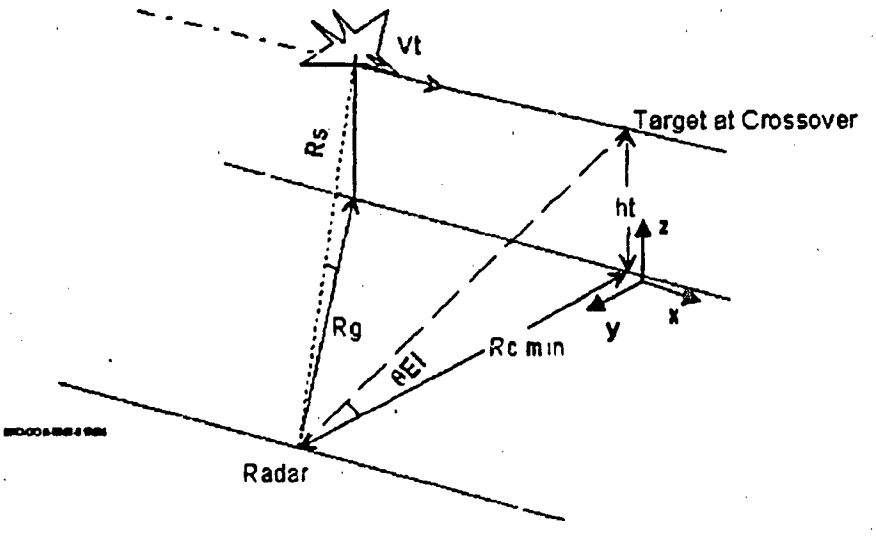

The ground projection of the flight path is given below.

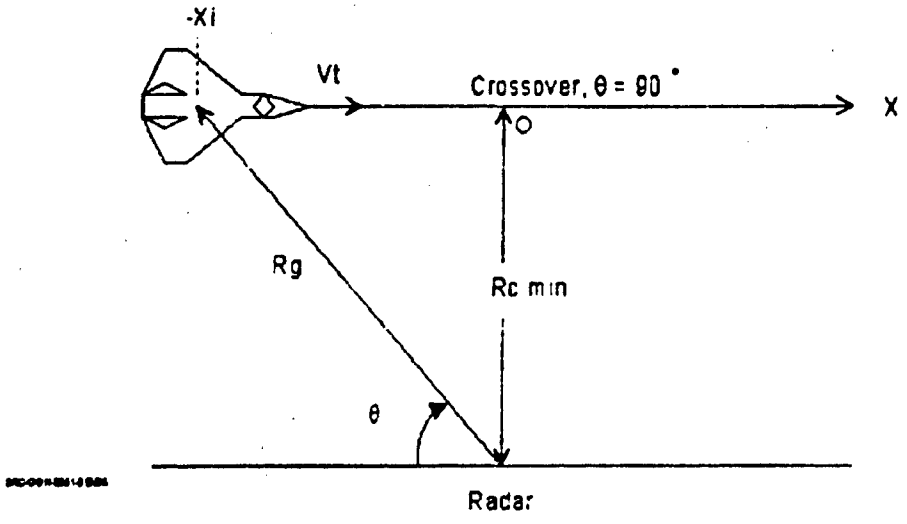

The maximum azimuth angular velocity for a radar antenna pedestal tracking a target in level flight passing at Rc_{min} in front of the radar with a velocity of V_{target} may be calculated.

Assumptions:

R_{max} = 25000 m. (Maximum target range)

R_{min} = 1500 m. (Minimum target range)

$Rc_{min} = R_{min}$ (Minimum pass distance of target at crossove

V_{target} = 426 m/sec. (Target velocity = Mach 1.2)

Calculations:

$$\omega_{max} = \frac{V_{target}}{Rc_{min}} \qquad \omega_{max} = 0.284 \text{ rad/sec} \qquad \text{(Maximum azimuth angular velocit}$$

$$\theta dot_{max} = \omega_{max} \cdot \frac{180}{\pi} \qquad \theta dot_{max} = 16.272 \text{ deg/sec}$$

If the minimum pass distance is varied, the maximum azimuth angular velocity is:

$tr := 0 .. \frac{R_{max} - R_{min}}{500}$ target range index

$Rc_{tr} := R_{min} + 500 \cdot tr$ m. (Pass distance calculation)

$\omega_{tr} := \frac{V_{target}}{Rc_{tr}}$ rad/sec. (Maximum azimuth angular velocit

$\theta dot_{tr} := \omega_{tr} \cdot \frac{180}{\pi}$ deg/sec.

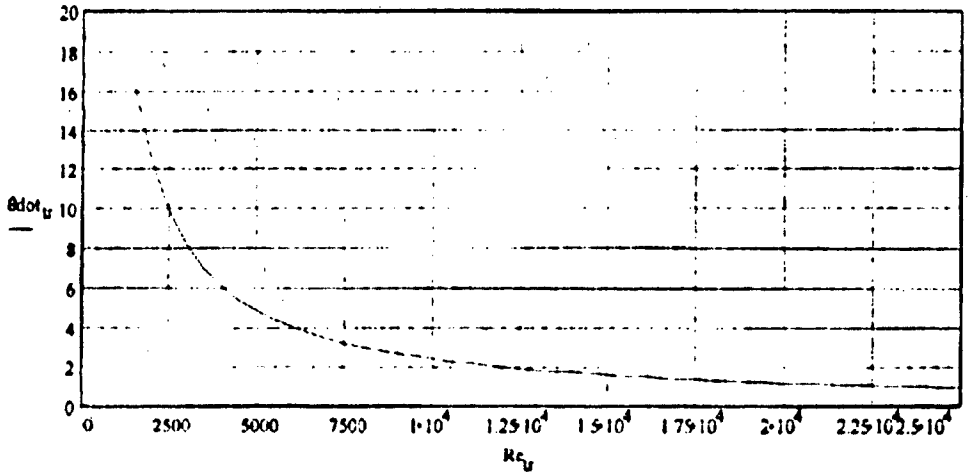

Maximum azimuth angular velocity (deg/sec.) vs. pass distance

Looking at the azimuth angular velocity of the radar antenna pedestal for the pass course flight, the equations of motion are:

$Xi := 16000$ m. (Targets initial cross range distance)

$t := 0, 0.1 .. \frac{2 \cdot Xi}{V_{target}}$ sec. (Target flight time)

$x(t) := Xi - V_{target} \cdot t$ m. (Target cross range distance)

$\theta dot(t) := \frac{R_{min} \cdot V_{target}}{\left[(x(t))^2 + R_{min}^2\right]} \cdot \frac{180}{\pi}$ deg/sec. (Angular velocity of the rada

$$\theta 2dot(t) := -2 \cdot V_{target}^{2} \cdot R_{min} \cdot \frac{x(t)}{\left(R_{min}^{2} - (x(t))^{2}\right)^{2}} \cdot \frac{180}{\pi} \quad \text{deg/sec}^2 \quad \text{(Angular acceleration of the rada}$$

$$Rg(t) := \sqrt{(x(t))^{2} - R_{min}^{2}} \quad \text{m.} \quad \text{(Ground range distance)}$$

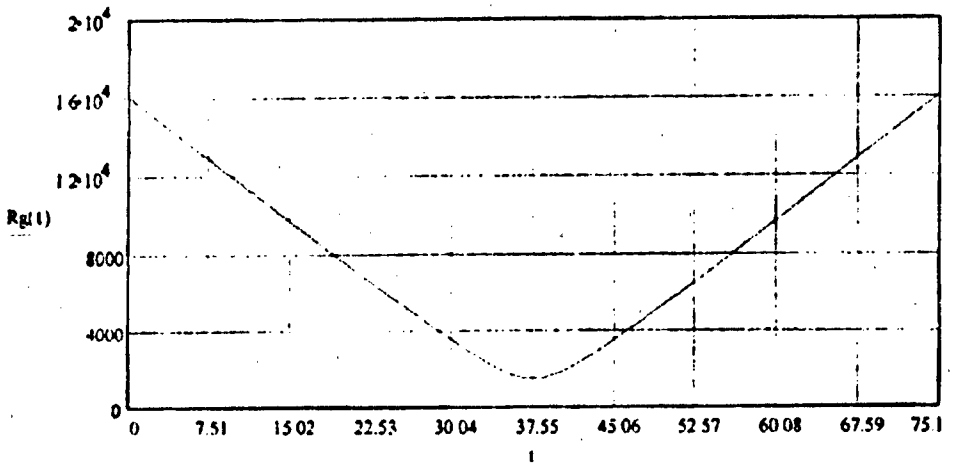

Ground range distance (m.) vs. flight time

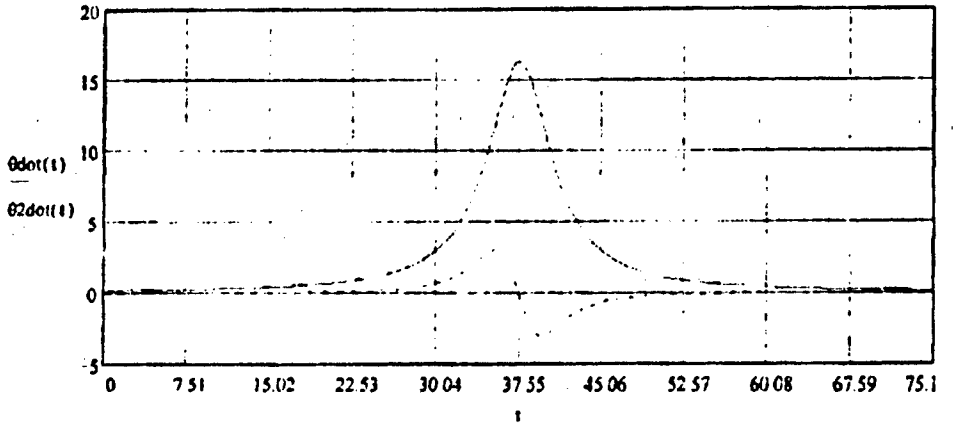

Angular velocity of antenna pedestal vs. flight time
Angular acceleration of antenna pedestal vs. flight time

The maximum elevation angular velocity for a radar antenna pedestal tracking a target in level flight passing at Rc_{min} in front of the radar with a velocity of V_{target} may be calculated.

Assumptions:

ht := 1500 m. (Target height during flight)

Calculations:

$Elev\_ := atan\left(\frac{ht}{R_{min}}\right) \cdot \frac{180}{\pi}$ deg. (Maximum elevation angl

Elev_ = 45 deg.

$Elev(t) := atan\left(\frac{ht}{Rg(t)}\right) \cdot \frac{180}{\pi}$ deg. (Antenna elevation)

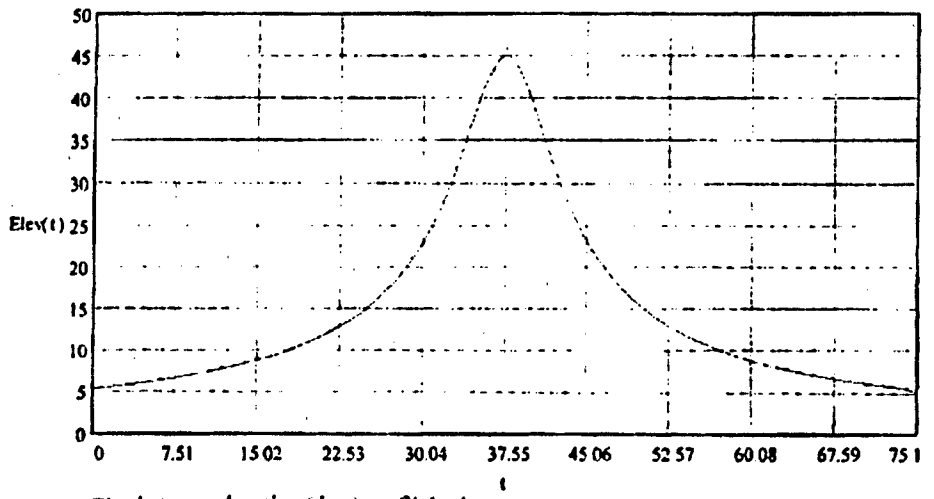

Antenna elevation (deg.) vs. flight time

Looking at the elevation angular velocity of the radar antenna pedestal for the pass course flight, the equations of motion are:

$$\theta dotEL(t) := \frac{\frac{-ht \cdot x(t)}{\left[(x(t))^2 + R_{min}^2\right]^{1.5}} \cdot V_{target}}{1 - \frac{ht^2}{(x(t))^2 + R_{min}^2}} \cdot \frac{180}{\pi}$$ deg/sec. (Elevation angular velocity of the radar)

$$\theta 2dotEL(t) = \left[\frac{-ht \cdot V_{target}^2}{\left[(x(t))^2 - R_{min}^2\right]^{1.5} + ht^2 \cdot \left[(x(t))^2 - R_{min}^2\right]^{1.5}} \cdots + \left[\frac{ht \cdot x(t) \cdot V_{target}}{\left[(x(t))^2 - R_{min}^2\right]^{1.5} + ht^2 \cdot \left[(x(t))^2 - R_{min}^2\right]^{1.5}} \cdot \left[3 \cdot x(t) \cdot V_{target} \cdot \left[(x(t))^2 - R_{min}^2\right]^{.5} \cdots - \frac{ht^2 \cdot x(t) \cdot V_{target}}{\left[(x(t))^2 - R_{min}^2\right]^{.5}} \right] \right] \cdot \frac{180}{\pi}$$

deg/sec^2 (Elevation angular acceleration of the rada

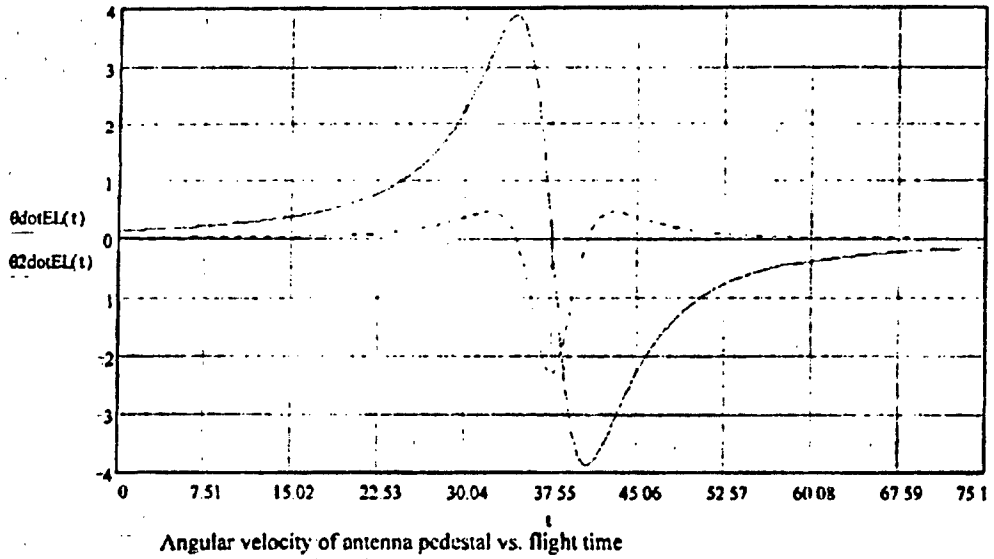

Angular velocity of antenna pedestal vs. flight time
Angular acceleration of antenna pedestal vs. flight time

Barton, D.K., "Modern Radar System Analysis," Artech House. 1988, Norwood, MA., pg. 173.

Barton, D.K., "The 1993 Moscow Air Show," Microwave Journal, May, 1994.,pg. 37.

Beard, J.K. "Three simple, robust two-state Kalman filters," SRC Technical Memorandum JKB-93-05, 3 May 1993.

Beard, J.K. "Description of the tracker CSC for pulse-Doppler radars", SRC Technical Memorandum JKB-93-06, 5 June 1993.

Beard, J.K. "A Doppler resolve methodology for pulse-Doppler radars." SRC Technical Memorandum JKB-93-11, 23 August 1993.

Beard, J.K., "An Analysis Model for ESA Point Designs," SRC Technical Memo, March 30, 1993.

Beard, J.K., "A 14 Bit A to D Gives a 100 dB Noise Floor in the WFS Signal Processor Upgrade," SRC Technical Memo, April 12, 93.

Beard, J.K., "Dynamic Range of Digital Data," SRC Technical Memo, August 4, 92.

Beard, J.K., "A Beam Steering Controller Concept for Phased Arrays," SRC Technical Memo, August 12, 1992.

Begovich, N.A., "Frequency Scanning," Microwave Scanning Antennas, vol III, 1966, Academic Press. Inc., New York, Robert Hansen editor, pg. 136.

Cheston, C.C, Frank, J.,"Phased Array Radar Antennas," Radar Handbook, Merrill Skolnik, editor., McGraw-Hill Publishing, 1990, pg.7.59.

Child, J. "High-resolution A-D converters sport new twists on old architectures," Computer Design Product Focus Review & Buying Guide Issue, March 28, 1994.

Costlow, T., "Drive makers spinning new technologies," Electronic Engineering Times, No. 819, October 17, 1994.

Dionne et al. "Method for Enhancing Low-Noise CFA Performance." in Electron Devices Meeting CH2865-4/90/0000-0529 IEEE, 1990.

Dittman and Norgradi. "Cooling and Insulating Small Hard Tube Modulators." Power Modulator Symposium CH2839-9/90/0000-134, IEEE Conference Records, 1990.

Emry, M.L., "A/D Testing and Characterization," SRC Technical Memo, May 18, 93.

Goutzoulis, A, Davies, K., Zomp, J. et al, "A Hardware-Compressive Fiber-Optic True Time Delay Steering System for Phased-Array Antennas," Microwave Journal, Vol. 37, No. 9, September, 1994, pg. 126 - 140.

Grishin et al. "An Investigation of Transmission of Broadband Noise through a TWT." Soviet Journal of Communications Technology & Electronics volume 31 No. 8 pages 152 through 158, 1990.

House, R., "Simple tests reveal data-acq boards whose accuracies match their resolution," Personal Engineering, Volume 11, Number 6, June, 94.

Johnson, M.W., "Test High-Speed, High Resolution A-D Converters," Electronic Design, November 8, 1990.

Kummer, W.H. "Feeding and Phase Scanning." Microwave Scanning Antennas, vol III, 1966, Academic Press, New York, Robert Hansen, editor, pgs. 85-102.

Lazerson and Shlyakhter. "Electronic Suppression of Noise in TWT of O Type." Radiotechnika and Elektrotechnika volume 36 No. 3, pages 528-533, 1991.

Leonard, R.K. Jr., "Data Converters: Getting to Know Dynamic Specs," Electronic Design, November 8, 1990.

Mailloux, R.J., "New Directions in Phased Array Developement", Journal of Electronic Defense, vol. 17, No. 7, July, 1994, pg. 33.

McMaster, George. "Current Status of Cross-Field Devices Technical Digest." in Electron Devices Meeting, CH2528-8/88/0000-0358, IEEE 1988.

MSIC publication, "The Range Resolve Algorithm"

"New and Innovative Ideas in Processing and Simulation Technologies: Program Overview and Status," Quarterly Progress Review, 28 APRIl 1993.

"New and Innovative Ideas in Processing and Simulation Technologies: Program Overview and Status," Quarterly Progress Review, 23 November 1993.

Nogradi, Istvan. "Envelope Technique for Trigger Amplifiers." 19th Power Modulator Symposium CH2839-9/90/0000-052 IEEE, 1990.

Nograd, Istvan. "Array-type Pulsed Power Modulators." 28th Intersociety Energy Conversion Engineering Conference ISBN 0-8412-2772-5, 1993.

Norgradi, Istvan. "Hardfet Modulator." Twentieth Power Modulator Symposium CH3180-7/92/0000-0189, IEEE Conference Records, 1992.

Nogradi, Istvan. "Modified Hardfet Modulator." URSI, National Radio Science Meeting Paper #7.1120, 1993.

Nogradi, Istvan. "HARDFET Radar Modulator." High Voltage Workshop, 1989 and published with experimental results at the "Hardfet Modulator." Power Modulator Symposium Library of Congress Library Catalogue No.: 92-53252, 1992.

Nogradi, Istvan. "The Modified Hardfet Modulator." International Union of Radio

Science Meeting (URSI) Paper #93479, 1993.

Pobedonostsev et al. "Multiple-Beam Microwave Tubes." International Microwave Symposium CH3277-1/93/0000-1131, IEEE, 1993.

Rhea, J.,"DOD Turns to GaAs Technology for Ground Based Radars," Microwaves & RF, May, 1991, pg. 47-53.

Skolnik, M.I., Sherman, J.W., Ogg, F.C., "Statistically Designed Density-Tapered Arrays," IEEE Transactions on Antennas and Propagarion, July, 1964, pg. 408.

Smullin and Haus. "Noise in Electron Devices" Library of Congress Catalog Card No: 58-12714, Copyright MIT, 1958.

Steyskal, H.,"Digital Beamforming Antennas: An Introduction," Journal of Electronic Defense, Vol. 17, No.7, July, 1994 , pg 37.

Stiglitz, M., "Unraveling the M?MIC Knot," Journal of Electronic Defense, Vol. 17, No. 5, May, 1994, pg. 43-47.

Tang, R., Burns, R.W., "Array Technology," Proceedings of the IEEE, Vol. 80, No.1, January, 1992, pg. 173.

"The multimedia drive," IEEE Spectrum, April, 1994.

Torok, Les. "Precision Inductance Modeling is the basis for Accurate PFN Simulation." Library of Congress Catalogue No.: ISBN 1076-8467.

Wersman et al. "Modulation Capabilities of Different Grid Design for a Cs-Ba Tacitron." Twenty-first International Power Modulator Symposium ISSN 1076-8467, 1994.

H-1. Introduction

The Wavelet Transform (WT), Inverse Wavelet Transform (IWT), and Wavelet Packet Transform (WPT) can be used for joint time/frequency analysis of signals. In radar systems, this function corresponds to simultaneous extraction of range and range rate from a target return. Specialized wavelet transforms can require fewer mathematical operations than conventional techniques (e.g., Fast Fourier Transforms - FFT) to perform this analysis, and can yield more-useful results. Wavelet processing can also be used to convert between time domain and frequency domain signal representations, in effect duplicating the capabilities of standard FFT techniques.

The mathematical properties of wavelets have been studied since the early 1950's. Related mathematical systems that describe the velocity/momentum characteristics of sub-atomic particles were developed in the 1920's by the originators of Quantum Mechanics and underlie Heisenberg's well-known Uncertainty Principle.

In the early- and mid-1980's several researchers developed the theory of "perfect reconstruction" quadrature mirror filters (QMFs) and implemented subband coding communications systems built around these filters (*Signal Processing* 10(3) , M. Vetterli, 1986). In the late 1980's, the useful properties of specific classes of wavelets were "re-discovered" (I. Daubechies, *Communications on Pure and Applied Mathematics* XLI, 1988), and the QMF implementation of the Wavelet Transform was publicized.

Much of the information on wavelets has been treated as proprietary, trade secret, or protected intellectual property. In the last year, standard techniques and toolkits have been published (*Electronic Engineering Times*, October 10 1994; *Adapted Wavelet Analysis from Theory to Software*, A. K. Peters Ltd, May 1994) which allow wavelets to be seen as system implementation tools, rather than mathematical research projects.

H-2. Technical Discussion

The WT decomposes an input signal into components by iteratively correlating the input with each of a set of basis functions. Most other transforms (Fourier, Cosine, Harr, etc.) also

perform decomposition by correlation. Implementation methods, however, vary widely between transform types.

The most familiar type of transform, the FFT, uses sinusoidal basis functions, with a constant frequency step between successive members of the set. The transform outputs (i.e., the components of the input waveform) correspond to voltage levels in the signal at the frequencies of the basis functions. The set of all components is the spectrum of the signal.

There are many different classes of wavelet basis functions. The most-widely used ones are orthonormal and satisfy the following conditions :

$$\sum_{k\in Z} a_{2k} = 1 \qquad \sum_{k\in Z} a_{2k+1} = 1 \qquad \sum_{k\in Z} a_k a_{k+2l} = 0 \qquad \sum_{k\in Z} a_k a_k^* = 2 \qquad (l \neq 0)$$

where the a_k are "wavelet coefficients", and the set of k is a subset of the integers.

There are infinitely many sets of functions that satisfy these criteria. Basis functions that are "compactly supported" can be used to perform joint time/frequency analysis. "Compact support" can be taken to mean that the number of non-zero coefficients is less than the number of samples of the input signal being analyzed.

For example, one frequently-implemented set of coefficients is :

$$a_{-2} = \left(\left(1+\cos\alpha+\sin\alpha\right)\cdot\left(1-\cos\beta-\sin\beta\right)+2\sin\beta\cdot\cos\alpha\right)\div 4$$

$$a_{-1} = \left(\left(1-\cos\alpha+\sin\alpha\right)\cdot\left(1+\cos\beta-\sin\beta\right)-2\sin\beta\cdot\cos\alpha\right)\div 4$$

$$a_0 = \left(1+\cos\left(\alpha-\beta\right)+\sin\left(\alpha-\beta\right)\right)\div 2 \qquad a_1 = \left(1+\cos\left(\alpha-\beta\right)-\sin\left(\alpha-\beta\right)\right)\div 2$$

$$a_2 = 1-a_{-2}-a_0 \qquad a_3 = 1-a_{-1}-a_1 \qquad \left(-\pi \le \alpha,\ \beta < \pi\right)$$

Note that these equations define a maximum of six non-zero coefficients, and that there are an infinite number of sets of coefficients that satisfy the equations, with each such set defined by the values of α and β.

Flow Graphs of typical implementations of the FFT and the WT are shown in **Figures H-1** and **H-2**, respectively. DQMF is a Decimating Quadrature Mirror Filter (DQMF), which will be defined later. HP and LP are the high-pass and low-pass outputs of the DQMF filter pairs. The numbers of samples input and output at each processing node are adjacent to the flow lines between nodes.

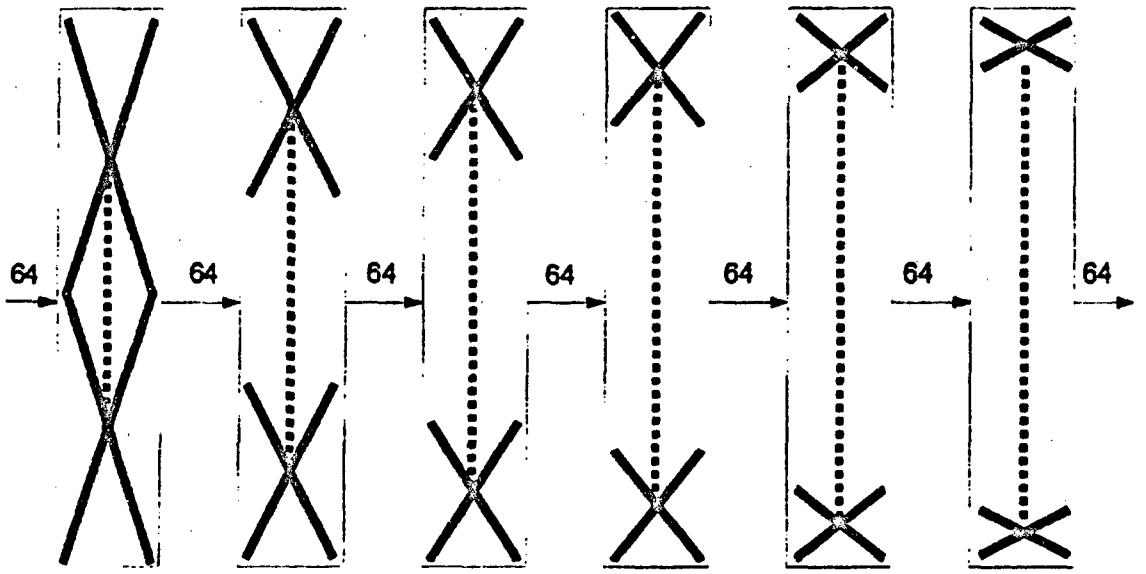

Figure H-1: Flow Graph of FFT (Simplified)

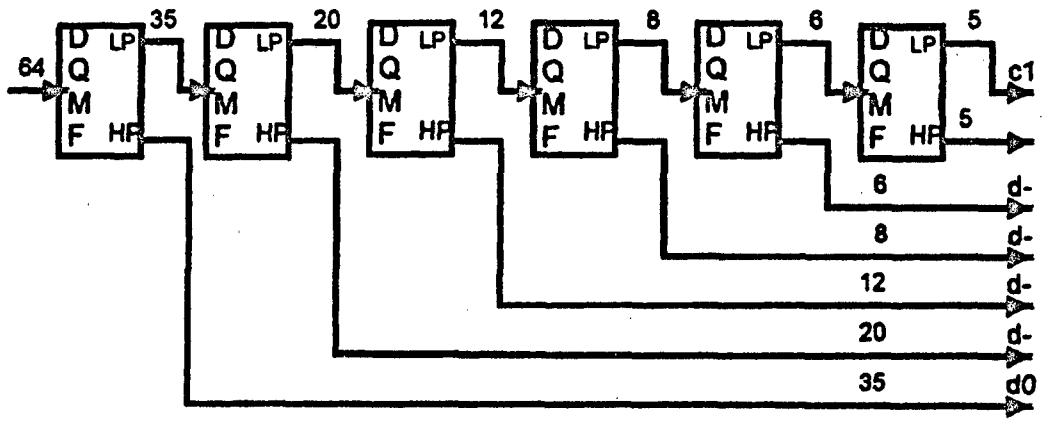

Figure H-2: Flow Graph of Basic Wavelet Transform (Simplified Nomenclature)

Note that each stage of the standard FFT algorithm applies N/2 'butterfly' operations to N input samples, and outputs N results. This simplifies the memory access patterns of "in-place" versions of the algorithm and allows efficient use of high degrees of parallelism in multi-processor implementations.

Each stage of most WT9 implementations, however, produces more samples than were input to the stage. As shown in **Figure H-2**, the output of each DQMF is expanded by approximately the number of non-zero wavelet coefficients. Memory allocation and addressing are more complicated for the WT than for the FFT. Parallelism is possible if the memory control hardware of the computer on which the WT is executed has appropriately powerful addressing and data access capabilities. Alternatively, the output expansion can be avoided by using the "Periodic" version of the WT, instead of the "Aperiodic" (continuous) version shown here.

Each DQMF is a pair of Finite Impulse Response (FIR, also known as transversal, correlation, or convolution) filters. One of the filters performs a high-pass function, and the other, a low-pass. The cutoff frequencies of the filters in each pair are identical, and their bandwidths are complementary. The multiplier values used by each filter are scaled, translated versions of the wavelet basis function coefficients. For every set of consecutive input samples, each filter calculates a set of consecutive output samples, each of which is the sum of the products of all its multipliers with the input samples (i.e., the filter computes "dot" or "inner" products). For example, with the coefficients defined above, each output sample is the product of two six-term vectors. Half the outputs of each filter are used as inputs of the next stage, and half are made available as transform outputs, effectively reducing the sampling rate by half at each stage. Note that it is sensible to say that the filters have "complementary" bandwidths since it is assumed that the input to the WT is band-limited and has no negative-frequency components.

For standard versions of the WT, the same set of multiplier coefficients is used by every DQMF (i.e., all filters have the same transfer function). This differs from the FFT, which synthesizes a set of bandpass filters, each with a different center frequency and different filter coefficients. Another difference between the WT and FFT is that the division of the WT into successive stages is inherent in the definition of the transform, whereas in the FFT, it results from implementation considerations (The Discrete Fourier Transform has a single-stage

implementation. The multi-stage FFT computes the same result as the DFT, but performs less arithmetic).

Each output from an FFT or a WT has a specific resolution in time and frequency. These resolutions can be visualized as the extents of rectangular areas in a 2-dimensional plot of time versus frequency. In other words, the transform outputs tile the time/frequency plane.

For the FFT, the time resolution of each output is the number of samples times the inter-sample period, and the nominal frequency resolution is the difference in frequencies of two adjacent basis sinusoids. The resolution of each output is identical to the resolution of every other output, and the FFT does not allow localization of signals in the time domain. Therefore, each tile in the time/frequency plane spans the entire time dimension, with a minimal extent in the frequency dimension.

The WT is a multi-resolution transform. Each output provides a different combination of time and frequency resolutions and different degrees of uncertainty for simultaneous localization of signals in the time and frequency domains. For the example WT of **Figure H-2**, time and frequency resolutions are inversely related, by octaves. Output c_1 has a frequency resolution of 1/64 of the Nyquist rate, a center frequency of 3/128, and a time resolution of the entire data acquisition period. It is approximately equivalent to the bin 1 output of an FFT. Output d_4 has a frequency resolution of 1/32 of the Nyquist rate, a center frequency of 3/64, and a time resolution of 1/2 the data acquisition period. The other output resolutions progress up to d_0, which has resolutions of 1/2 and 1/32, and a center frequency of 3/4.

Each tile in the WT output time/frequency plane has a different shape, with small extents in the low-frequency part of the plane and large extents in the high-frequency part. The time/frequency localization capabilities of this transform are clearly non-optimal for radar applications, since it can resolve the times (ranges) of signals (targets) at high frequencies (large Doppler shifts) but not their specific frequencies (range rates).

The Wavelet Packet Transform (WPT) overcomes these difficulties (R. R. Coifman, Y. Meyer, S. R. Quake, M.L. Wickerhauser, *Progress in Wavelet Analysis and Applications*, June 1992). The WPT uses linear combinations of wavelet functions as its basis functions. The WPT

is implemented by use of additional DQMFs to process the High-Pass outputs of higher-level filters (the d_x outputs of **Figure H-2**).

If all outputs from all filters (including the ones added for the WPT) are processed, the implementation has a tree or pyramid structure, instead of the linear structure of **Figure H-2.** As a result, all transform outputs have minimal-frequency, maximal-time resolutions. If only selected portions of the filter sequence are expanded, the WPT can implement any combination of time and frequency resolutions independent of filter center frequencies, subject to the constraints that the resolutions are inverse and that the nominal passbands of the outputs do not overlap.

For example, a WPT that emulated the FFT could be generated by carrying the filter tree to the finest level of frequency resolution from every branch, and allowing the time resolution to degrade. Or the inverse of **Figure H-2** could be synthesized, with good range resolution associated with low frequencies.

Wavelet transforms provide great flexibility in tailoring the transform to match the application. In addition to the choice of filter resolutions and transform structure mentioned above, the choice of basis function affects the transform functionality. Bases can be chosen to optimize recognition of specific signals or waveforms in a background of noise or interference. Basis functions can be derived from descriptions of expected signal and noise characteristics, or experimentally selected from pre-defined "libraries" by evaluation of system characteristics in simulated or actual operating conditions (M. L. Wickerhauser, *Adapted Wavelet Analysis*, 1994).

H-2.1.1.1 Potential Radar Applications

A partial search of recent technical literature (published in 1993 and 1994) yielded 98 items relevant to wavelets. This included a textbook, several conference proceedings, two single-topic issues of monthly journals, and a comprehensive literature survey. The high level of current interest is indicated by the 976 entries for 1993 in the literature survey, which projects a 1994 total of about 2000 entries.

Most of the literature is general, theoretical, and mathematical. Much of the remainder is directed toward image processing, data coding and compression, audio processing, multi-

dimensional processing, or multi-sensor processing. The current immaturity of the field is indicated by the fact that only about 10 percent of the articles refer to actual implementations or applications. Only two of the 98 sources mentioned above explicitly concern radar systems.

The obvious application of the WT and WPT is for generation of range-Doppler maps in Doppler (e.g., high-PRF) radar systems. They are also capable of doing the types of baseband signal processing that are traditionally performed by FFTs and FIR digital filters (e.g., MTI and matched filter/correlation processing). It is not clear whether wavelet techniques would be more efficient than existing techniques for these applications.

Wavelets may provide an attractive alternative to standard CFAR techniques for target detection. A target detection sub-system could be implemented analogously to an image-processing feature-extraction subsystem, with the desired features being copies, subject to distortion and noise, of the transmitted signal. Current feature-extraction algorithms (A. E. Cetin, R. Ansari, *Signal Recovery From Wavelet Transform Maxima*, IEEE Transactions on Signal Processing, Vol. 42, No. 1, January 1994) are rather complex, which leaves the practicality of this approach open to question.

The largest advantages of wavelet processing over other techniques seem to be in the areas of wideband, multi-sensor, and/or multi-dimensional processing. These advantages make wavelets particularly effective in sonar signal processing (L. G. Weiss, *Wavelets and Wideband Correlation Processing*, IEEE Signal Processing Magazine, January, 1994). These processing methods should be directly adaptable to radar systems that employ high-bandwidth signals (e.g., pseudo-noise or LFM) or perform dynamic beam forming. These seem to be the most attractive areas of research for development of practical wavelet applications. However, because the study team found no articles that explicitly addressed these methods in the initial literature search, this claim is currently speculative.

ACRONYMS

A&T	Acquisition and Testing
A/D	Analog Devices
ADC	Analog-to-Digital Converter
AGC	Automatic Gain Control
ASPRO	Associative Processor
ASTB	Airborne Seeker Test Bed
BIFODEL	Binary FO Delay Lines
BIT/Cal	Built-In Test/Calibration
BPF	BandPass Filter
BT	Time Bandwidth Products
BWO	Backward Wave Oscillator
CFA	Cross-Field-Amplifier
CFAR	Constant False Alarm Rate
CIO	Controlled Input/Output
COHO	Coherent Oscillator
COTS	Commercial-Off-The-Shelf
CPI	Coherent Processing Interval
CRGP	Countering Range-Gate Pulloff
CRT	Chinese Remainder Theorem
CW	Continuous Wave
DAS	Data Acquisition Subsystem
DF	Direction Finding
DIA	Defense Intelligence Agency
DIO	Data Input/Output
DQMF	Decimating Quadrature Mirror Filter
DSP	Digital Signal Processor
DT&E	Developmental Test and Evaluation
DTSE&E	Director of Test, System Engineering and Evaluation
DTL	Digital Test Laboratory
EAR	Electronically Agile Radar
ECCM	Electronic Counter-CounterMeasures
ECM	Electronic CounterMeasures
ERP	Effective Radiated Power
ESA	Electronically Steered Array
FFT	Fast Fourier Transform
FIR	Finite Impulse Response
FLEXAR	Flexible Array Radar
FO	Fiber Optic
FOV	Field Of View
FSU	Former Soviet Union
GaAs	Gallium Arsenide
GFE	Government Furnished Equipment
GPS	Global Positioning System
HF	High Frequency
HP	Hewlett Packard
HPA	High Power Amplifier
HPSP	Hughes Parallel Signal Processor-1000
HWIL	Hardware-In-The-Loop
IC	Integrated Circuit (Chips)
IF	Intermediate Frequency
IMM	Interacting Multiple Model
IPR	In-Process Review
I/Q	In-Phase/Quadrature-Phase
IRIG	Inter-Range Instrumentation Group
IWT	Inverse Wavelet Transform
KANS	Klystron And Noise Study
LFM	Linear Frequency Modulation
LH	Left Hand
LNA	Low Noise Amplifier
LPRF	Low Pulse Repetition Frequency
LRU	Line Replaceable Unit
M&S	Models and Simulations
MDS	Minimum Detectable Signal
MIMD	Multiple Instruction, Multiple Data
MIPS	Million Instructions Per Second
MMIC	Monolithic Microwave Integrated Circuit
MOPA	Master Oscillator Power Amplifier
MR	MagnetoResistive
MSIC	Missile and Space Intelligence Center
MTBF	Mean-Time Between Failure
MTTR	Mean-Time To Repair
NDI	Non-Developmental Item
NJ	Noise Jamming
OBA	Optimal Bayesian Algorithm
OCXO	Oven Controlled Crystal Oscillator
OIS	Operator Interface Subsystem
OSHA	Occupational Safety and Health Administration
PCM	Phase Control Module
PC	Personal Computer
PDAF	Probabilistic Data Association Filter
PFN	Pulse Forming Network
PLL	Phase Locked Loop
PLO	Pase Locked Oscillator
PPI	Plan-Position Indication
PRF	Pulse Repetition Frequency
PRI	Pulse Repetition Interval
PRML	Partial-Response, Maximum Likelihood
PSP	Programmable Signal Processor
QMF	Quadrature Mirror Filter
RAID	Redundant Array of Inexpensive Disks
RCS	Radar Cross Section
RDP	Radar Data Processor
RF	Radio Frequency
RIS	Radar Interface Subsystem

RMS	Root Mean Square
RPP	Radar Post Processor
RGPO	Range Gate Pulloff
RH	Right Hand
RHI	Range-Height Indicator
ROW	Rest-Of-World
RPP	Radar Post Processor
RTRS	Reconfigurable Transportable Radar Set
S&TI	Scientific and Technical Intelligence
SAM	Surface to Air Missile
SAR	Synthetic Aperture Radar
SAW	Surface Acoustic Wave
SCI	Storage Concept Incorporated
SCV	SubClutter Visibility
SDIO	Strategic Defense Initiative Office
SEAD	Suppression of Enemy Air Defense
SHARC	Super Harvard Architecture Computer
SLB	Side Lobe Blanking
SNR	Signal to Noise Ratio
SOTA	State Of The Art
SRC	Scientific Research Corporation
STALO	Stable Local Oscillator
STAMO	Stable Master Oscillator
SWR	Standing Wave Ratio
T&C	Timing and Control
TBM	Tactical Ballistic Missile
TD	Time Delay
TER	Target Engagement Radar
TIR	Target Illumination Radar
T/R	Transmit and Receive
TSPI	Time, Space, Position Indicator
TTB	Technical Test Bed
TTD	True Time Delay
TTR	Target Tracking Radar
TWT	Traveling-Wave-Tubes
UHF	Ultra High Frequency
USD	Under Secretary of Defense
VCXO	Voltage Controlled Crystal Oscillator
VGPO	Velocity Gate Pull-Off
VL	Vertical Linear
VLSI	Very Large Scale Integration
VSWR	Voltage Standing Wave Ratio
VUE	Visual User Environment
WDM	Wavelength Division Multiplexing
WFS	WaveForm Simulator
WORM	Write Once Read Multiple
WPT	Wavelet Packet Transform
WT	Wavelet Transform